ECMWF COPERNICUS REPORT

Copernicus Atmosphere Monitoring Service

Validation report of the CAMS near-real time global atmospheric composition service

June - August 2018

Issued by: KNMI

Date: 17 December 2018

Ref: CAMS84_2018SC1_D1.1.1_JJA2018_v1

IMPLEMENTED BY ECMWF

Validation report of the CAMS near-real-time global atmospheric composition service. Period June - August 2018

EDITORS:
A. Wagner (MPG), M. Schulz (MetNo), Y. Christophe (BIRA-IASB),
M. Ramonet (LSCE), H.J. Eskes (KNMI)

AUTHORS:
S. Basart (BSC), A. Benedictow (MetNo), Y. Bennouna (CNRS-LA),
A.-M. Blechschmidt (IUP-UB), S. Chabrillat (BIRA-IASB), H. Clark (CNRS-LA),
E. Cuevas (AEMET), H. Flentje (DWD), K. M. Hansen (AU), U. Im (AU),
J. Kapsomenakis (AA), B. Langerock (BIRA-IASB), A. Richter (IUP-UB),
N. Sudarchikova (MPG), V. Thouret (CNRS-LA), T. Warneke (UBC), C. Zerefos (AA)

REPORT OF THE COPERNICUS ATMOSPHERE MONITORING SERVICE, VALIDATION SUBPROJECT.

AVAILABLE AT:
http://atmosphere.copernicus.eu/quarterly_validation_reports

CITATION:
Wagner, A., M. Schulz, Y. Christophe, M. Ramonet, H.J. Eskes, S. Basart, A. Benedictow, Y. Bennouna, A.-M. Blechschmidt, S. Chabrillat, H. Clark, E. Cuevas, H. Flentje, K.M. Hansen, U. Im, J. Kapsomenakis, B. Langerock, A. Richter, N. Sudarchikova, V. Thouret, T. Warneke, C. Zerefos, Validation report of the CAMS near-real-time global atmospheric composition service: Period June - August 2018, Copernicus Atmosphere Monitoring Service (CAMS) report, CAMS84_2018SC1_D1.1.1_JJA2018_v1.pdf, December 2018.

STATUS:
Version 1, Final

DATE:
17/12/2018

Executive Summary

The Copernicus Atmosphere Monitoring Service (http://atmosphere.copernicus.eu, CAMS) is a component of the European Earth Observation programme Copernicus. The CAMS global near-real time (NRT) service provides daily analyses and forecasts of reactive trace gases, greenhouse gases and aerosol concentrations. This document presents the validation statistics and system evolution of the CAMS NRT service for the period up to 1 September 2018. Updates of this document appear every 3 months.

This summary is split according to service themes as introduced on the CAMS website: air quality & atmospheric composition, climate forcing, ozone layer and UV. Specific attention is given to the ability of the CAMS system to capture recent events. We focus on the 'o-suite' composition fields, which are the daily analyses and forecasts produced by the IFS (Integrated Forecast System) modelling system at ECMWF, using the available meteorological and atmospheric composition observations which are ingested in the ECMWF 4D-Var assimilation system. The model and assimilation configuration is summarised in section 2. We furthermore assess the impact of the composition observations by comparing the validation results from the 'o-suite' to a 'control' configuration without assimilation. Also, the pre-operational delayed-mode analyses and high-resolution forecasts of CO_2 and CH_4 are assessed in this report.

The o-suite data delivery for the period June - August 2018 (JJA-2018) was excellent, with an availability of 100% at 10 and 22 utc (two forecasts per day).

Air quality and atmospheric composition

Tropospheric ozone (O_3)

CAMS o-suite ozone is validated with surface and free tropospheric ozone observations from the GAW and ESRL networks, IAGOS airborne data and ozone sondes. For free tropospheric ozone against ozone sondes the o-suite modified normalized mean biases (MNMBs) are on average small, ±10% over the Northern Hemisphere (NH), between ±30% for stations in the Tropics, and between ±15% for the Arctic (Fig. S.1). Over Antarctica o-suite biases are observed between 0% and +20%, whereas the control run shows negative biases. For JJA2018 good agreement is found over the NH mid latitudes in the free troposphere, which is confirmed with IAGOS evaluations over Paris and Frankfurt. In the UTLS region, both runs show larger positive and negative MNMBs. Surface ozone compares well with IAGOS over Europe. Good agreements with the IAGOS free troposphere ozone profiles is also found over Western Africa and North America, the Pacific ocean and Asia, with sometimes large differences in the UTLS region (e.g. Los Angeles, San Francisco).

In comparison with surface observations we find a steady improvement of the o-suite over the past 5 years over European GAW stations. Biases are generally around ±10%, and within ±20% (the Arctic is discussed below). The o-suite slightly overestimates surface ozone for Europe and the US during June and August 2018 with MNMBs up to 12%. Both runs overestimate the low O_3 observations (monsoon season) for Asia with MNMBs up to 60%. For the tropics, surface ozone is reproduced

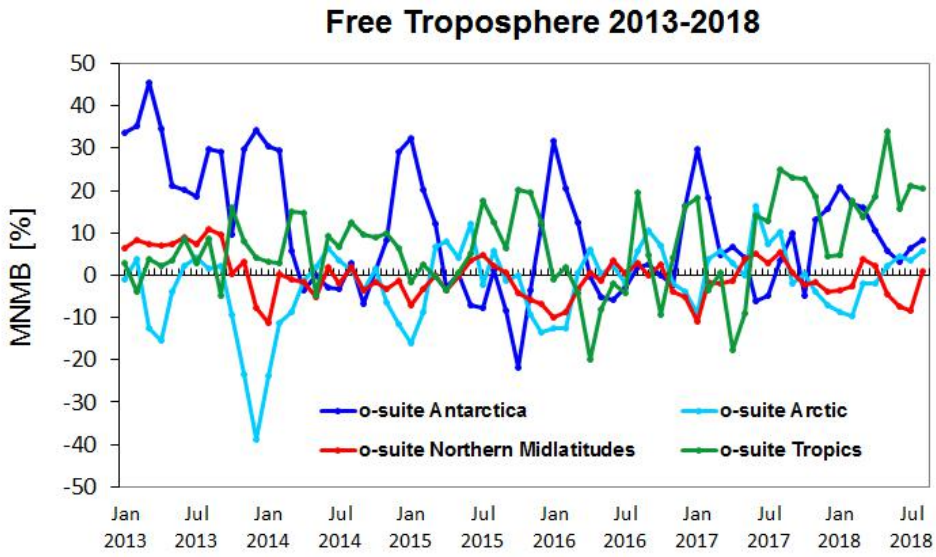

Figure S.1: Time series of MNMB of ozone in the o-suite, compared against ozone sondes, averaged over different latitude bands. The free troposphere is defined here as the layer between 750 and 300 hPa.

well with MNMBs within 5%. For Antarctica negative biases are observed for the control run, which is efficiently corrected by the assimilation in the o-suite (MNMBS < 10%).

Tropospheric Nitrogen dioxide (NO_2)

Model validation, with respect to SCIAMACHY/Envisat NO_2 data before April 2012 and GOME-2/MetOp-A NO_2 data afterwards, shows that tropospheric NO_2 columns are well reproduced by the NRT model runs, indicating that emission patterns and NO_x photochemistry are generally well represented, although modelled shipping signals are more pronounced than in the satellite retrievals. Tropospheric NO_2 columns over some local emission hotspots (e.g. Moscow, and Red Basin in China) are overestimated, while wintertime and springtime values over Europe are underestimated. Since December 2014, the agreement between satellite retrievals and model results for time series over East-Asia and Europe is better than for previous years (Fig. S.2), as observed columns of NO_2 decreased recently, likely associated with reduced emissions, and (in contrast to the observations) simulated values show an increase over the whole timeseries available. Spring and summertime values over East-Asia are overestimated by the o-suite since 2015, a feature which did not occur for previous years. Mainly in summer and autumn the models regularly show an overestimation over several regions with fire activity (Canada, Siberia, and Nepal).

Tropospheric Carbon Monoxide (CO)

Model validation with respect to GAW network surface observations, IAGOS airborne data, FTIR observations (NDACC and TCCON) and MOPITT / IASI satellite retrievals reveals that the absolute values, latitude dependence and seasonality, as well as day-to-day variability of CO can be reproduced well by the CAMS-global analyses and forecasts. Biases are between 0% and -30% for European stations, and between -10 and -13% in Asia. A similar bias in Europe in the lower layers is observed by IAGOS. For stations in the southern hemisphere the comparison with NDACC and GAW measurements shows that data assimilation reduces the large positive MNMBs in the control run.

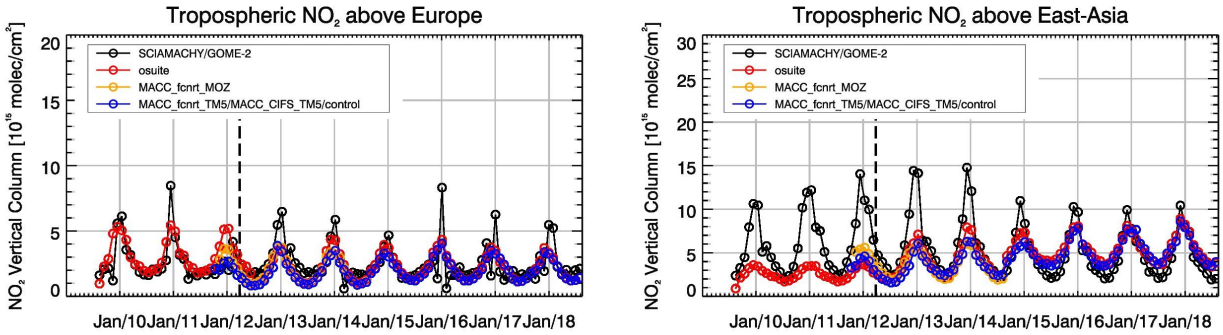

Figure S.2: Time series of tropospheric NO_2 columns from SCIAMACHY (up to March 2012), GOME-2 (from April 2012 onwards) compared to model results for Europe and East-Asia. The o-suite is in red, control is in blue (the model run without data assimilation is termed control since Sep 2014).

In the free troposphere the bias is close to 0, while a small positive bias of about 10% is found in the UTLS. CO plumes in June related to forest fires in North America are mostly well detected but underestimated by the o-suite. Other pollution episodes over North America and Asia are sometimes captured, and sometimes missed, depending on the location. The o-suite does not in all cases better represent the profiles than the control run. Complex vertical variability observed over airports in Africa is generally captured by the o-suite, although absolute values may sometimes differ. Comparisons with NDACC-FTIR observations and with MOPITT and IASI satellite observations generally confirm the very small biases within 5% in the free troposphere, and the accurate description of seasonal and day-to-day variability. In contrast, the control run shows a pronounced positive bias in the tropics and southern hemisphere, demonstrating the positive impact of the assimilation. Prominent positive biases are only observed over East Asia and the Syberian fire region.

Formaldehyde

Model validation, with respect to SCIAMACHY/Envisat HCHO data before April 2012 and GOME-2/MetOp-A HCHO data afterwards, shows that modelled monthly HCHO columns represent well the magnitude of oceanic and continental background values and the overall spatial distribution in comparison with mean satellite HCHO columns. Compared to GOME-2 satellite retrievals, an overestimation of values regularly occurs over Australia and Central Africa, which could be both related to biogenic emissions or fire emissions. For time series over East-Asia and the Eastern US, both regions where HCHO columns are probably dominated by biogenic emissions, models and retrievals agree rather well. However, the yearly cycle over East-Asia is underestimated by the models.

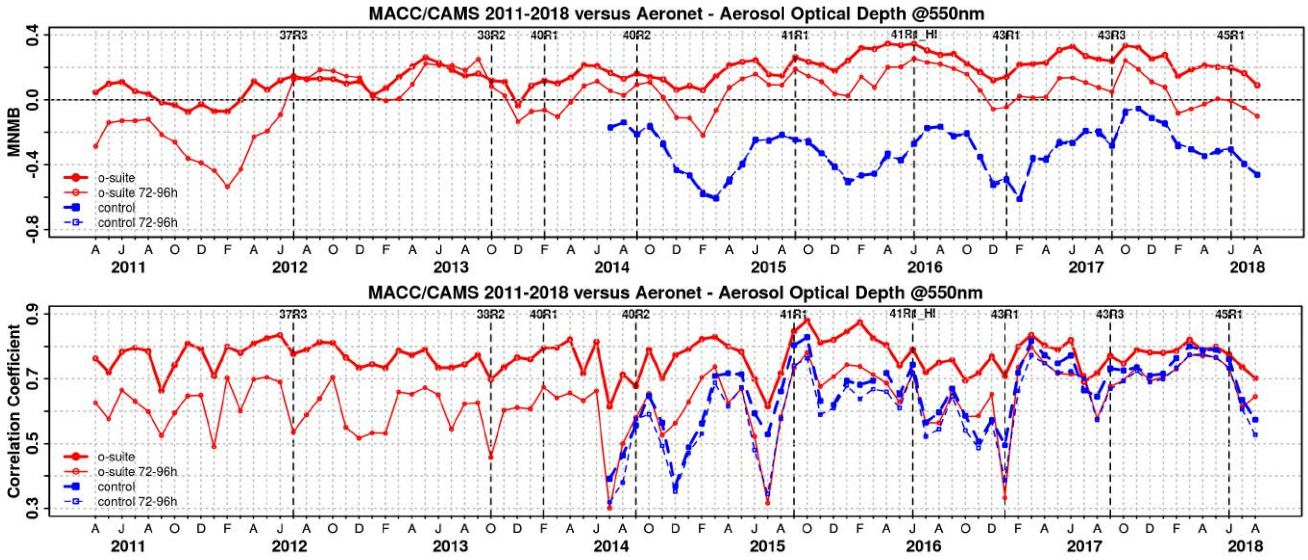

Figure S.3. Aerosol optical depth at 550nm in IFS 00Z model simulations for April 2011 – August 2018 against daily matching Aeronet Version3 level 1.5 data. a) Modified normalized mean bias (MNMB); o-suite (thick red curve); o-suite at last forecast day (light red curve); Control (blue dashed); Control at last forecast day (light blue dashed); b) Corresponding correlation coefficient. Model version changes are marked as vertical bars.

Aerosol

We estimate that the o-suite aerosol optical depth showed an average positive bias in the latest three months of +15%, measured as modified normalized mean bias against daily Aeronet (V3 level 1.5) sun photometer data. The +3 day forecasted aerosol distribution shows 14% less aerosol optical depth (AOD) than that from the initial forecast day, as shown in Figure S.3-a. The spatio-temporal correlation, shown in figure S.3-b, shows month-to-month variation in JJA 2018 similar to summer 2017, indicating the simulation reproduces approximately 60% of the day to day AOD variability across all Aeronet stations. We find a high AOD bias in Southern Latitudes. The o-suite forecast at +3 days shows slightly lower correlation, as a consequence of imperfect forecasted meteorology and fading impact of the initial assimilation of MODIS AOD and MODIS fire info on model performance. However, the forecast and also control experiment have improved clearly since February 2017. The second o-suite running each day at 12UTC shows almost identical performance as the o-suite starting at 00UTC.

The AOD performance of the o-suite with respect to the AERONET data exhibits no pronounced seasonal cycle since 2014. Since October 2017, global AOD is dominated by organics and sea salt. Sea salt AOD increased further due to the latest model upgrade in June 2018 with the new sea salt emission scheme activated.

The aerosol Ångström exponent (AE) contains information about the size distribution of the aerosol, and implicitly composition. The o-suite AE changes from a positive global bias against Aeronet (V3 Level 1.5) data of +5% to -2%, indicating a change to slightly more coarse particles since latest model upgrade to version 45R1 in June 2018, consistent with an increase in sea salt.

PM10 data are evaluated as defined by the IFS aerosol model. An evaluation of these PM10 surface concentrations against an average from data in the period 2000-2009 at 160 background sites in North America and Europe indicate that PM10 concentrations exhibit on average in the latest period an underestimation with MNMB bias of -7% in Europe and an overestimation of + 20% in North America. This regional bias difference is also found for AOD. The fraction of data within factor 2 of observed values has increased compared to earlier years.

For June to August 2018, the CAMS global o-suite reproduces the main locations of dust activity in the Sahara and the Middle East in comparison with MODIS satellite observations. However, CAMS tends to overestimate the dust concentrations over Mauritania and underestimates the North Atlantic dust transport and the desert dust sources in Iraq. The o-suite reproduces the daily variability of AERONET observations with a high correlation coefficient of 0.89 on average for all the AERONET sites, while the control experiment and the SDS-WAS Multi-model show a correlation coefficient of 0.84 and 0.87 respectively. Both CAMS experiments (o-suite and control), as well as the SDS-WAS Multi-model, underestimate the AERONET observations resulting in a mean bias of -0.03 for control, -0.05 for o-suite and -0.05 the SDS-WAS Multi-model. During summer, the maximum occurrence of strong and fast dust outbreaks occurs in the Sahara, associated with small mesoscale convective systems that the CAMS model is not able to resolve. The prediction of these convective systems is the main reason for the weaker skills of the o-suite over the Sahara and North-Western Maghreb during this season, with a correlation coefficient of 0.56 and bias of -0.21 for the Sahara. Otherwise, in the Sahel, a strong underestimation (mean bias of -0.21) is observed, despite the fact that the model can reproduce the observed daily variability with a high correlation of 0.80. The strong underestimations observed in the o-suite in the Sahel are also spread to the Tropical North Atlantic (mean bias of -0.27 for the o-suite) in agreement with the underestimation observed in the comparison with the satellites. Otherwise, the comparison of the 48h and 72h forecasts for both CAMS experiments shows that the prediction is stable during the 3-days forecasts with correlation coefficients of 0.84 (0.89), 0.85 (0.83), and 0.82 (0.82) for the 24, 48 and 72h forecasts respectively, for o-suite (control). In the Subtropical North Atlantic, the correlation coefficient for o-suite decreases from 0.80 to 0.67 for the 48 to 72 hour forecast, similar to the control in which the correlation decreases from 0.70 to 0.61. The results indicate limitations of the CAMS model to predict Mauritanian sources.

Backscatter coefficients are low-biased in the planetary boundary layer (PBL). Possible reasons are missing of ammonia and nitrate in the model (foreseen to be activated soon), assumption of too high particle densities (too compact materials) in the mass to backscatter conversion, and the lack of a vertical transport barrier at the top of the PBL, causing dilution with free troposphere air. Free troposphere (FT) background backscatter coefficients are biased high, probably due to wrong re-distribution between PBL and FT. This is not fixed by the assimilation, which instead adds aerosol to the whole profile. The backscatter bias on a specific level thus depends on its relative position w.r.t. to the boundary layer height (BLH). The model BLH agrees reasonably (within a few 100 m) with observations under favourable measurement conditions. Very often, however, meteorological conditions prevent formation, unambiguousness or detectability of the BLH or make the latter a challenge.

System performance in the Arctic

The CAMS model runs are validated using surface ozone measurements from 4 sites within the IASOA networks and ozone concentrations in the free troposphere are evaluated using balloon sonde measurement data.

For the period from December 2014 to August 2018 the simulations of the surface ozone concentrations are on average in good agreement with the observations apart from ozone depletion events in spring (March to June).

During June – August 2018 there is generally an overestimation of the surface ozone concentrations in the Arctic for both the o-suite and the control run (NMB = 2% to 21%). The control run performs better with higher correlation coefficients (r = 0.19 – 0.40 for the o-suite compared to r = 0.15 – 0.62 for the control run).

Ozone concentrations in the free troposphere are in good agreement with observations with low relative bias (up to 10% for the o-suite and -10%-10% for the control run). In the UTLS, the o-suite has a slightly higher positive bias for the Arctic sites.

Comparison with FTIR observations from the NDACC network shows that the CO tropospheric columns are well simulated at the two arctic sites with low positive bias (<4%), while there is a large positive bias for the control (12-15%). The assimilation has a positive effect on the correlation coefficient: r = 0.94-0.95 for the o-suite and 0.34-0.57 for the control run. The results for the stratospheric are similar with slightly higher biases for the o-suite (<6%). Comparison MOPITT versions 7 shows that modeled CO total columns are in good agreement with the satellite retrievals with low bias in the Arctic (±10%).

System performance in the Mediterranean

The model is compared to surface O_3 observations from the AirBase network. Our analysis shows that model MNMBs vary between -20% and 30% depending on the station. Temporal correlation coefficients between simulated and observed surface ozone for both the o-suite and control runs are highly significant over the entire Mediterranean from Gibraltar to Cyprus.

CAMS model can reproduce the daily variability of AERONET observations (with correlation coefficients of 0.70, 0.82 and 0.59, respectively for Western, Central and Eastern Mediterranean). Although, the operational CAMS model tends to overestimate the observed AOD values by AERONET sites resulting with an MB of 0.01, 0.03 and 0.02, respectively for Western, Central and Eastern Mediterranean. During summer, the enhancement of the photochemical processes (which favours the formation of secondary aerosols) together with the lack of precipitation increase the background levels in the Basin. Underestimations of these background aerosols are corrected during the assimilation cycle increasing the AOD levels. At surface levels, PM10 and PM2.5 results of CAMS o-suite and control show similar skill scores in comparison with EIONET-Airbase observations. For PM2.5, CAMS model tends to overestimate the observations meanwhile PM10 tends to be underestimated in the Spanish Mediterranean sites. From June to August, the overestimations observed in the comparison against EIONET-Airbase cause that the o-suite overpredict the number of exceedances of the EU PM10 daily threshold (i.e. 50 $\mu g/m^3$).

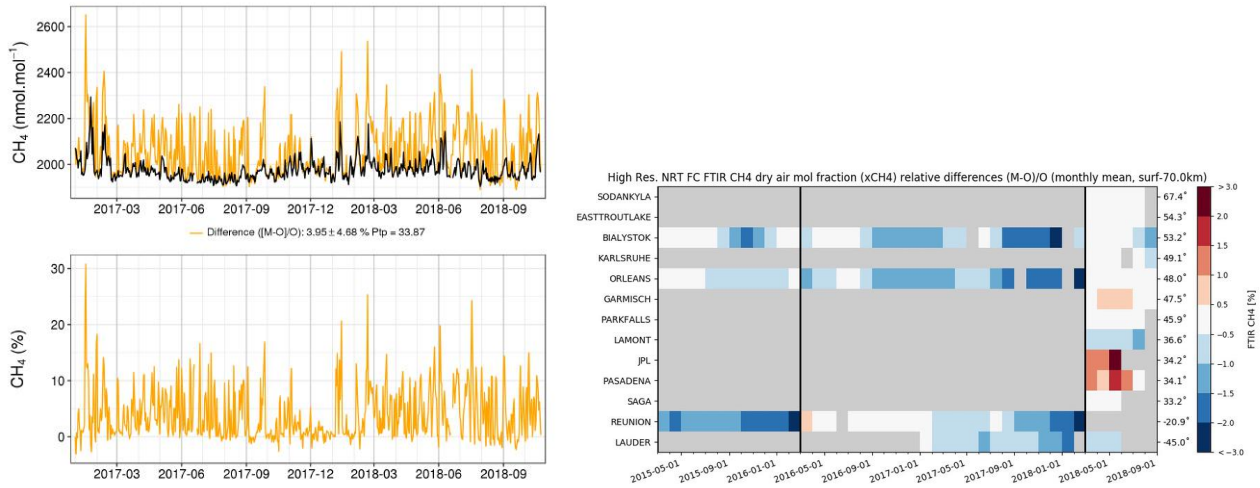

Figure S.4: Left: CH_4 time series (daily means) at the ICOS tall tower of Saclay, located 20 km south of Paris (above) and relative differences (below). Right: monthly mean relative bias for column averaged CH_4 mole fractions at TCCON sites compared to the high resolution forecast, showing positive outliers at JPL and Pasadena sites located in Los Angeles, California.

Climate forcing

Greenhouse gases

CO_2 and CH_4 surface concentrations from the ICOS network, and total or partial columns from TCCON and NDACC stations have been used to validate the high resolution forecast experiment.

The comparison at background surface and total column sites show that CO_2 and CH_4 long term increases are respectively overestimated and underestimated by the model. Consequently we observe at several sites, characterized by relatively low seasonal and synoptic variabilities, a switch from positive to negative biases for CH_4, and the reverse for CO_2.

We observe significant overestimation of CH_4 concentrations (ICOS) and total columns (TCCON) at stations close to megacities of Paris and Los Angeles, indicating an issue with the emission inventories, and the difficulty to represent the pollution plumes emitted from megacities (Figure S.4).

Both surface and total column measurements indicate an overestimation of the the amplitude of the CO_2 seasonal cycle in the northern hemisphere by 1 to 2%.

On average, over the period covering October 2017 to September 2018, the high resolution forecast experiment reduces the daytime bias compared to the analysis experiment, by 2.8 ppb and 0.8 ppm for CH_4 and CO_2 respectively (using sites with a corrrelation coefficient higher than 0.5). During the night the bias reductions are 1.2 ppb and 0.9 ppm respectively. The RMSE is also reduces in the high resolution forecast by about 1 ppm for CO_2. It is also reduced for CH_4 by few ppb at background stations like AMS or MHD, but it is increased at the Trainou tall tower by 10 to 50 ppb, depending on the elevation. This increase of the RMSE at Trainou, 100km south of Paris, can probably be explained by the mis-representation of hot spot emissions, which can have higher effect with high resolution simulations.

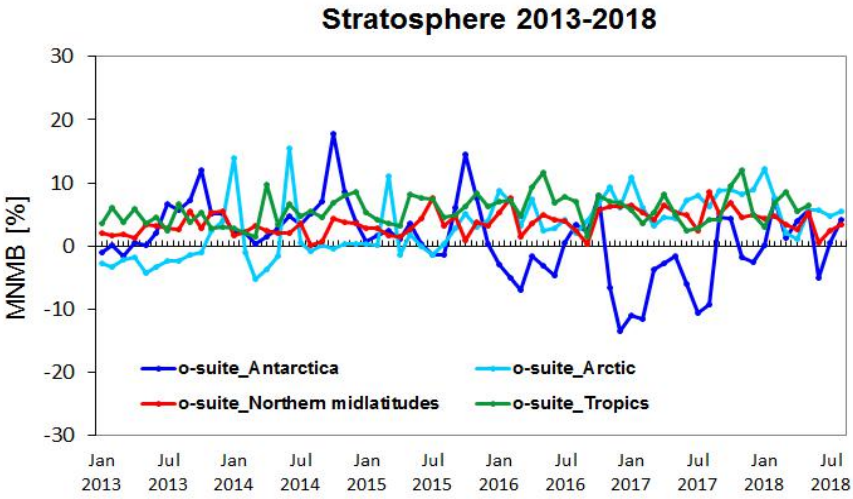

Figure S.5: MNMBs (%) of ozone in the stratosphere from the o-suite against aggregated sonde data in the Arctic (light blue), Antarctic (dark blue) northern midlatitudes (red) and tropics (green)) from 2013 to August 2018.

Ozone layer and UV

Ozone partial columns and vertical profiles

Ozone columns and profiles have been compared with the following observations: vertical profiles from balloon-borne ozonesondes; ground-based remote-sensing observations from the NDACC (Network for the Detection of Atmospheric Composition Change, http://www.ndacc.org); and satellite observations by two instrument (OMPS-LP, ACE-FTS). Furthermore, the o-suite analyses are compared with those delivered by the independent assimilation system BASCOE.

Compared to ozone sondes (Fig. S.5) the model O_3 partial pressures are slightly overestimated in all latitude bands (MNMB between 4 and +12%) except above the Antarctic.

Comparisons with the NDACC network include 16 stations for UVVIS and FTIR stratospheric columns, microwave profiles for Ny Alesund (78.9°N) and Bern (47°N) and LIDAR profiles at Hohenpeissenberg (47.8°N) and Observatoire Haute Provence (OHP), France (43°N). The comparison with the UVVIS stations are generally in agreement with the o-suite, while it indicates a latitudinal dependence of the biases for the control run. The result from MWR and LIDAR comparisons for the current period are in line with those of previous reports.

The comparison with independent satellite observations is generally in good agreement for the considered period: for ACE-FTS, the NMB is mainly within 10% between 5km and 40km, and mostly within 5% between 15km and 35km except in the tropics. OMPS-LP has less regular profiles, but the NMB still remain within 15% for most parts of the 20-40 km range.

Other stratospheric trace gases

Due to the lack of stratospheric chemistry in the C-IFS-CB05 scheme, the only useful product in the stratosphere is ozone. Other species, like NO_2, have also been evaluated but the results are only indicative.

Events

North Atlantic dust transport over the Iberian Peninsula during August 2018: In early-August 2018, MODIS satellite detected a North Atlantic dust plume with origin in Northern Algeria on 1st August. The dust plume moved in an arc shape over the Atlantic and arrived in Southern Portugal on 2nd August, to North-western Spain on early 3rd August and Central Spain on late 3rd August. This dust trajectory was nicely tracked by the AERONET sunphotometers in the Iberian Peninsula and resulted in a maximum AOD value of 1.2 over Portugal. The CAMS o-suite can timely reproduce the AOD spatial distribution of the dust plume over the Arabian Peninsula in comparison with the AERONET observations, despite the model underestimate of the observed maximum values. At surface levels, the CAMS o-suite correctly predicted the observed evolution of dust particulate matter over the Eastern Iberian Peninsula, with values up to 120 $\mu g/m^3$ on 4th August.

Alaska fire events, July 2018: Several fire events were detected during July 2018 in Alaska region. The CO peak detected by MOPITT and IASI between July 7 and 9 was well captured by CAMS-global with similar CO concentrations. A second fire event detected around July 22 was also well captured, but somewhat underestimated by about 20%.

Table of Contents

1. Introduction

The Copernicus Atmosphere Monitoring Service (CAMS, http://atmosphere.copernicus.eu/) is a component of the European Earth Observation programme Copernicus. The CAMS global near-real time (NRT) service provides daily analyses and forecasts of trace gas and aerosol concentrations. The CAMS near-real time services consist of daily analysis and forecasts with the ECMWF IFS system with data assimilation of trace gas concentrations and aerosol properties. This document presents the system evolution and the validation statistics of the CAMS NRT global atmospheric composition analyses and forecasts. The validation methodology and measurement datasets are discussed in Eskes et al. (2015).

In this report the performance of the system is assessed in two ways: both the longer-term mean performance (seasonality) as well as its ability to capture recent events are documented. Table 1.1 provides an overview of the trace gas species and aerosol aspects discussed in this CAMS near-real time validation report. This document is updated every 3 months to report the recent status of the near-real time service. The report covers results for a period of at least one year to document the seasonality of the biases. Sometimes reference is made to other model versions or the reanalysis to highlight aspects of the near-real time products.

This validation report is accompanied by the "Observations characterization and validation methods" report, Douros et al. (2017), which describes the observations used in the comparisons, and the validation methodology. This report can also be found on the global validation page, http://atmosphere.copernicus.eu/user-support/validation/verification-global-services.

Key CAMS NRT products and their users are: Boundary conditions for regional air quality models (e.g. AQMEII, air quality models not participating in CAMS); Long range transport of air pollution (e.g. LRTAP); Stratospheric ozone column and UV (e.g. WMO, DWD); 3D ozone fields (e.g. SPARC). As outlined in the MACC-II Atmospheric Service Validation Protocol (2013) and MACC O-INT document (2011), relevant user requirements are quick looks of validation scores, and quality flags and uncertainty information along with the actual data. This is further stimulated by QA4EO (Quality Assurance Framework for Earth Observation, http://www.qa4eo.org) who write that “all earth observation data and derived products is associated with it a documented and fully traceable quality indicator (QI)”. It is our long-term aim to provide such background information. The user is seen as the driver for any specific quality requirements and should assess if any supplied information, as characterised by its associated QI, are "fit for purpose" (QA4EO task team, 2010).

CAMS data are made available to users as data products (grib or netcdf files) and graphical products from ECMWF, accessible through the catalogue on http://atmosphere.copernicus.eu/.

A summary of the system and its recent changes is given in section 2. Subsequent sections gives an overview of the performance of the system for various species, and during recent events. Routine validation results can be found online via regularly updated verification pages, http://atmosphere.copernicus.eu/user-support/validation/verification-global-services.
Table 1.2 lists all specific validation websites that can also be found through this link.

Table 1.1: Overview of the trace gas species and aerosol aspects discussed in this CAMS near-real time validation report. Shown are the datasets assimilated in the CAMS analysis (second column) and the datasets used for validation, as shown in this report (third column). Green colors indicate that substantial data is available to either constrain the species in the analysis, or substantial data is available to assess the quality of the analysis. Yellow boxes indicate that measurements are available, but that the impact on the analysis is not very strong or indirect (second column), or that only certain aspects are validated (third column).

Species, vertical range	Assimilation	Validation
Aerosol, optical properties	MODIS Aqua/Terra AOD PMAp AOD	AOD, Ångström: AERONET, GAW, Skynet, MISR, OMI, lidar, ceilometer
Aerosol mass (PM10, PM2.5)	MODIS Aqua/Terra	European AirBase stations
O_3, stratosphere	MLS, GOME-2A, GOME-2B, OMI, SBUV-2, OMPS	Sonde, lidar, MWR, FTIR, OMPS, ACE-FTS, OSIRIS, BASCOE and MSR analyses
O_3, UT/LS	MLS	IAGOS, ozone sonde
O_3, free troposphere	Indirectly constrained by limb and nadir sounders	IAGOS, ozone sonde
O_3, PBL / surface		Surface ozone: WMO/GAW, NOAA/ESRL-GMD, AIRBASE
CO, UT/LS	IASI, MOPITT	IAGOS
CO, free troposphere	IASI, MOPITT	IAGOS, MOPITT, IASI, TCCON
CO, PBL / surface	IASI, MOPITT	Surface CO: WMO/GAW, NOAA/ESRL
NO_2, troposphere	OMI, GOME-2, partially constrained due to short lifetime	SCIAMACHY, GOME-2, MAX-DOAS
HCHO		GOME-2, MAX-DOAS
SO_2	GOME-2A, GOME-2B (Volcanic eruptions)	
Stratosphere, other than O_3		NO_2 column only: SCIAMACHY, GOME-2
CO_2, surface, PBL		ICOS
CO_2, column	GOSAT	TCCON
CH_4, surface, PBL		ICOS
CH_4, column	GOSAT, IASI	TCCON

Table 1.2: Overview of quick-look validation websites of the CAMS system.

Reactive gases – Troposphere
GAW surface ozone and carbon monoxide: http://macc.copernicus-atmosphere.eu/d/services/gac/verif/grg/gaw/gaw_station_ts!CIFS/TM5 AN IAGOS tropospheric ozone and carbon monoxide: http://www.iagos.fr/cams/ Surface ozone from EMEP (Europe) and NOAA-ESRL (USA): http://www.academyofathens.gr/cams Tropospheric nitrogen dioxide and formaldehyde columns against satellite retrievals: http://www.doas-bremen.de/macc/macc_veri_iup_home.html Tropospheric CO columns against satellite retrievals: http://cams.mpimet.mpg.de
Reactive gases - Stratosphere
Stratospheric composition: http://www.copernicus-stratosphere.eu NDACC evaluation in stratosphere and troposphere (the NORS server) http://nors-server.aeronomie.be
Aerosol
Evaluation against Aeronet stations: http://aerocom.met.no/cams-aerocom-evaluation/ More in-depth evaluations from the Aerocom website: http://aerocom.met.no/cgi-bin/aerocom/surfobs_annualrs.pl?PROJECT=CAMS&MODELLIST=CAMS-VALreports&FULL=explicit&INFO=nohover&PERFORMANCE=ind&YEARFILTER=ALLYEARS&PSFILTER=ALLVARS&Type0=SCATTERLOG&Ref0=AERONETSunNRT&Run0=ECMWF_OSUITE&Parameter0=OD550_AER&St WMO Sand and Dust Storm Warning Advisory and Assessment System (SDS-WAS) model intercomparison and evaluation: http://sds-was.aemet.es/forecast-products/models
Satellite data monitoring
Monitoring of satellite data usage in the Reanalysis and Near-Real-Time production: http://copernicus-atmosphere.eu/d/services/gac/monitor/

Naming and color-coding conventions in this report follow the scheme as given in Table 1.3.

Table 1.3. Naming and color conventions as adopted in this report.

Name in figs	**experiment**	**Color**
{obs name}	{obs}	black
o-suite D+0 FC	0001	red
control	gsyg	blue
GHG high-resolution run	gqpe / ghqy	orange
GHG global analysis	gqiq	blue

2. System summary and model background information

The specifics of the different CAMS model versions are given below (section 2.1) including an overview of model changes. Other systems used in CAMS are listed in section 2.2. An overview of products derived from this system is given in section 2.3. Timeliness and availability of the CAMS products is given in section 2.4.

2.1 System based on the ECMWF IFS model

Key model information is given on the CAMS data-assimilation and forecast run o-suite and its control experiment, used to assess the performance of the assimilation. The forecast products are listed in Table 2.1. Table 2.2 provides information on the satellite data used in the o-suite. Further details on the different model runs and their data usage can be found at http://atmosphere.copernicus.eu/documentation-global-systems.
Information on older MACC experiment types, including MACC_fcnrt_MOZ and MACC_CIFS_TM5 can be found in older Validation reports available from http://www.gmes-atmosphere.eu/services/aqac/global_verification/validation_reports/.

Table 2.1: Overview of model runs assessed in this validation report.

Forecast system	Exp. ID	Brief description	Upgrades (e-suite ID)
o-suite	0001	Operational CAMS DA/FC run	20180626-present 20170926-20180625 20170124-20170926 20160621-20170124 20150903-20160620 20140918-20150902
Control	gzhy gsyg gnhb gjjh geuh g4o2	control FC run without DA	20180626-present (gzhy) 20170926-20180625 (gsyg) 20170124-20170926 (gnhb) 20160621-20170124 (gjjh) 20150901-20160620 (geuh) 20140701-20150902 (g4o2)
GHG run	ghqy gf39	High resolution T1279, NRT CO_2 and CH_4 without DA	20160301-20170621 (ghqy) 20150101-20160229 (gf39)
	gqpe	High resolution Tco1279 (~9km) NRT CO_2, CH_4 and linCO forecast, initialized from GHG analysis gqiq and CAMS operational CO analysis	20170101-present
	gqiq	GHG analysis Tco399 (~25km)	20170101-present

Table 2.2: Satellite retrievals of reactive gases and aerosol optical depth that are actively assimilated in the o-suite.

Instrument	Satellite	Provider	Version	Type	Status
MLS	AURA	NASA	V4	O3 Profiles	20130107 -
OMI	AURA	NASA	V883	O3 Total column	20090901 -
GOME-2A	Metop-A	Eumetsat	GDP 4.8	O3 Total column	20131007 -
GOME-2B	Metop-B	Eumetsat	GDP 4.8	O3 Total column	20140512 -
SBUV-2	NOAA-19	NOAA	V8	O3 21 layer profiles	20121007 -
OMPS	Suomi-NPP	NOAA / EUMETSAT		O3 Profiles	20170124 -
IASI	MetOp-A	LATMOS/ULB Eumetsat	-	CO Total column	20090901 - 20180621 20180622 -
IASI	MetOp-B	LATMOS/ULB Eumetsat	-	CO Total column	20140918 - 20180621 20180622 -
MOPITT	TERRA	NCAR	V5-TIR V7-TIR V7-TIR Lance	CO Total column	20130129 - 20160124 - 20180626 20180626
OMI	AURA	KNMI	DOMINO V2.0	NO2 Tropospheric column	20120705 -
GOME-2A/2B	METOP A/B	Eumetsat	GDP 4.8	NO2 Tropospheric column	20180626 -
OMI	AURA	NASA	v003	SO2 Tropospheric column	20120705-20150901
GOME-2A/2B	METOP A/B	Eumetsat	GDP 4.8	SO2 Tropospheric column	20150902 -
MODIS	AQUA / TERRA	NASA	Col. 5 Deep Blue Col. 6, 6.1	Aerosol total optical depth, fire radiative power	20090901 - 20150902 - 20170124 -
PMAp	METOP-A METOP-B	EUMETSAT		AOD	20170124 - 20170926 -

2.1.1 o-suite

The o-suite consists of the IFS-CB05 chemistry combined with the CAMS bulk aerosol model. The chemistry is described in Flemming et al. (2015) and Flemming et al. (2017), aerosol is described in Morcrette et al. (2009). The forecast length is 120 h. The o-suite data is stored under **expver '0001'** of **class 'MC'**. On 21 June 2016 the model resolution has seen an upgrade from T255 to T511, and forecasts are produced twice per day. The latest upgrade of the system is based on IFS version cy45r1_CAMS (https://confluence.ecmwf.int/display/COPSRV/Current+global+production+suites) and took place on 26 June 2018, see. The validation for this upgrade is described in Eskes et al., 2018. The update relevant for this report (for MAM-2018) is the 26 September 2017 upgrade, https://confluence.ecmwf.int/pages/viewpage.action?pageId=79955183. The performance of this upgrade is discussed in Eskes et al., 2017. A summary of the main specifications:

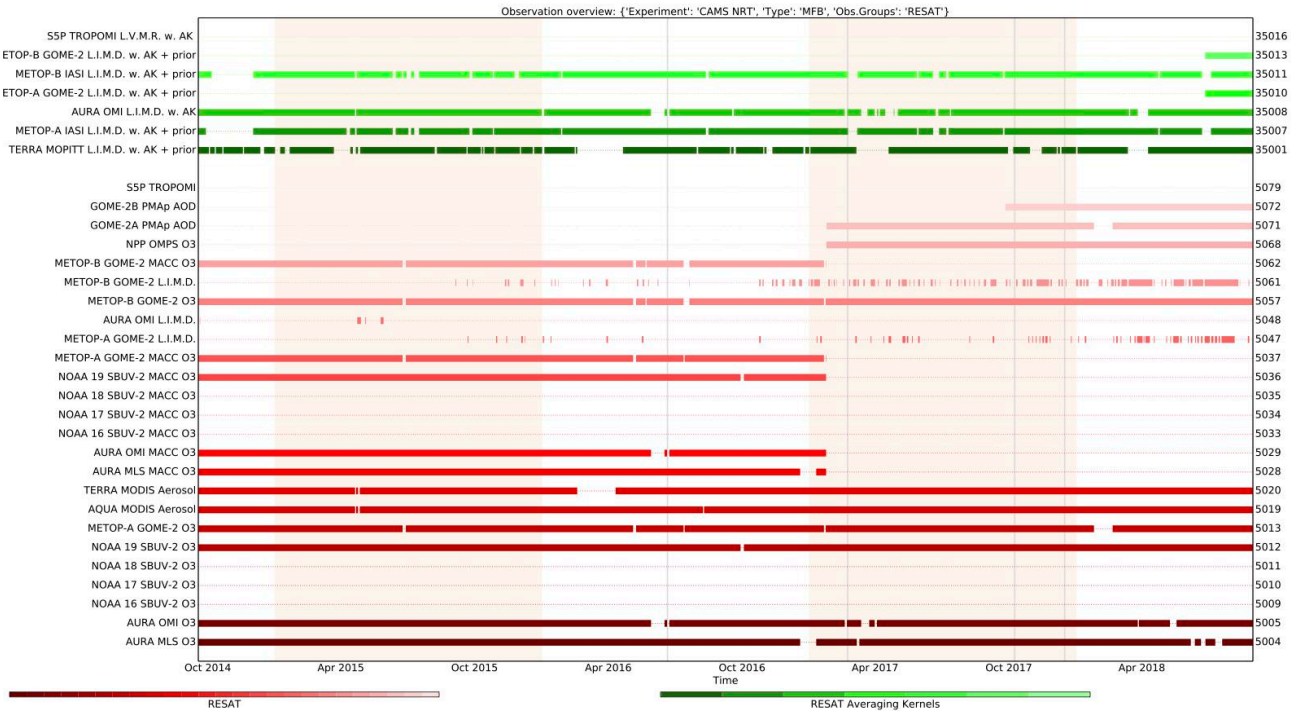

Figure 2.1: Satellite observation usage in the real-time analysis, for ozone, CO, aerosol AOD, from October 2014 onwards. Top seven rows: products assimilated with averaging kernels. New assimilated products since the 24 January 2017 upgrade are the PMaP AOD including GOME-2B and OMPS ozone profile observations. Note that the lines mentioning "MACC O3" should be discarded.

- The modified CB05 tropospheric chemistry is used (Williams et al., 2013), originally taken from the TM5 chemistry transport model (Huijnen et al., 2010)
- Stratospheric ozone during the forecast is computed from the Cariolle scheme (Cariolle and Teyssèdre, 2007) as already available in IFS, while stratospheric NOx is constrained through a climatological ratio of HNO_3/O_3 at 10 hPa.
- Monthly mean dry deposition velocities are based on the SUMO model provided by the MOCAGE team.
- Data assimilation is described in Inness et al. (2015) and Benedetti et al. (2009) for chemical trace gases and aerosol, respectively. Satellite data assimilated is listed in Table 2.2 and Fig. 2.1.
- Anthropogenic and biogenic emissions are based on MACCity (Granier et al., 2011) and a climatology of the MEGAN-MACC emission inventories (Sindelarova et al., 2014)
- NRT fire emissions are taken from GFASv1.2 (Kaiser et al. 2012).

The aerosol model includes 12 prognostic variables, which are 3 bins for sea salt and desert dust, hydrophobic and hydrophilic organic matter and black carbon, sulphate aerosols and its precursor trace gas SO_2 (Morcrette et al., 2009). Aerosol total mass is constrained by the assimilation of MODIS AOD (Benedetti et al. 2009). A variational bias correction for the MODIS AOD is in place based on the approach used also elsewhere in the IFS (Dee and Uppala, 2009).

New source scheme for Secondary Organic Aerosols (part of the Organic Matter), based on scaled CO emissions. This is a change form the current AEROCOM-based emissions. The impact is an increase of organic matter aerosol concentrations. The upgrade of 24 January 2017 introduced the

following adjustments: 1. Reduced dust emissions over Taklamakan desert and India. 2. Dust emissions adjusted towards more larger particles. 3. Reduction in sulphate aerosol. 4. Mass fixer for aerosols.

A history of updates of the o-suite is given in Table 2.4, and is documented in earlier MACC-VAL reports:
http://www.gmes-atmosphere.eu/services/aqac/global_verification/validation_reports/.

A list with changes concerning the assimilation system can be found at
http://atmosphere.copernicus.eu/user-support/operational-info/global-system-changes.
The CAMS o-suite system is upgraded regularly, following updates to the ECMWF meteorological model as well as CAMS-specific updates such as changes in chemical data assimilation. These changes are documented in e-suite validation reports, as can be found from the link above. Essential model upgrades are also documented in Table 2.4.

On 26 September 2017 the system has been upgraded to cy43r3. A validation report for this upgrade (Eskes et al., 2017) is available here:
https://atmosphere.copernicus.eu/sites/default/files/repository/CAMS84_2015SC2_D84.3.1.3_201706_esuite_v1_0.pdf

2.1.2 Control

The control run (relevant expver = **gsyg** since 26/11/2017) applies the same settings as the respective o-suites, based on the coupled IFS-CB05 system with CAMS aerosol for cy41r1/cy40r2, except that data assimilation is not switched on. The only two exceptions with regard to this setup are:

- at the start of every forecast the ECMWF operational system is used to initialise *stratospheric* ozone, considering that stratospheric ozone, as well as other stratospheric species are not considered to be a useful product of this run. The reason for doing so is that this ensures reasonable stratospheric ozone as boundary conditions necessary for the tropospheric chemistry.
- The full meteorology in the control run is also initialized from the ECMWF operational NWP analyses. Note that this is different from the o-suite, which uses its own data assimilation setup for meteorology. This can cause slight differences in meteorological fields between o-suite and control, e.g. as seen in evaluations of upper stratospheric temperatures.

2.1.3 High-resolution CO_2 and CH_4 forecasts and delayed-mode analyses

The pre-operational forecasts of CO_2 and CH_4 use an independent setup of the IFS as the osuite, at a resolution of TL1279, i.e. ~16 km horizontal, and with 137 levels. This system runs in NRT, and does not apply data assimilation for the greenhouse gases.

The land vegetation fluxes for CO_2 are modelled on-line by the CTESSEL carbon module (Boussetta et al., 2013). A biogenic flux adjustment scheme is used in order to reduce large-scale biases in the net ecosystem fluxes (Agusti-Panareda, 2015). The anthropogenic fluxes are based on the annual mean EDGARv4.2 inventory using the most recent year available (i.e. 2008) with estimated and climatological trends to extrapolate to the current year. The fire fluxes are from GFAS (Kaiser et al., 2012). Methane fluxes are prescribed in the IFS using inventory and climatological data sets,

Table 2.4: Long-term o-suite system updates.

Date	o-suite update
2009.08.01	Start of first NRT experiment f7kn with coupled MOZART chemistry, without aerosol. Also without data assimilation.
2009.09.01	Start of first MACC NRT experiment f93i, based on meteo cy36r1, MOZART v3.0 chemistry, MACC aerosol model, RETRO/REAS and GFEDv2 climatological emissions, T159L60 (IFS) and 1.875°×1.875° (MOZART) resolution.
2012.07.05	Update to experiment fnyp: based on meteo cy37r3, MOZART v3.5 chemistry, where changes mostly affect the stratosphere, MACCity (gas-phase), GFASv1 emissions (gas phase and aerosol), T255L60 (IFS) and 1.125°×1.125° (MOZART) resolution. Rebalancing aerosol model, affecting dust.
2013.10.07	Update of experiment fnyp from e-suite experiment fwu0: based on meteo cy38r2, no changes to chemistry, but significant rebalancing aerosol model. Assimilation of 21 layer SBUV/2 ozone product
2014.02.24	Update of experiment fnyp from e-suite experiment fzpr: based on meteo cy40r1. No significant changes to chemistry and aerosol models.
2014.09.18	Update to experiment g4e2: based on meteo cy40r2. In this model version IFS-CB05 is introduced to model atmospheric chemistry.
2015.09.03	Update to experiment g9rr: based on meteo cy41r1.
2016.06.21	Update to experiment 0067: based on meteo cy41r1, but a resolution increase from T255 to T511, and two production runs per day
2017.01.24	Update to cycle 43R1_CAMS, T511L60
2017.09.26	Update to cycle 43R3_CAMS, T511L60
2018.06.26	Update to cycle 45R1_CAMS, T511L60

consistent with those used as prior information in the CH_4 flux inversions from Bergamaschi et al. (2009). The anthropogenic fluxes are from the EDGAR 4.2 database (Janssens-Maenhout et al, 2012) valid for the year 2008. The biomass burning emissions are from GFAS v1.2 (Kaiser et al., 2012). The high resolution forecast experiments also included a linear CO scheme (Massart et al., 2015).

The experiments analyzed in this report are:

- "**ghqy**" from March 2016. The initial conditions used in ghqy on 1st of March 2016 are from the GHG analysis (experiment gg5m). Furthermore, the meteorological analysis used to initialize the ghqy forecast changed resolution and model grid in March 2016. Note that the CO_2, CH_4 and linear CO tracers are free-running.
- "**gqpe**" from January 2017 to present. It runs with a TCO1279 Gaussian cubic octahedral grid (equivalent to approximately 9km horizontal resolution). Note that the CO_2, CH_4 and linear

CO tracers are initialized with the GHG analysis (gqiq) for CO_2 and CH_4 and the CAMS operational analysis for CO.

- The greenhouse gas analysis experiment "**gqiq**" runs on a TCO399 grid (equivalent to around 25km) and 137 vertical levels, and is available from January 2017. This experiment runs in delayed mode (4 days behind real time) and makes use of observations from TANSO-GOSAT (methane and CO_2) and MetOp-IASI (methane).

2.2 Other systems

2.2.1 BASCOE

The NRT analyses and forecasts of ozone and related species for the stratosphere, as delivered by the Belgian Assimilation System for Chemical ObsErvations (BASCOE) of BIRA-IASB (Lefever et al., 2014; Errera et al., 2008), are used as an independent model evaluation of the CAMS products. The NRT BASCOE product is the ozone analysis of Aura/MLS-SCI level 2 standard products, run in the following configuration (version 05.07):

- The following species are assimilated: O_3, H_2O, HNO_3, HCl, HOCl, N_2O and ClO.
- It lags by typically 4 days, due to latency time of 4 days for arrival of non-ozone data from Aura/MLS-SCI (i.e. the scientific offline Aura/MLS dataset).
- Global horizontal grid with a 3.75° longitude by 2.5° latitude resolution.
- Vertical grid is hybrid-pressure and consists in 86 levels extending from 0.01 hPa to the surface.
- Winds, temperature and surface pressure are interpolated in the ECMWF operational 6-hourly analyses.
- Time steps of 20 minutes, output every 3 hours

See the stratospheric ozone service at http://www.copernicus-stratosphere.eu/. It delivers graphical products dedicated to stratospheric composition and allows easy comparison between the results of o-suite, BASCOE and TM3DAM. The BASCOE data products (HDF4 files) are also distributed from this webpage. Other details and bibliographic references on BASCOE can be found at http://bascoe.oma.be/. A detailed change log for BASCOE can be found at http://www.copernicus-stratosphere.eu/4_NRT_products/3_Models_changelogs/BASCOE.php.

2.2.2 TM3DAM and the multi-sensor reanalysis

One of the MACC products was a 30-year reanalysis, near-real time analysis and 10-day forecast of ozone column amounts performed with the KNMI TM3DAM data assimilation system, the Multi-Sensor Reanalysis (MSR) system (van der A et al., 2010, 2013),
http://www.temis.nl/macc/index.php?link=o3_msr_intro.html.
The corresponding validation report can be found at
http://www.copernicus-atmosphere.eu/services/gac/global_verification/validation_reports/.

The NRT TM3DAM product used for the validation of the CAMS NRT streams is the ozone analysis of Envisat/SCIAMACHY (until April 2012), AURA/OMI, and MetOp-A/GOME-2, run in the following configuration:

- total O_3 columns are assimilated
- Global horizontal grid with a 3° longitude by 2° latitude resolution.

- Vertical grid is hybrid-pressure and consists in 44 levels extending from 0.1 hPa to 100 hPa.
- Dynamical fields from ECMWF operational 6-hourly analysis.

An update of the MSR (MSR-2) was presented in van der A et al. (2015), which extended the record to 43 years based on ERA-interim reanalysis meteo and with an improved resolution of 1x1 degree.

2.2.3 SDS-WAS multimodel ensemble

The World Meteorological Organization's Sand and Dust Storm Warning Advisory and Assessment System (WMO SDS-WAS) for Northern Africa, Middle East and Europe (NAMEE) Regional Center (http://sds-was.aemet.es/) has established a protocol to routinely exchange products from dust forecast models as the basis for both near-real-time and delayed common model evaluation. Currently, twelve regional and global models (see the complete list in the following link https://sds-was.aemet.es/forecast-products/forecast-evaluation/model-inter-comparison-and-forecast-evaluation/at_download/file) provides daily operational dust forecasts (i.e. dust optical depth, DOD, and dust surface concentration).

Different multi-model products are generated from the different prediction models. Two products describing centrality (multi-model median and mean) and two products describing spread (standard deviation and range of variation) are daily computed. In order to generate them, the model outputs are bi-linearly interpolated to a common grid mesh of 0.5º x 0.5º. The multimodel DOD (at 550 nm) Median from nine dust prediction models participating in the SDS-WAS Regional Center is used for the validation of the CAMS NRT streams.

2.3 CAMS products

An extended list of output products from the NRT stream o-suite are available as 3-hourly instantaneous values up to five forecast days. These are available from ECMWF (through ftp in grib2 and netcdf format, http://atmosphere.copernicus.eu/global-near-real-time-data-access).

2.4 Availability and timing of CAMS products

The availability statistics provided in Table 2.6 are computed for the end of the 5-day forecast run. The CAMS production KPI is defined as the percentage of cycles in which all the general data dissemination tasks are completed before the deadlines: 10 UTC for the 00:00 and 22 UTC for the 12:00 UTC run. This was in part based on requirements from the regional models. We note that at present most regional models can still provide their forecasts even if the global forecast is available a bit later. Note that since 21 June 2016 two CAMS forecasts are produced each day.

For the period March - May 2018, 98.9% of the forecasts were delivered on time. two model cycles were late: 2018032812 - started late due to power failure; 2018041300 - finished late due to fire in Computer Hall

Table 2.6: Timeliness of the o-suite from Dec 2014 to the end of May 2018. From June 2016 onwards CAMS has produced two forecasts per day.

Months	**On time, 22 utc**	**80th perc**	**90th perc**	**95th perc**
Dec-Feb '14-'15	97%	D+0, 19:43	D+0, 20:28	D+0, 21:13
Mar-May 2015	96%	D+0, 19:38	D+0, 21:03	D+0, 21:40
Jun-Aug 2015	95%	D+0, 20:24	D+0, 20:53	D+0, 21:54
Sept-Nov 2015	95%	D+0, 19:44	D+0, 20:55	D+0, 21:51
Dec-Feb '15-'16	100%	D+0, 18:39	D+0, 18:57	D+0, 19:43
Mar-May 2016	98%	D+0, 19:32	D+0, 19:47	D+0, 20:00
Jun-Aug 2016 (00 and 12 cycle)	100%	D+0, 08:53 D+0, 20:55	D+0, 09:04 D+0, 21:01	D+0, 09:18 D+0, 21:18
Sep-Nov 2016	98.9%	D+0, 08:44 D+0, 20:44	D+0, 08:51 D+0, 20:48	D+0, 08:52 D+0, 20:51
Dec 2016 - Feb 2017	99.4%	D+0, 09:02 D+0, 21:01	D+0, 09:11 D+0, 21:02	D+0, 09:18 D+0, 21:04
Mar-May 2017	100%	D+0, 09:08 D+0, 21:07	D+0, 09:14 D+0, 21:09	D+0, 09:19 D+0, 21:11
Jun-Aug 2017	100%	D+0, 09:05 D+0, 21:05	D+0, 09:07 D+0, 21:08	D+0, 9:09 D+0, 21:10
Sep-Nov 2017	100%	D+0, 09:02 D+0, 21:00	D+0, 09:05 D+0, 21:04	D+0, 9:09 D+0, 21:07
Dec 2017 - Feb 2018	98.33%	D+0, 08:55 D+0, 20:54	D+0, 08:59 D+0, 20:59	D+0, 09:01 D+0, 21:02
Mar-May 2018	98.9%	D+0, 09:00 D+0, 21:00	D+0, 09:06 D+0, 21:03	D+0, 09:08 D+0, 21:06
Jun-Aug 2018	100%	D+0, 09:11 D+0, 21:07	D+0, 09:14 D+0, 21:09	D+0, 09:20 D+0, 21:11

3. Tropospheric Ozone

3.1 Validation with sonde data in the free troposphere

Model profiles of the CAMS runs were compared to free tropospheric balloon sonde measurement data of 38 stations taken from the NDACC, WOUDC, NILU and SHADOZ databases for August 2017 to August 2018 (see Fig. 3.1.1 - 3.1.2). Towards the end of the period, the number of available soundings decreases, which implies that the evaluation results may become less representative. The figures contain the number of profiles in each month that are available for the evaluation. The methodology for model comparison against the observations is described in Douros et al., 2017. The free troposphere is defined as the altitude range between 750 and 200hPa in the tropics and between 750 and 300hPa elsewhere.

MNMBs for the o-suite are mostly within the range ±20%, for all months, in all zonal bands, except for the Tropics, where larger positive MNMBs up to 34% appear, see Fig. 3.1.1.-3.1.2. The control run generally shows larger negative MNMBs, (up to -40%).

Over the Arctic, the o-suite mostly shows slightly positive MNMBs during summer and spring (MNMBs up to 10%), while during the winter season the MNMBs get negative (within -10%) see, Fig. 3.1.1.

Over the NH mid-latitudes MNMBs for the o-suite are on average close to zero all year round (maxima are -8% to +6%), which is generally a clear improvement compared to the control run, which shows larger negative MNMBs during the respective period.

Over the Tropics and over Antarctica, ozone mixing ratios are mostly overestimated by the o-suite (up to 34%) by the o-suite, see Fig. 3.1.2. The control run sows large negative MNMBs for Antarctica.

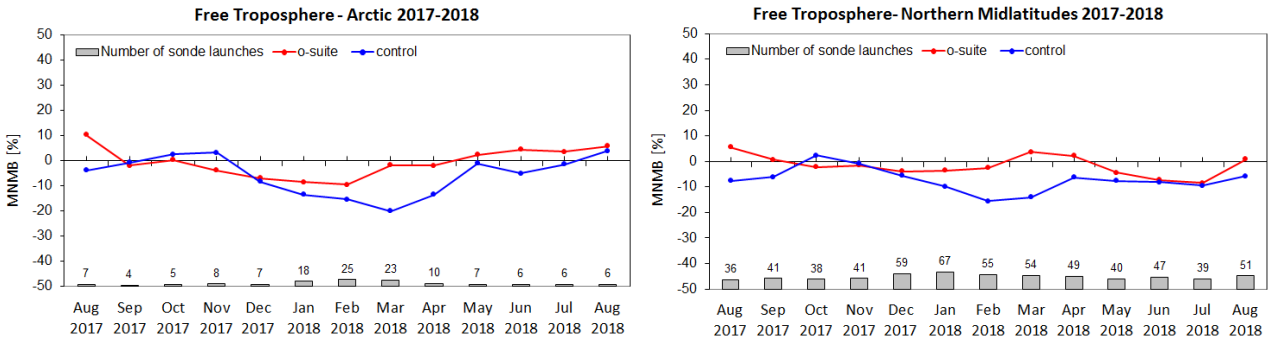

Figure 3.1.1: MNMBs (%) of ozone in the free troposphere (between 750 and 300 hPa) from the IFS model runs against aggregated sonde data over the Arctic (left) and the Northern mid latitudes (right). The numbers indicate the amount of individual number of sondes.

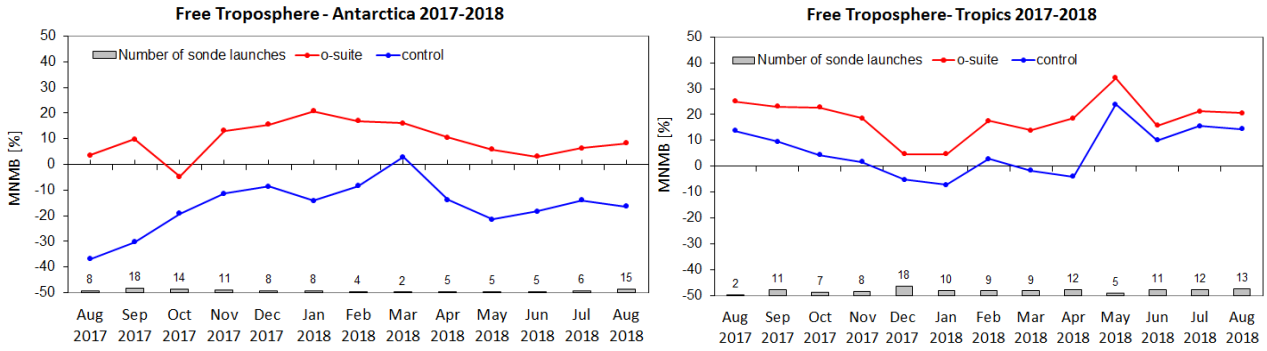

Figure 3.1.2: MNMBs (%) of ozone in the free troposphere (between 750 and 200hPa (Tropics) / 300hPa) from the IFS model runs against aggregated sonde data over the Tropics (left) and Antarctica (right). The numbers indicate the amount of individual number of sondes.

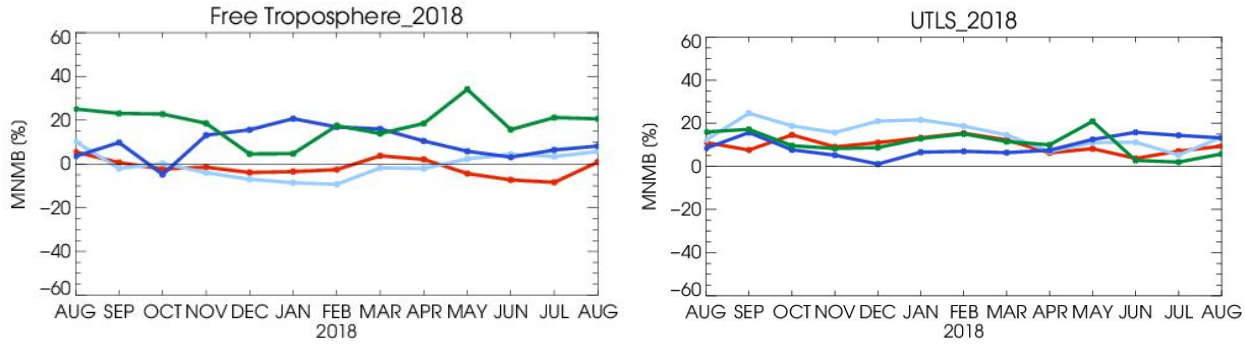

Figure 3.1.3: MNMBs (%) of ozone in the free troposphere (left, between 750 and 200hPa (Tropics) / 300hPa) and UTLS (right, between 300 and 100hPa (Tropics) / 60hPa) from the IFS model runs against aggregated sonde data over the Tropics (green) and Antarctica (blue), Arctic (light blue) and Northern Midlatitudes (red).

3.2 Ozone validation with IAGOS data

The daily profiles of ozone measured at airports around the world, are shown on the website at http://www.iagos.fr/macc/nrt_day_profiles.php. For the period from June - July 2018, the data displayed on the web pages and in this report include only the data as validated by the instrument PI. The available flights and available airports are shown in Fig. 3.2.1 top and bottom respectively. Performance indicators have been calculated for different parts of the IAGOS operations.

Six aircrafts were operating during this period. With these aircrafts, operating fully over the three month period, we can expect a total of about 1260 flights. The actual number of flights within the period was 757 (1514 profiles) giving a performance of 60 %. These flights are shown in Fig. 3.2.1 (top). Fifty one percent (50%) of the operational flights had usable measurements of ozone and 76% of flights had usable CO. Delivering these O_3 and CO data were two aircraft from Lufthansa operating from Frankfurt, two aircraft operated by Air France based in Paris, one from China Airlines based in Taipei and one from Hawaiian Airlines since fall 2017, with flight operations from Honolulu. Fig. 3.2.1 (bottom) shows the available airports, with a plotting circle scaled to the highest number of flights at an airport.

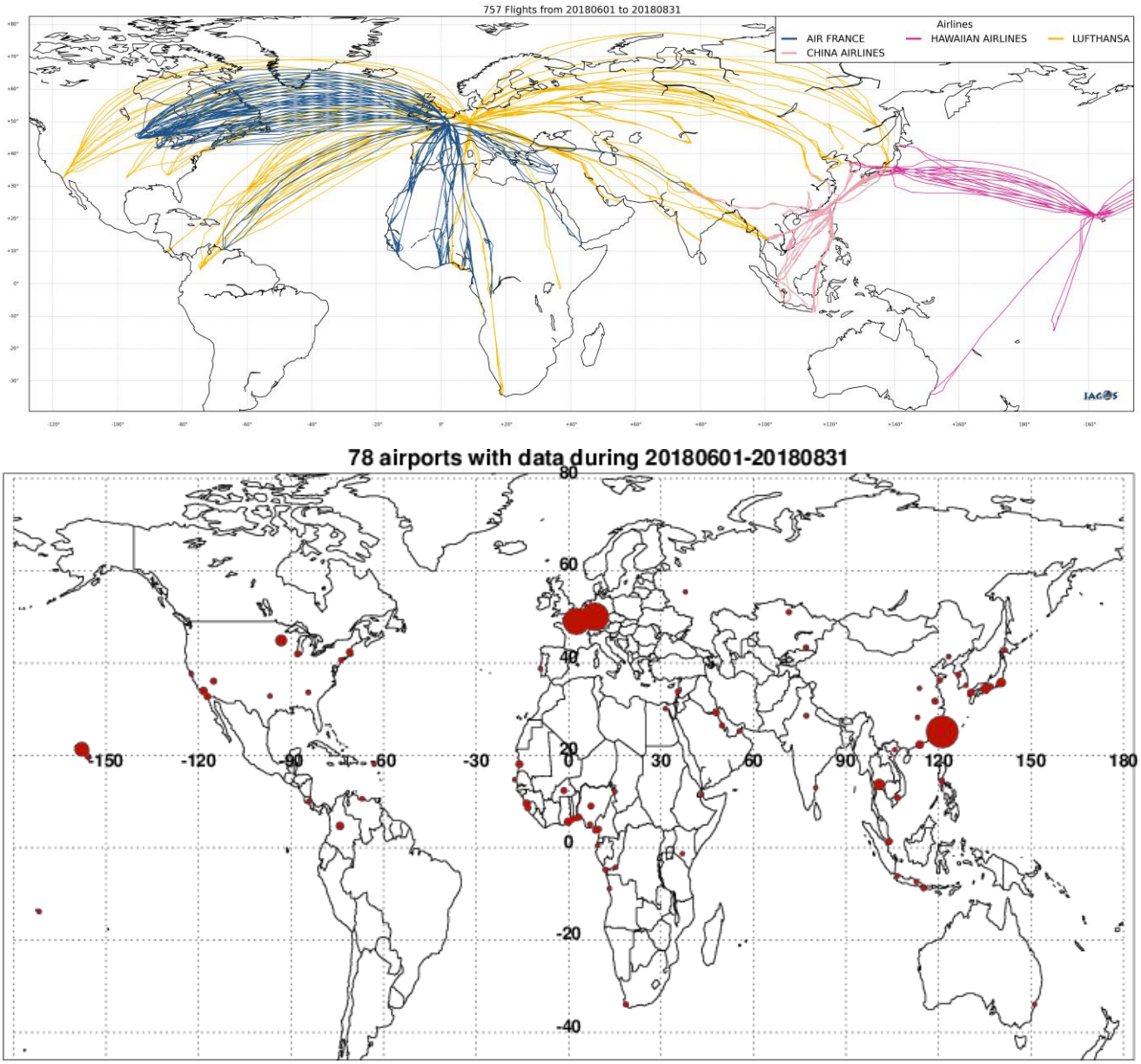

Figure 3.2.1. Map of the flights (top) and the visited airports (bottom) during the period June - July 2018, by the IAGOS-equipped aircraft. The size of the plotting circle represents the number of profiles available.

Europe

Figure 3.2.2 presents ozone time series at Frankfurt during June – July 2018. Ozone is well represented throughout the profiles until the UTLS region where ozone is generally overestimated by the o-suite and overestimated or underestimated by the control run as clearly seen in Fig. 3.2.3. Some examples of individual profiles are presented in Fig. 3.2.4.

In the time series at Frankfurt (Fig 5.2.2), the days around 9 June, an increase in ozone is observed in the boundary layer and free troposphere. In Fig. 5.2.3 profiles for 9 and 10 June are presented. On 9 and 10 June, the profiles are nearly constant from the surface to the UTLS (Fig. 5.2.4.a) with a value of in the range 60-70 ppbv. The profiles obtained with the models agree well with

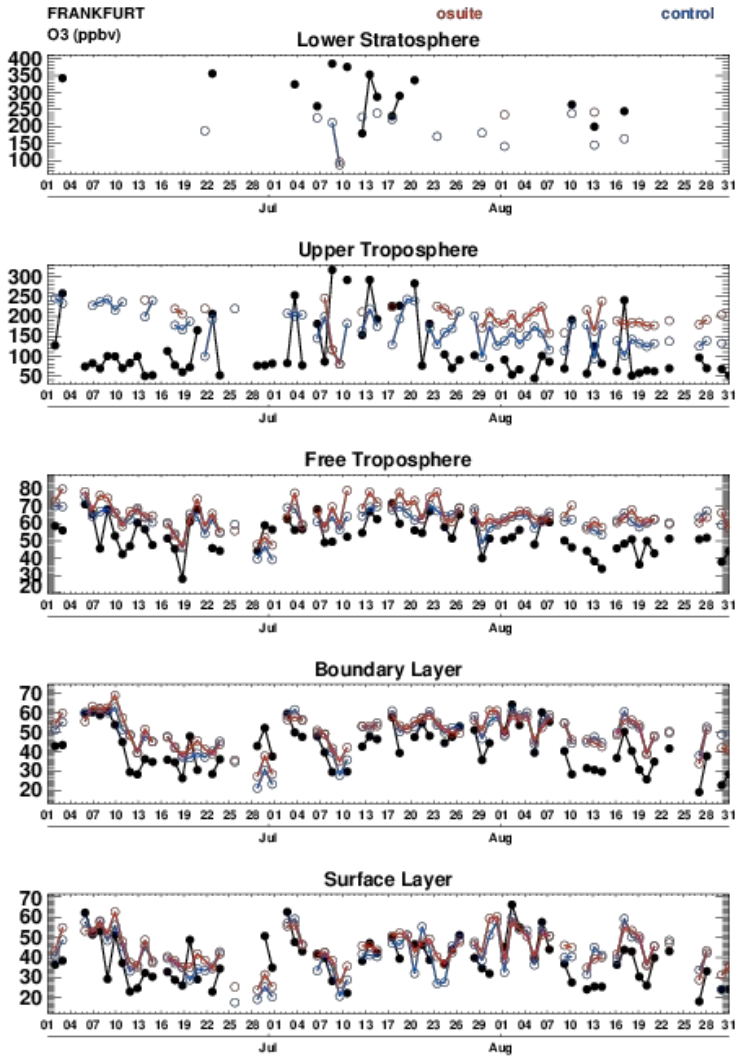

Figure 3.2.2. Time series of daily mean ozone over Frankfurt during JJA 2018 for 5 layers, Surface, Boundary layer, Free Troposphere, Upper Troposphere and Lower Stratosphere.

observations in the boundary layer with values slightly overestimated on day 10. In the free troposphere the magnitude is overestimated on day 9 with slightly better results from the control run, while the agreement is better on day 10 for both models.

Around 20th June the timeseries present an increase of ozone values in all layers (Fig. 5.2.3). As mentioned in the regional report for JJA 2018, at this period, the weather is characterized by anticyclonic conditions over North and Western Europe bringing mostly dry and warm weather. On 20th June a peak in the free troposphere of 80 ppbv appears near the altitudes of 3000 m (Fig. 5.2.4.a). Both models reproduce a maximum in the free troposphere at a slightly higher altitude (4000 m) but with a much smoother profile. On 21th June the ozone profile presents a complex shape with several peaks: a maximum of 50 ppbv and 90 ppbv is observed near 3500 m and 5000 m respectively, and a third peak is also observed in the UTLS at 9000 m with a mixing ratio of 200 ppbv (Fig. 5.2.4.a).

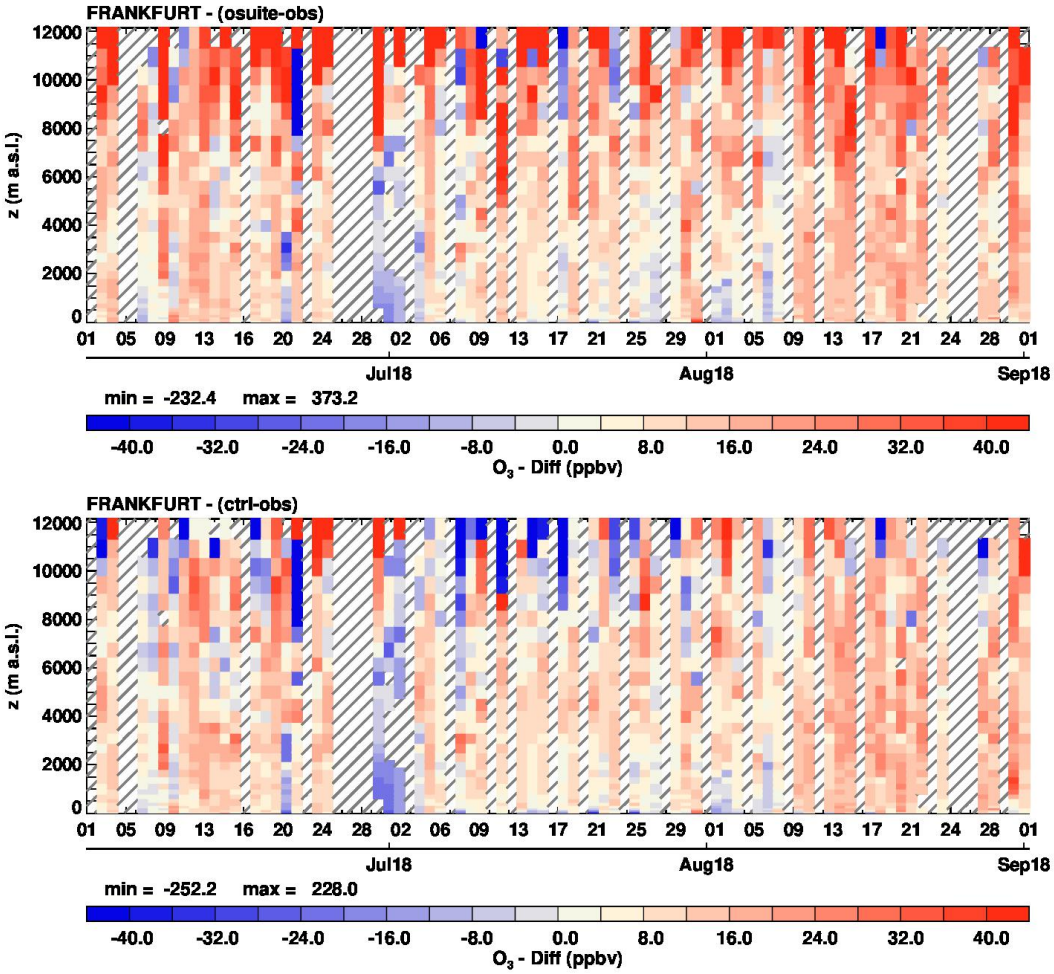

Figure 3.2.3 Time series of the absolute differences (model - observations) in daily profiles for ozone over Frankfurt during JJA 2018. Left panel correspond to o-suite and right panel to control run.

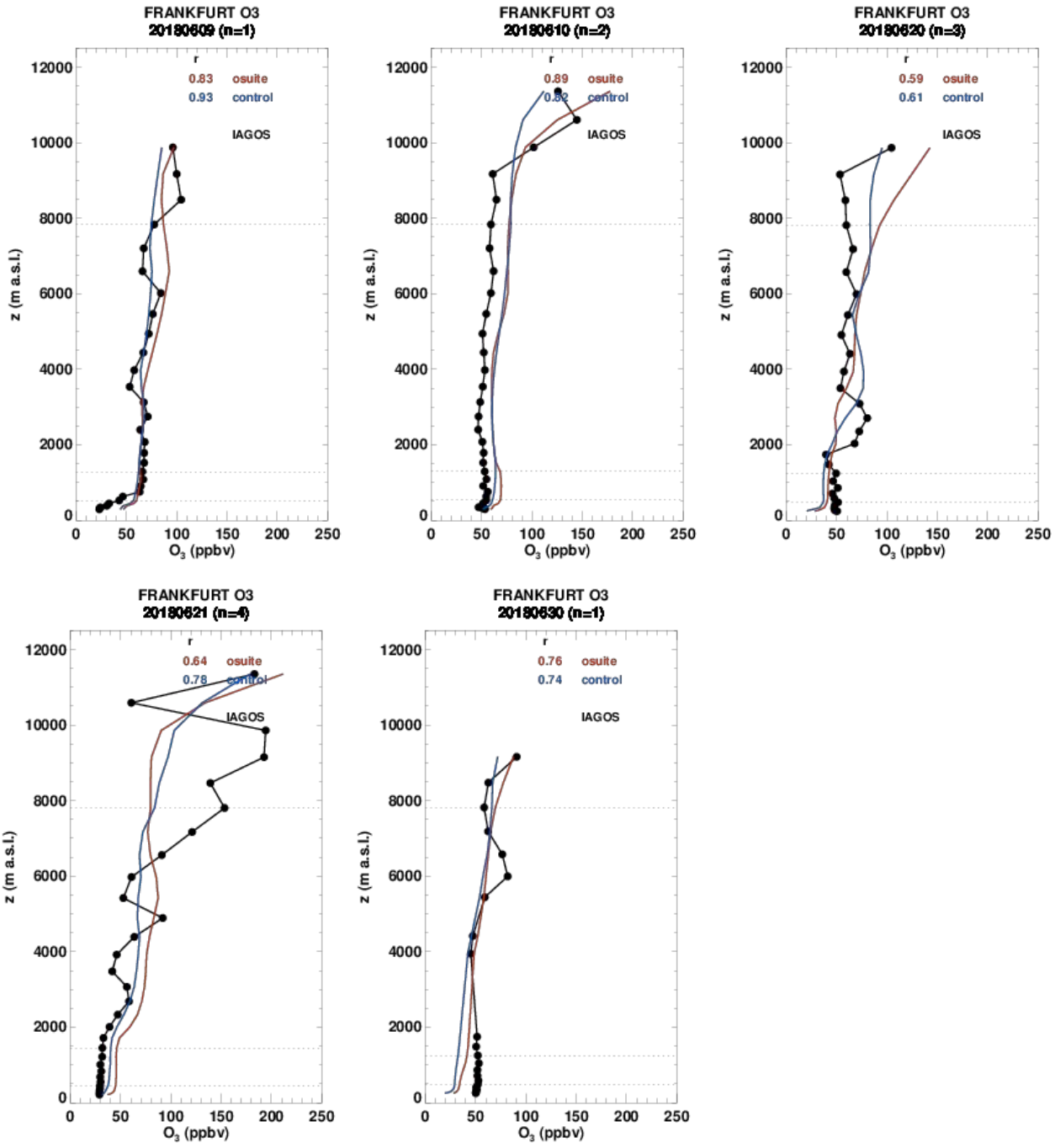

Figure 3.2.4.a Selection of daily profiles for ozone from IAGOS (black) and the two NRT runs (o-suite:red, control: blue) over Europe during JJA 2018.

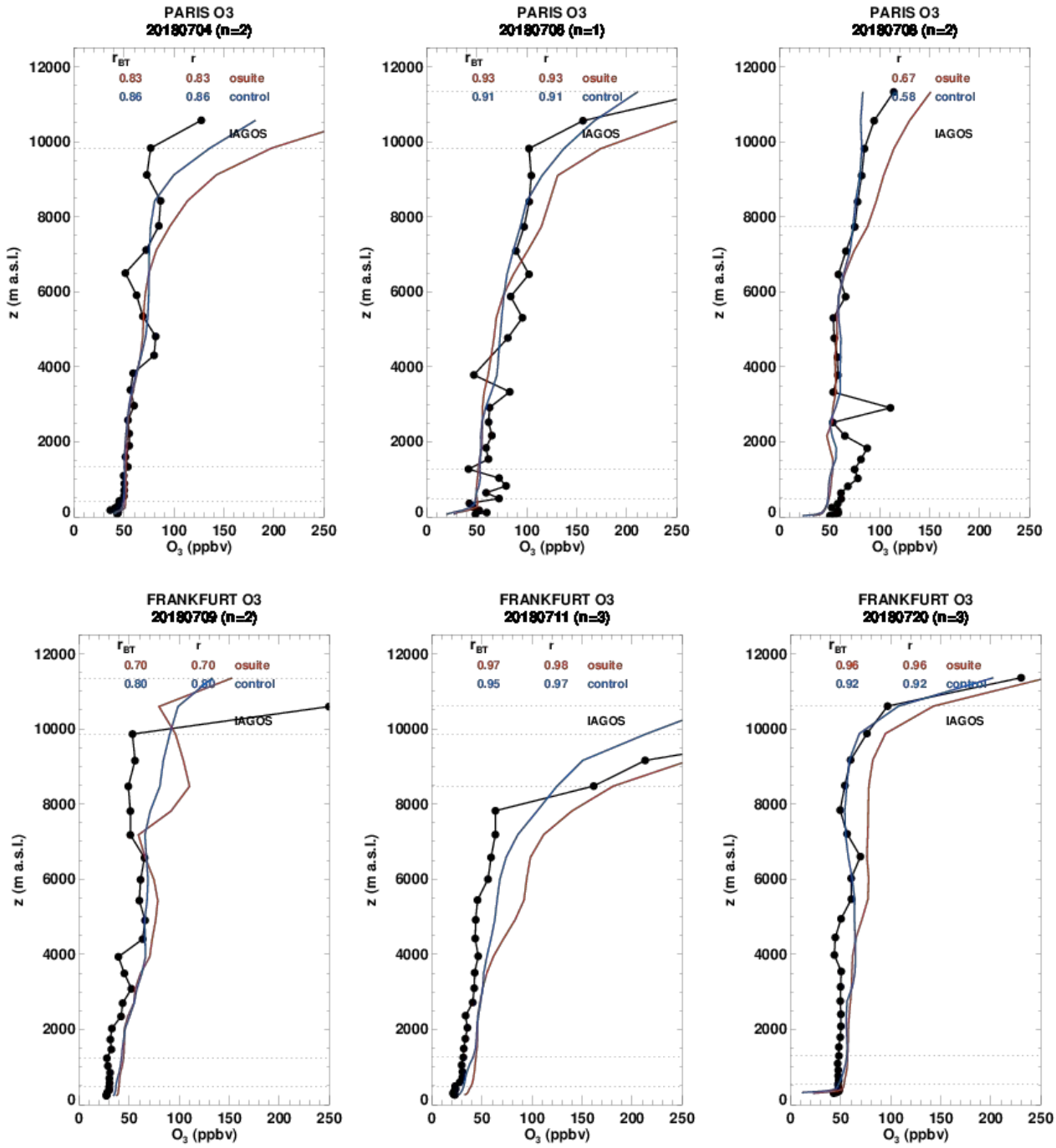

Figure 3.2.4.b Selection of daily profiles for ozone from IAGOS (black) and the two NRT runs (o-suite:red, control: blue) over Europe during JJA 2018.

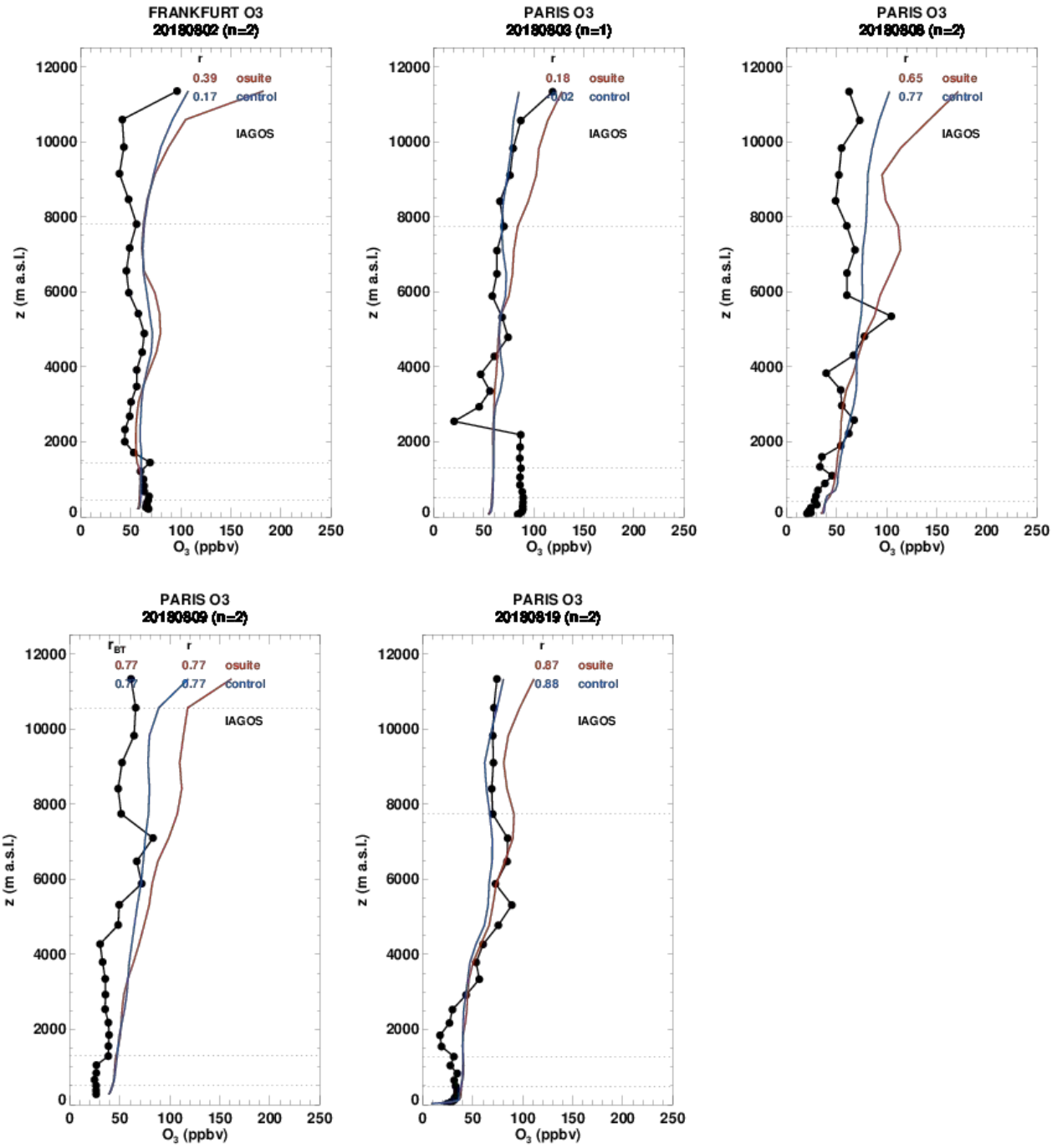

Figure 3.2.4.c Selection of daily profiles for ozone from IAGOS (black) and the two NRT runs (o-suite:red, control: blue) over Europe during JJA 2018.

The increase in ozone in the free troposphere is detected by both models but the profile is almost constant in this layer with a magnitude of about 80 ppbv. The peak in the UTLS is not reproduced by the models. The magnitude of all these maxima is always underestimated by the models as shown by the blue color on Fig. 3.2.3.

As already mentioned in the regional report, July was the third hottest in France since 1900 according to Météo France (http://www.meteofrance.fr/actualites/64662417-juillet-2018-3e-mois-de-juillet-le-plus-chaud-depuis-1900). Paris met the strongest episodes of ozone pollution since summer 2003. Fig. 3.2.4.b shows profiles at Paris on 6th and 8th July with ozone. These profiles present complex shapes with peaks in the boundary layer and also in the lower part of the free troposphere. On 6th July, the profile present two peaks with mixing ration of about 80 ppbv in the boundary layer and in the free troposphere at 3000 m. On 8th July, the profile presents a peak near 2000 m and another near 3000 m of about 90 ppbv and 110 ppbv. The complex shape of these profiles is not reproduced by the models and ozone mixing ratios are underestimated with nearly constant profiles from the surface to about 6000 m. In the UTLS, for these days the agreement is better for the control run. An increase in the boundary layer and free troposphere is also observed at Frankfurt at the end of June and beginning of July (Fig. 3.2.2). As it can be seen on the time series and time series of the differences (3.2.3), for these days ozone is often underestimated by both models (blue color). This can also been seen on the profile for 30th June shown on Fig. 3.2.4.a.

During the month of July, several anomalies of high ozone are also observed in the UTLS (Fig. 3.2.2). Profiles at Frankfurt on 9th, 11th and 20th July and Paris on 4th July are presented in Fig. 3.2.4.b, showing a descent of the tropopause. These stratospheric intrusions are in general detected by the models but the different results often diverge in the UTLS and it is not systematically the same model that provides the best agreement.

As also mentioned in the regional report, in the beginning of August, southwestern Europe especially undergoes a severe heat wave and temperatures are also high across other parts of Europe. For France, it is the second record-breaking heat wave after 2003 according to Météo France. High ozone increases in the surface and boundary layers can be noted on the time series of Frankfurt at this period (Fig. 3.2.2). Two profiles observed at the beginning of August in Paris and Frankfurt are also presented in Fig. 3.2.4.c. At Frankfurt on 2nd August, ozone mixing ratio is constant from the surface to the boundary layer with 70 ppbv. This increase is detected by the models as shown on the time series (Fig. 3.2.2) at Frankfurt, and the profile obtained with the models agrees reasonably with observations and ozone values are slightly underestimated by both models (Fig. 3.2.4.c). At Paris ozone mixing ratio reaches 90 ppbv between the surface and 2000 m (Fig. 3.2.4.c). For this extreme episode, the models behave similarly and underestimate largely the magnitude of ozone mixing ratio by almost 50%.

On 19th August at Paris, high ozone is observed in the free troposphere between 6000 and 8000 m with about 80 ppbv. This feature might be related to the long range transport of pollution from forest fires in North America (California and British Columbia). CO values are also high in the same range of altitudes (see section 4.2). This increase is detected by the models and control run show a better performance as the maximum is found slightly higher for CAMS global. The models provide values close to observations in that region of the atmosphere but the profile is almost constant from the boundary layer to mid-troposphere which leads to overestimations by both models in the boundary layer.

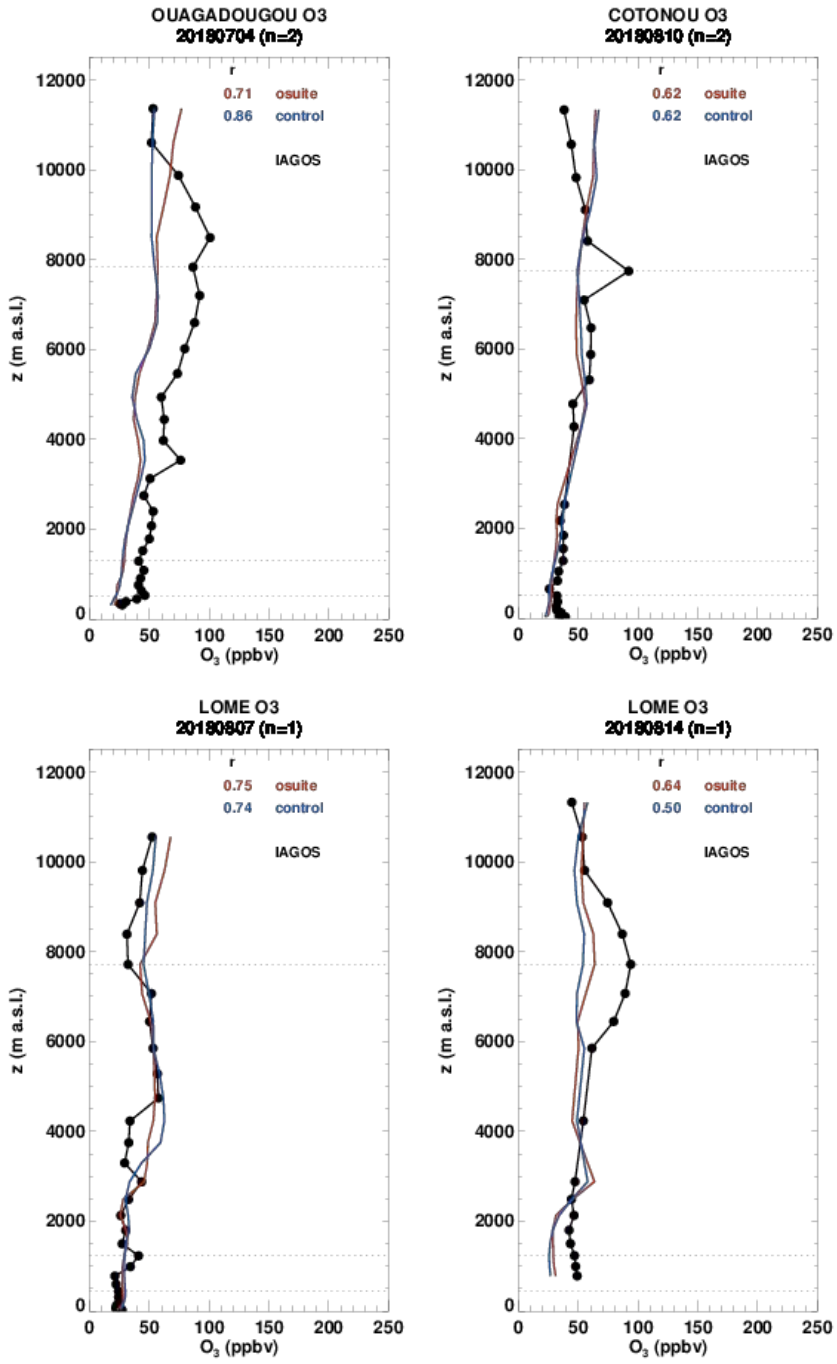

Figure 3.2.5 Selection of daily profiles for ozone from IAGOS (black) and the two NRT runs (o-suite: red, control: blue) over West Africa during JJA 2018.

West Africa

Several destinations across West Africa have been visited during the period June - July 2018. These include some situated on the Gulf of Guinea (Cotonou, Conakry, Lome) where pollution from oil industries effects the profiles all year round, some situated inland (Ouagadougou). All these cities are subject to anthropogenic emissions from vehicles and to biomass burning during the dry season, from December to March and from June to October in the northern and southern hemisphere

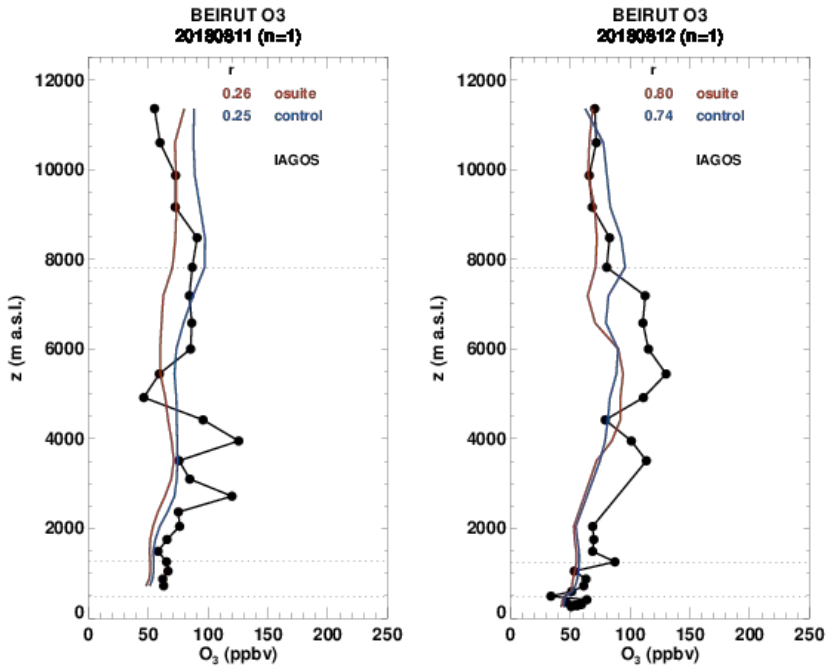

Figure 3.2.6 Selection of daily profiles for ozone from IAGOS (black) and the two NRT runs (o-suite: red, control: blue) over the Middle East during JJA 2018.

respectively. We do not therefore expect to see a big influence of biomass burning on the profiles shown here for JJA. In Fig. 3.2.5 examples of ozone profiles sampled in this region are shown. The ozone profiles selected hereafter present anomalies in the free troposphere and UTLS likely related to the transport of pollution from forest fires (in the southern hemisphere) as they are often correlated with peaks in CO (see section 4.2). In the examples presented here, the results from the o-suite and control run are almost identical at all locations. The overall shape of the profiles is well reproduced with the exception of the sharp peaks which are much smoother in the results from the models, and the magnitudes are often underestimated throughout the free troposphere and in the boundary layer.

Middle-East

Some profiles are available in the Middle East with ozone mixing ratios in the mid and upper troposphere: on 11th and 12th August at Beirut (Fig. 3.2.6). These summertime ozone maximum over the Middle East are due to a complex contribution of dynamical and chemical factors, and of anthropogenic and natural influence (Li. et al, 2001). The profiles at Beirut present complex shapes with maxima in the lower part of the free troposphere and high ozone values in the upper troposphere (Fig. 3.2.6). On 11th August, the peaks are found near 3000 m and 4000 m with the same magnitude of about 130 ppbv. Ozone values reach 80 ppbv between 6000 and 9000 m. The shape of the profile obtained with the model is much smoother than that of observations. The profile obtained with the models presents two maxima, one likely reflecting the observed increase of ozone values in the lower part of the troposphere and the other the observed increase in the upper troposphere. The altitude of these maxima is closer to that of the observations, but the magnitudes are underestimated in the lower part of the free troposphere. In the upper troposphere the agreement is better especially for control run. On 12th August, two maxima are also observed in the free troposphere near 3500 m and in between 6000-7000 m with values of about 120 ppbv and 130 ppbv respectively. Both models produce a single maximum in the free troposphere with a

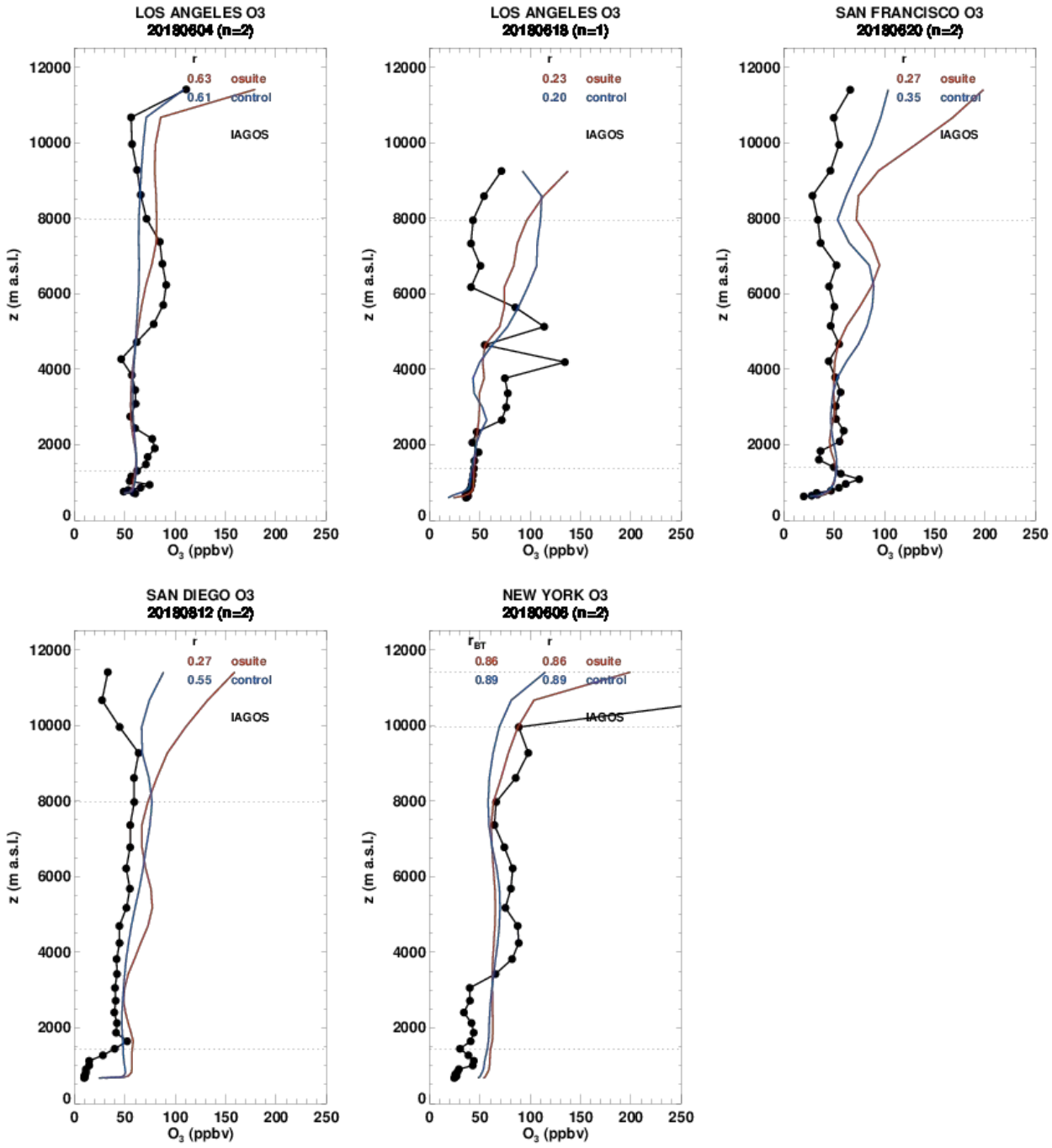

Figure 3.2.7.a Selection of daily profiles for ozone from IAGOS (black) and the two NRT runs (o-suite: red, control: blue) over North America during JJA 2018.

magnitude much smaller than observations of about 80 ppbv. In the upper troposphere the performance is better for CAMS global than control run in this case.

North America

During the period June-August 2018, most available ozone profiles in North America are at Californian airports: Los Angeles, San Francisco and San Diego (Fig. 3.2.6.a). At these airports ozone

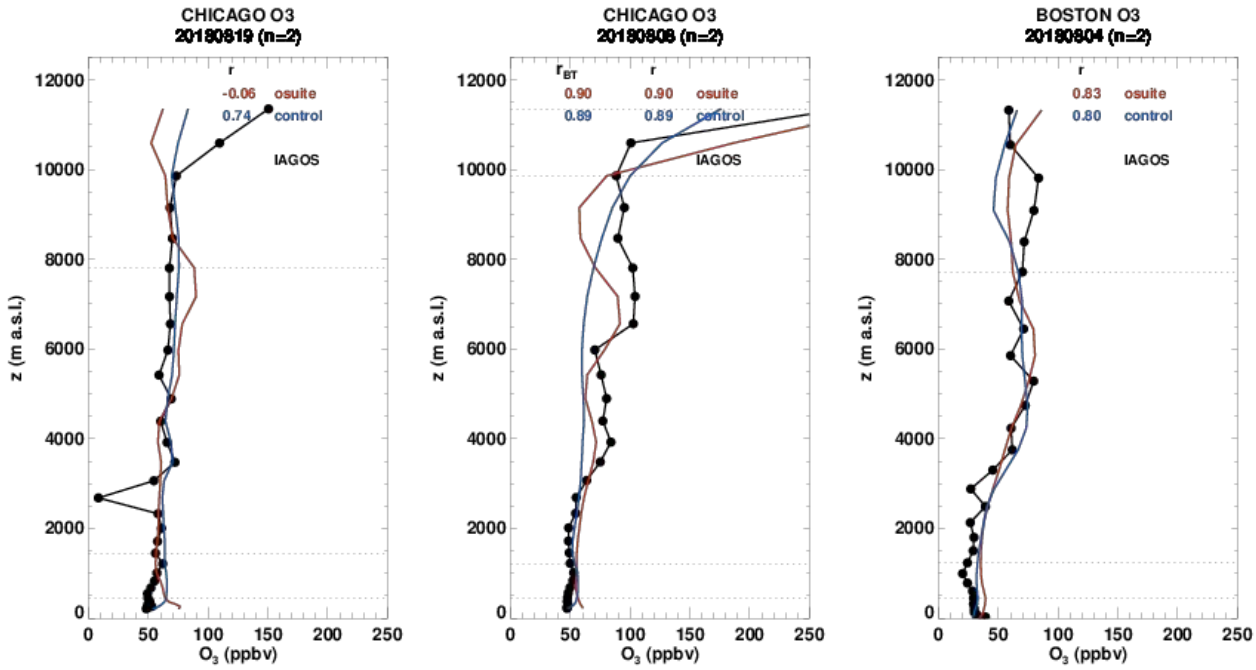

Figure 3.2.7.b Selection of daily profiles for ozone from IAGOS (black) and the two NRT runs (o-suite: red, control: blue) over North America during JJA 2018.

is in general well reproduced in the lower part of the troposphere. In the profiles at Los Angeles on 4th and 18th June, high ozone values are observed in the free troposphere. On 4th June, ozone values are high between 4000 m and 8000 m with about 80 ppbv. On 18th June two peaks are observed at 5500 m and 4000 m, with 110 ppbv and 130 ppbv respectively. These two peaks are not reproduced by the models which present high values of ozone higher in the free troposphere. On 20th June at San Francisco, the models present a maximum in the upper part of the free troposphere which is not present in observations. Meanwhile, the sharp peak observed in the boundary layer is well reproduced by both models with a smoother shape and hence with an underestimated maximum value. In San Diego on 12th August, a small peak is observed in the lower part of the free troposphere. This feature is not reproduced by the models but the values are closed to observations at the altitude of the peak, however the profile is constant profile in the boundary layer leading to overestimations in this layer.

Some profiles are also available at the airports of New York, Chicago and Boston (Fig. 3.2.6a-b). In New York on 6th June, ozone values reach 90 ppbv between 4000 m and 8000 m. These values are slightly underestimated by both models, and the constant profile obtained lead to overestimations in the boundary layer like in the previously commented case of San Diego. For the profiles at San Diego and Boston in August, the overall agreement between models and observations is good, with the exception of the negative anomaly in ozone on 19th August (at 2500 m) which is not reproduced by the models, and 8th August for which control run provides a much worse performance than CAMS global as the maxima observed in the upper free troposphere are not detected at all by the latter.

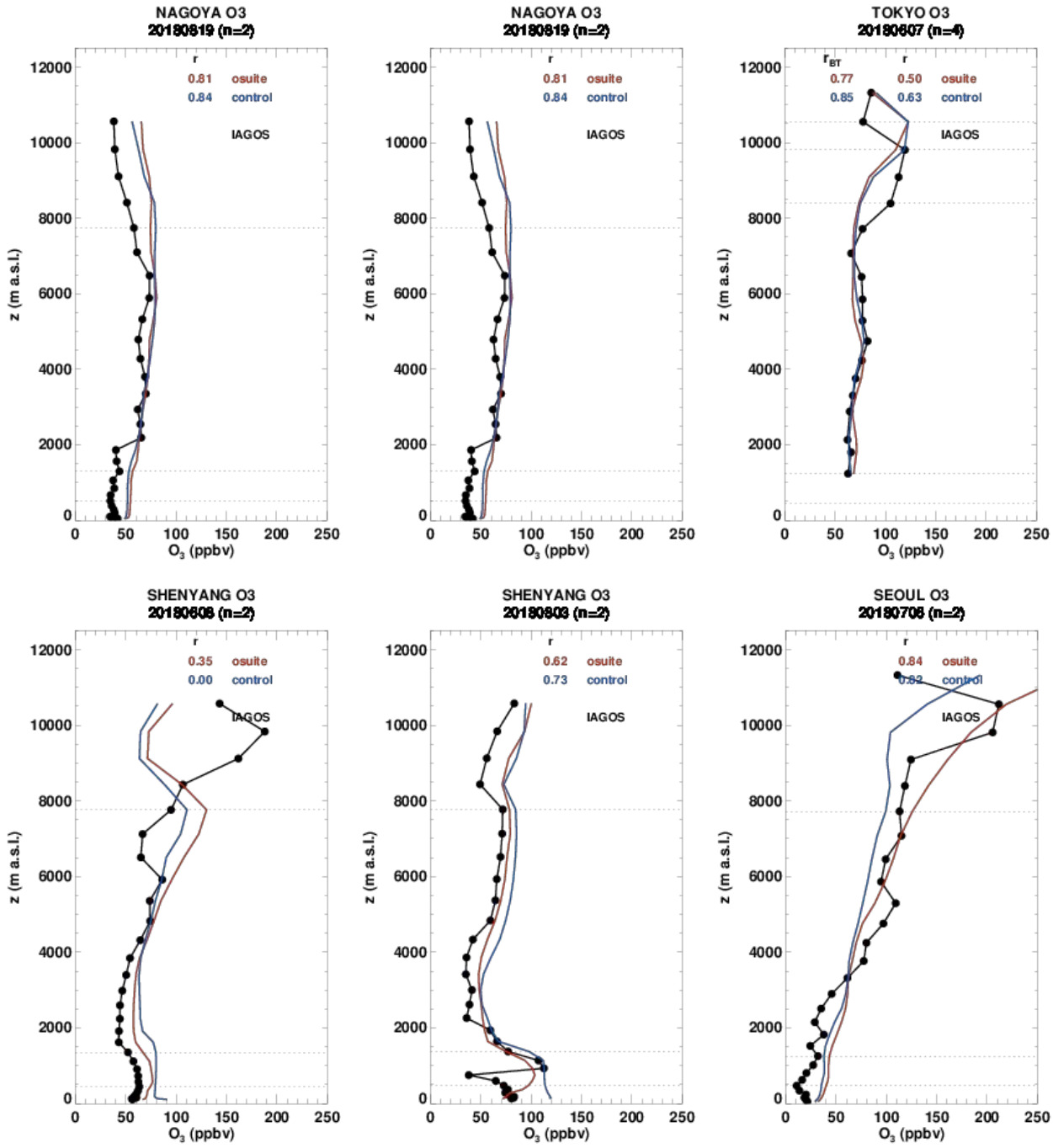

Figure 3.2.8.a Selection of daily profiles for ozone from IAGOS (black) and the two NRT runs (o-suite:red, control: blue) over Northeastern Asia during JJA 2018.

At most locations, the models behave similarly in the lowest part of the troposphere with a reasonable agreement with observations in most cases. The largest discrepancies between models and observations are found in the mid-troposphere and UTLS where the results of the two models can be different.

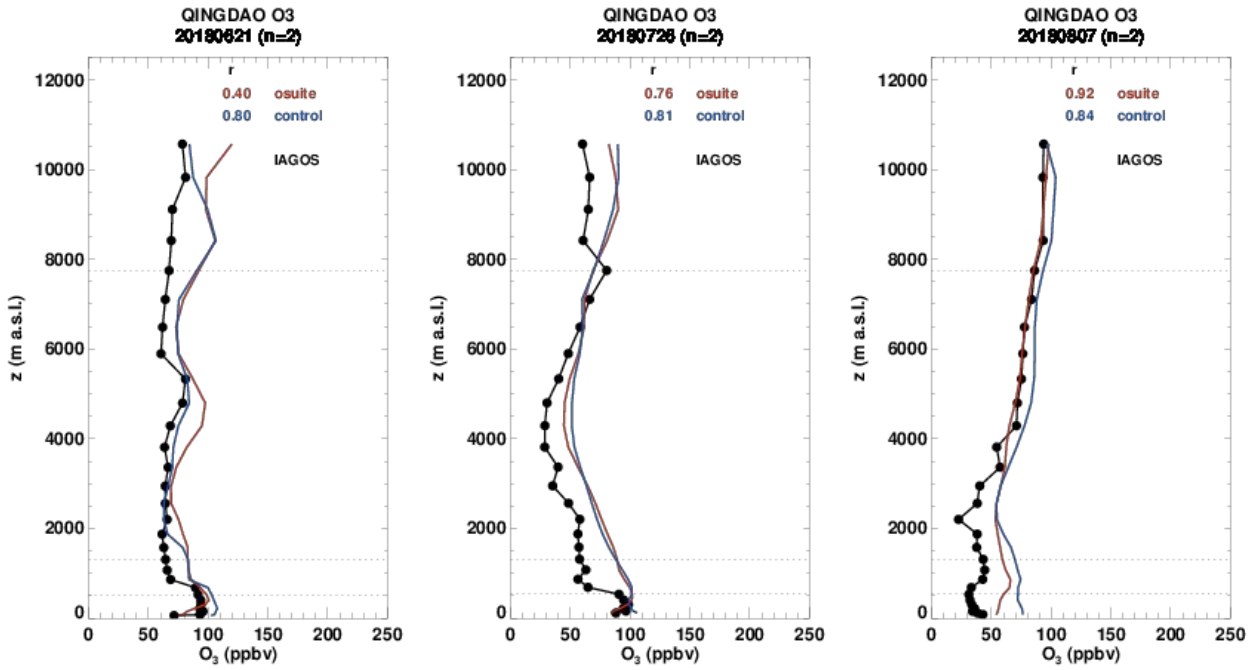

Figure 3.2.8.b Selection of daily profiles for ozone from IAGOS (black) and the two NRT runs (o-suite:red, control: blue) over Northeastern Asia during JJA 2018.

North-eastern Asia

In Fig. 3.2.8.a, several profiles are presented for the airports of: Nagoya (Japan), Tokyo (Japan), Shenyang (China), Qingdao (China), and Seoul (Korea). For these airports of North eastern Asia, the models mostly present very similar results. In the surface and boundary layer the models agree well with observations with some slight overestimations ozone and a slightly better performance from the CAMS global. In the free troposphere, the agreement is good for both models. In the UTLS, the presence of ozone peaks is not always detected. As an example at Tokyo on 7th June, a peak of ozone near 10000 m is detected by the models but a little higher in altitude and with a similar magnitude. On 6 July at Seoul, the peak in the UTLS is not represented by the models.

Pacific

As mentioned before, the Hawaiian aircraft started monitoring operations in October 2017. The pristine environment of the Island makes Hawaii a key location for addressing air quality and climate change issues, and for the validation of models. During the period June-July 2018, the airport of Honolulu has been sampled during the first half of the summer (Fig. 3.2.9). As it can be seen on the time series the models in general agree well with the observations in the surface and boundary layer. This is also shown on Fig. 3.2.10 with the time series of the absolute differences (model-observations). In the free troposphere the results from the models are also similar, and the values are underestimated or overestimated with no systematic behaviour. In the UTLS the results from the control run are better than those of CAMS-control which present large overestimations.

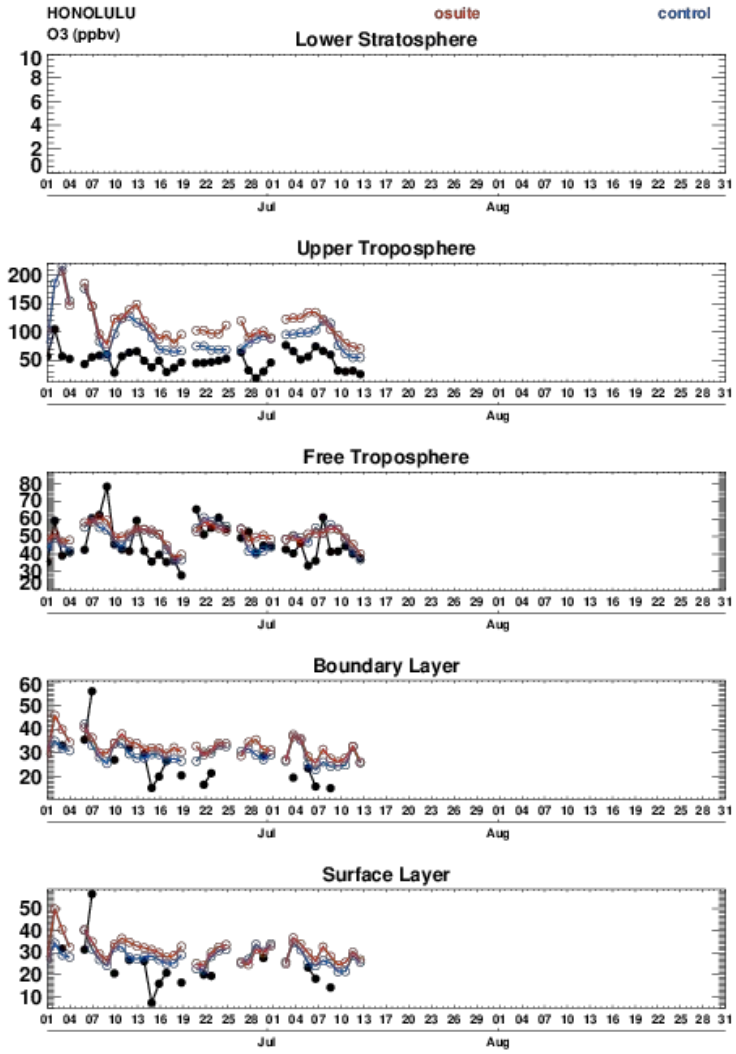

Figure 3.2.9. Time series of daily mean ozone over Honolulu during JJA 2018 for 5 layers, Surface, Boundary layer, Free Troposphere, Upper Troposphere and Lower Stratosphere.

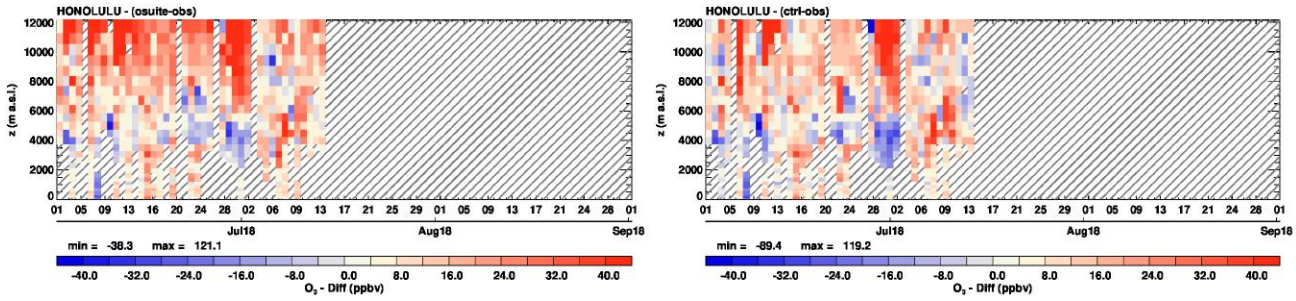

Figure 3.2.10. Time series of the absolute differences (model - observations) in daily profiles for ozone Honolulu during JJA 2018. Left panel corresponds to o-suite and right panel to control run.

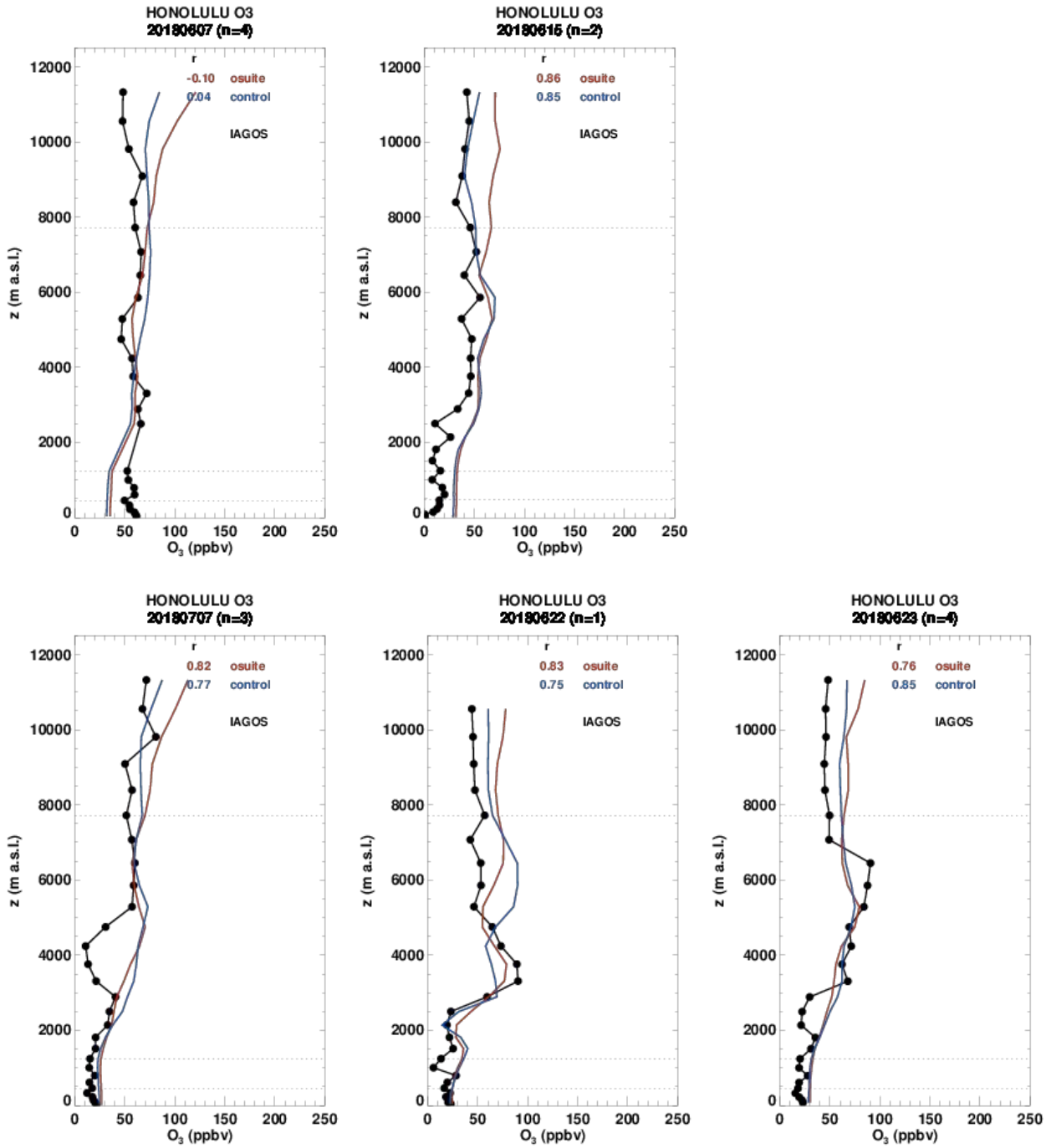

Figure 3.2.11 Selection of daily profiles for ozone from IAGOS (black) and the two NRT runs (o-suite: red, control: blue) over the Pacific during JJA 2018.

In Fig. 3.2.11 several profiles at Honolulu which present anomalies at different altitudes are shown. On 7th June a high peak is observed in the surface, boundary and free troposphere layers as shown on the time series (Fig. 3.2.9). The profile for that day shows that ozone values are nearly constant from the surface to the altitude of about 3500 m with 70 ppbv. The models have similar behaviour, both underestimate ozone p to 4000 meters, with the largest underestimations in the lowest layers (see also Fig.3.2.10).

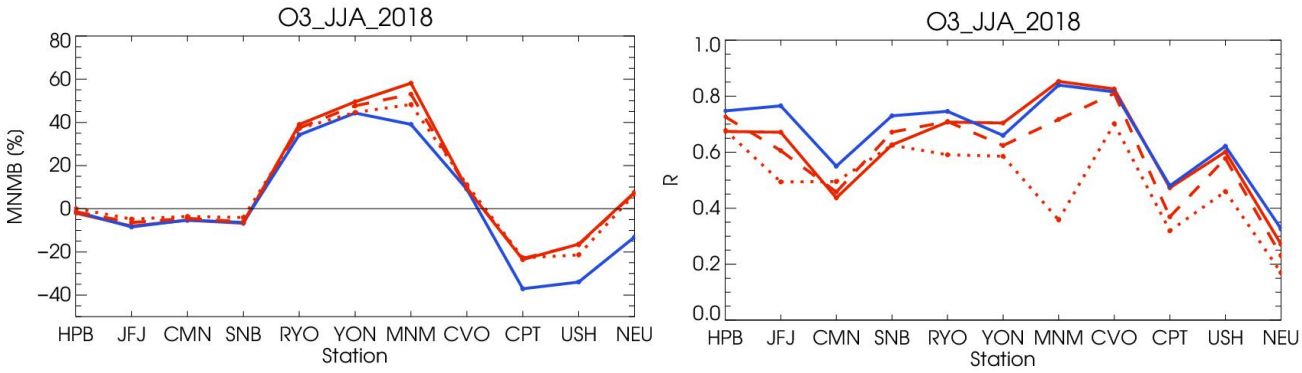

Figure 3.3.1: Modified normalized mean bias in % (left) and correlation coefficient (bottom right) of the NRT model runs compared to observational GAW data in the period June 2018 to August 2018 (o-suite: solid red, D+2: red-dashed, D+4: red-points, and control: blue).

On 15th June, a negative anomaly is observed in the lowest layers as shown by the extremely low values of ozone in the surface and boundary layer (Fig. 3.2.9). The corresponding profile shows that mixing ratio ozone is lower than 20 ppbv in the surface and boundary layer, and both models overestimates by roughly 50%. On 7th July like on 15 June, ozone values are low in the surface and boundary layer. Moreover in this case there is also a marked minimum in ozone at the altitude of 4000 m. Although the agreement of the models with observations is good in the surface and boundary layer, the aforementioned minimum is not detected by the models which present large overestimations.

On the 22th and 23th June the profiles at Honolulu present a complex shape with high ozone values in the free troposphere between 3000 m and 7000 m (Fig. 3.2.11). This increase of ozone values in the free troposphere can also be seen in the time series (Fig. 3.2.9). For 22ndJune ozone values are nearly constant between these altitudes with a value of 80 ppbv on average. On 23rd a peak is observed at the altitude of about 3500 m reaching almost 100 ppbv. For this event, the models detect an increase in the free troposphere (Fig. 3.2.9), and the profile obtained on 10th June agrees well with observations: the shape of the profile is well reproduced and maximum ozone values are of the same magnitude. On 23rd June, the models reproduce correctly the peak aforementioned again with an altitude and magnitude close to observation, however the models produce a second peak near 6000 m which is not present in observations. In this case the result from CAMS global is better than that of control run, the second maximum being less pronounced for CAMS global.

3.3 Validation with GAW and ESRL-GMD surface observations

For the Near Real Time (NRT) validation, 11 GAW stations and 14 ESRL stations are currently delivering O_3 surface concentrations in NRT, and the data are compared to model results. In the following, a seasonal evaluation of model performance for the 2 NRT runs (o-suite and control) has been carried out for the period from June to August 2018. The latest validation results based on GAW stations can be found on the CAMS website,
http://www.copernicus-atmosphere.eu/d/services/gac/verif/grg/gaw/, and based on ESRL on
http://www.academyofathens.gr/kefak/cams/index.html.

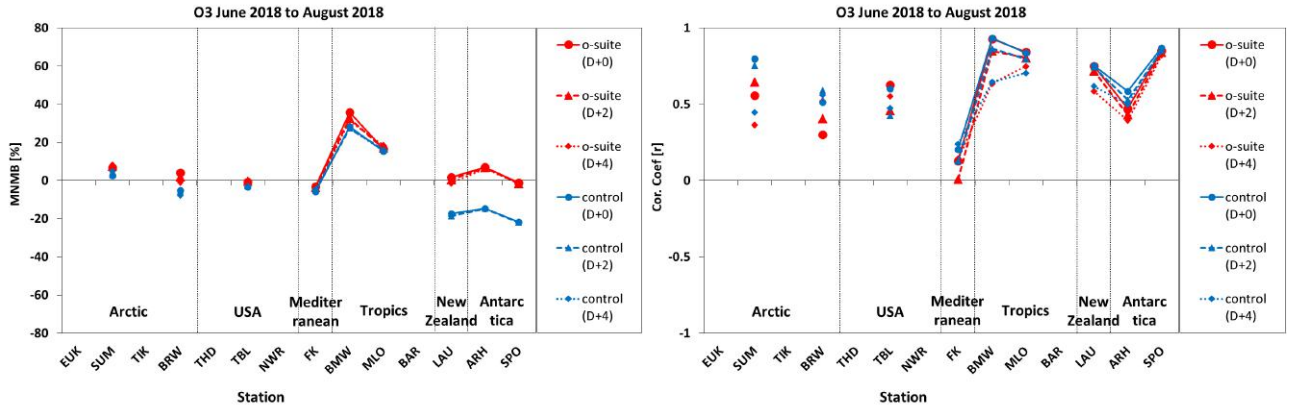

Figure 3.3.2: Modified normalized mean bias in % (left) and correlation coefficient (right) of the NRT forecast runs compared to observational ESRL data in the period June 2018 to August 2018. Circles correspond to D+0, triangles to D+2 and rhombs to D+4 metrics respectively.

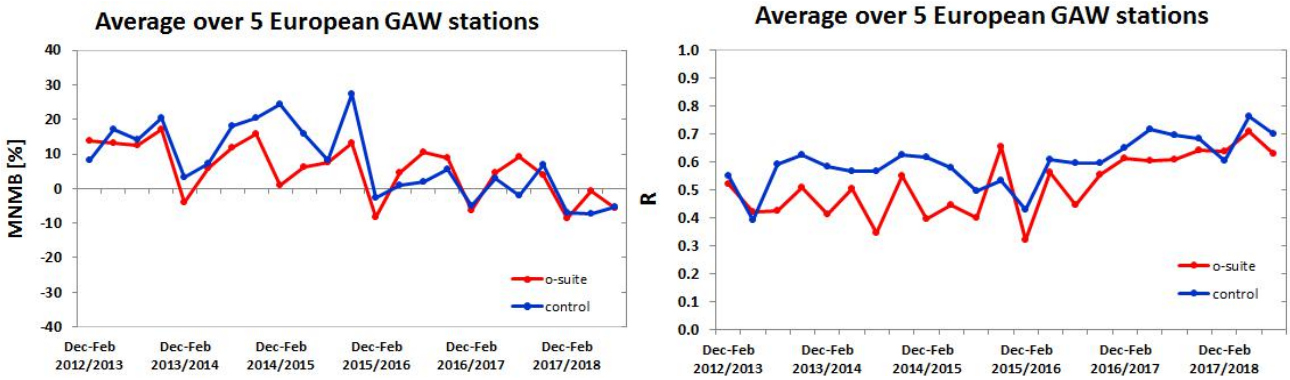

Figure 3.3.3: Long term (Dec. 2012 – August 2018) evolution of seasonal mean MNMB (left) and correlation (right), as averaged over 5 GAW stations in Europe, for o-suite (red) and control (blue).

Modified normalized mean biases in % (left, panel) and correlation coefficients (right, panel) for different forecasts days (D+2, red-dashed and D+4, red- pointed) with respect to GAW and ESRL observations are shown in Figs. 3.3.1 and 3.3.2. It indicates that MNMBs for both o-suite and control run mostly remain stable up to D+4 (forecast run from 96h to 120h). Correlations between simulated and observed surface ozone values remain almost stable up to D+2 (forecast run from 48h to 72h), but then drop (correlations for D+4 are lower than correlations for D+2 and D+0), see Fig. 3.3.1 and 3.3.2, right graph).

A comparison of the seasonal-mean MNMB over Europe (Fig. 3.3.3) from December 2012 to present shows that the MNMB over European GAW stations is minimal during the winter season, and tends to increase in other months. Also on average the MNMB for the o-suite shows a slight improvement over the years, while it remains higher, and more variable for the consecutive control runs. Temporal correlation is consistently better for control than for the o-suite. The GAW results are summarized in Figs 3.3.1 and 3.3.3.

Looking at different regions, for European stations (HPB, JFJ, ZUG, SNB, CMN, PRS), observed O_3 surface mixing ratios are very close to the observations. MNMBs are between -1 and -8% for booth runs, see Fig. 3.3.1. Correlations for the European stations are between 0.43 and 0.67 for the o-suite and between 0.54 and 0.76 for the control run, see Fig. 3.3.1.

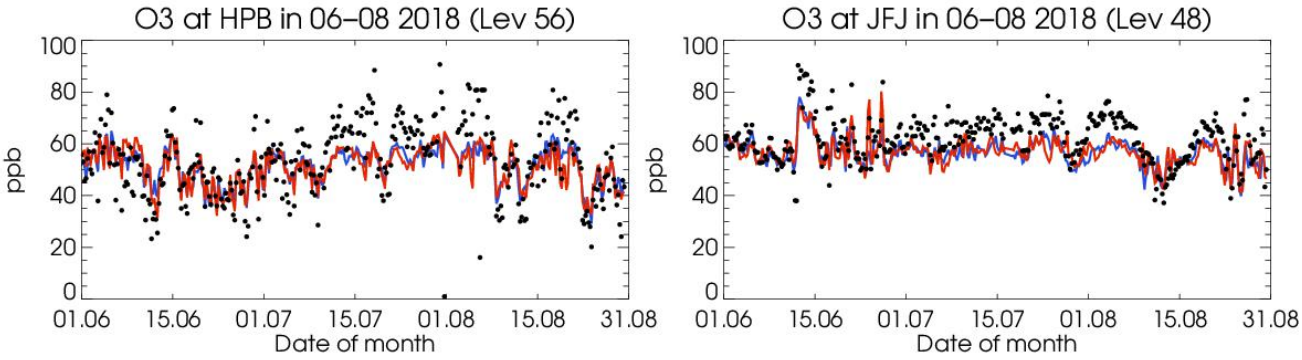

Figure 3.3.4: Time series for the o-suite (red) and control (blue) compared to GAW observations at Hohenpeissenberg (47.8°N, 11.02°E) and Jungfraujoch (39.03°N, 141.8°E)

Over Arctic stations (BRW and SUM), the o-suite overestimate surface ozone values by 4% at Point Barrow and 7% at Summit. On the other hand the control run overestimate surface ozone by 3% at Summit and underestimate it by 5% at Point Barrow. Notable is that the control runs reproduces better than the o-suite the day to day surface ozone variability over the Arctic stations ($r_{o\text{-}suite}$≈0.30 and $r_{control}$≈0.51 at BRW and $r_{o\text{-}suite}$≈0.56 and $r_{control}$≈0.80 at SUM).

For stations located in Asia (RYO, YON, MNM) both runs strongly overestimate O3 mixing ratios with MNMBs between 39% and 58% for the o-suite and between 34% and 44% for the control run, see Fig 3.3.6. Correlation coefficients range between 0.70 and 0.85.

For TBL USA station, the observed ozone mixing ratios are very well reproduced by the o-suite (MNMB≈0%) and slightly underestimated (MNMB≈-3%) by the control run. Correlations between o-suite and observations are 0.60 for both the o-suite and the control run.

The observed ozone mixing ratios are strongly overestimated by both runs over Bermuda (BER) station in the Tropics ($MNMB_{o\text{-}suite}$≈36% and $MNMB_{control}$≈28%). Both runs are also overestimate surface ozone values by 15% at Mauna Loa (MLO) station. However correlations between simulated and observed surface ozone are high for both the o-suite and the control run over both Bermuda (r>0.9) and Mauna Loa stations (r>0.8).

O_3 mixing ratios of the southern hemispheric stations (CPT, USH) are underestimated with MNMBs between -16 and -23% by the o-suite. The control run shows larger underestimations up to -37%, see Fig 3.3.8. Correlation coefficients range around 0.47 and 0.6. At Lauder (LDR) station in New Zealand the o-suite reproduces well O_3 mixing ratios (MNMB≈0%) while the control run underestimate it by -20%. Correlations between simulated and observed surface ozone values are 0.75 for both runs.

Finally for South Pole station in Antarctica (SPO), the data assimilation almost corrects the negative offset in the control run (o-suite MNMBs= -1%, control MNMB= -20%), see Fig 3.1.3.7 (right panel). For Neumayer station (NEU) the MNMB is 7% for the o-suite and -13% for the control, Fig. 3.3.8. At Arrival Heights station (ARH) the o-suite overestimates surface ozone values by 6% while the control run underestimates it by -15%. Correlations between simulated and observed surface ozone are high for both runs at ARH station SPO stations ($r_{o\text{-}suite}$≈0.50 and $r_{control}$≈0.60) and even higher at SPO (r≈0.85 for both runs)

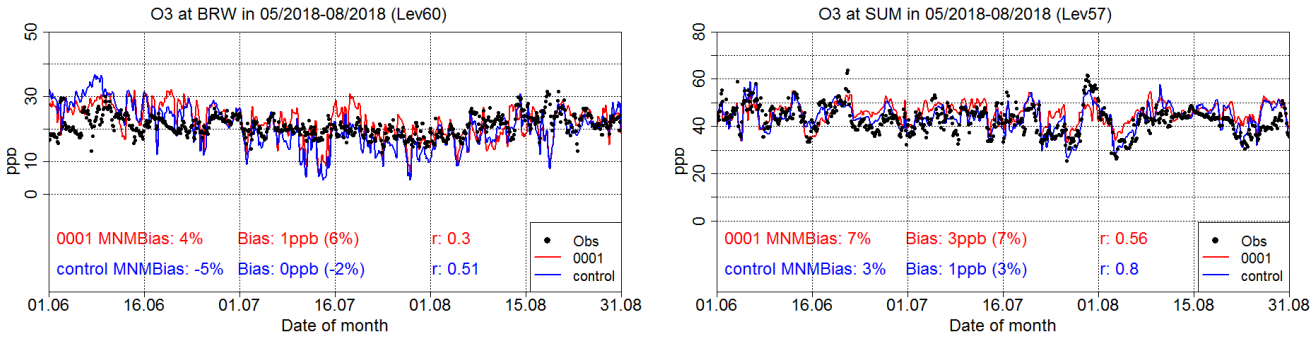

Figure 3.3.5: Time series for the o-suite (red) and control (blue) compared to ESRL observations at Summit, Greenland station (72.57°N, 38.48°W, left) and at Point Barrow, Alaska station (71.32°N, 156.51°W, right)

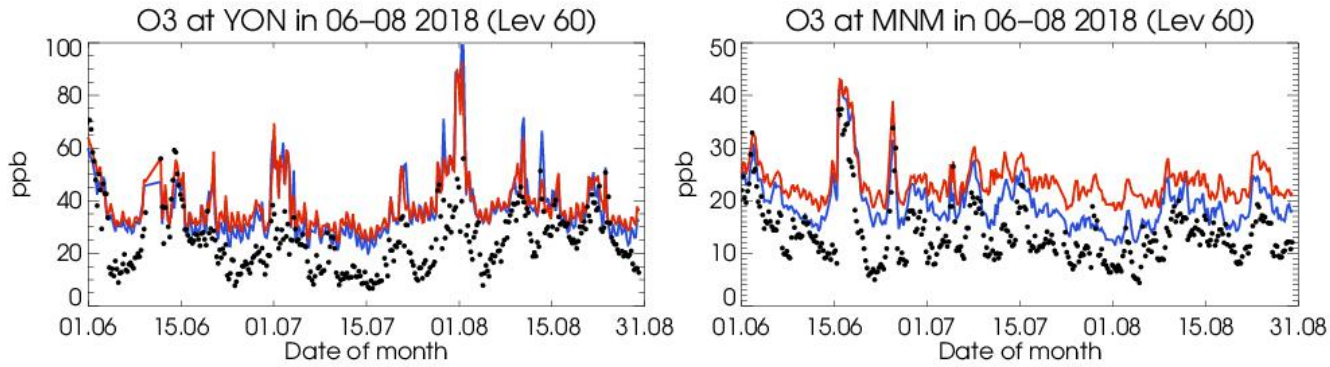

Figure 3.3.6: Time series for the o-suite (red) and control (blue) compared to GAW observations for Yonagunijima (24.47°N, 123.02°E) and Minamitorishima (24.29°N, 153.98°E)

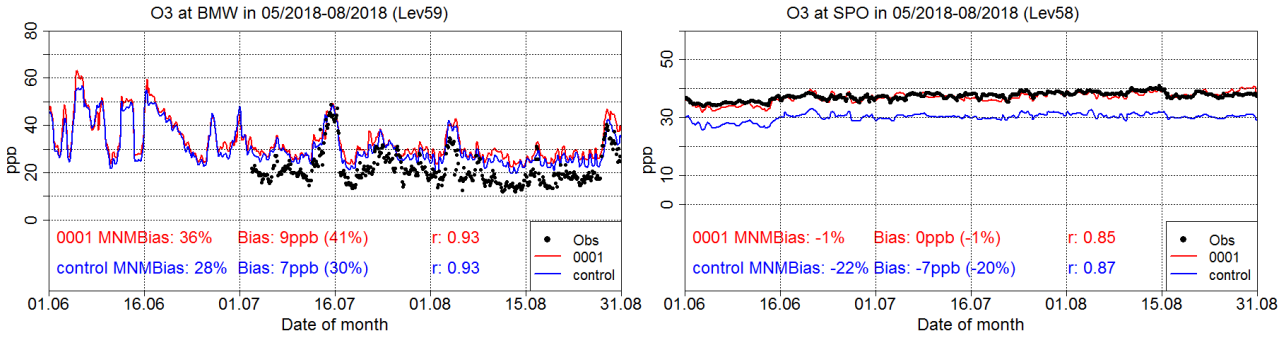

Figure 3.3.7: Time series for the o-suite (red) and control (blue) compared to ESRL observations (black dots) at Tudor Hill, Bermuda station (32.27°N, 64.88°W) and at South Pole, Antarctica station (90.00°S, 24.80°W).

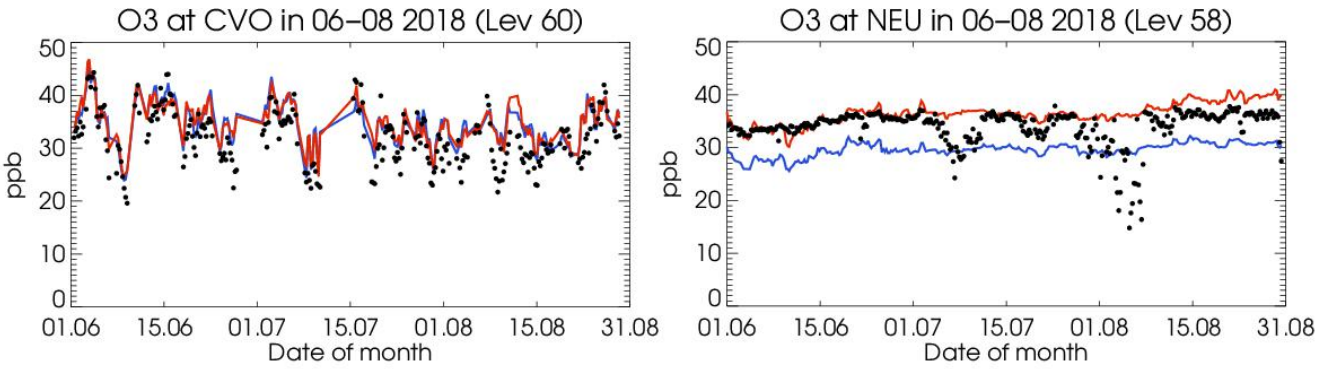

Figure 3.3.8: Time series for the o-suite (red) and control (blue) compared to GAW observations (black dots) at Cape Point (34.55°S, 18.48°W) and GAW observations at Neumayer (70.65°S, 8.25°W).

3.4 Validation with AirBase observations in Mediterranean

The surface ozone validation analysis over the Mediterranean is based on an evaluation against station observations from the Airbase Network (http://acm.eionet.europa.eu/databases/airbase/). In addition, 2 stations from the Department of Labour Inspection - Ministry of Labour and Social Insurance, of Cyprus (http://www.airquality.dli.mlsi.gov.cy/) are used in the validation analysis. For the validation analysis, stations in the Mediterranean located within about 100 km from the shoreline of the Mediterranean shore are used. Table 3.4.1 shows the names, coordinates, elevation and the MNMBs and correlations obtained with the 2 forecast runs (o-suite and control). It indicates that the variance explained by each station of both the o-suite and control is high and correlations are highly significant over Western, Central and Eastern Mediterranean (with the exception of Finokalia station in Crete). It should be noted that the control run reproduces slightly better than the o-suite the surface ozone day to day variability over the Eastern Mediterranean (see Table 3.4.1).

In terms of biases, o-suite MNMBs vary between -20% and 30% depending on the stations over the Mediterranean shore of Spain. The Control MNMBs are on average 1.5% lower than o-suite MNMBs. Over the stations Plan Aups/Ste Baume in France and Gharb in Malta the o-suite overestimate surface ozone concentrations by 9% and 6% respectively. Again the Control MNMBs are 1.5% lower than o-suite MNMBs. Over Finokalia station in Crete both the o-suite underestimate surface ozone by -4%and -6% respectively. Finally over Agia Marina and Oros Troodos stations in Cyprus the o-suite overestimate surface ozone mean concentrations by 7%. The Control MNMBs are on average 1.5% lower than o-suite MNMBs.

The spatial distribution of MNMBs and the correlation coefficients of the o-suite over the Mediterranean are shown in 3.1.4.2, where it is evident that correlations over the entire Mediterranean from Gibraltar to Cyprus are highly significant. It is also evident that the CAMS NRT runs have a better performance over Central and eastern Mediterranean compared to the Mediterranean shore of Spain in terms of biases.

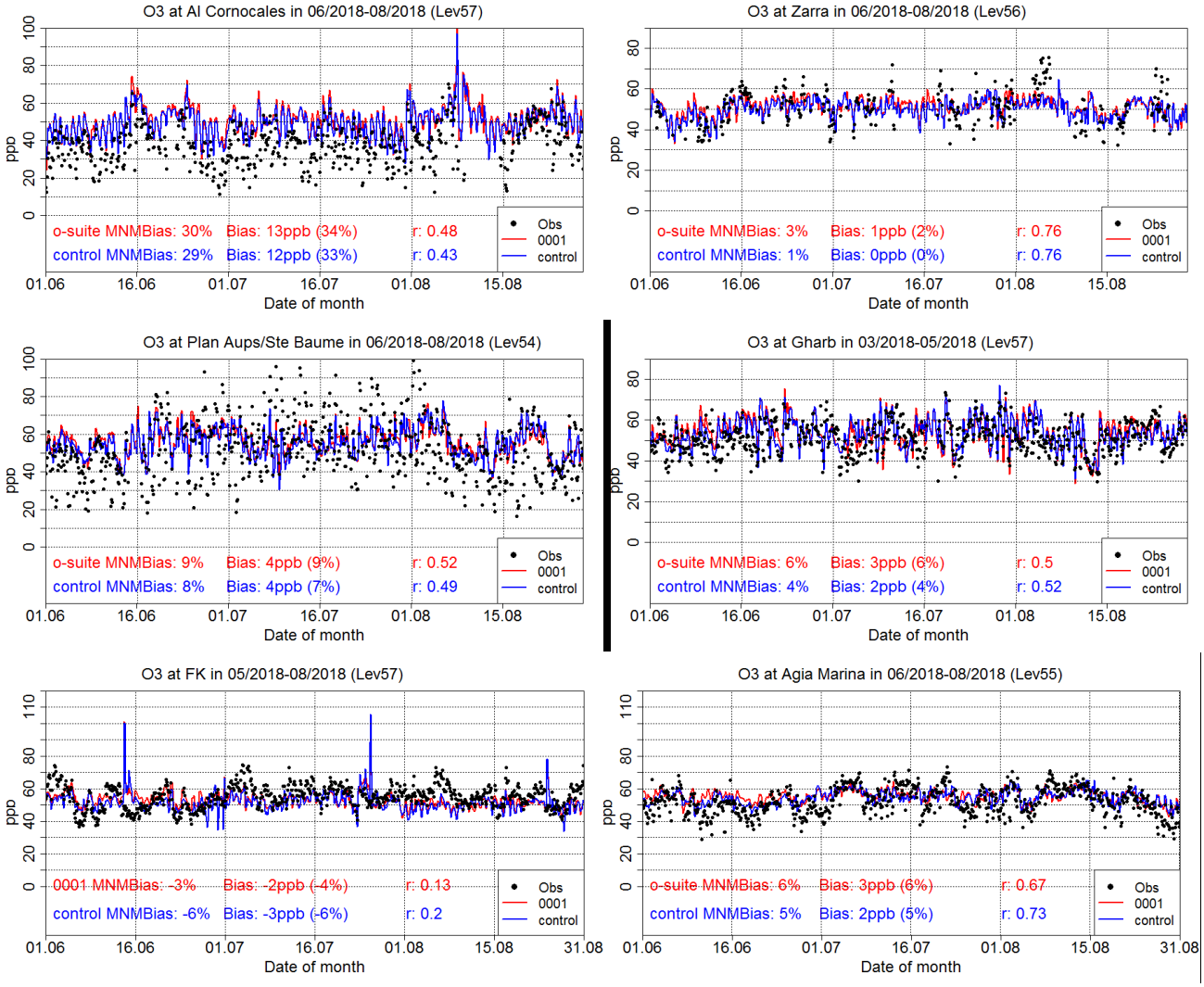

Figure 3.4.1: Time series for the o-suite (red) and Control (blue) compared to Airbase observations at Al Cornocales, Spain station (36.23°N, 5.66 °W, top left), at Zarra, Spain station (39.08°N, 1.10°W, top right), at Plan Aups/Ste Baume, France station (43.34°N, 5.73°E, center left), at Gharb, Malta station (36.07°N, 14.20°E, center right at Finokalia, Crete Greece station (35.32°N, 25.67°E, bottom left) and compared to observations provided by the Department of Labour Inspection - Ministry of Labour and Social Insurance of Cyprus) at Agia Marina, Cyprus station (35.04°N, 33.06 °E, low right).

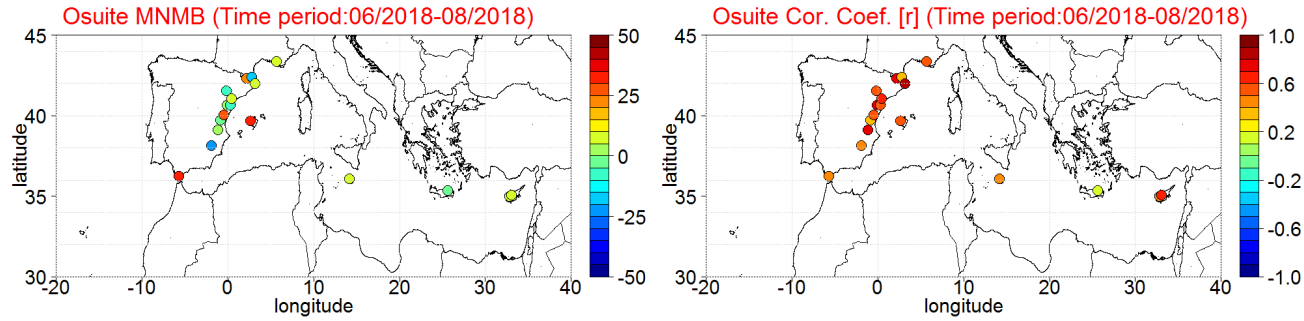

Figure 3.4.2: Spatial distribution of MNMB in % (left) and correlation coefficient (right) of the o-suite run compared to observational data during the period from 1 June 2018 to 31 August 2018.

Table 3.4.1: Coordinates, elevation, corresponding model level (level 60 is the surface level), as well as validation scores (MNMBs and correlations for the period JJA 2018) obtained with the 2 forecast runs (o-suite and control), for each one of the selected Mediterranean stations. MNMBs and correlations with blue denote stations where control run performs better while with red are denoted stations where o-suite performs better.

						Distance from the	MNMB		Cor. Coef	
Station Name	Stat_ID	Lon	Lat	Alt (m)	Level	shore (km)	o-suite	control	o-suite	control
Al Cornocales	ES1648A	-5.66	36.23	189	57	16	30.2	29.0	0.48	0.43
Caravaka	ES1882A	-1.87	38.12	1	60	73	-22.3	-23.3	0.50	0.48
Zarra	ES0012R	-1.10	39.08	885	56	70	3.3	1.1	0.76	0.76
VIillar Del Arzobispo	ES1671A	-0.83	39.71	430	60	48	-1.6	-2.7	0.31	0.33
Cirat	ES1689A	-0.47	40.05	466	60	37	28.7	27.2	0.51	0.54
Bujaraloz	ES1400A	-0.15	41.51	327	60	60	-9.1	-2.8	0.56	0.60
Morella	ES1441A	-0.09	40.64	1150	53	51	0.7	-2.0	0.74	0.82
Bc-La Senia	ES1754A	0.29	40.64	428	59	21	-5.7	-7.8	0.56	0.57
Ay-Gandesa	ES1379A	0.44	41.06	368	58	15	8.2	6.2	0.68	0.66
Ak-Pardines	ES1310A	2.21	42.31	1226	57	81	24.9	22.4	0.73	0.71
Hospital Joan March	ES1827A	2.69	39.68	172	57	3	31.5	29.3	0.51	0.44
Al-Agullana	ES1201A	2.84	42.39	214	60	25	-15.7	-18.9	0.32	0.30
Av-Begur	ES1311A	3.21	41.96	200	56	9	7.9	5.6	0.83	0.83
Plan Aups/Ste Baume	FR03027	5.73	43.34	675	54	21	9.0	7.7	0.52	0.49
Gharb	MT00007	14.20	36.07	114	57	31	5.9	4.4	0.50	0.52
Aliartos	GR0001R	23.11	38.37	110	59	18	NA	NA	NA	NA
NEO	-	21.67	37.00	50	60	2	NA	NA	NA	NA
Finokalia	GR0002R	25.67	35.32	250	57	4	-3.1	-6.2	0.13	0.20
Oros Troodos	-	32.86	34.95	1819	49	11	6.9	6.3	0.44	0.57
Agia Marina	CY0002R	33.06	35.04	532	55	14	7.1	5.1	0.67	0.73

3.5 Validation with IASOA surface observations

Model results were compared to O_3 observations from the Villum Research Station, Station Nord in north Greenland (81.6°N 16.7°W), Eureka, Nunavut, Canada (80.1°N 86.4°W), Zeppelin Mountain, Svalbard (78.9°N 11.9°E), and Tiksi, Russia (71.6°N 128.9°E) from the IASOA network, Fig. 3.5.1.

The data from Svalbard and VRS are covering the period from December 2014 to August 2018. Data from Eureka covers the period August 2016 – August 2018, and data from Tiksi covers the period September 2016 – August 2018. Ozone depletion events in March – June in 2015 – 2018 are not captured by the model simulations during spring at any of the sites. These events are related to halogen chemistry reactions that are not represented in the model simulations. The simulations are on average in good agreement with the observations apart from the spring depletion events.

For the period June – August 2018 the measurements are not quality controlled. The model simulations overestimate the measured O_3 concentrations at all sites resulting in a positive bias of 2% - 21% for the o-suite and 3% - 22% for the control run (Table 3.1.2) like previous years. The control run performs better than the o-suite in terms of the correlation; r = 0.19 – 0.40 for the o-suite compared to r = 0.15 – 0.62 for the control run.

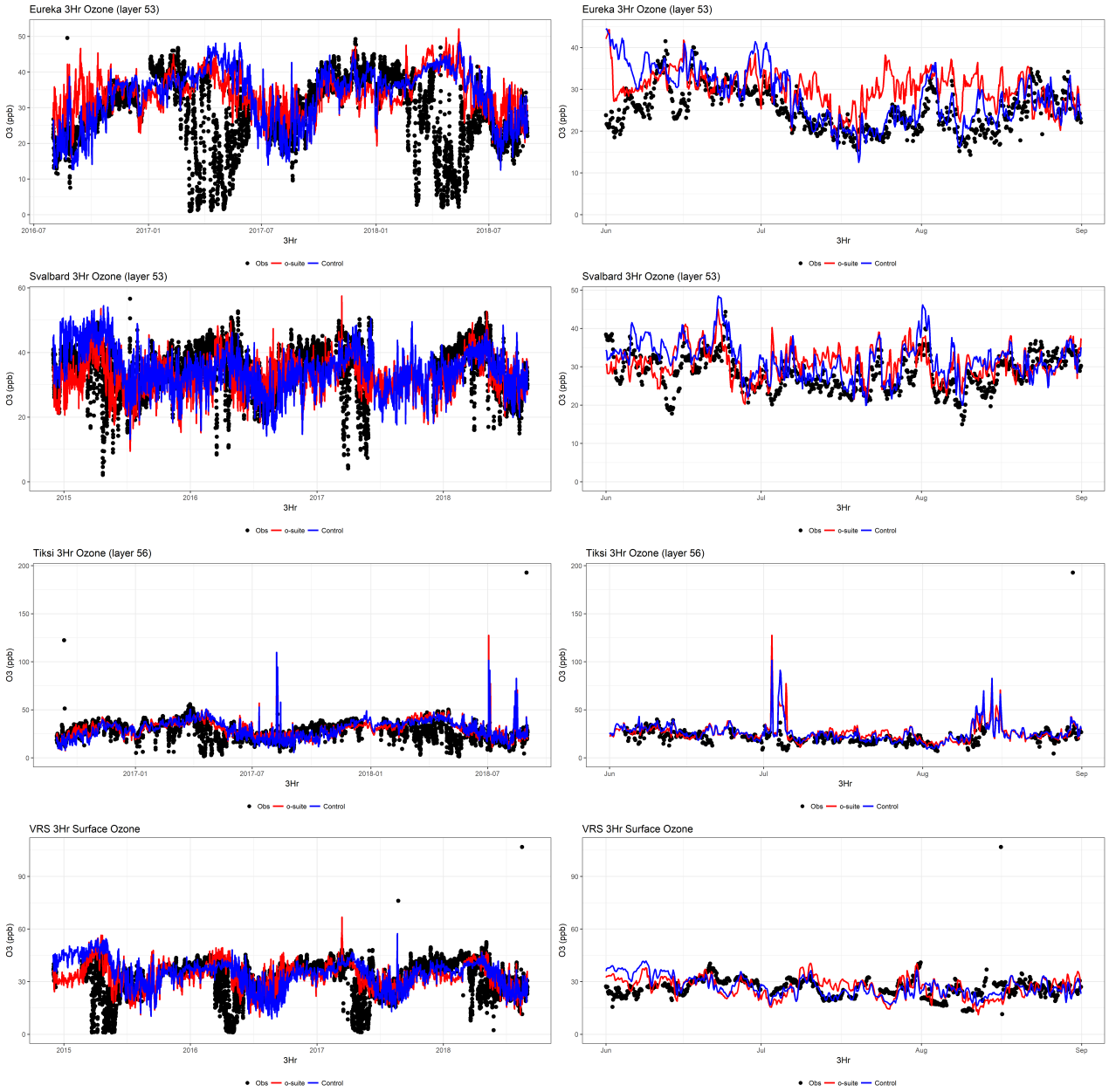

Figure 3.5.1: Time series for o-suite (red) and Control (blue) compared to observations (black dots) at Eureka, Nunavut, Canada (Top row), Svalbard (second row), Tiksi, Russia (third row) and the Villum Research Station, Station Nord, Greenland (bottom row) for the full period (left) and for June-August (right).

Table 3.5.1. Normalised Mean Bias (NMB) and correlation coefficient (r) of the Control and the O-suite simulations for the sites Eureka, Svalbard, Tiksi and Villum Research Station (VRS) for the period June – August 2018.

		NMB	R
Eureka	o-suite	0.20	0.27
	control	0.12	0.60
Svalbard	o-suite	0.09	0.40
	control	0.12	0.62
Tiksi	o-suite	0.21	0.19
	control	0.22	0.26
VRS	o-suite	0.02	0.19
	control	0.03	0.15

4. Carbon monoxide

4.1 Validation with Global Atmosphere Watch (GAW) Surface Observations

For the Near-Real-Time (NRT) validation, 10 GAW stations have delivered CO surface mixing ratios in NRT and data is compared to model results as described in Douros et al (2017) and is used for CAMS model evaluation for June – August 2018. The latest validation results can be found on the CAMS website: http://www.copernicus-atmosphere.eu/d/services/gac/verif/grg/gaw/

For stations in the Northern Hemisphere, both runs mostly show slightly negative MNMBs. For the stations located in the Southern Hemisphere, both runs show a strong positive offset, which is reduced by the data assimilation for the o-suite.

For stations in Europe, and the Southern hemisphere, the MNMBs and correlation coefficients indicate that the forecast remains stable till the D+4 (forecast run from 96h to 120h).

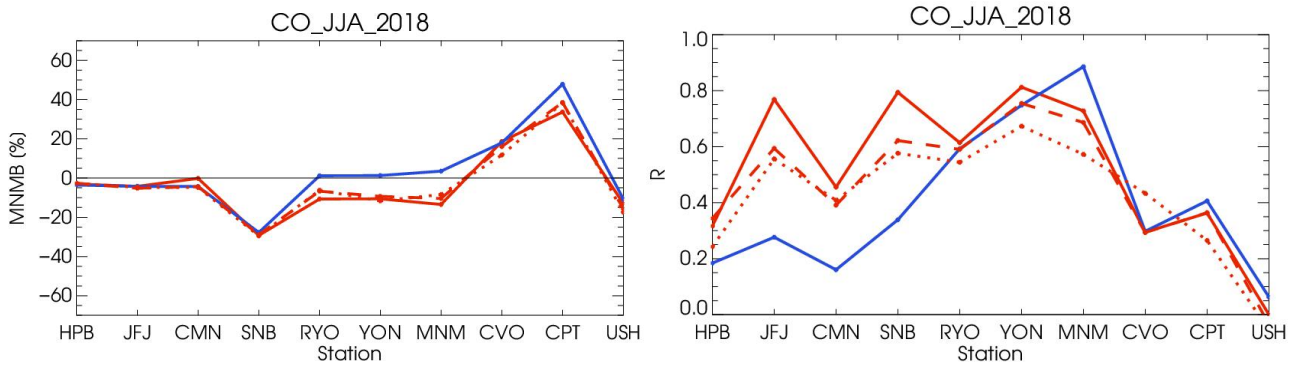

Figure 4.1.1: Modified normalized mean bias in % (left) and correlation coefficient (bottom right) of the NRT model runs compared to observational GAW data in the period June 2018 to August 2018 (o-suite: solid red, D+2: red-dashed, D+4: red-points, and control: blue).

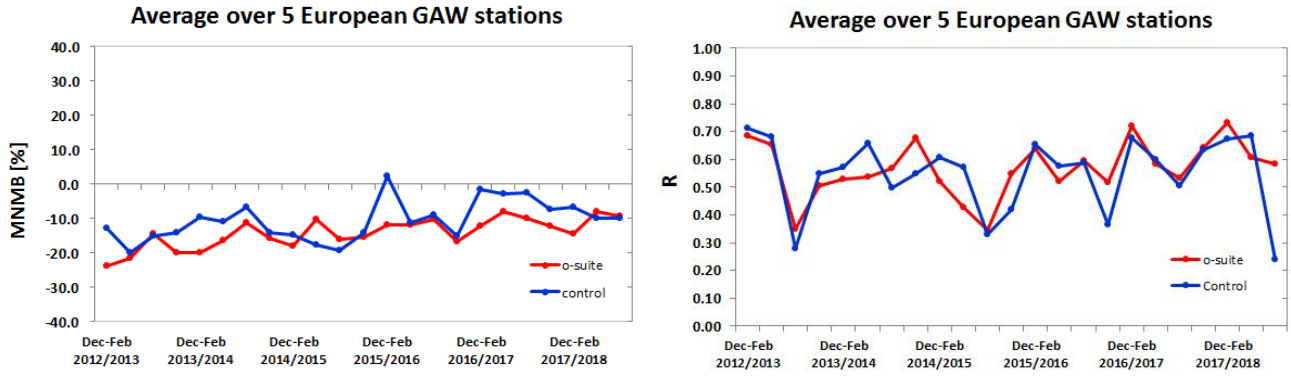

Figure 4.1.2: Long term (Dec. 2012 – August 2018) evolution of seasonal mean MNMB (left) and correlation (right), as averaged over 5 GAW stations in Europe, for o-suite (red) and control (blue).

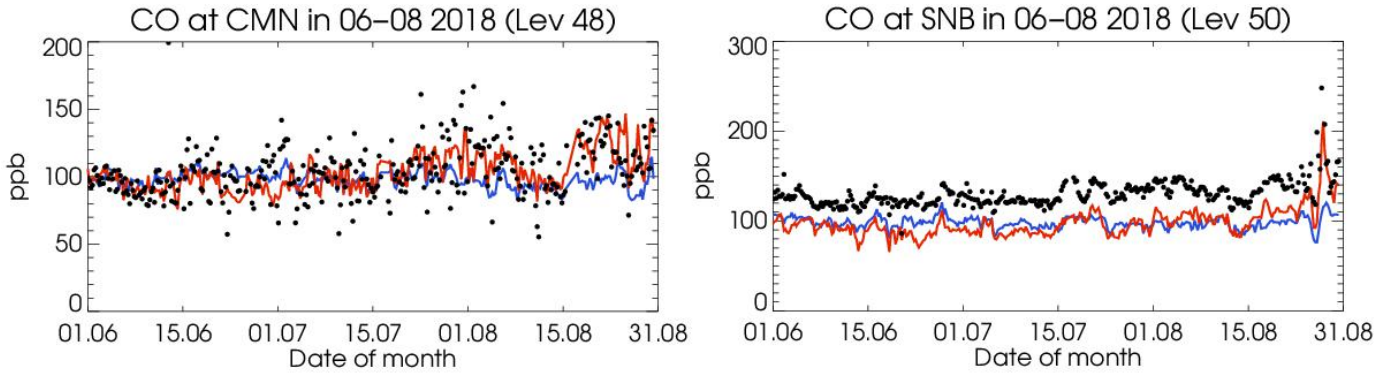

Figure 4.1.3: Time series for the o-suite (red) and control (blue) compared to GAW observations at Monte Cimone (44.18°N, 10.70°E) and Sonnblick (47.05°N, 12.96°E)

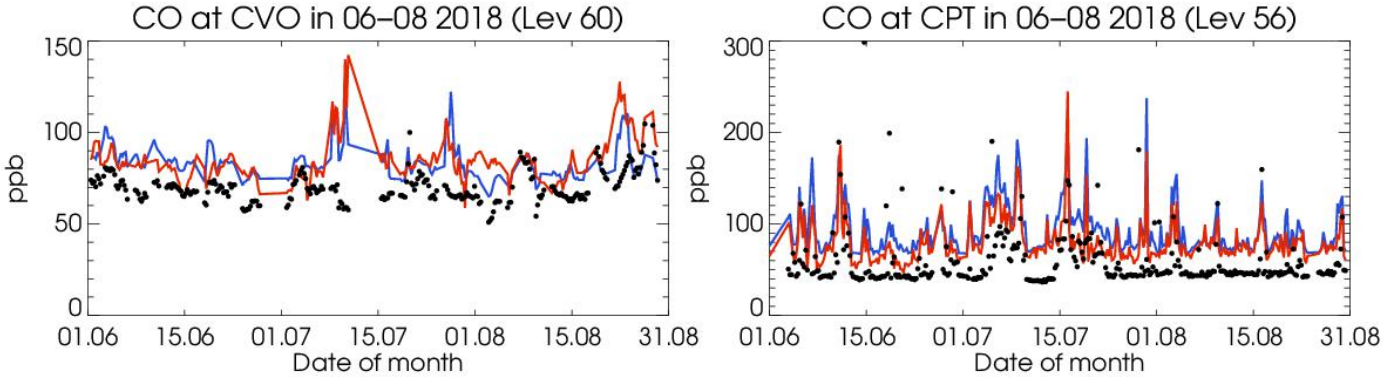

Figure 4.1.4: Time series for the o-suite (red) and control (blue) compared to GAW observations at and Cape Verde (16.9°N, 24.9°W) and Cape Point (34.35°S, 18.5°E).

A comparison of the seasonal-mean MNMB over Europe (Fig. 4.1.2) from December 2012 to present shows a slowly improving MNMB from about -20% in 2013 to -10% for more recent periods. Temporal correlation remains relatively constant at r=0.6 on average, except for the last quarter (JJA), where the correlation of the control run drops to 0.24.

For European stations, the o-suite shows an underestimation of observed CO mixing ratios, with MNMBs between 0% and -30%. The control shows slightly higher CO mixing ratios for European stations with MNMBs between -4% and -27%. Correlation coefficients are between 0.33 and 0.79 for the o-suite and between 0.16 and 0.33 for the control run.

For stations in Asia (RYO, YON, MNM) the control run shows a good correspondence with the observations with MNMBs between 1 and 3%. The data assimilation reduces the CO mixing ratios and introduces a negative bias (MNMBs between -10 and -13%), see Fig. 4.1.5. Correlation coefficients range between 0.59 and 0.88.

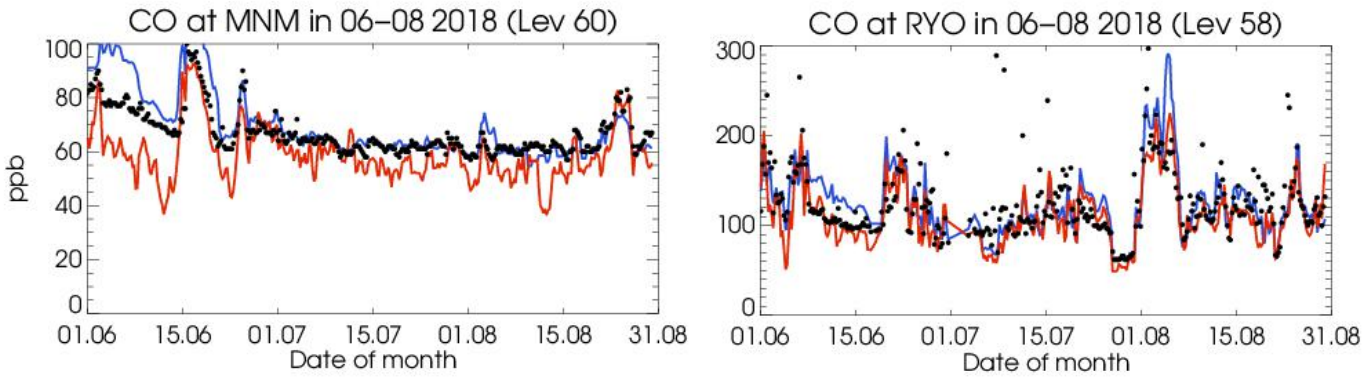

Figure 4.1.5: Time series for the o-suite (red) and control (blue) compared to GAW observations for Minamitorishima (24.29°N, 123.02°E) and Ryori (39.03°N, 141.82°E).

4.2 Validation with IAGOS Data

The daily profiles of ozone and CO measured at airports around the world are shown on the website at http://www.iagos.fr/macc/nrt_day_profiles.php. For the period June-August 2018, data from several aircraft have been validated, as discussed in Sec. 3.2.

Figure 4.2.1 shows the time series of daily mean values in different atmospheric layers over Paris and Frankfurt. At Frankfurt, the models underestimate CO in both the boundary and surface layer (Fig. 4.2.2). This behaviour is more obvious in the individual profiles over Europe (Fig. 4.2.3). In the low stratosphere, models in general overestimate the amount of CO. The best agreement between models and observations is found in the free and upper troposphere.

As shown in section 3.2, an increase of ozone is observed at Frankfurt at the surface and boundary layers at the beginning of June around day 9. This increase is correlated with high CO for the same days as shown in the time series (Fig. 4.2.1). CO profiles at Frankfurt on 8, 9 and 10th June are presented in Fig. 4.2.3, with values reaching about 200 ppbv in the boundary layer. This increase is detected by the models but largely underestimated by about 50% (Fig. 4.2.1 and 4.2.3).

At the end of August at Frankfurt, high CO is observed in all layers according to the time series (Fig. 4.2.1). Fig. 4.2.3 presents CO profiles for the 27, 28 and 30th of August. For these three days, CO mixing ratios are of about 200 ppbv in the boundary layer. On 27th and 28th August, the profiles present a wide plume of CO in the mid-troposphere between 3000 and 8000 m in the first case, and between 3000 m and 6000 m in the second case, both reaching values of 400 ppbv. For the profile on 30th August a plume is still present between 3000 m and 6000 m, but with a much smaller magnitude with 200 ppbv. These plumes are likely related to the long range transport of smoke from North American forest fires (see regional report). For these days, boundary layer values are underestimated by both models, and the wide and extreme plumes are well detected by the models although magnitudes are underestimated, with a slightly better performance from the o-suite on 28th August. On day 30th, the models do not reproduce the small peak observed in the same range of altitudes.

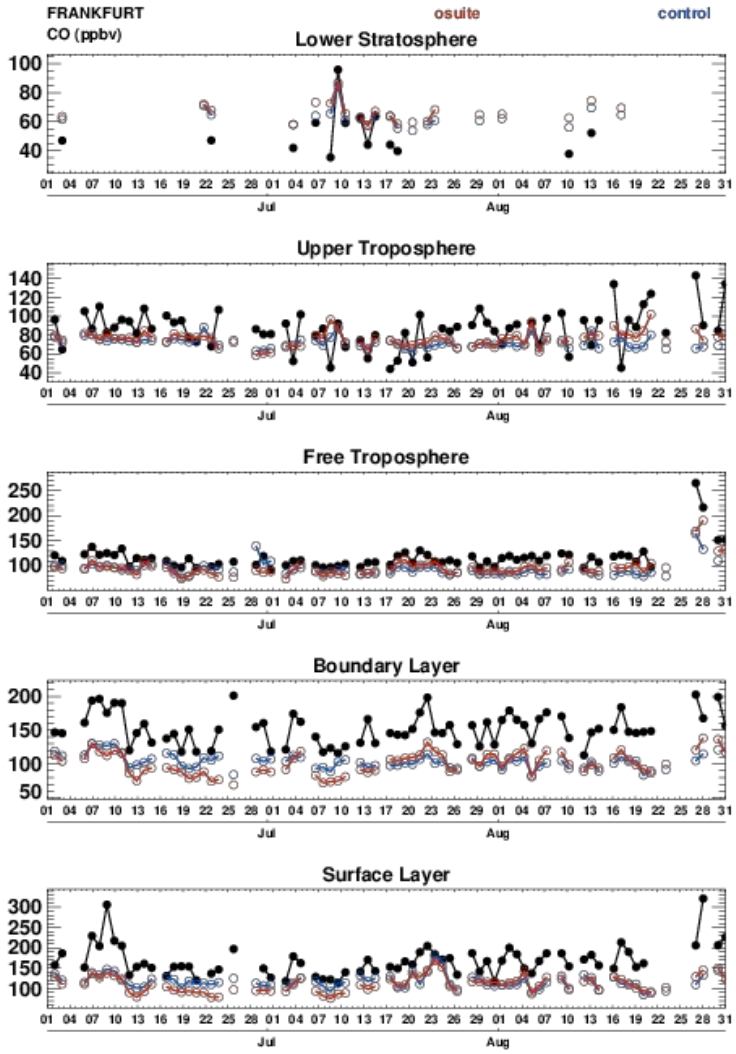

Figure 4.2.1. Time series of daily mean CO over Frankfurt during JJA 2018 for 5 layers, Surface, Boundary layer, Free Troposphere, Upper Troposphere and Lower Stratosphere.

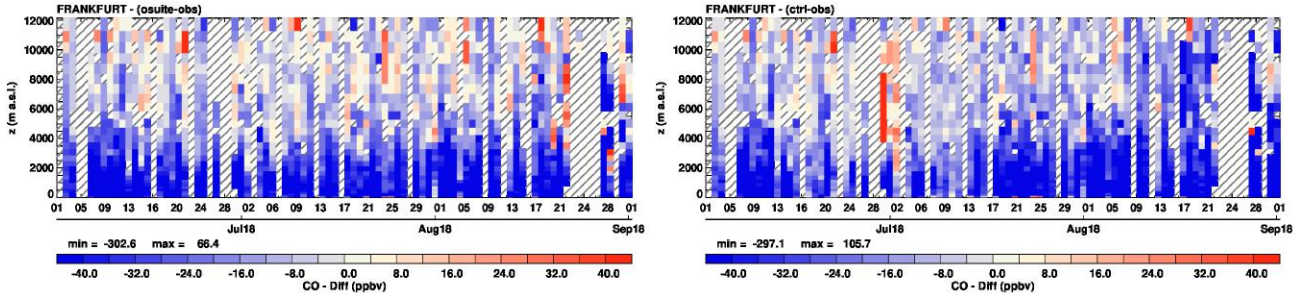

Figure 4.2.2. Time series of the absolute differences (model - observations) in daily profiles for CO over Frankfurt during JJA 2018. Left panel corresponds to o-suite and right panel to control run.

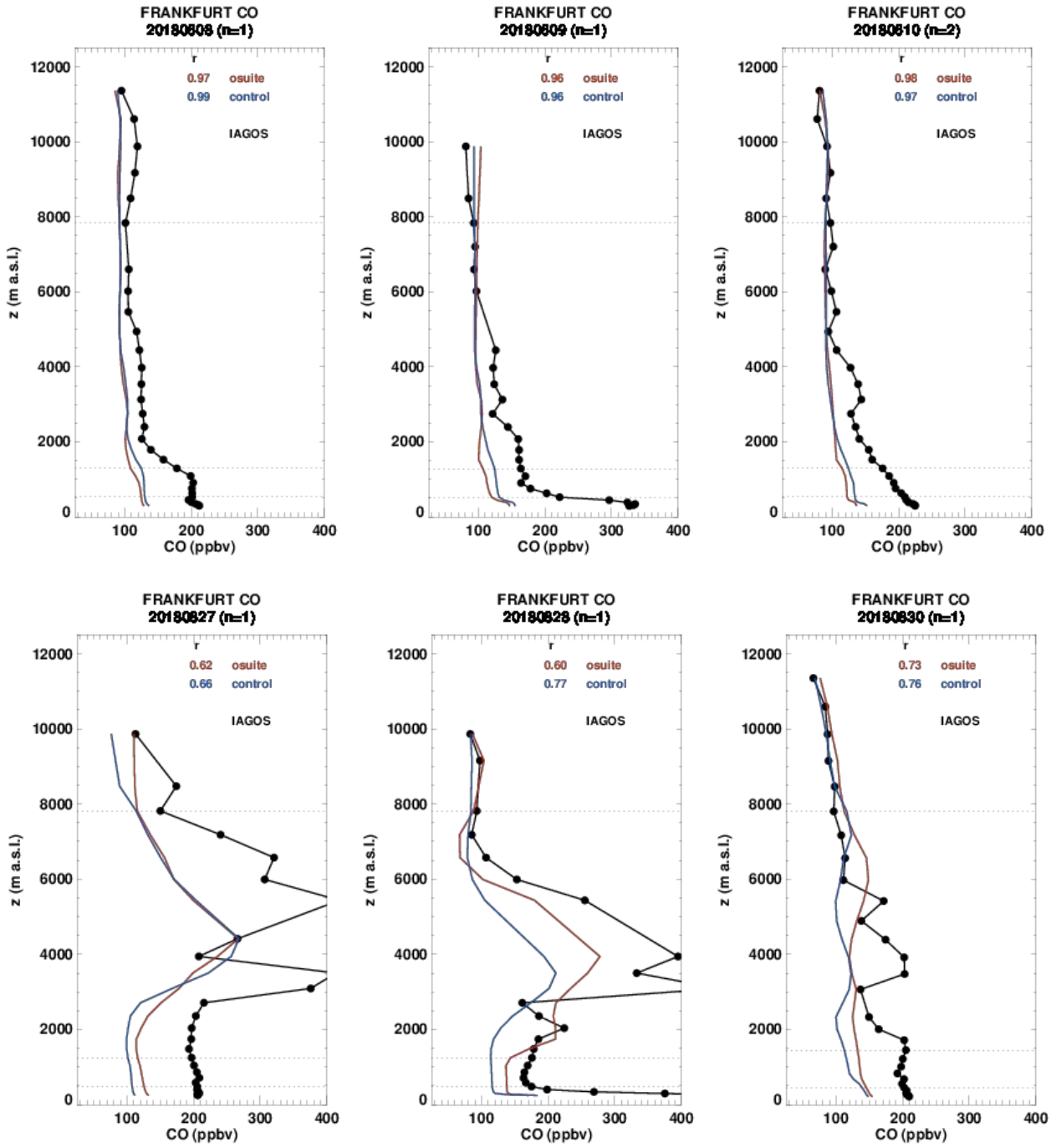

Figure 4.2.3.a Selection of daily profiles for CO from IAGOS (black) and the two NRT runs (o-suite: red, control: blue) over Europe during June-August 2018.

As mentioned before in section 3.2, during the summer Paris experienced the strongest episodes of ozone since 2003. Fig. 4.2.3 presents profiles at Paris on 6th, 7th and 8th July. On 6th July a peak is observed in the boundary layer with 150 ppbv. For 7th and 8th, CO values are nearly constant in the boundary layer with 100 ppbv and 150 ppbv respectively. These features are correlated with increases in ozone in the same days as previously described (see section 3.2).

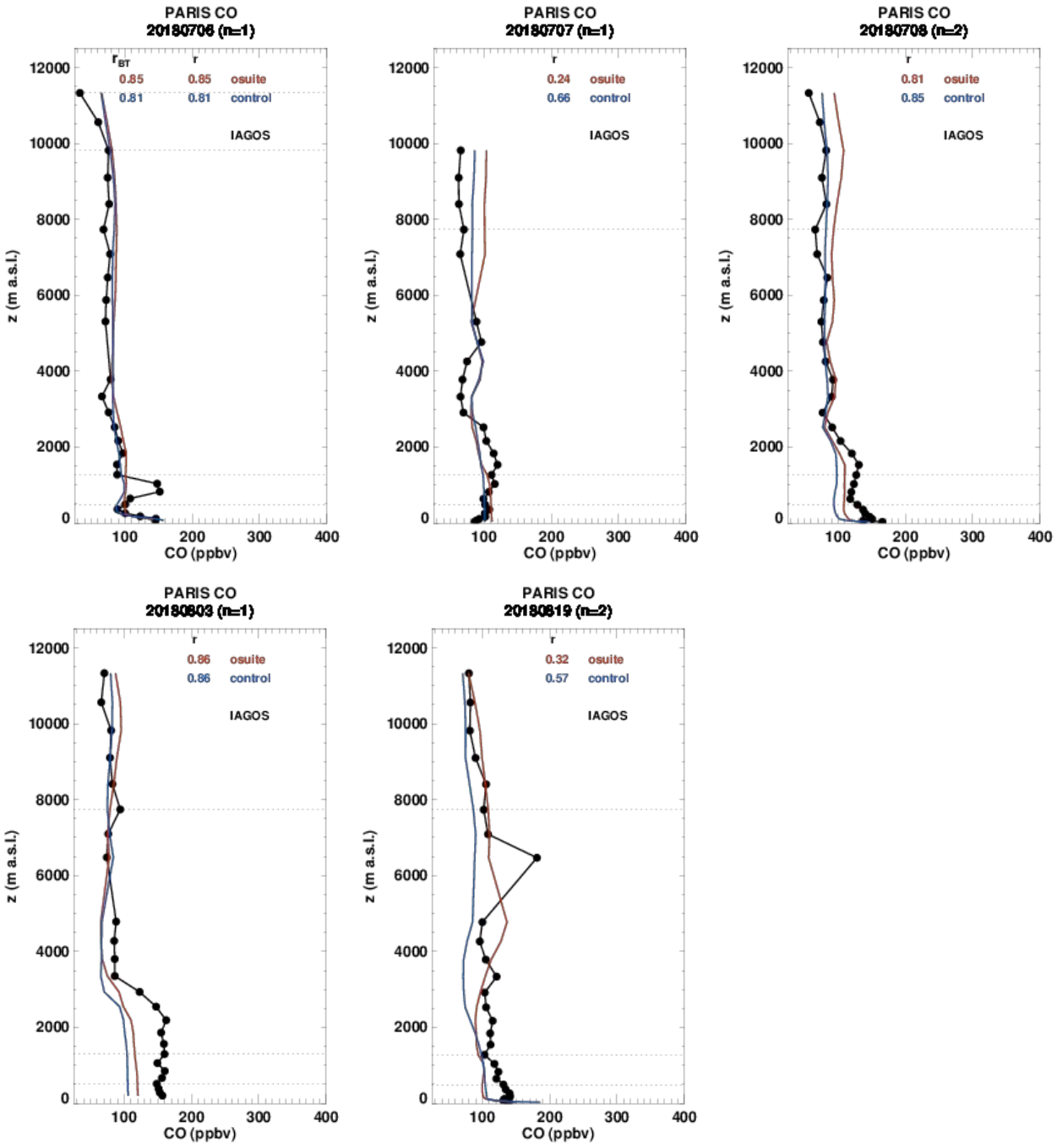

Figure 4.2.3.b Selection of daily profiles for ozone from IAGOS (black) and the two NRT runs (o-suite: red, control: blue) over Europe during June-August 2018.

During the heat wave period in late July- early August (see section 3.2), the observations show an increase in CO values correlated to that of ozone in the lower part of the troposphere. On 3rd August, the profile at Paris shows CO mixing ratios of 200 ppbv from the surface up to 1500 m (Fig. 4.2.3). These values are largely underestimated by both models which present similar results.

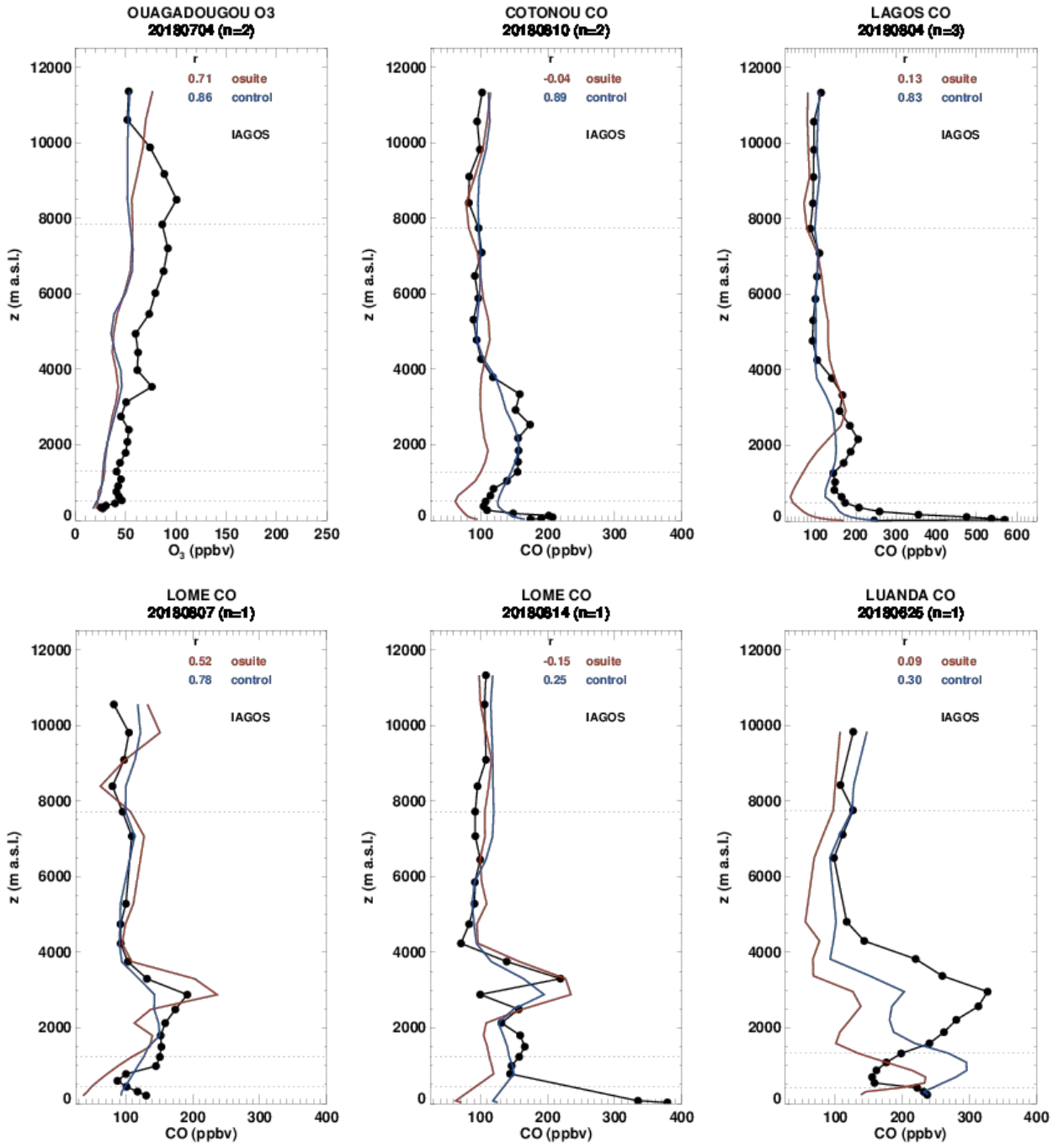

Figure 4.2.4.a Profiles of CO from IAGOS (black) and the two NRT runs over West Africa during JJA 2018.

On 19th August at Paris, a peak of about 180 ppbv is observed in the free troposphere near 6500 m. This feature is likely due to the long range transport of pollution from forest fires in North America (California and British Columbia). It is correlated to high ozone values in the same region of the atmosphere (see profiles in section 3.2). The o-suite detects an increase but slightly lower near 5000 m and with an underestimated magnitude of 120 ppbv. In the case of control run, no maximum is detected in the free troposphere.

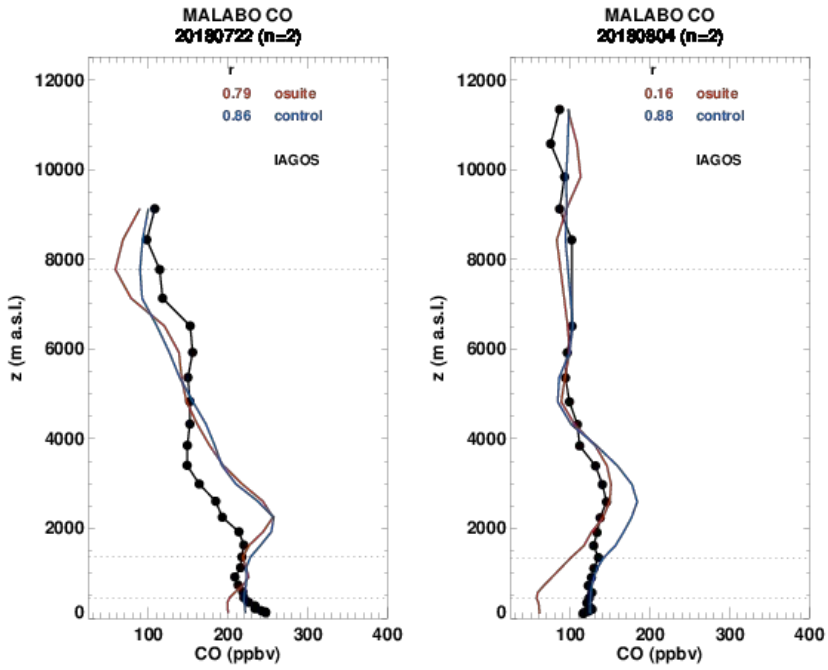

Figure 4.2.4.b Profiles of CO from IAGOS (black) and the two NRT runs over West Africa during JJA 2018.

West Africa

Fig. 4.2.4-a-b highlights some examples of profiles for CO over West Africa sampled by Air France aircraft during June - August 2018. The profiles presented here are for airports of Ouagadougou, Cotonou, Lome, Lagos, Malabo and Luanda. These cities are affected by anthropogenic emissions from vehicles, oil industries, and from biomass burning which stretches across Africa just north of the equator from December to March and south of the equator from June to October. The increases in CO are generally seen at the correct altitudes by both o-suite and control run, which reproduces reasonably the shapes of the profiles. In the surface and boundary layer control run often provides better results than the o-suite which underestimates CO. The worst performance is obtained at Luanda, where both models overestimate CO in the boundary layer, and largely underestimate the peak in the lower part of the free troposphere between 1500 m and 4000 m, with a magnitude of 100 ppbv for the o-suite against 330 ppbv according to observations.

North America

Over North American airports similarly to Europe, it has been shown in previous reports that CO is usually underestimated at the surface and boundary layers by the two runs, while there is a good agreement in the free troposphere. In Fig. 4.2.5, two profiles at Chicago and one profile at San Diego are presented, on 8th and 19th August, and on 12th August respectively. On 8th August, in the surface layer CO mixing ratio is of about 200 ppbv, and the profile is nearly constant from the boundary layer to 4000 m with about 150 ppbv. This profile also shows a small maximum near 6000 m. The o-suite agrees well with the observations in the boundary layer while the peak is not reproduced by the control run, which presents a smooth profile underestimating CO in all layers up to 7000 m.

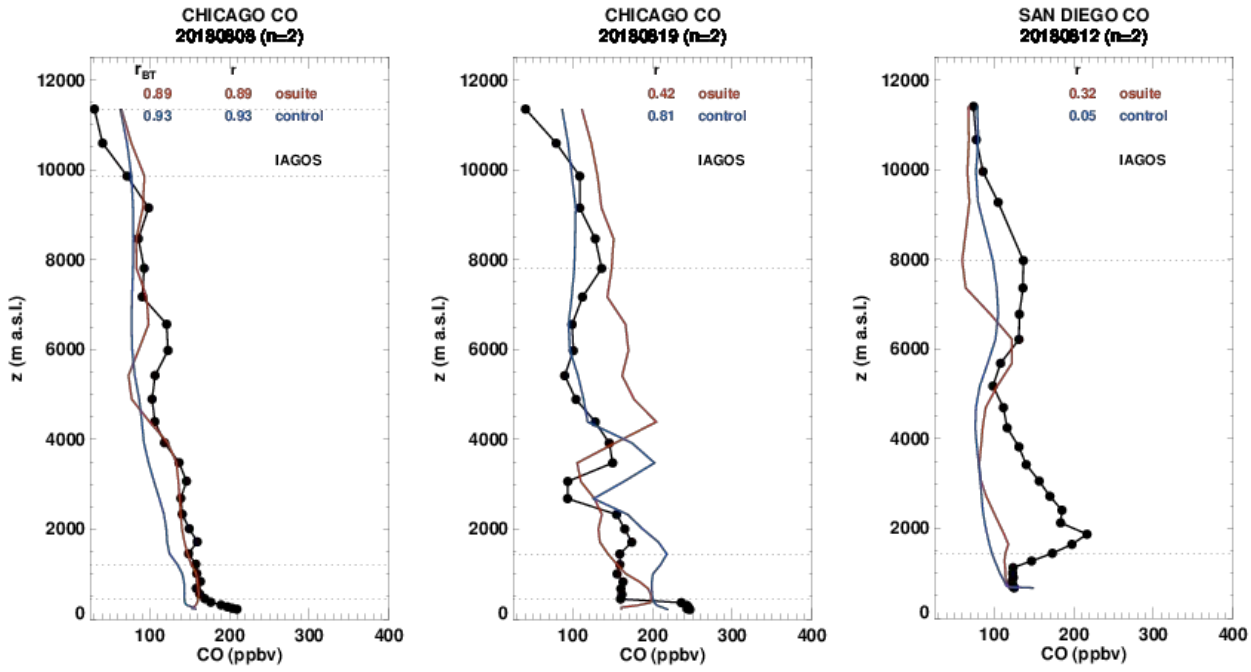

Figure 4.2.5. Profiles of CO from IAGOS (black) and the two NRT runs over North America during JJA 2018.

The profile on 19th August has a complex shape with maximum near 2000 m, 4000 m and 8000 m with a similar magnitude of 150 ppbv. The profiles obtained with the models also present a complex shape, with different results for the o-suite and control run in the altitudes of the maxima. The performance of the control run is better than that of the o-suite, which presents a shape rather different from the observations. However, the magnitudes obtained by the control run are overestimated in the boundary layer and lower part of the free troposphere. On 12th August, observations present high CO values in the lower part of the free troposphere between 2000 m and 4000 m, and also in the upper troposphere between 6000 m and 8000 m with similar values of about 150 ppbv on average. The shape of the profile is not reproduced by the models, and mixing ratios are strongly underestimated in these ranges of altitudes.

Northeastern Asia

Fig. 4.2.6 highlights profiles at several locations in China (Hong Kong, Shenyang, Taipei), Japan (Tokyo, Osaka). It should be noted that the worse performance of the models is obtained at Hong Kong airport where the profiles of the models are nearly constant from the boundary layer to the UTLS with small CO mixing ratios while observations show high CO in the boundary layer and also some maxima in free troposphere. At the other airports (Shenyang, Osaka, Nagoya, Tokyo and Taipei), the complex shapes of the profiles are in general well reproduced by both models with sometimes shifts in the altitude of the maxima (except for 19th June at Nagoya and 28th August at Tokyo). Regarding the magnitude, no systematic behaviour (underestimation/overestimation) can be found here. At Taipei, surface mixing ratios are often overestimated. For all airports, in general the results from the o-suite are better than those of control run. The worst case is the example of Shenyang on 8th August where CO values are extremely overestimated in all layers by the control.

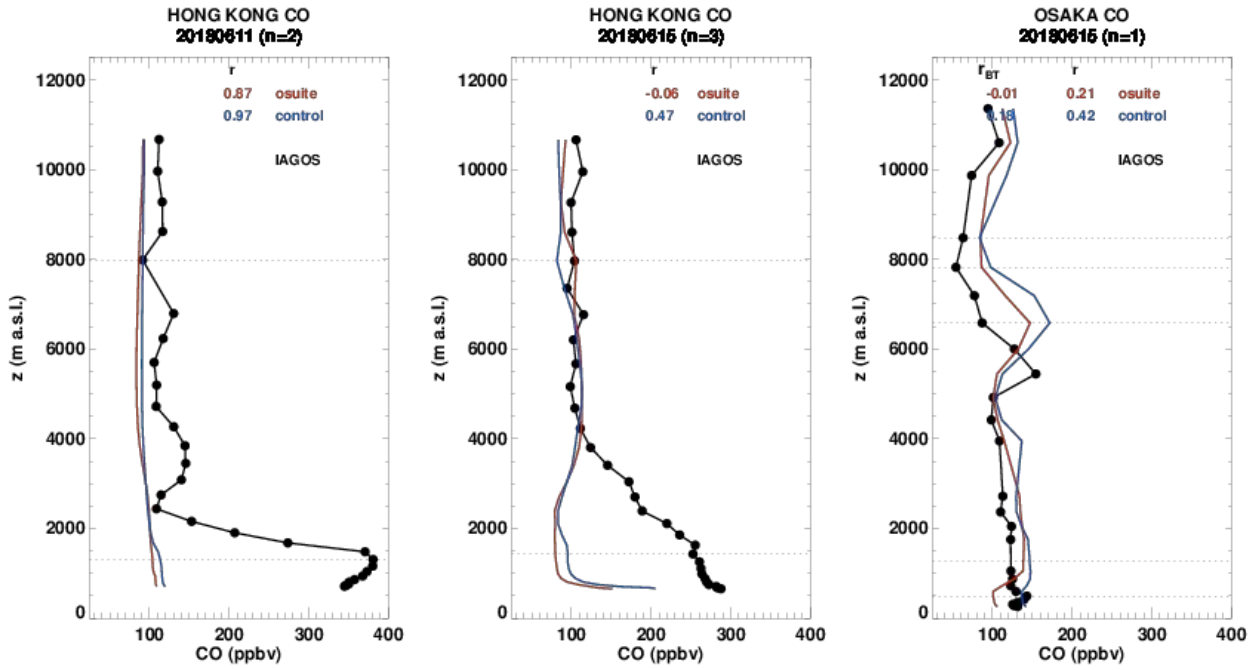

Figure 4.2.6.a Profiles of CO from IAGOS (black) and the two NRT over North Eastern Asia during JJA 2018.

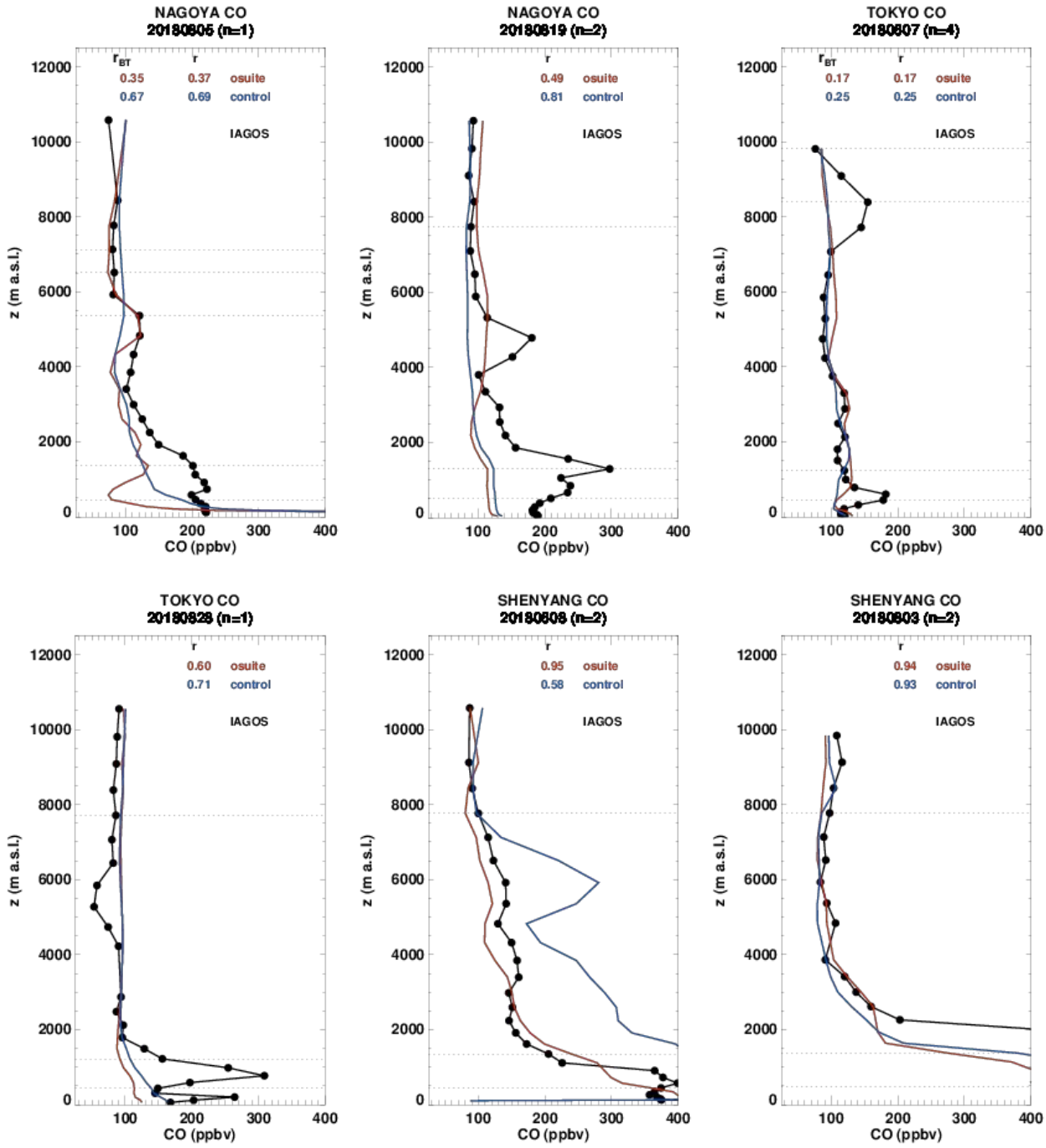

Figure 4.2.6.b Profiles of CO from IAGOS (black) and the two NRT over North Eastern Asia during JJA 2018.

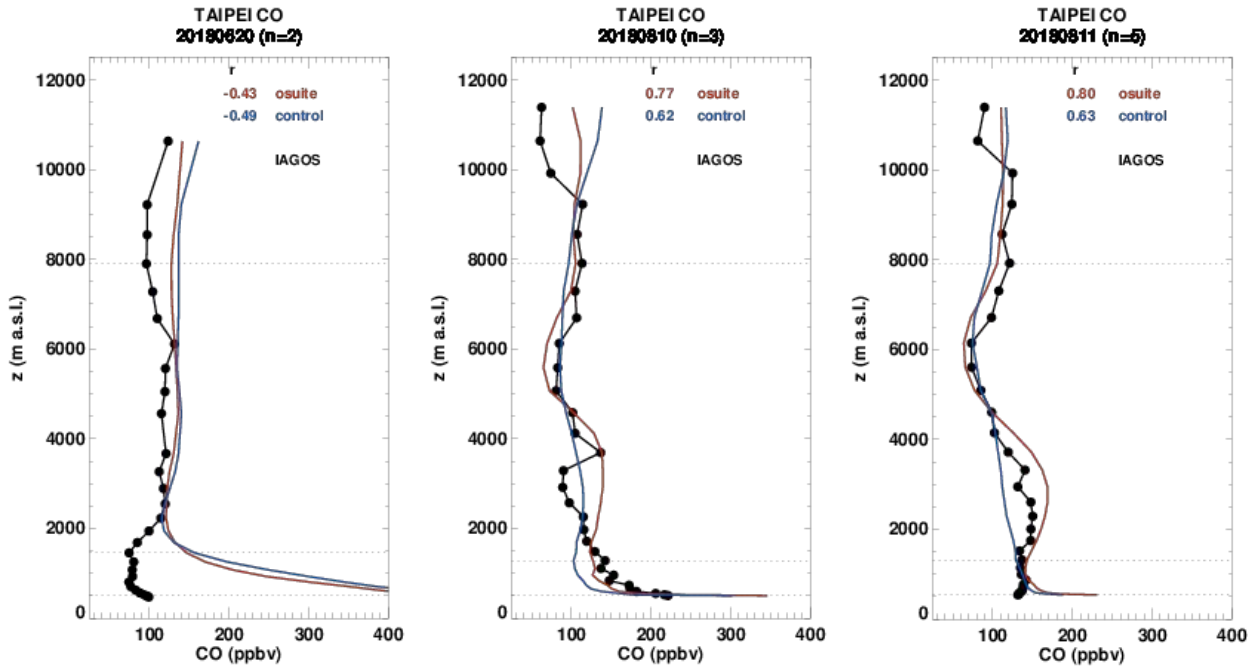

Figure 4.2.6.c Profiles of CO from IAGOS (black) and the two NRT over North Eastern Asia during JJA 2018.

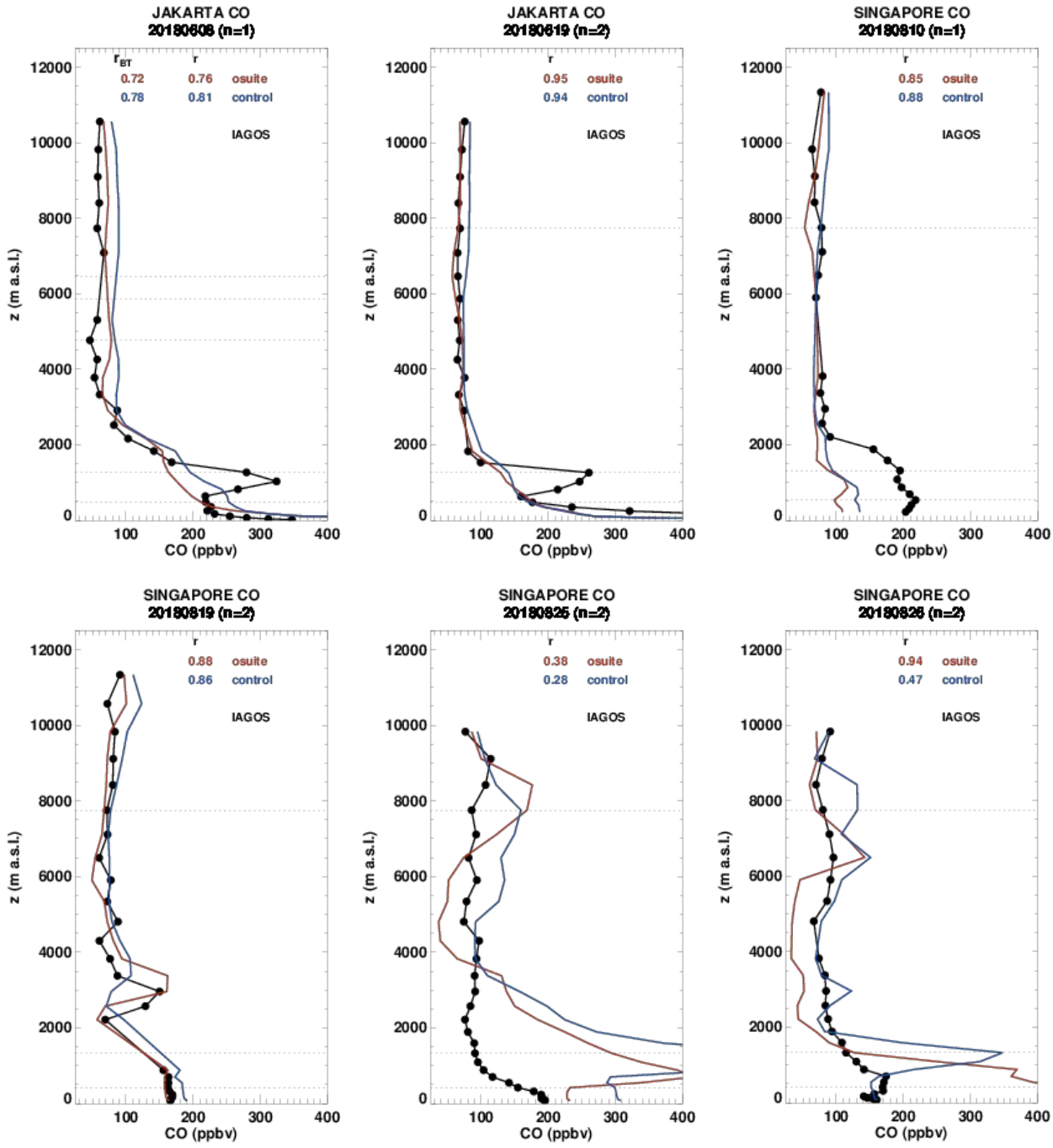

Figure 4.2.7.a: Profiles of CO from IAGOS (black) and the two NRT over Indonesia during JJA 2018.

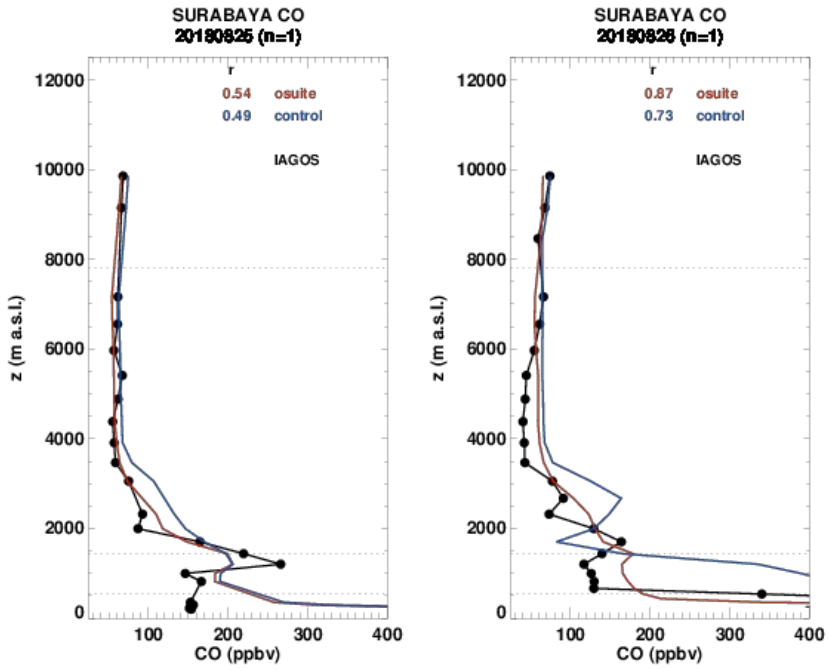

Figure 4.2.7.b: Profiles of CO from IAGOS (black) and the two NRT over Indonesia during JJA 2018.

Indonesia

In Fig. 4.2.7, several profiles from airports in Indonesia are presented: Jakarta, Singapore and Subaraya. In most profiles the behaviour of the models is similar. The best agreement is found in the UTLS. In the free troposphere the agreement is good in general except in Singapore for some cases. The discrepancies between the models and the observations are the largest at the surface and boundary layer. The CO peaks observed in the boundary layer at Jakarta (8th and 19th June) are not detected by the models. On 25th and 26th August at Singapore very high CO values are produced by the models in the surface and boundary layers reaching more 400 ppbv for the o-suite, but these patterns are not present in the observations. Conversely, on 8th August at Singapore again, CO mixing ratios are underestimated in the surface and boundary layer by a factor 2. On 19th August, the models agree well with observations and the peak of CO in the lower part of the free troposphere is well reproduced by both models. In Subaraya, surface mixing ratios are largely overestimated by both models on 25th August. On 26th August at Subaraya, control run overestimates values in the boundary layer and the lower part of the free troposphere, while CAMS global agrees well with observations in all layers.

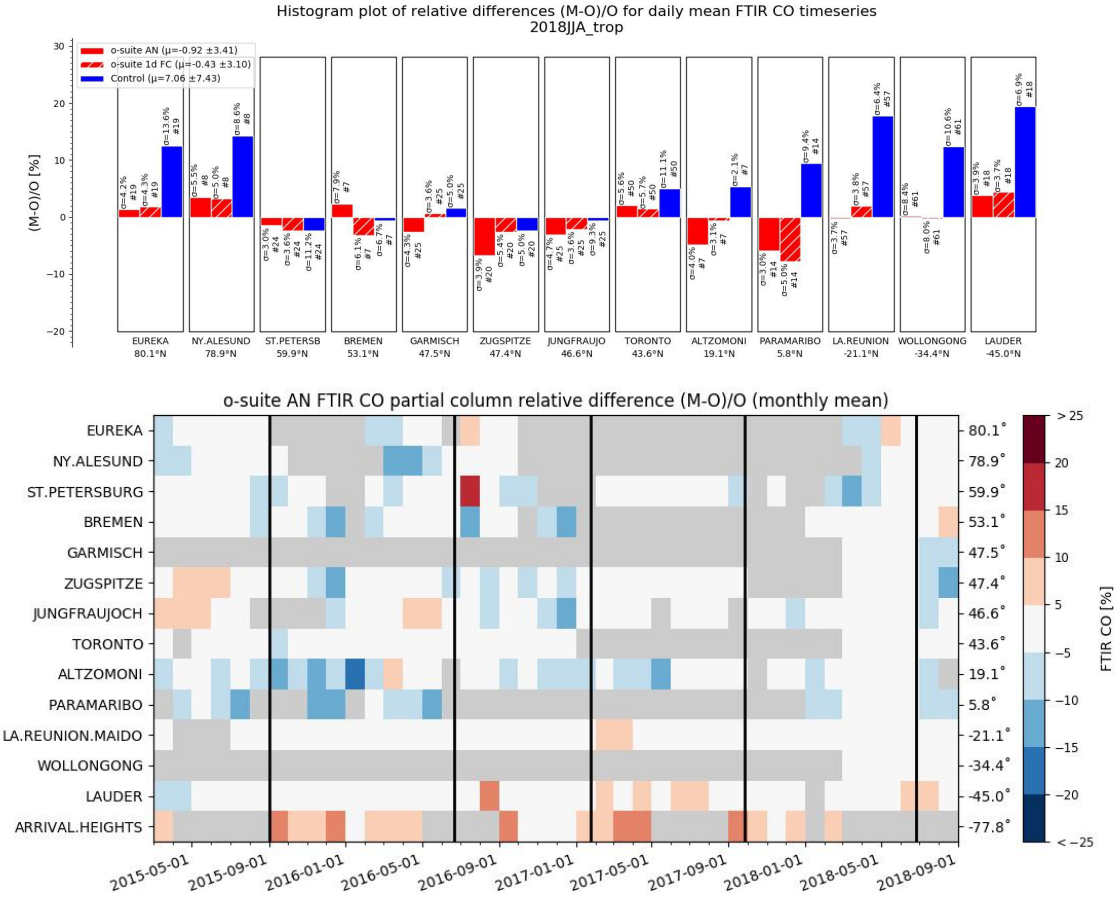

Figure 4.3.1: Seasonal relative mean bias for tropospheric CO columns (MB, %), standard deviation (STD, %) and number of observations used for the considered period JJA (top) and monthly mean biases for a longer time period (bottom, model upgrades are indicated in black).The overall uncertainty for the CO measurements is approximately 5% and the osuiteAN averaged bias for all stations is -1%. Stations are sorted with decreasing latitude (northern to southern hemisphere).

4.3 Validation against FTIR observations from the NDACC network

In this section, we compare the CO profiles of the CAMS models with FTIR measurements at different FTIR stations within the NDACC network. These ground-based, remote-sensing instruments are sensitive to the CO abundance in the troposphere and lower stratosphere, i.e. between the surface and up to 20 km altitude. Tropospheric CO profiles and columns are validated. A description of the instruments and applied methodologies can be found at http://nors.aeronomie.be.

Figure 4.3.1 show that the o-suite tropospheric columns of CO agree well with the FTIR data. All biases for the o-suite AN and 1d FC are within the measurements uncertainty. For the NH mid latitude stations, the bias has become slightly negative (<-5%) in JJA compared to the previous reporting period MAM 2018. For the SH, the bias changes sign but remains within the 5% range.

For all stations in the southern hemisphere, the control run overestimates the CO with MBs up to 20%.

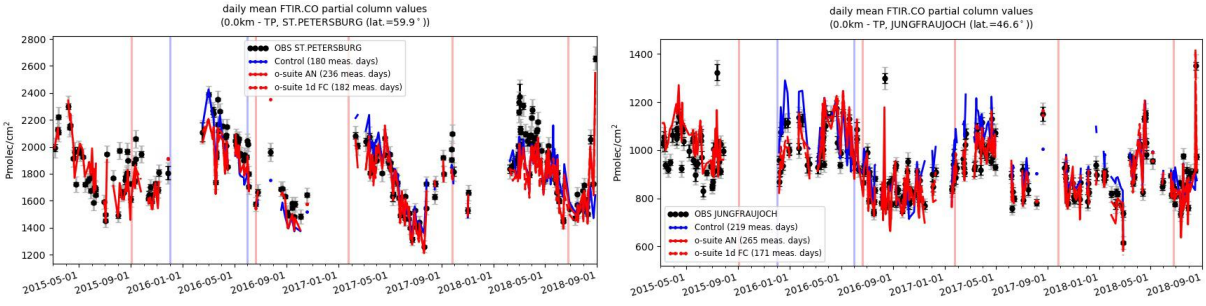

Figure 4.3.2: Daily mean values of tropospheric CO columns by the o-suite (AN and 1d FC, red) and the Control run (blue) compared to NDACC FTIR data at St Petersburg and Jungfraujoch for the period March 2015-August 2018. During March 2018 the osuite underestimated the CO columns at St. Petersburg.

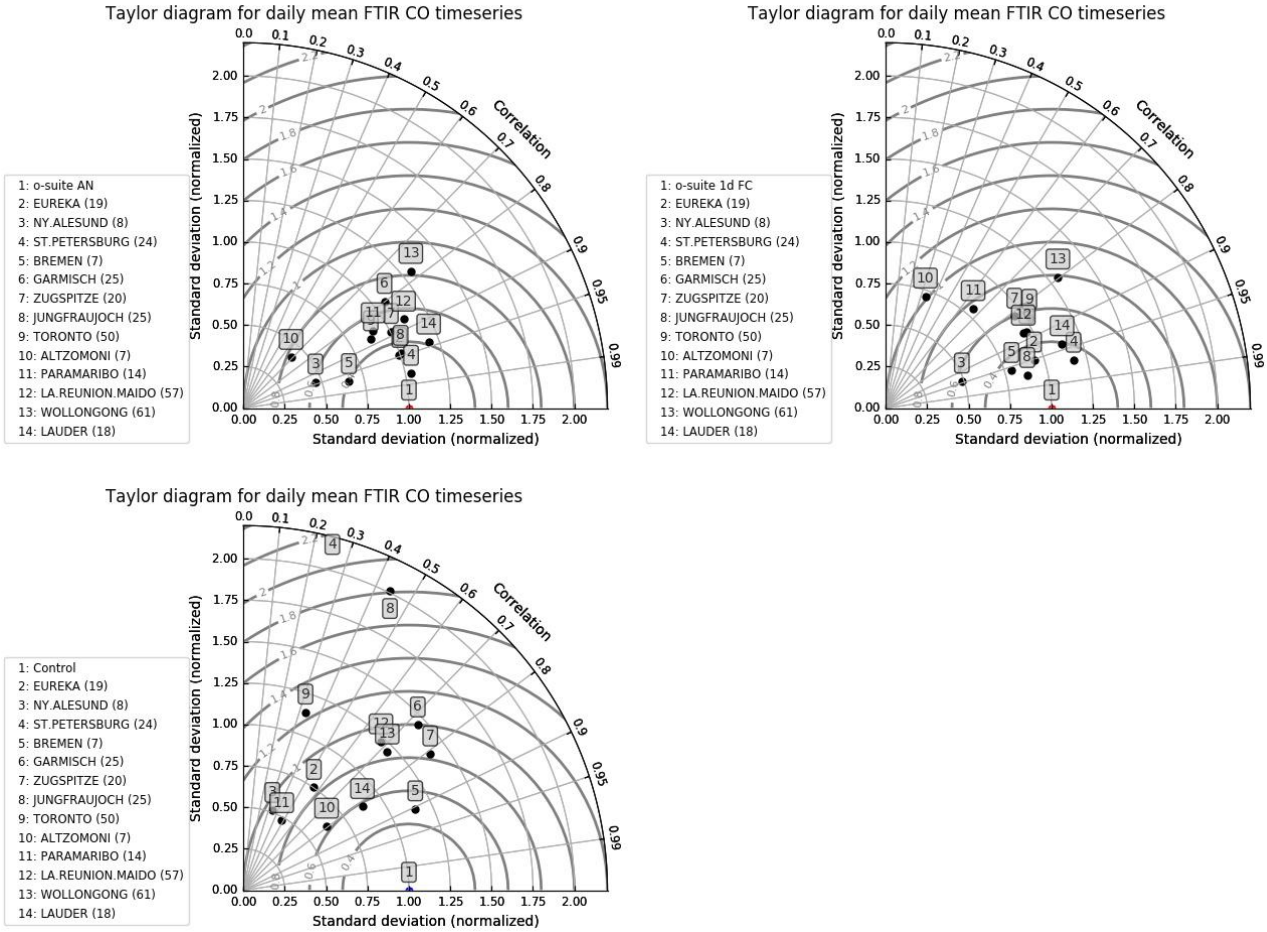

Figure 4.3.3: Taylor diagrams relating the standard deviations for the model / ground-based time series of tropospheric CO column data and their correlation, for o-suite analysis (top-left), o-suite 1-day forecast (top-right) and control (bottom). All time series are normalized such that the std of the model is 1. The o-suite FC and control run have higher variability in the CO columns. For the o-suite AN the std corresponds to the measurements std (leaving out stations 10,3,5 with low measurement count).

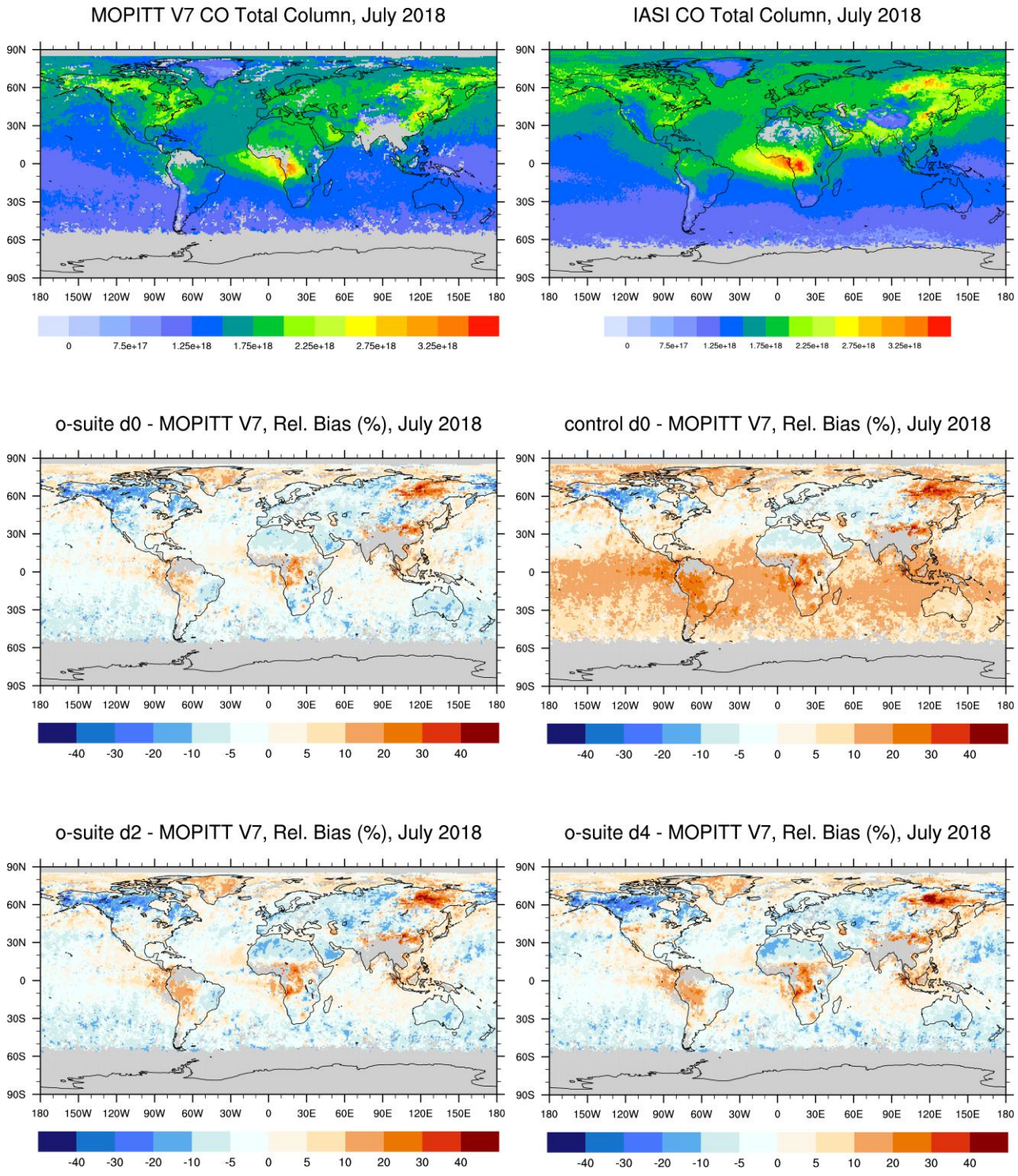

Fig. 4.4.1: CO total columns for MOPITT V7 (top left) and IASI (top right) satellite retrievals and relative difference between the model runs and MOPITT for July 2018: o-suite (middle left), control run (middle right), o-suite 2nd forecast day (bottom left), o-suite 4th forecast day (bottom right). Grey color indicates missing values.

The Taylor diagrams in Figure 4.3.3 provide information on the correlation of all three models under consideration with the FTIR time series. Leaving out the sites with few measurements, the assimilation has a positive effect on the correlation coefficient. Looking at the correlation values, the o-suite 1d FC (averaged correlation for all sites is 0.84) seems to perform slightly worse

compared the o-suite AN (averaged correlation for all sites is 0.88). The variability in the FTIR tropospheric columns is in general smaller than the variability of the corresponding model columns (approximately by a factor of 0.9).

4.4 Evaluation with MOPITT and IASI data

In this section, modeled CO total columns are compared to MOPITT versions 6 and 7 (thermal infrared radiances) (Emmons et. al., 2009, Deeter et al., 2010) and IASI satellite retrievals (Clerbaux et al., 2009). Figure 4.4.1 shows the global distribution of CO total columns retrieved from MOPITT V7 (top left) and IASI (top right) and the relative biases of the model runs with respect to MOPITT V7, averaged for July 2018.

In July 2018, both, MOPITT and IASI show high CO values over the biomass burning area in central Africa, over Siberia and north-east of China. IASI observations show somewhat higher values than MOPITT. The modeled CO geographical distribution and magnitude of values show that the model performs reasonably well. The relative difference between the model runs and MOPITT shows that both model runs have positive biases over Siberia and North-east China (up to 50 %) and over biomass burning areas in central Africa (up to 40%). Also, the control run shows an overestimation of CO total columns over biomass burning regions in South America (up to 40 %). Both model runs show negative biases over Alaska by about 20%. In general, the o-suite performs better than the control run without data assimilation, with some overestimation (by about 10%) in the equatorial region and high northern latitudes over the ocean with some regional exceptions and underestimation (by about 10%) in the mid-latitudes. The control run shows overestimations in the Southern Hemisphere by about 20-30% and in the high northern latitudes over the ocean (up to 20%) and underestimations over large parts of Eurasia and North Africa (by about 10%).

Figure 4.4.1 shows no significant difference between the o-suite analysis and 2nd and 4th forecast days, but a slightly growing positive bias over the fire active regions. Figure 4.4.2 shows time series of CO total column for MOPITT V6 and V7, IASI and the model runs over the eight selected regions. For the comparison with MOPITT, the modelled CO concentrations were transformed using MOPITT V7 averaging kernels (Deeter, 2004). Both, MOPITT and IASI CO total columns are assimilated in the o-suite run, while a bias correction scheme is applied to IASI data to bring it in line with MOPITT.

MOPITT and IASI CO total columns show a relatively similar variability over different regions. IASI CO values were lower compared to MOPITT over most regions with some seasonal exceptions till 2016. Since then IASI and MOPITT are more consistent over Europe, US and East Asia regions. Significant difference between MOPITT and IASI data are observed over the Alaskan and Siberian fire regions in winter seasons, with IASI CO total column values lower up to 30 %. In North and South Africa, deviations become larger since 2016 with IASI values higher than MOPITT up to 20%. Modelled seasonality of CO total columns is in relatively good agreement with the retrievals. In general, the comparison between the o-suite and control runs shows that assimilation of satellite CO has a more positive, pronounced impact on model results over East and South Asia, South Africa, and since the

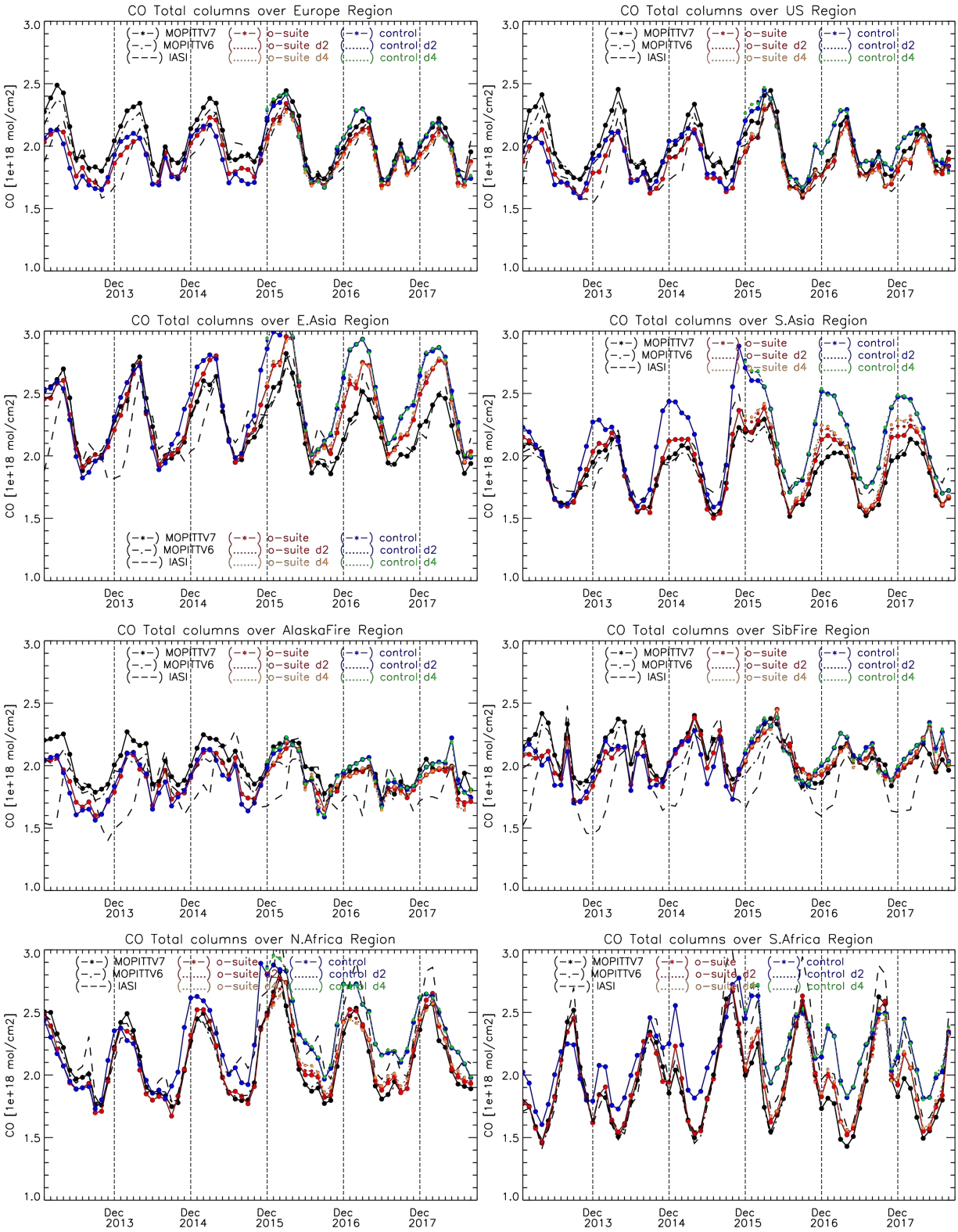

Fig. 4.4.2: Time series of CO total columns for satellite retrievals MOPIT V6 and V7, IASI (black) and the model runs over the selected regions: o-suite (red, solid), control (blue, solid), o-suite 2nd forecast day (red, dotted), o-suite 4th forecast day (orange, dotted), control 2nd forecast day (blue, dotted), control 4th forecast day (green, dotted).

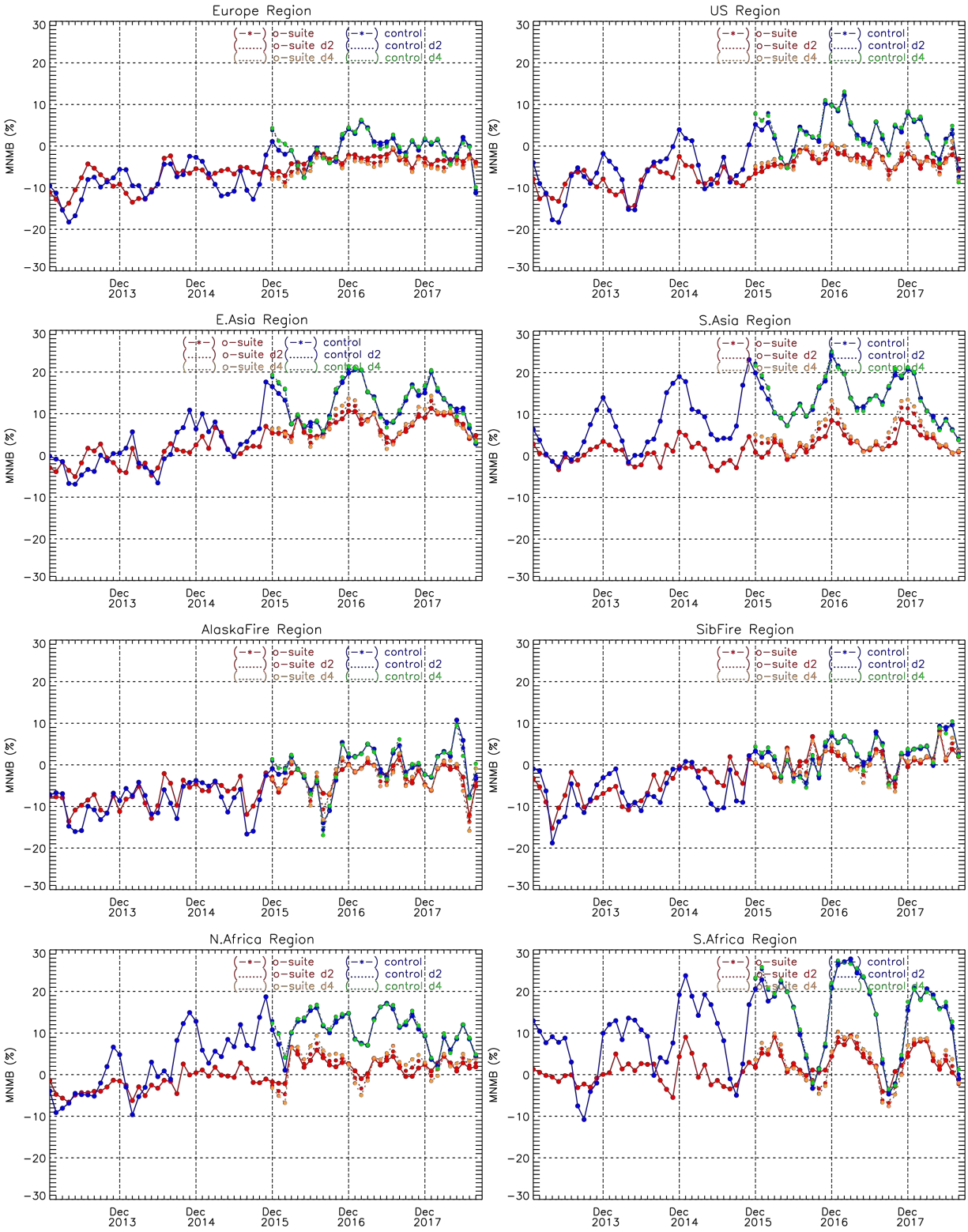

Fig. 4.4.3: Modified normalized mean bias (%) for CO total columns from the model simulations vs MOPITT V7 retrievals over selected regions. O-suite (red, solid), control run (blue, solid), o-suite 2nd forecast day (red, dotted), o-suite 4th forecast day (orange, dotted), control 2nd forecast day (blue, dotted), control 4th forecast day (green, dotted).

end of 2016 over US region in winter and spring seasons, and smaller impact over the other regions. Since June 2016 the o-suite shows very good agreement with the satellite retrievals over Europe and the US regions with biases less than 5%. During summer 2018, which is seasonal minimum in North Africa and south Asia, the control run shows a better performance compared to previous summers, reflecting in smaller positive biases. In July 2018, over the Alaskan fire region an untypical underestimation of satellite data by both model runs shows up (more details will be shown in the case studies section).

The modified normalized mean bias (MNMB) of the model runs compared to MOPITT V7 (Fig. 4.4.3) allows quantifying the impact of the assimilation on the model performance. The o-suite model run shows negative biases over Europe, the US and Alaskan fire regions with some seasonal exceptions. The control run shows a systematic positive bias up to 20% over South Asia in November-December 2014, 2015, 2016, and 2017. Over Southern Africa the control run overestimates satellite retrieved values up to 25% in the seasonal maximum in winter and spring 2015, 2016, and 2017. In general, the o-suite is within +/- 10% in all regions, while the control run shows larger biases in East and South Asia and North and South Africa, as well as stronger seasonal cycles. For the control run, d0, d2 and d4 forecast days are almost similar. For the o-suite run, d2 and d4 forecast days show growing positive/negative biases up to 5% compared to the analysis d0 in East and South Asia and North and South Africa.

In August 2018 the control run shows untypical negative biases of about 10% over Europe, while the o-suite follows its typical value by about -5%. In the same month, over the US the control run has a -6% bias and growing negative biases for the forecast day 4 up to -10%. In Alaska, the o-suite shows an untypical negative bias of more than 10% in July, while biases in control run are slightly smaller. For the Siberian fire region the o-suite run is in good agreement with the observations, while the control run shows a positive bias by about 10% in June and July. In North Africa and South and East Asian regions the control run shows better performance compared to previous summers (positive bias is less than 10%) and o-suite is very close to observations with almost no bias.

5. Tropospheric nitrogen dioxide

5.1 Evaluation against GOME-2 retrievals

In this section, model columns of tropospheric NO_2 are compared to SCIAMACHY/Envisat NO_2 satellite retrievals (IUP-UB v0.7) [Richter et al., 2005] for model data before April 2012, and to GOME-2/MetOp-A NO2 satellite retrievals (IUP-UB v1.0) [Richter et al., 2011] for more recent simulations. This satellite data provides excellent coverage in space and time and very good statistics. However, only integrated tropospheric columns are available and the satellite data is always taken at the same local time, roughly 10:00 LT for SCIAMACHY and 09:30 LT for GOME-2, and at clear sky only. Therefore, model data are vertically integrated, interpolated in time and then sampled to match the satellite data. GOME-2 data were gridded to model resolution (i.e. 0.4° deg x 0.4° deg). Model data were treated with the same reference sector subtraction approach as the satellite data. Uncertainties in NO_2 satellite retrievals are large and depend on the region and season. Winter values in mid and high latitudes are usually associated with larger error margins. As a rough estimate, systematic uncertainties in regions with significant pollution are on the order of 20% – 30%.

Figure 5.1.1 shows global maps of GOME-2 and model monthly mean tropospheric NO_2 columns as well as differences between retrievals and simulations for August 2018 as an example of the maps for summer 2018. The overall spatial distribution and magnitude of tropospheric NO_2 is well reproduced by both model runs, indicating that emission patterns and NO_x photochemistry are reasonably represented. Some differences are apparent between observations and simulations, with generally larger shipping signals simulated by the models. For example, shipping signals are much more pronounced in model simulations to the south of India. Emissions over central European pollution hotspots around the Benelux countries are underestimated. However, other local maxima of values observed over anthropogenic emission hotspots in East Asia (e.g. over the heavily populated Sichuan Basin; 30°N, 105°E), India and others such as Teheran, Mecca, around Lebanon/Israel and Moscow are overestimated. NOx boreal forest fire emissions over Siberia and Alaska/Canada seem to be overestimated by both model runs (see http://gmes-atmosphere.eu/d/services/gac/nrt/fire_radiative_power/ to compare to satellite based fire radiative power), a feature which reoccurs during fire seasons in these regions and is known from previous NRT reports. Note that an overestimation also occurs in the same regions for HCHO, though less pronounced.

Closer inspection of the seasonal variation of tropospheric NO_2 in some selected regions (Fig. 5.1.2) reveals significant differences between the models and points to some simulation problems. Over regions where anthropogenic emissions are major contributors to NO_x emissions, models catch the shape of the satellite time series rather well. However, over East-Asia absolute values and seasonality were in previous years strongly underestimated by all model runs (most likely due to an underestimation of anthropogenic emissions) for all seasons apart from summertime minima, with the o-suite showing the best results since an upgrade in July 2012. As wintertime NO_2 column retrievals decreased since 2014, model simulated wintertime maxima are in better agreement with the satellite retrieved ones for recent years. However, this decrease in values is not reproduced by the simulations which in contrast to satellite observations show an increase over the complete

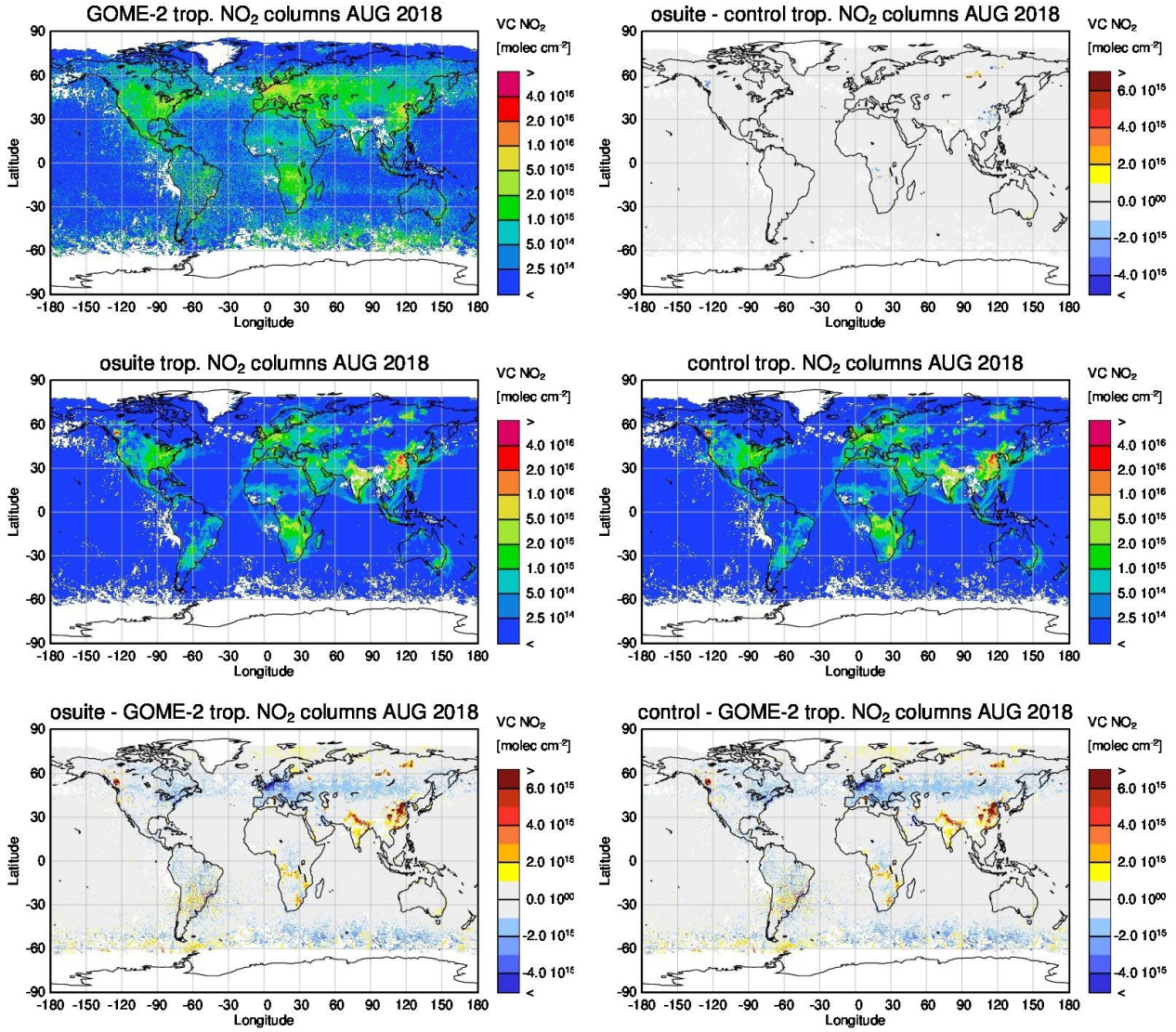

Figure 5.1.1: Global map comparisons of satellite retrieved and model simulated tropospheric NO_2 columns [molec cm^{-2}] for August 2018. The top row shows monthly mean tropospheric NO_2 columns retrieved by GOME-2 as well as the difference between o-suite and control, the second row shows the corresponding tropospheric NO_2 columns for model simulated averages. The third row shows differences of monthly means between models and GOME-2. GOME-2 data were gridded to model resolution (i.e. 0.4° deg x 0.4° deg). Model data were treated with the same reference sector subtraction approach as the satellite data.

timeseries of simulations available and as such, the better agreement for more recent years cannot be attributed to an improvement of the simulations. Moreover, summertime model minima increased in 2015 compared to previous years, which is in contrast to the satellite retrievals, so that the simulated values for the summers since 2015 are about 50% larger than satellite retrieved ones. The observed July and August means of 2018 over East-Asia are a bit lower compared to previous years, but it has to be seen if this trend continues over the next summers. As for East-Asia, a decrease in satellite retrieved values also occurred in 2015 over Europe where a peak is usually found around January, which was, as a result, only slightly underestimated by the models for January 2015. The underestimation of tropospheric NO_2 columns over Europe may be caused to some extent by a change of emission inventories in 2012. However, the situation changed over the

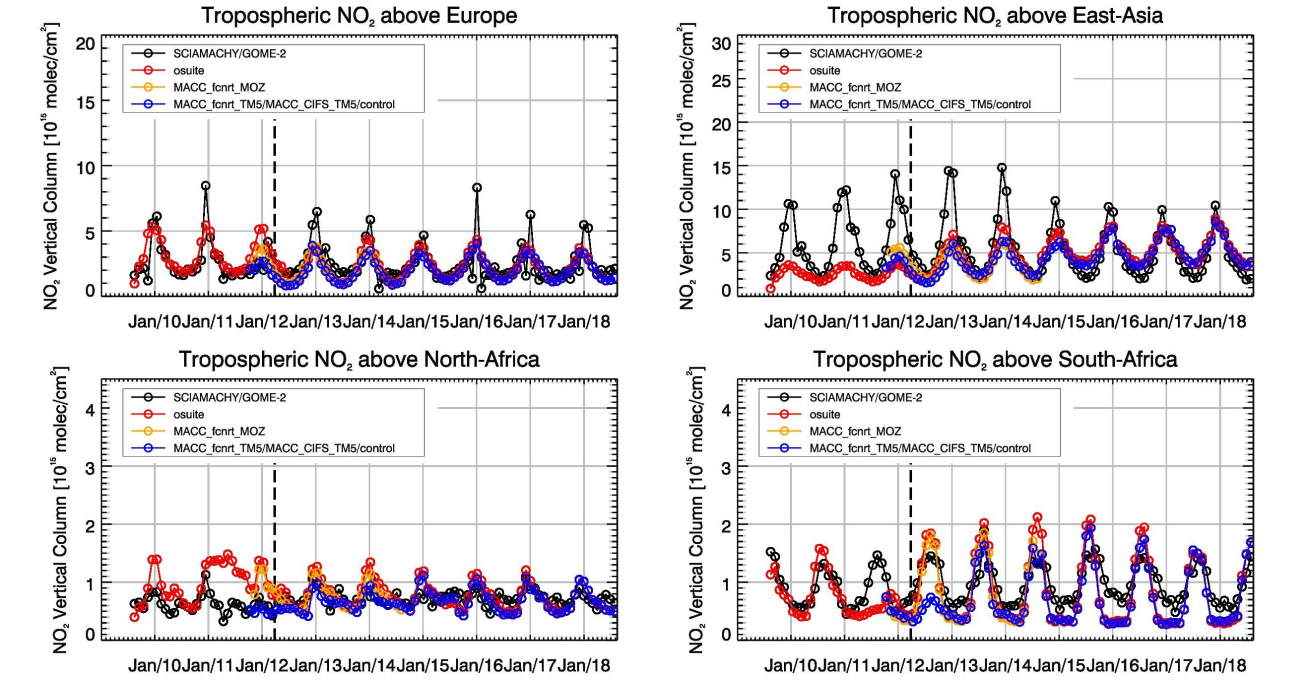

Figure 5.1.2: Time series of average tropospheric NO_2 columns [10^{15} molec cm^{-2}] from SCIAMACHY (up to March 2012) and GOME-2 (from April 2012 onwards) compared to model results for different regions (see Annex 2 for definition of regions). Upper panels represent regions dominated by anthropogenic emissions, lower panels represent those dominated by biomass burning. The blue line shows MACC_fcnrt_TM5 from November 2011 to November 2012, MACC_CIFS_TM5 results from December 2012 to August 2014 and control results from September 2014 onwards (the model run without data assimilation is termed control since Sep 2014). Vertical dashed black lines mark the change from SCIAMACHY to GOME-2 based comparisons in April 2012.

last three winter periods, for which GOME-2 shows (compared to previous years) a strong increase in January peak values, combined with a decrease in values for December and February, that is not reproduced by the models. It is not clear if the GOME-2 observations are realistic here, although a first inspection of daily GOME-2 satellite images did not point to problems regarding the retrieval.

Over regions where biomass burning is the major contributor to NO_x emissions, seasonality and amplitude of model columns are determined by fire emissions. The seasonality for the two regions in Africa was simulated reasonably well for 2010 and after October 2011. In the time period in between, a bug in reading fire emissions lead to simulation errors for all MOZART runs. Over North-Africa, the o-suite shows improved results since an update in July 2012 and the change to IFS-CB05 in September 2014. However, tropospheric NO_2 columns around December are still overestimated by the models. Summertime NO_2 columns over North-Africa are underestimated compared to the satellite data from 2015 onwards. The models (especially the o-suite) generally overestimate the seasonal cycle for South-Africa, particularly for 2014 -2016 with an overestimation of the seasonal maximum which usually occurs around August (e.g. by a factor of 1.4 larger compared to GOME-2 retrievals in 2016). However, summertime values are in better agreement since the upgrade of the o-suite in 2017, but summertime minima remain underestimated.

For details on the NO_2 evaluation: http://www.doas-bremen.de/macc/macc_veri_iup_home.html.

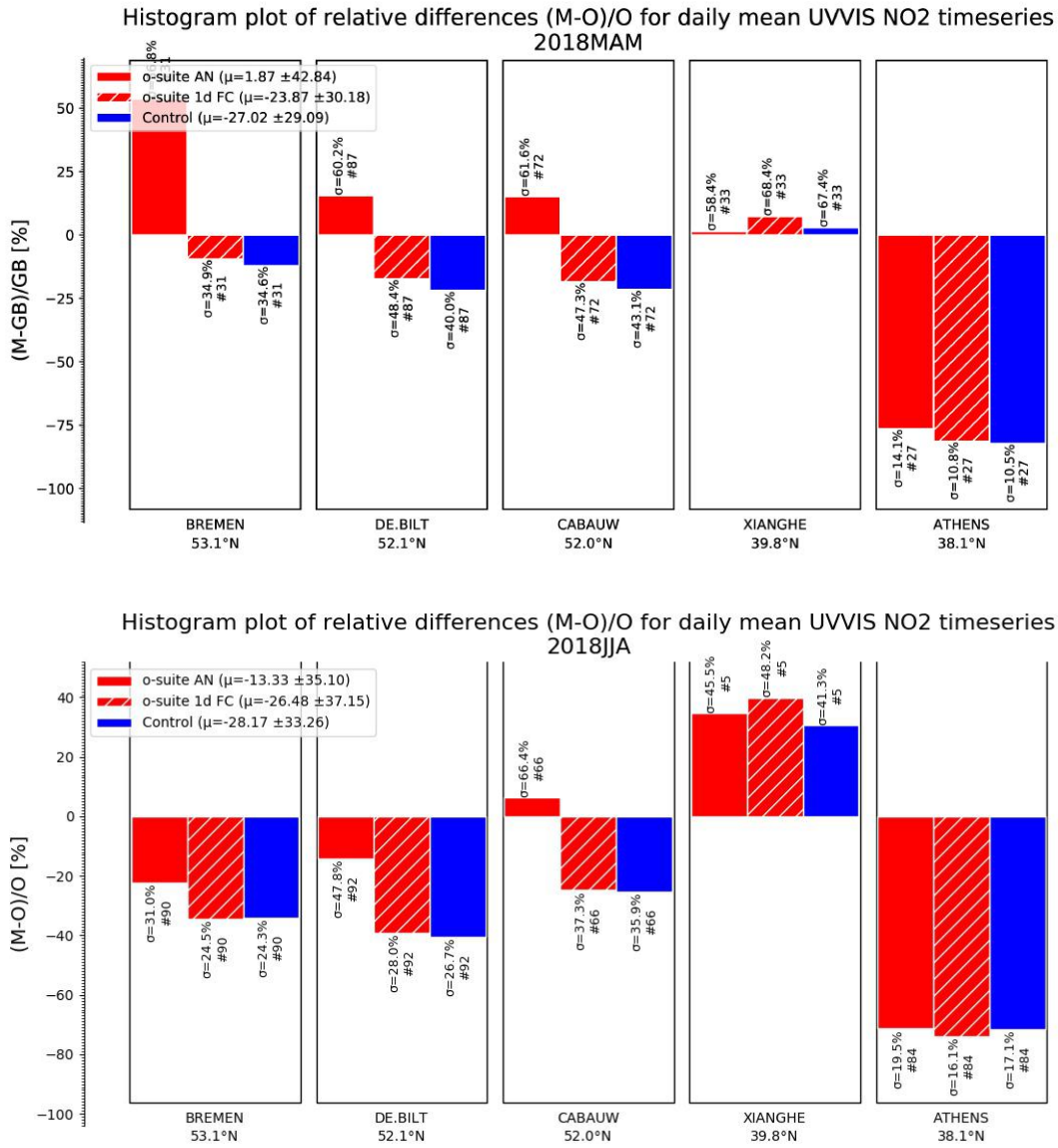

Figure 5.2.1: Table diagram showing the seasonal bias (March-May and June –August 2018) for five stations, sorted by latitude. Compared to the previous validation period MAM, the relative biases in JJA have changed from positive to negative for Bremen and De Bilt for the osuiteAN.

5.2 Evaluation against ground-based DOAS observations

In this section, we compare the NO_2 columns of the CAMS models with UVVIS DOAS profile measurements at Xianghe (39.8°N, 117°E, station near Beijing, altitude 92m) and column data from the other stations.[1] This ground-based, remote-sensing instrument is sensitive to the NO_2 abundance in the lower troposphere, up to 1km altitude with an estimated uncertainty of 8%. Tropospheric NO_2 profiles and columns are validated (up to 3.5km or 10km). A description of the instruments and applied methodologies is the same all DOAS OFFAXIS measurements, see

[1] No contribution from Reunion and OHP due to instrument failure.

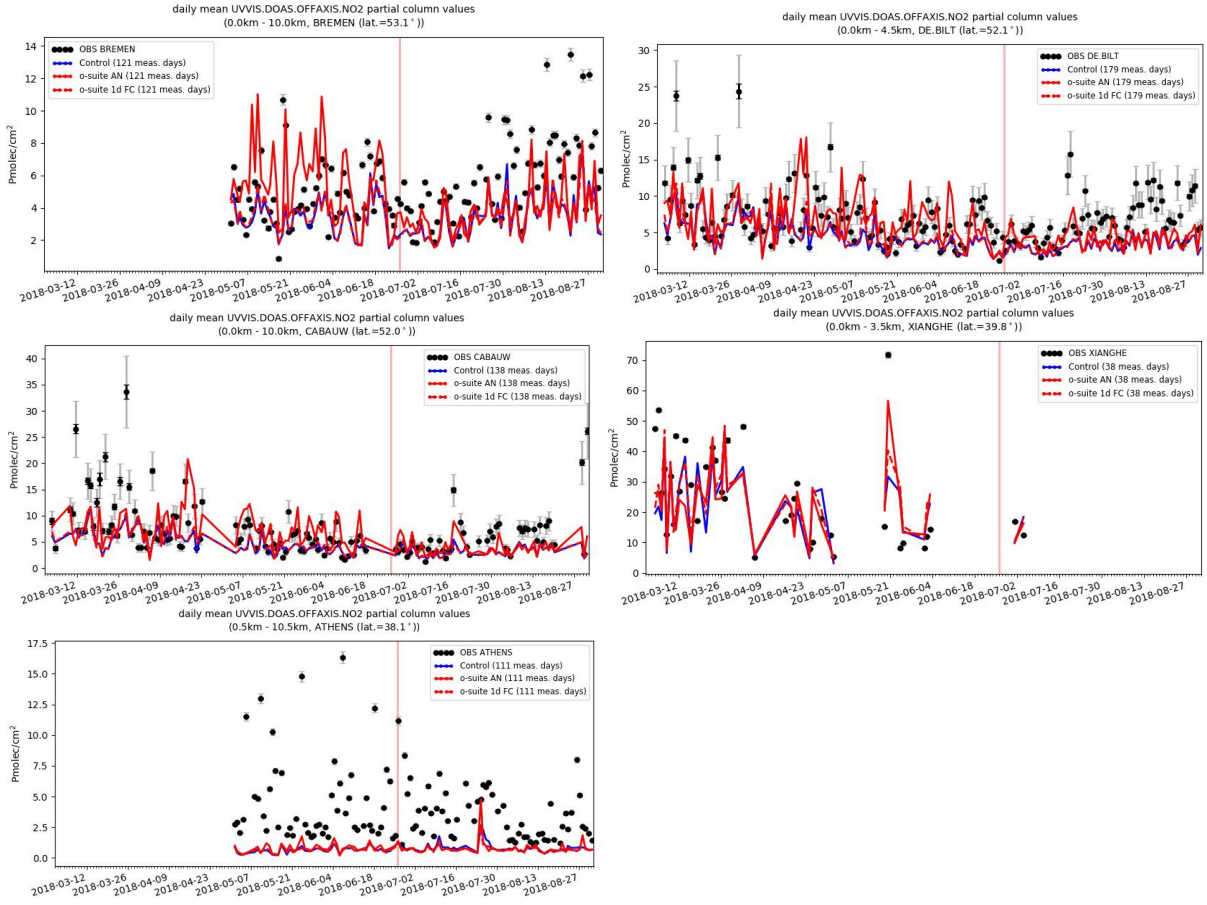

Figure 5.2.2: Time series of NO_2 partial columns at the five different sites. For all sites except Athens, background concentrations are well captured by the model and the o-suite AN seems to miss the high pollution days since the model update in June 2018.

http://nors.aeronomie.be. It is important to mention here that the model partial column values are calculated from the smoothed model profiles. This guarantees that the model levels where the measurement is not sensitive do not contribute to the observed bias. We should mention that the measurement data is still catalogued as rapid delivery and not in the consolidated NDACC database.

Fig. 5.2.1 shows the biases for the latest validation periods March-May and June-August 2018 at the different sites. Both Bremen and Athens are outliers (both stations cover the time period only partially Fig 5.2.2). At Athens a strong underestimation is observed. The o-suite AN was able to capture some of the high pollution events in the previous validation period, but for the JJA period, the high pollution events at Bremen, De Bilt and Cabauw are not well captured.

6. Formaldehyde

6.1 Validation against satellite data

In this section, simulations of tropospheric formaldehyde are compared to SCIAMACHY/Envisat HCHO satellite retrievals (IUP-UB v1.0) [Wittrock et al., 2006] for model data before April 2012 and to GOME-2/MetOp-A HCHO data (IUP-UB v1.0) [Vrekoussis et al., 2010] afterwards. As the retrieval is performed in the UV part of the spectrum where less light is available and the HCHO absorption signal is smaller than that of NO_2, the uncertainty of monthly mean HCHO columns is relatively large (20% – 40%) and both noise and systematic offsets have an influence on the results. However, absolute values and seasonality are retrieved more accurately over HCHO hotspots.

In Figure 6.1.1, monthly mean satellite HCHO columns are compared to model results for August 2018. The magnitude of oceanic and continental background values and the overall spatial distribution are well represented by the o-suite and control. The models overestimate values over Northern Australia, Indonesia/Malaysia and Central Africa which could be fire or biogenic emissions. The same is true for boreal fire emissions over Siberia and Alaska/Canada, where an overestimation is also found for tropospheric NO_2 (see chapter 3.2) which is more pronounced though.

Time series in Fig. 6.1.2 highlight three cases:

- East-Asia and the Eastern US, where HCHO is dominated by biogenic emissions. Model results and measurements generally agree rather well. However, all model runs underestimate the yearly cycle over East-Asia since 2012. In contrast to MOZART runs, MACC_CIFS_TM5 overestimated satellite values for the Eastern US since the middle of 2013. However, the newer IFS-CB05 runs perform well for Eastern US since 2015. For recent years and both regions, there is virtually no difference between the most recent o-suite run with IFS-CB05 chemistry and the corresponding control run without data assimilation. The variability or “ups and downs” in HCHO columns observed by GOME-2 since December 2014 is due to the lack of data (caused by instrument degradation) for these regions during Northern Hemisphere winter months (see Fig. 6.1.1 for the spatial coverage of HCHO data in December 2017). This also explains the negative values in the GOME-2 time series for Eastern US which occur in the time series since December 2015 and is a likely reason for the relatively large underestimation of values during DJF 2016/2017 by the models compared to the retrievals. Summertime maxima are still underestimated by the now higher resolution runs over East-Asia since 2016.
- North-Africa, where biomass burning as well as biogenic sources largely contribute to HCHO and its precursors. Satellite observations over North-Africa are generally slightly overestimated by IFS-CB05 chemistry model runs since 2014 and also the latest higher resolution model versions since July 2016.

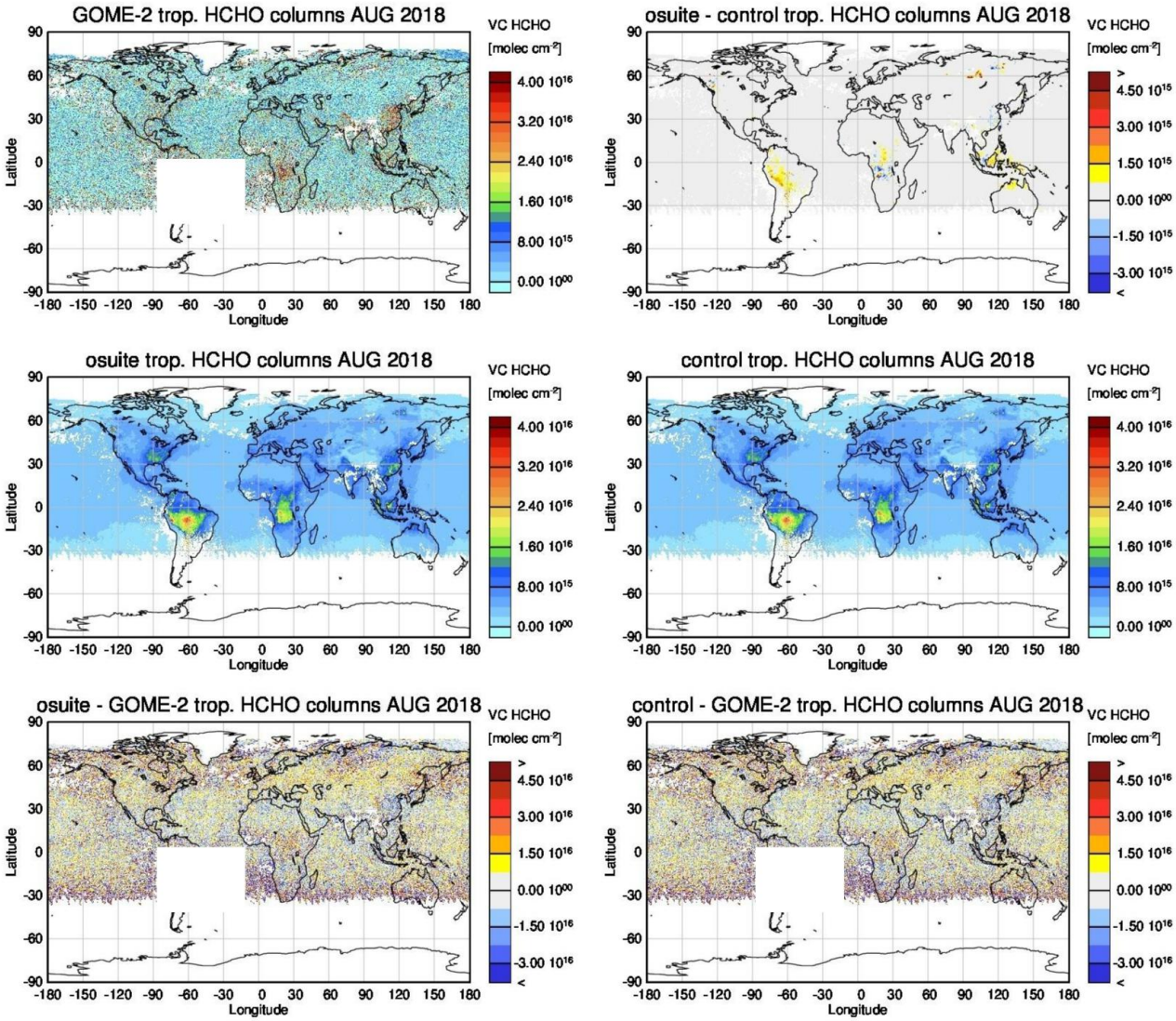

Figure 6.1.1: Global map comparisons of satellite retrieved and model simulated tropospheric HCHO columns [molec cm^{-2}] for August 2018. The top row shows monthly mean tropospheric HCHO columns retrieved by GOME-2, the second row shows the same but for model simulated averages. The third row shows differences of monthly means between models and GOME-2. GOME-2 data were gridded to model resolution (i.e. 0.4° deg x 0.4° deg). Model data were treated with the same reference sector subtraction approach as the satellite data. Satellite retrieved values in the region of the South Atlantic anomaly are not valid and therefore masked out (white boxes in all images except those which show model results only).

- Indonesia, where HCHO is also dominated by biogenic sources and biomass burning. Old MOZART based model versions generally overestimated satellite values here (by a factor of 3 – 4 in the second half of 2010) and failed to reproduce the observed seasonality. This may be due to the use of fire emissions including El Nino years which experience much larger fire activities. MOZART simulations and observations agreed much better since late 2012. IFS-CB05 runs agree very well with satellite retrieved ones for December 2014 to August 2015. For September and October 2015, satellite retrieved HCHO columns show a pronounced maximum. 2015 was a strong El Nino year, which caused droughts and higher fire activity in Indonesia. As for previous

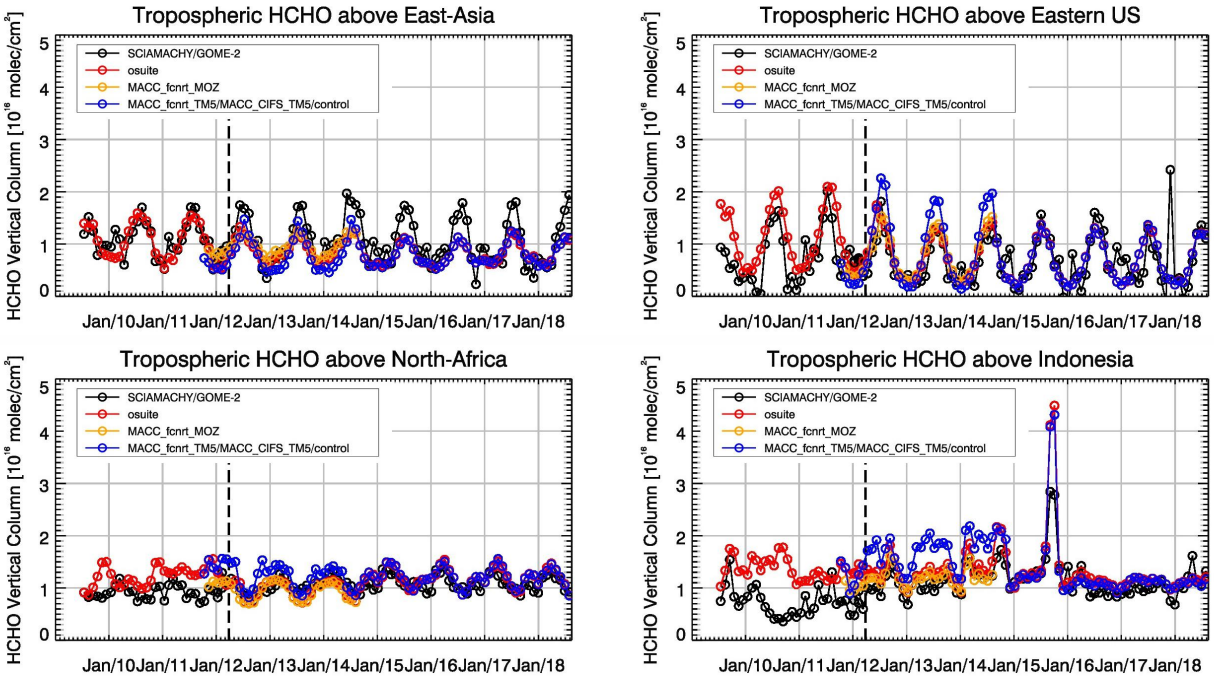

Figure 6.1.2: Time series of average tropospheric HCHO columns [10^{16} molec cm^{-2}] from SCIAMACHY (up to March 2012) and GOME-2 (from April 2012 onwards) compared to model results for different regions. The blue line shows MACC_fcnrt_TM5 from November 2011 to November 2012, MACC_CIFS_TM5 results from December 2012 to August 2014 and control results from September 2014 onwards (the model run without data assimilation is termed control since Sep 2014). The regions differ from those used for NO_2 to better focus on HCHO hotspots: East-Asia (25-40°N, 110-125°E), Eastern US (30-40°N, 75-90°W), Northern Africa (0-15°N, 15°W-25°E) and Indonesia (5°S-5°N, 100-120°E). Negative satellite retrieved values over Eastern US are due to a lack of data (caused by instrument degradation) during Northern Hemisphere winter months for this region. Vertical dashed black lines mark the change from SCIAMACHY to GOME-2 based comparisons in April 2012.

El Nino years, fire emissions used by IFS-CB05 seem to be largely overestimated, resulting in model simulated HCHO columns which are almost twice as large as those retrieved by GOME-2. Further investigations (see previous reports) show that this is not caused by cloud flagging applied to the satellite and model data. The recent higher resolution runs in general overestimate values over Indonesia as well. There is little variation from one month to another in both, satellite observations and model simulations since middle of 2016, apart from a decrease in retrieved HCHO columns for Dec 17/ Jan 18 and an increase in May 2018 which is not reproduced by the simulations.

For details on the HCHO evaluation: http://www.doas-bremen.de/macc/macc_veri_iup_home.html.

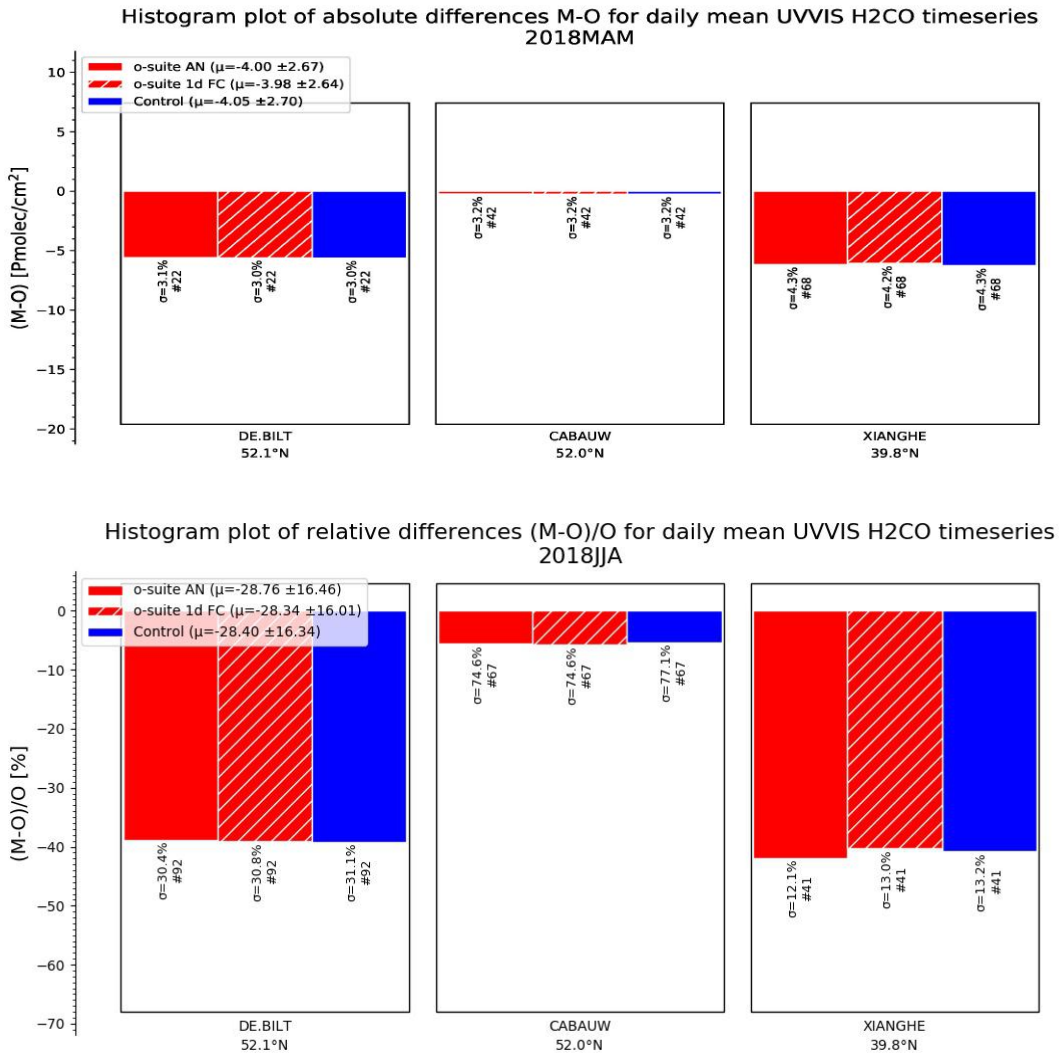

Figure 6.2.1: Table diagram showing the seasonal absolute bias (March–May and June-August 2018) for three stations, sorted by latitude. Due to some high pollution events at De Bilt and Xiange in JJA, biases have increased.

6.2 Evaluation against ground-based DOAS observations

In this section, we compare the H_2CO columns of the CAMS models with UVVIS DOAS measurements at Xianghe, Cabauw and De Bilt.[2] These ground-based, remote-sensing instruments are sensitive to the HCHO abundance in the lower troposphere. Tropospheric HCHO profiles and columns are validated (up to 3.5km (Xianghe) or 10km (Cabauw and De Bilt)). A description of the instruments and applied methodologies is the same as for the MWR O_3 and FTIR O_3 and CO validations see http://nors.aeronomie.be. It is important to mention here that the model partial column values are calculated for the smoothed model profiles. This guarantees that the model levels where the measurement is not sensitive do not contribute to the observed bias. We should

[2] No contribution from Reunion and OHP due to instrument failure.

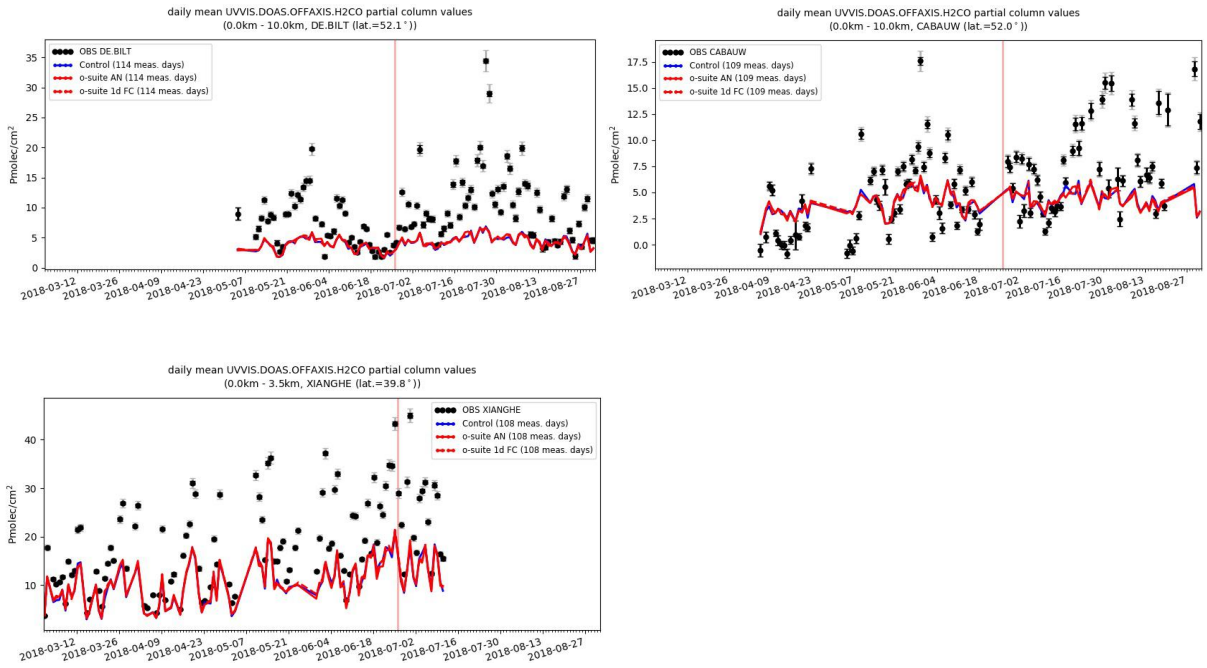

Figure 6.2.2: Time series of H2CO partial columns at the five different sites. All models underestimate the H2CO concentrations.

mention that the measurement data is still catalogued as rapid delivery and not in the consolidated NDACC database.

Fig. 6.2.1 shows the absolute biases for March-May and June-August 2018 at the different sites, which show an underestimation of all models at all sites. From Fig. 6.2.1 and 6.2.2 we see little difference between the o-suite and the control run. Although the background column values are well captured by the models, the high emission events are not.

7. Aerosol

7.1 Global comparisons with Aeronet and EMEP

The comparison of the CAMS simulation of time series of aerosol optical depth can be compared for all Aeronet stations via: http://aerocom.met.no/cams-aerocom-evaluation/

More detailed evaluation including scores, maps, scatterplots, bias maps and histograms illustrating the performance of the aerosol simulation in the IFS system are made available through the AeroCom web interface. The model run can be compared here to eg. the CAMS interim and other models, such as the AeroCom Median model.

Correlation, based on daily aerosol optical depth and NRT Aeronet observations, has been rather stable recently. The o-suite forecast at +3 days shows only slightly lower correlation. See figure S3.

Part of the month-to-month variation in correlation is due to the varying quality and coverage of the Aeronet network. This has been improved by the version 3 from Aeronet. We use therefore version 3 level 1.5 for all global comparison to Aeronet.

The performance of the o-suite model exhibits some seasonal variation in AOD depending on region (Fig. 7.1.1-a). Noteworthy is the persistent AOD overestimation over North America (Fig. 7.1.1-b), but also the change from underestimation to overestimation in East Asia since February 2017. The latitudinal display of model and Aeronet AOD in the period investigated here (Fig. 7.1.2) shows the positive bias against Aeronet NRT in the Southern but also Northern Hemisphere.

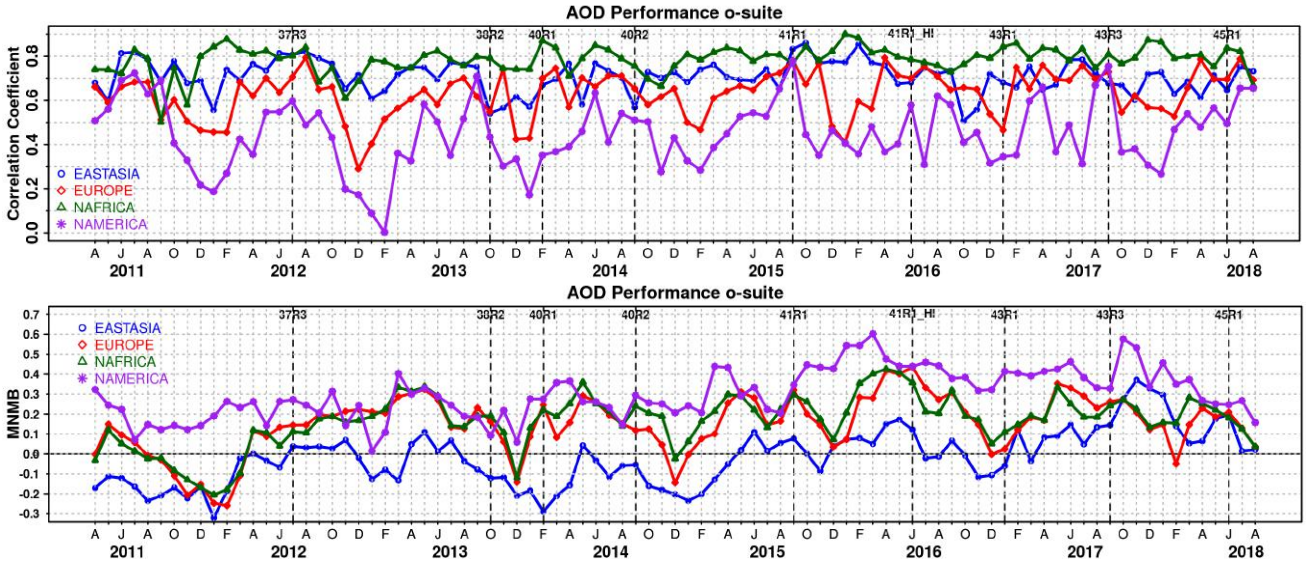

Figure 7.1.1. (top) Correlation coefficient and (bottom) modified normalized mean bias (MNMB) in AOD, since 2011, based on daily AOD comparison (Aeronet V3 level 1.5 data) in four world regions [Eastasia (blue); Europe (red); NAfrica (green); NAmercia (purple)] for the o-suite.

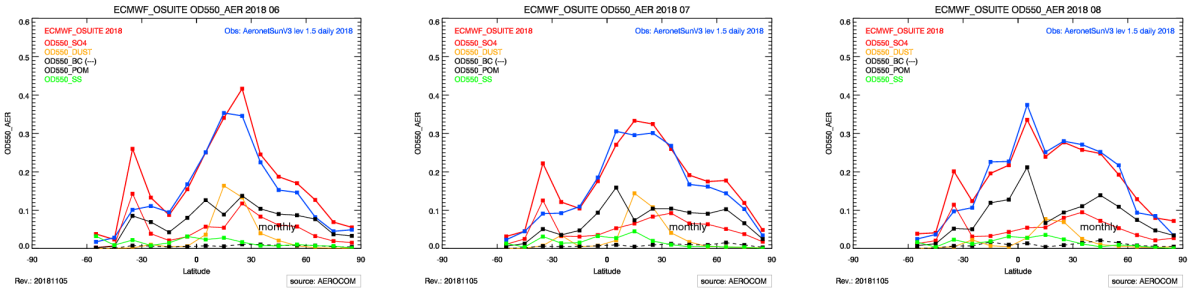

Figure 7.1.2. Aerosol optical depth of o-suite (red) compared to latitudinally aggregated Aeronet V3 level 1.5 data (blue) for the three months covered by this report.

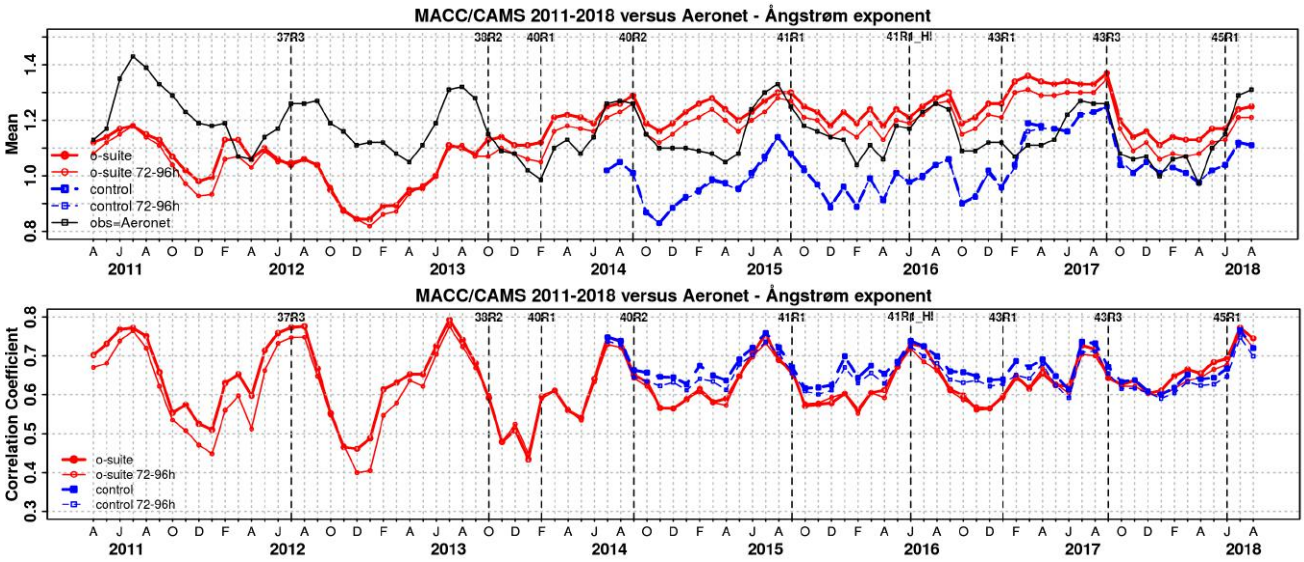

Figure 7.1.3. a) (top) Evolution of mean Ångström exponent in o-suite and control at Aeronet sites (Aeronet V3 level 1.5 data), based on matching monthly mean values. o-suite (thick red curve); o-suite at last forecast day (light red curve); control (blue dashed curve); control at last forecast day (light blue dashed curve). b) (bottom) Correlation using daily matching Ångström exponent.

The simulated aerosol size distribution may be validated to first order using the wavelength dependent variation in AOD, computed as Ångström exponent, with higher Ångström exponents indicative of smaller particles. We find in JJA 2018 a very small bias (Figure 7.1.3-a). Temporal and spatial variability is difficult to capture, but correlation from all daily data is higher than for AOD (Figure 7.1.3-b and S3). Figure 7.1.4 shows that the Sep 2017 and Jun 2018 model changes are responsible for a shift in Ångström exponent. More organic matter seems to shift the size distribution to smaller sizes. The model upgrade in Feb 2017 with a bugfix for sea salt and improved parameterisations for SO4 lead to sea salt increased with 45% while sulphate further decreased a bit. Also dust AOD had an increase on average, but this increase was found also in earlier years and reflects increased source strength in N-Africa in spring. Sea salt has increased further due to a new sea salt emission scheme implemented in the latest model upgrade and is back to earlier 2011-2013 levels.

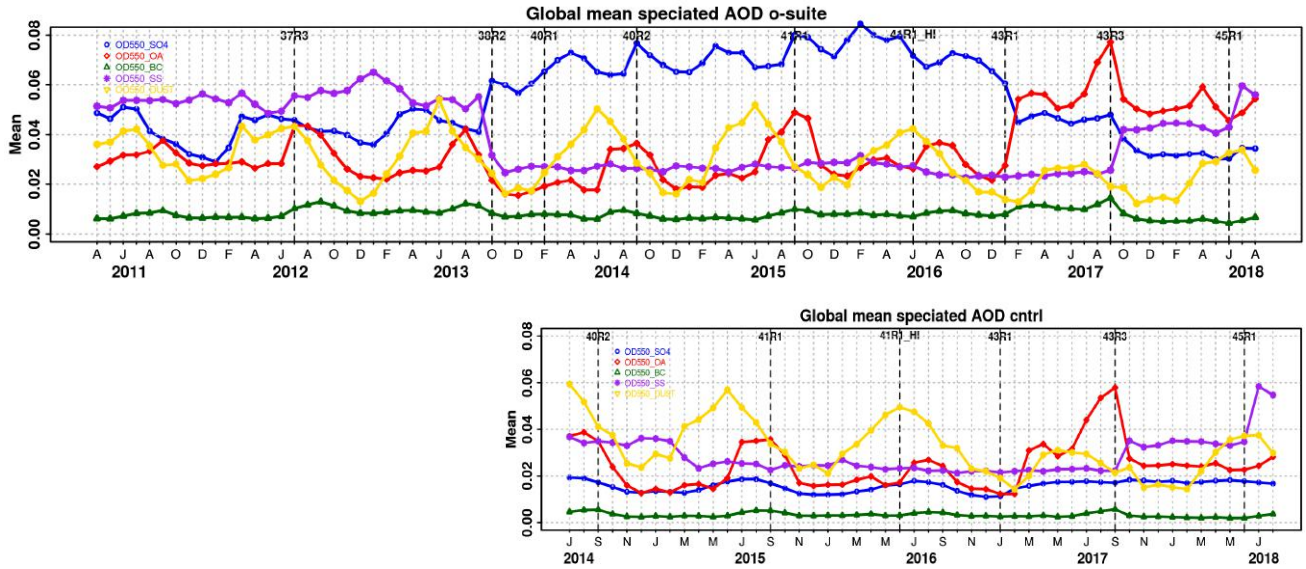

Figure 7.1.4. Evolution of the aerosol components of total AOD@550nm [OD550_SO4 = sulphate(blue); OD550_OA = organics(red); OD550_BC = black carbon(green); OD550_SS = sea salt(purple); OD550_DUST = dust(yellow)] in o-suite and control simulation.

The o-suite uses data assimilation to obtain a first guess aerosol field. In the forecast period, however, a-priori model parameterisations and emissions (except fire emissions, which are kept in the forecast equal to the latest GFAS emission values) determine more and more the shape and amplitude of the aerosol fields. The performance of the day three forecasted AOD fields as compared to the first guess is shown in Figure S3 in the summary of this report. Table 7.1.1 shows an average global decrease in total aerosol optical depth during the first four forecast days, dominated by sulphate and organics. The control run with no assimilation shows significant less AOD (-25% compared to o-suite, see figure S3). All this supports the conclusion that either a-priori IFS aerosol and aerosol precursor sources are too small or sinks are too effective in the IFS model.

Table 7.1.1. Mean global total and speciated AOD in the o-suite for the last two periods covered by the VAL report and change after 3 forecast days.

	o-suite		o-suite	
	Mean MAM 2018 0-24h	Change wrt to first day on day 4	Mean JJA 2018 0-24h	Change wrt to first day on day 4
AOD@550	0.126	-18%	0.172	-14%
BC-OD@550	0.005	-29%	0.005	-21%
Dust-OD@550	0.026	0%	0.031	3%
OA-OD@550	0.049	-30%	0.050	-24%
SO4-OD@550	0.032	-25%	0.033	-21%
SS-OD@550	0.043	-14%	0.053	-7%

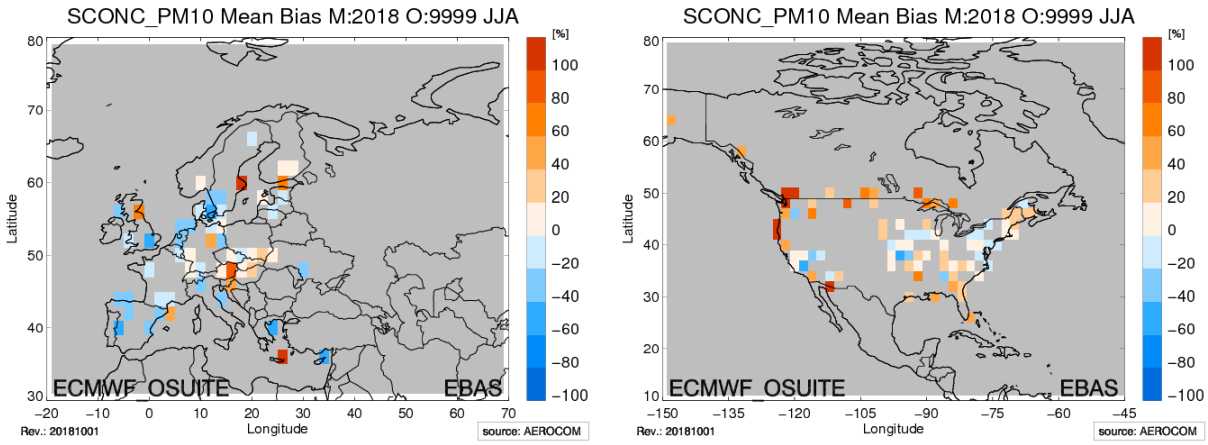

Figure 7.1.5. Bias [%] map of monthly mean PM10 concentrations at EMEP (Europe) and IMPROVE sites (North America); simulated o-suite versus EMEP/IMPOVE derived climatological average (2000-2009).

Surface concentration of particulate matter below 10 µm (PM10) from the o-suite experiment have been validated against data from 160 background IMPROVE and EMEP stations. A climatological average has been constructed from data in the period 2000-2009 as available in the EBAS database hold at NILU. The data availability is not the same at all stations, and sometimes covers only a few years.

A negative MNMB bias of in Europe and an overestimate in North America appears (figure 7.1.5), consistent with the AOD bias in the two regions. Figure 7.1.6 is showing the evolution of mean observed and simulated PM10. The biggest change appeared in July 2017 with the bias of o-suite now becoming positive overall. Shown is also the statistics of being within factor 2, a more robust metrics for a comparison to climatological data. This statistics has clearly improved over time, indicating best PM10 performance in summer months for the o-suite. O-suite is also better most of the times than the control simulation.

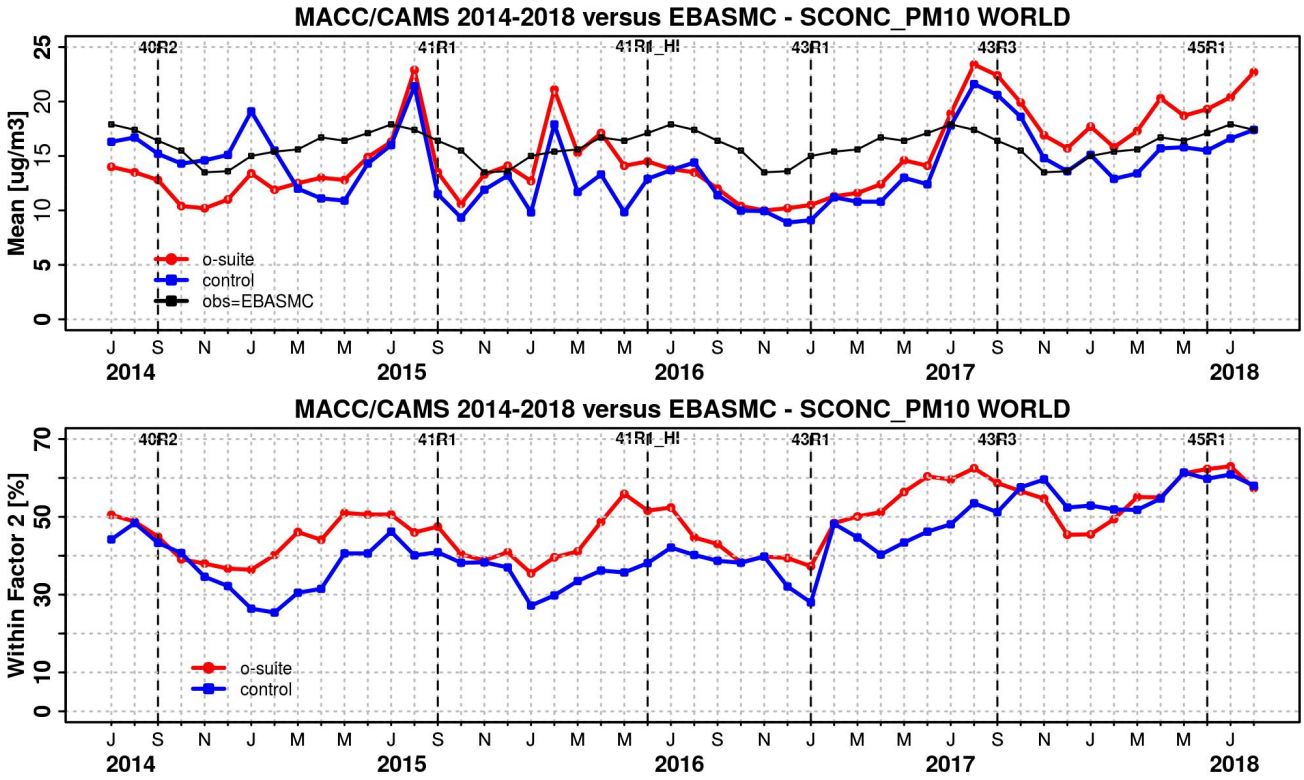

Figure 7.1.6. Temporal evolution of monthly mean average PM 10 concentrations at EMEP (Europe) and IMPROVE sites (North America) and data fraction within a factor 2 of observed; ca 160 sites, observed data averaged from data available in EBAS from 2000-2009.

7.2 Dust forecast model intercomparison: Validation of DOD against AERONET, and comparisons with Multi-model Median from SDS-WAS

The 72-hour forecasts (on a 3-hourly basis) dust aerosol optical depth (DOD) from CAMS o-suite and control have been validated for the period 1 June 2018 – 31 August 2018 against AERONET direct-sun cloud-screened observations, MODIS/Terra and Aqua Collection 6.1 Level 3 (1º x 1º) and SDS-WAS Multi-model Median DOD. The SDS-WAS Multi-model Median DOD is obtained from twelve dust prediction models participating in the Sand and Dust Storm Warning Advisory and Assessment System (SDS-WAS) Regional Center for Northern Africa, Middle East and Europe (http://sds-was.aemet.es/).

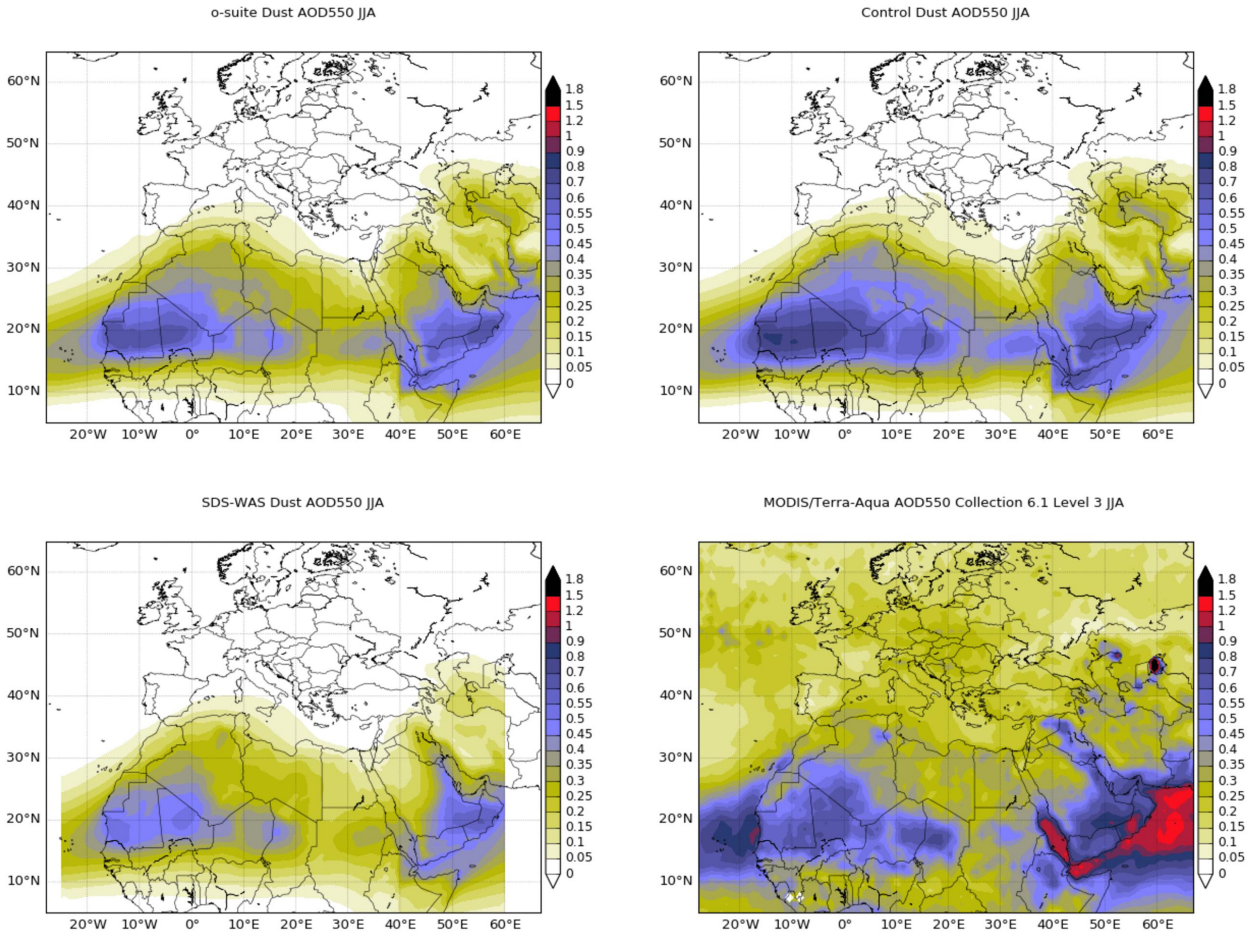

Figure 7.2.1: Averaged DOD 24h forecast from o-suite (top left) and control (top right), DOD of the multi-model SDS-WAS Median product (bottom left) as well as AOD from MODIS/Terra-Aqua Collection 6.1 Level 3 combined Dark target and Deep Blue product (bottom right) for the study period.

For the summer, the major dust activity is concentrated over the Sahara (in the Bodelé Basin and the Mali/Mauritania border as well as South Algeria, Sudan and Ethiopia) and the southern Arabian Peninsula (Southern Saudi Arabia, Oman and Yemen) and Iraq, as demonstrated by MODIS in Figure 7.2.1. The CAMS o-suite does forecasts the main areas of dust activity in the Sahara in comparison with MODIS, although the o-suite and control show higher DOD values over Mauritania (see Figure 7.2.1) in which also the SDS-WAS Multi-model product presents a lower signal. Otherwise, the North Atlantic dust transport appears strongly underestimated in comparison with MODIS. Over Capo Verde, CAMS o-suite showes a seasonal DOD average of 0.35, while MODIS observes a seasonal average up to 0.7 (not shown here), indicating that the CAMS model is underestimating the dust contribution. Over the Mediterranean, dust transport is observed over Central-Western parts of the Basin. In the Middle East, both CAMS experiments show maximum DOD concentrations over Oman and Yemen in agreement with the MODIS observations. The CAMS model underestimates the dust sources in Iraq, as shown by the comparison with MODIS (Figure 7.2.1).

For June to August, the o-suite reproduces the daily variability of AERONET observations with a correlation coefficient of 0.89, averaged over all the AERONET sites, while the control experiment and the SDS-WAS Multi-model show a correlation coefficient of 0.84 and 0.87 respectively. Regarding mean bias (MB), both CAMS experiments (o-suite and control), as well as the SDS-WAS Multi-model, underestimate the AERONET observations resulting in an MB of -0.03 for control and -0.05 for o-suite and the SDS-WAS Multi-model.

Tropical North Atlantic and Western/Central Mediterranean (see Santa Cruz de Tenerife and Tunis Carthage in Figure 7.2.2 and Table 7.2.1) regions present the best results in the AERONET comparison in terms of correlation. Both experiments can reproduce the daily variability with correlation coefficients between 0.90-0.94 (0.88-0.90) for o-suite (control). Over the Sahara (see Tamanrasset in Figure 7.2.2 and Table 7.2.1), o-suite shows better results than control with an increase of the correlation coefficient from 0.44 (control) to 0.56 (o-suite) although the o-suite shows a higher underestimation (MB of -0.08) than the control experiment which tends to overestimate the AERONET observations (MB of 0.05). The SDS-WAS Median Multi-model shows slightly better results than o-suite with a correlation coefficient of 0.59 for the Sahara, although it underestimates the observations with an MB of -0.11. In the Sahel (see Banizoumbou in Figure 7.2.2 and Table 7.2.1), the o-suite shows strong underestimations (MB of -0.21, slightly higher than control with MB of -0.10) although the model reproduces the observed daily variability (with a correlation value of 0.80 for o-suite and 0.71 for control). The strong underestimations observed in o-suite in the Sahel are also spread to the Tropical North Atlantic (MB of -0.27 for o-suite) in agreement with the underestimation observed in the comparison with MODIS (Figure 7.2.1).

In the North-Western Maghreb, the CAMS experiments show underestimations (MB of -0.15 for control and -0.21 for o-suite) in comparison with the AERONET observations and lower correlation coefficients in comparison with the SDS-WAS Median Multi-model (0.78 for o-suite, 0.64 for control and 0.81 for the SDS-WAS Median Multi-model). During summer, the maximum occurrence of strong and fast dust outbreaks occurs in the Sahara, associated with mesoscale convective systems. These convective systems are better resolved by the high-resolution regionals models that are included in the SDS-WAS Multi-model product.

In the Middle East (see Table 7.2.1 and the Kaust Campus and Mezaira AERONET sites in Figure 7.2.3), o-suite better reproduces the daily variability than control (with correlation coefficient of 0.71 for o-suite and 0.48 for control) and the SDS-WAS Multi-model presents lower correlations (0.59). Underestimations are observed in both CAMS experiments (MB of -0.16 for control and -0.05 for o-suite).

The CAMS o-suite model results are better than control over sub-Tropical North Atlantic region, characterised by long-range transport, with correlation values from 0.72 for control to 0.84 for o-suite (see Table 7.2.1 as well as Santa Cruz de Tenerife AERONET sites in Figure 7.2.2). Both CAMS models present high correlations between 0.86 and 0.93 and slight underestimations (MB between -0.01 and -0.03) over the Iberian Peninsula and the Central-Eastern Mediterranean. The Western Mediterranean region shows slightly lower correlation values (0.82 for control and 0.83 for o-suite). This is connected with the mesoscale convective systems that affect this part of the Basin that are typically observed during summer in the Maghreb and northern Sahara.

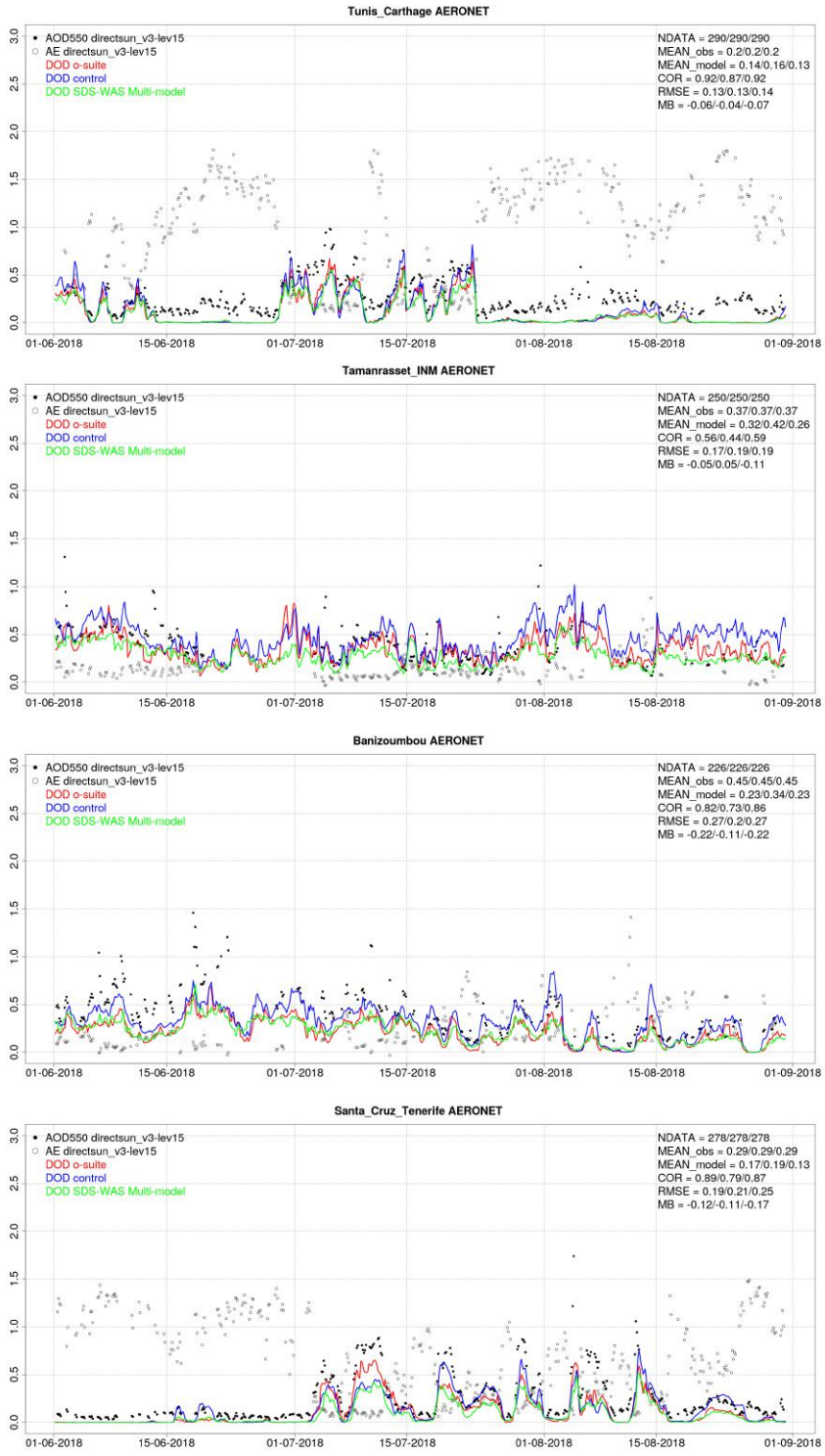

Figure 7.2.2: AOD from AERONET (black dots), DOD o-suite (red line), DOD control (blue line) and DOD Multimodel SDS-WAS Median (green line) for the study period over Tunis Carthage (North Western Magrebh), Tamanrasset (Sahara), Banizoumbou (Sahel) and Santa Cruz de Tenerife (sub-Tropical North Atlantic). Skill scores per each individual site and model (o—suite/control/SDS-WAS Multi-model) are shown in the upper right corner (NDATA: available 3-hourly values used for the calculations, MEAN observations, MEAN_model, COR, RMSE, MB).

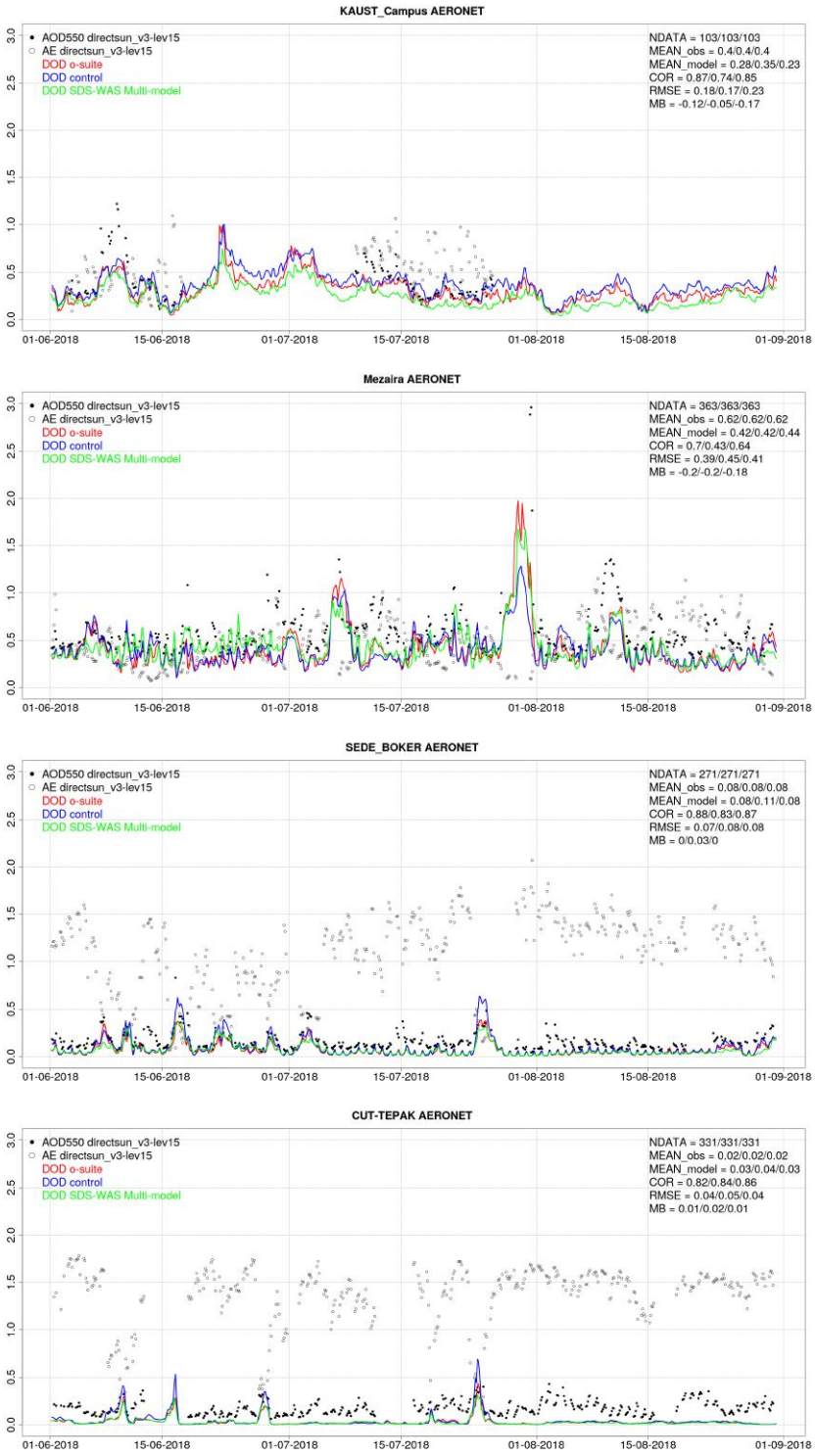

Figure 7.2.3: AOD from AERONET (black dots), DOD o-suite (red line), DOD control (blue line) and DOD Multimodel SDS-WAS Median (green line) for the study period over Kaust Campus (Middle East), Mezaira (Middle East), SEDE BOKER and CUT-TEPAK (Eastern Mediterranean). Skill scores per each individual site and model (o—suite/control/ SDS-WAS Multi-model) are shown in the upper right corner (NDATA: available 3-hourly values used for the calculations, MEAN observations, MEAN_model, COR, RMSE, MB).

Table 7.2.1: Skill scores (MB, FGE, RMSE and r) of 24h forecasts for CAMS o-suite, CAMS control and SDS-WAS Multi-model Median for the study period, and the number of data (NDATA) used. Dust AOD (DOD) from AERONET is the reference.

		control				o-suite DOD				SDS-WAS Median DOD			
	NDATA	**MB**	**FGE**	**RMSE**	**r**	**MB**	**FGE**	**RMSE**	**r**	**MB**	**FGE**	**RMSE**	**r**
Sahara	250	0.05	0.18	0.19	0.44	-0.05	-0.08	0.17	0.56	-0.11	-0.30	0.19	0.59
Sahel	721	-0.10	-0.17	0.25	0.71	-0.21	-0.53	0.30	0.80	-0.23	-0.51	0.32	0.79
Tropical North Atlantic	44	-0.21	-0.33	0.28	0.88	-0.27	-0.43	0.31	0.94	-0.36	-0.63	0.42	0.83
Subtropical North Atlantic	560	-0.04	0.32	0.17	0.72	-0.05	0.23	0.14	0.84	-0.10	0.01	0.19	0.81
North Western Maghreb	236	-0.15	-0.41	0.28	0.64	-0.21	-0.67	0.29	0.78	-0.23	-0.67	0.30	0.81
Western Iberian Peninsula	658	-0.03	1.40	0.10	0.90	-0.03	1.39	0.10	0.93	-0.04	1.36	0.12	0.90
Iberian Peninsula	1452	-0.02	1.53	0.09	0.86	-0.02	1.52	0.09	0.90	-0.03	1.51	0.10	0.89
Western Mediterranean	2699	-0.02	1.46	0.08	0.82	-0.02	1.42	0.09	0.83	-0.03	1.41	0.09	0.84
Central Mediterranean	2939	-0.01	1.37	0.08	0.90	-0.02	1.33	0.08	0.93	-0.03	1.30	0.09	0.93
Eastern Mediterranean	1524	0.02	1.61	0.07	0.84	0.00	1.56	0.06	0.86	0.00	1.57	0.06	0.87
Eastern Sahara	102	0.00	0.02	0.16	0.76	-0.08	-0.20	0.17	0.79	-0.10	-0.29	0.20	0.70
Middle East	755	-0.16	-0.29	0.35	0.48	-0.17	-0.35	0.32	0.71	-0.14	-0.26	0.32	0.59
All sites	**11940**	**-0.03**	**1.12**	**0.14**	**0.84**	**-0.05**	**1.05**	**0.14**	**0.89**	**-0.05**	**1.03**	**0.16**	**0.87**

The comparison of 1 to 3 day forecasts shows that the prediction is stable during the 3-days forecasts with correlation coefficients of 0.84 (0.89), 0.85 (0.83), and 0.82 (0.82) respectively for 24, 48 and 72h forecasts for all the sites for o-suite (control). In the Subtropical North Atlantic, the correlation coefficient (r) for o-suite decreases from 0.80 to 0.67 in going from the 48h to 72h forecast (see Table 7.2.2). In the control run the correlation decreases from 0.70 (for 48h) to 0.61 (for 72h). This indicates limitations of the CAMS model to predict Mauritanian sources.

Table 7.2.2: Skill scores (MB, FGE, RMSE and r) of 48h and 72h forecasts for CAMS o-suite and CAMS control for the study period, and the number of data (NDATA) used. Dust AOD (DOD) from AERONET is the reference.

		48h control				48h o-suite				72h control				72h o-suite			
	NDATA	**MB**	**FGE**	**RMSE**	**r**	**MB**	**FGE**	**RMSE**	**r**	**MB**	**FGE**	**RMSE**	**r**	**MB**	**FGE**	**RMSE**	**r**
Sahara	245	0.05	0.19	0.19	0.48	-0.02	0.01	0.17	0.49	0.06	0.18	0.18	0.51	0.00	0.04	0.15	0.56
Sahel	711	-0.10	-0.18	0.26	0.66	-0.20	-0.49	0.31	0.69	-0.10	-0.16	0.27	0.63	-0.18	-0.41	0.31	0.64
Tropical North Atlantic	44	-0.21	-0.33	0.27	0.88	-0.26	-0.45	0.32	0.88	-0.20	-0.27	0.28	0.83	-0.27	-0.41	0.34	0.83
Subtropical North Atlantic	553	-0.03	0.30	0.17	0.70	-0.06	0.15	0.16	0.80	-0.03	0.26	0.19	0.61	-0.07	0.11	0.19	0.67
North Western Maghreb	234	-0.15	-0.39	0.28	0.60	-0.20	-0.61	0.30	0.65	-0.14	-0.38	0.28	0.56	-0.19	-0.59	0.31	0.59
Western Iberian Peninsula	650	-0.03	1.38	0.11	0.89	-0.03	1.38	0.11	0.90	-0.03	1.37	0.11	0.89	-0.04	1.37	0.12	0.90
Iberian Peninsula	1441	-0.02	1.54	0.09	0.85	-0.03	1.52	0.09	0.89	-0.02	1.52	0.10	0.80	-0.03	1.51	0.10	0.82
Western Mediterranean	2671	-0.01	1.46	0.08	0.82	-0.02	1.44	0.08	0.82	-0.02	1.44	0.09	0.75	-0.02	1.43	0.09	0.77
Central Mediterranean	2931	-0.01	1.36	0.09	0.88	-0.02	1.31	0.09	0.90	-0.01	1.35	0.09	0.88	-0.02	1.32	0.09	0.89
Eastern Mediterranean	1507	0.02	1.60	0.07	0.83	0.00	1.56	0.07	0.83	0.02	1.60	0.07	0.82	0.01	1.56	0.07	0.82
Eastern Sahara	102	0.00	0.02	0.19	0.66	-0.05	-0.13	0.20	0.62	0.02	0.06	0.18	0.71	-0.04	-0.08	0.18	0.69
Middle East	746	-0.15	-0.28	0.35	0.46	-0.17	-0.33	0.35	0.57	-0.15	-0.27	0.35	0.50	-0.17	-0.31	0.35	0.54
All sites	**11835**	**-0.03**	**1.11**	**0.15**	**0.83**	**-0.05**	**1.05**	**0.15**	**0.85**	**-0.03**	**1.11**	**0.15**	**0.82**	**-0.04**	**1.06**	**0.16**	**0.83**

7.3 Backscatter profiles

Technical specifications of data sources, evaluated parameters and methods are described in the report CAMS-84 D8.1. In this section, the temporal and vertical variation of the backscatter coefficient (bsc) profiles are evaluated, statistically as bias, correlation, and standard deviation of o-suite '0001' and control run 'gzyh' vs ceilometers, and summarized in Taylor plots. Second topic is the reproduction of the planetary boundary layer (PBL), and thirdly the representation of individual aerosol types. Covariance plots of daily 2-D time-height sections serve for case studies and for development of a fractional skill score. The vertically integrated bsc is not in focus, because it has limited vertical extension and reveals similar but less accurate information like AOD. As several case studies have confirmed the reliability of the methodology, we focus towards evaluation metrics and interpretations of aerosols representation in the model versions.

Period Overview

The model aerosol optical depth (AOD) and ceilometer overviews exhibit periods with significant aerosol plumes over Germany. Figure 7.3.1 shows the maximum AOD over Germany, separately for contributions of mineral dust (SD), sea salt (SS), carbonaceous matter (CM), black (BC) and organic carbon (OC), as well as sulfate (SU). Two SD events occurred in the JJA 2018 period, 7-11 June and 7/8 Aug 2018. The other components follow their usual seasonality.

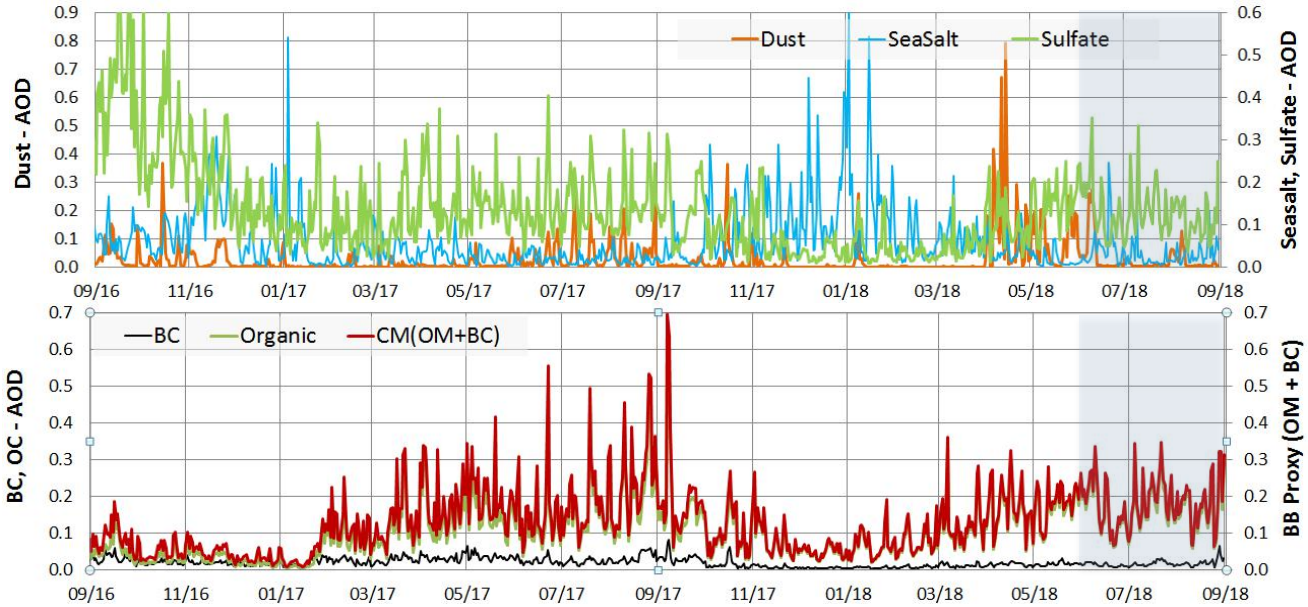

Figure 7.3.1: Maximum daily AOD over Germany for aerosols included in the IFS model from 09/2016 - 08/2018: sea salt (blue), dust (orange), sulfate (light green), black carbon (BC, black), organic matter (green), proxy for 'biomass burning' (as OC+BC - red). Note the different y-axes for the aerosol species.

Mean profiles:

Model bsc in the PBL are on average lower than observed (Fig 7.3.2, 7.3.3). Only in April 2018 the model on average showed a high mean bias in dust all below 4 km altitude. That the median bias is much lower, indicates that single Saharan dust events were overestimated in April 2018, not the background. While enhanced emissions of organic matter (OM) have been introduced in Jan 2017, and parametrizations of SO_2/SO_4 conversion/deposition were improved, nitrate and ammonia are still missing in the current model version, which contribute roughly 10-30% of aerosol mass (as NO_3NH_4 or $(NH_4)_2SO_4$) in the rural central European PBL. (According to pers. communication - S. Remy/Z. Kipling - nitrates and ammonium are ready in the current model and possibly get activated in the next cycle). The assimilation tends to fill this gap with other compounds and thereby overestimate e.g. organics and sulfate. Secondly, our forward operator (including mass→volume conversion) presently uses particle densities of the pure materials, not taking into account that dry atmospheric particles are often porous (sponge-like, even fractal) with entrapped air owing to coagulation and variable internal mixing, and thus exhibit reduced bulk density. A high-biased particle density results in low-biased equivalent volume, and a corresponding underestimation of all optical properties, because these depend strongly on the particle size. Density reductions for accumulation mode particles, composed of hydrophilic and hydrophobic materials may be as high as a factor 1.5 (~1.3 for surface). Thirdly, the capping transport barrier at the PBL top is less effective in the model, diluting high PBL concentrations with clean FT air. Geometrically, however, the PBL height on average seems reasonable (cf. next section).

Monthly mean bsc profiles in the model roughly follow observations, except that the PBL top is too smooth (7.3.2) and the PBL too clean. The monthly mean bsc profiles suggest that the aerosol mass, added to the whole column by the assimilation (run 0001), results in overall higher aerosol load than in the control run (gsyg, gzhy), but the assimilation fails to introduce a fully realistic step at the

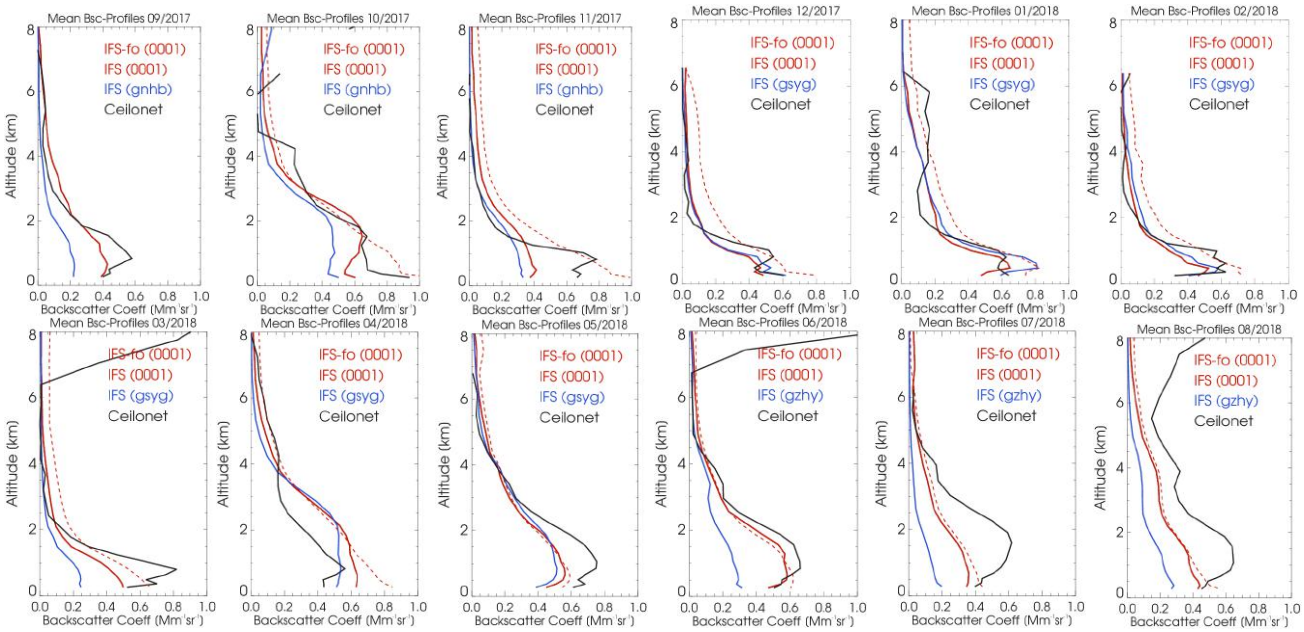

Figure 7.3.2: Monthly mean profiles of backscatter coefficients from osuite (red), control run gnhb/gsyg/gzhy (blue), and ceilometers (black) combined from 21 German stations in September 2017 to August 2018. Two profiles are given for the osuite each, calculated with forward operators from DWD (IFS-fo) and ECMWF (IFS), respectively. The profiles are partly contaminated by remaining cloud artefacts.

top of the PBL to lower values in the free troposphere (FT) as seen in the ceilometer profiles. Rather, the FT background is too high in several months due to adding an assimilated portion there. This aerosol mass is missing in the PBL, yielding a too low amplitude (coded in the standard deviation) of the model compared to observations (reference) in the Taylor plots, too. Except from April 2018 (where the model produced too much dust), the higher bsc observed throughout the extraordinary warm summer from May to August 2018 are not captured by the model. The generally better fit of the median profiles, indicates that the background is better captured than events.

As before, Figs. 7.3.2/3 show for the o-suite each two bsc profiles, calculated from the model mass mixing ratios, one using a forward-operator (fo) calculated by ourselves (DWD) and the other with the one implemented in the IFS. Noteably, the monthly mean difference between the bsc profile based on our (DWD) forward operator and the one calculated within the IFS (IFS-fo), jumps down to few % after April/May. The reason for this is not yet clear, but possibly result from larger uncertainties are the real particle density and the humidity-dependent water uptake.

Taylor Plots

The average coefficient of correlation between modelled and observed vertical backscatter profiles clusters around r = 0.4. The absolute values after normalization to the reference value (observations) at the standard deviation 1.0, are captured significantly better by the o-suite (red dots) then the control run (blue dots). There is however a very large day-to-day and also a seasonal variation of the performance (Figure 7.3.4).

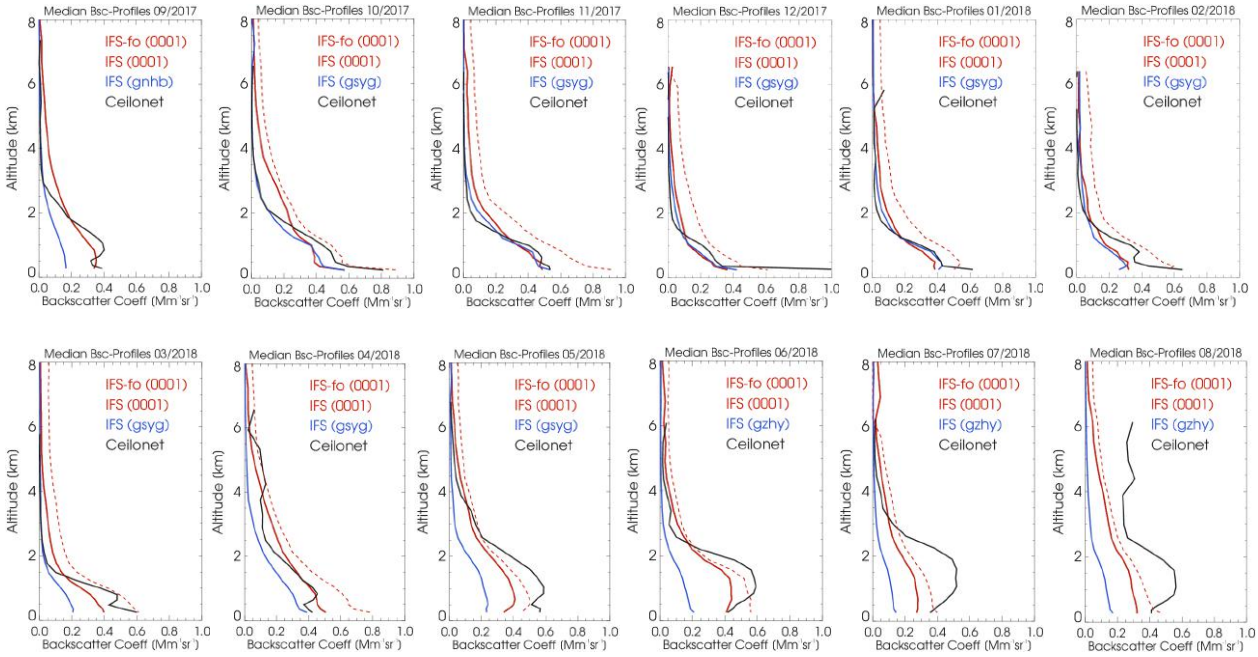

Figure 7.3.3: Monthly median profiles of backscatter coefficients from osuite (red), control run gnhb, gsyg, gzhy (blue), and ceilometers (black) combined from 21 German stations in September 2017 to August 2018. Two profiles are given for the osuite each, calculated with forward operators from DWD and ECMWF, respectively. The profiles are partly contaminated by remaining cloud artefacts.

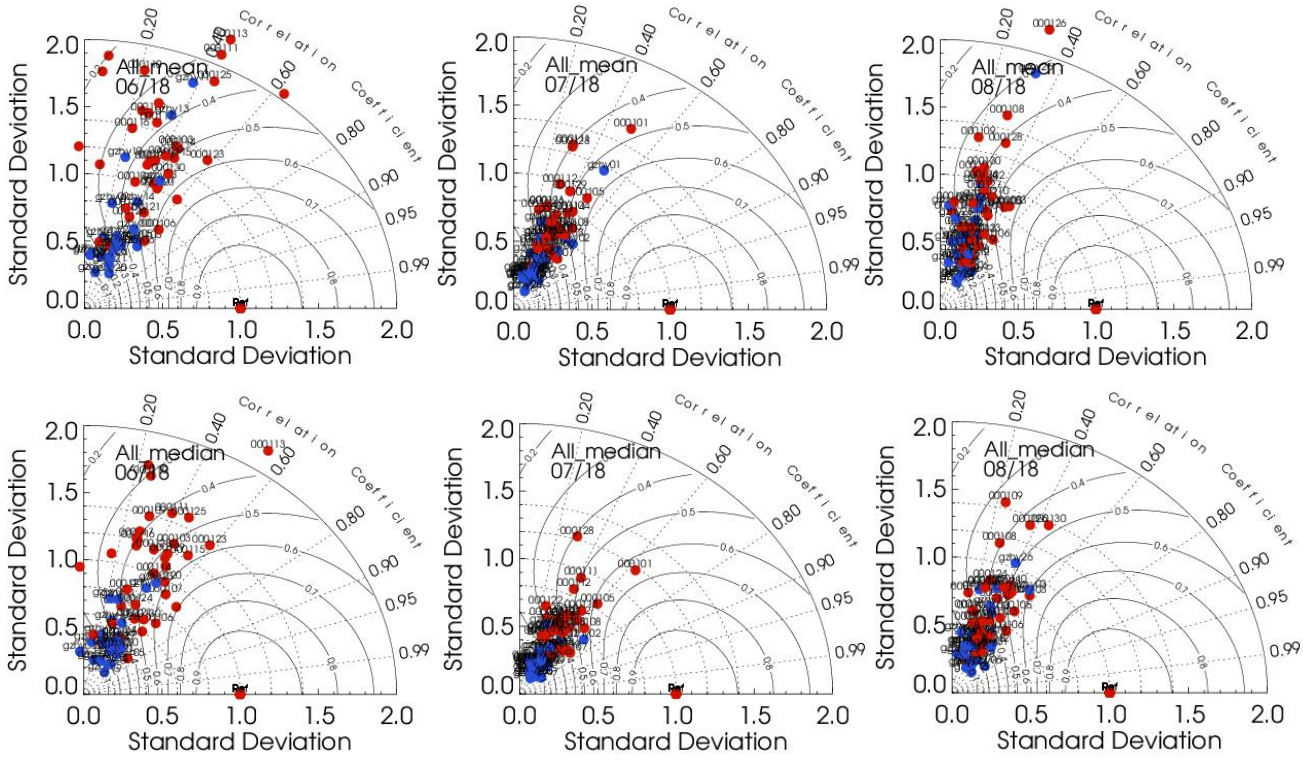

Figure 7.3.4: Taylor polar plots with daily average standard deviation of vertical profiles vs correlation coefficient, averaged over 21 German ceilometer sites for June, July, Aug 2018. O-suite red, control blue.

Summary

Backscatter coefficients are low-biased in the planetary boundary layer (PBL). Possible reasons are missing of ammonia and nitrate in the model, assumption of too high particle densities (for pure compact materials) in the mass to backscatter conversion, and the lack of vertical transport barrier at the top of the PBL, causing dilution with free troposphere air. Free troposphere (FT) background backscatter coefficients are biased high, probably due to wrong re-distribution between PBL and FT. This is not fixed by the assimilation, which instead adds aerosol to the whole profile. The bsc bias on a specific level thus depends on its relative position w.r.t. to the BLH.

Monthly average vertical backscatter profiles show a high low bias in the extraordinary warm summer 2018. Interestingly, the model profiles, based on DWD's forward operator and the one implemented in the IFS (IFS-fo), jump to smaller values of few % after April/May. The monthly Taylor plots over 21 German stations indicate that daily averages of Pearsons correlation coefficients cluster around 0.4, and that the o-suite on average has a lower bias than control.

7.4 Aerosol validation over the Mediterranean

Three-hourly aerosol optical depth (AOD) and surface concentration (PM10 and PM2.5) from o-suite experiment and control experiment have been validated for the period 1 June 2018 – 31 August 2018 against AERONET direct-sun cloud-screened observations.

Aerosol optical depth

CAMS o-suite can reproduce the daily variability of AERONET observations. In Western, Central and Eastern Mediterranean, the correlation coefficient increase from 0.67, 0.75 and 0.51 to 0.70, 0.82 and 0.59, respectively for control and o-suite during summer (see the correlation coefficient by sites in Figure 7.4.1). Underestimations observed in the Mediterranean Basin in control (MB of -0.06, -0.03 and -0.03 for Western, Central and Eastern Mediterranean regions respectively) are corrected in o-suite introducing overestimations in the Basin (MB of 0.01, 0.03 and 0.02 for Western, Central and Eastern Mediterranean regions respectively). The highest peaks on CAMS AOD simulations are linked to desert dust intrusions (see Barcelona, Rome Tor Vergata, Thessaloniki and Cairo EMA AERONET sites in Figure 7.4.2). During summer, the photochemical processes are enhanced (which favours the formation of secondary aerosols) and the lack of precipitation increase the background levels in the Basin. Underestimations of these background aerosols are corrected during the assimilation cycle increasing the AOD levels (see Figure 7.4.2).

Surface aerosol concentrations

For summer, PM10 and PM2.5 results of CAMS o-suite and control show similar skill scores in comparison with EIONET-Airbase observations (see Figure 7.4.3). For PM2.5, CAMS model tends to overestimate the EIONET-Airbase observations meanwhile PM10 tends to be underestimated in the Spanish Mediterranean sites (see Figure 7.4.3 and Figure 7.4.4). From June to August, the overestimations observed in the comparison against EIONET-Airbase cause that the o-suite overpredict the number of exceedances of the EU PM10 daily threshold (i.e. 50 $\mu g/m^3$; see Zorita, Hospital Joan March, Venaco and Gharb in Figure 7.4.5). Particularly, in Gharb station in Malta, there are two PM10 events in July (on 8th and 18th July) predicted by the o-suite that achieved 110 and 70 $\mu g/m^3$, respectively. They were associated with sea-salt contributions.

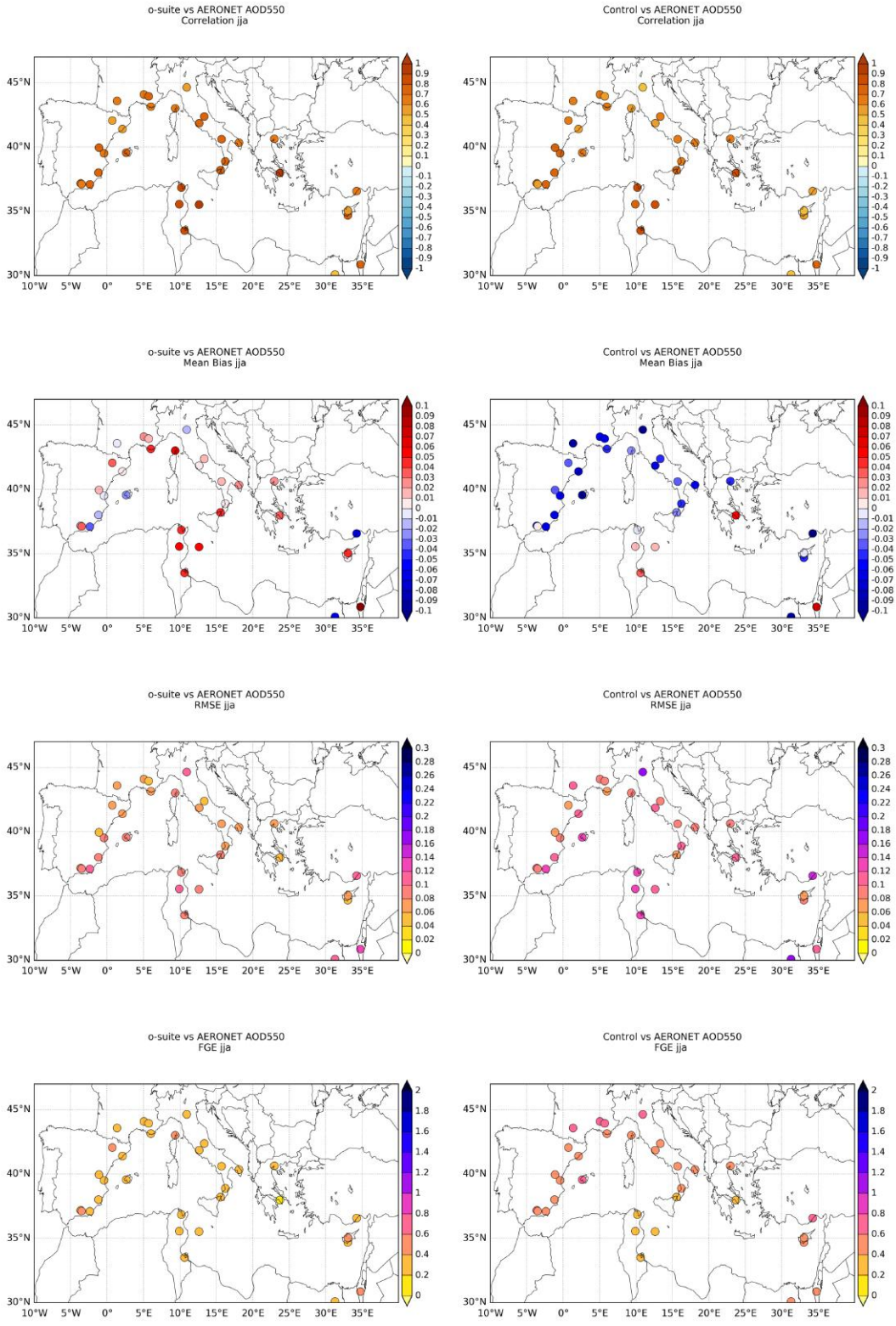

Figure 7.4.1: Skill scores (correlation coefficient, MB, RMSE and FGE) for 24-hour forecasts of CAMS o-suite and control for the study period. AOD from AERONET is the reference.

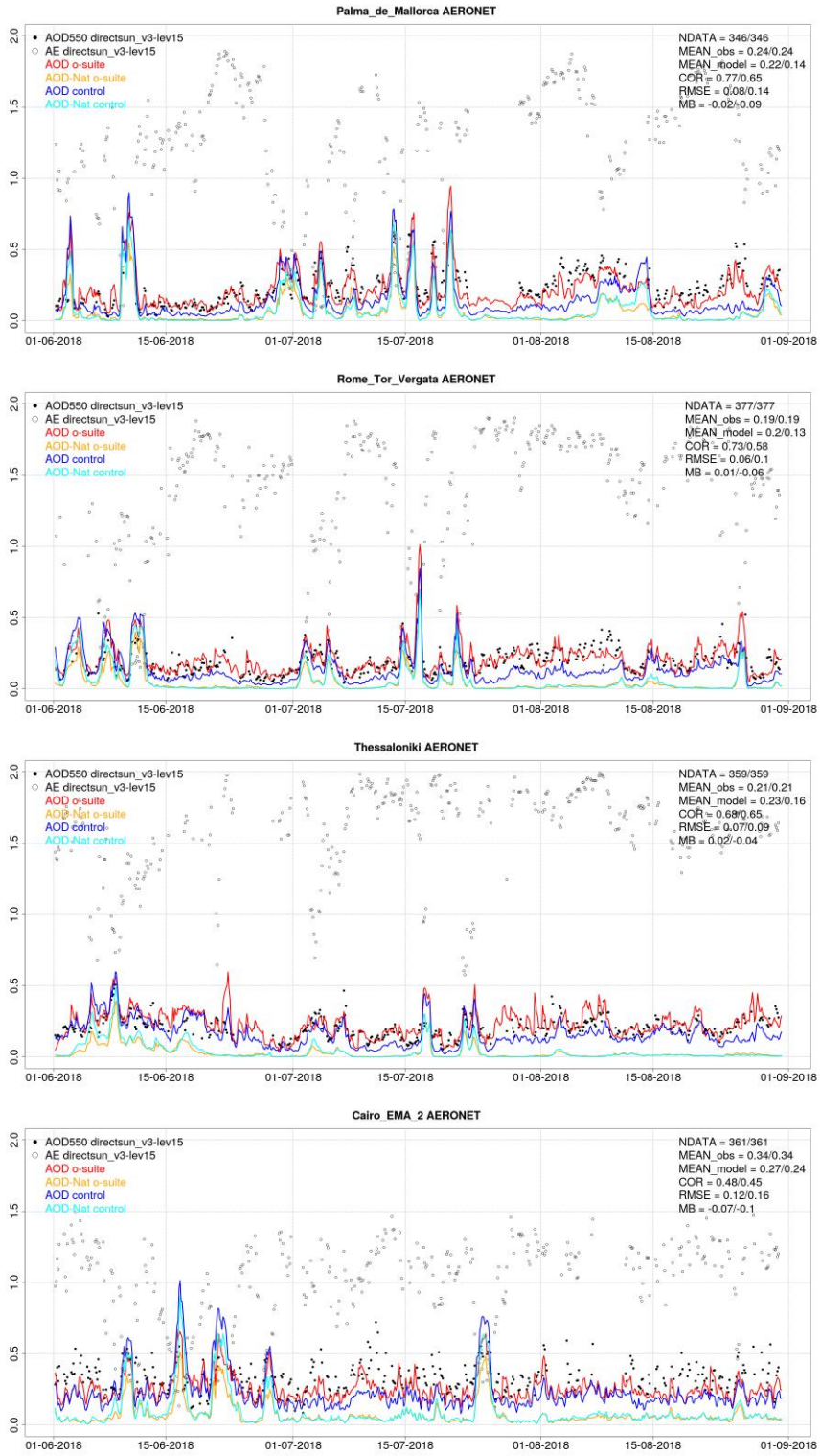

Figure 7.4.2: AOD from AERONET (black dot), AOD o-suite (red line), AOD control (blue line), AOD-Nat o-suite (orange line), AOD-Nat control (cyan line), for the study period over Palma de Mallorca (Balearic Islands, Spain), Rome Tor Vergata (Italy), Thessaloniki (Greece) and Cairo EMA 2 (Egypt). AOD-Nat corresponds to the natural aerosol optical depth that includes dust and sea-salt. Skill scores per each individual site and model (o—suite/control) are shown in the upper right corner (NDATA: available 3-hourly values used for the calculations, MEAN observations, MEAN_model, COR, RMSE, MB).

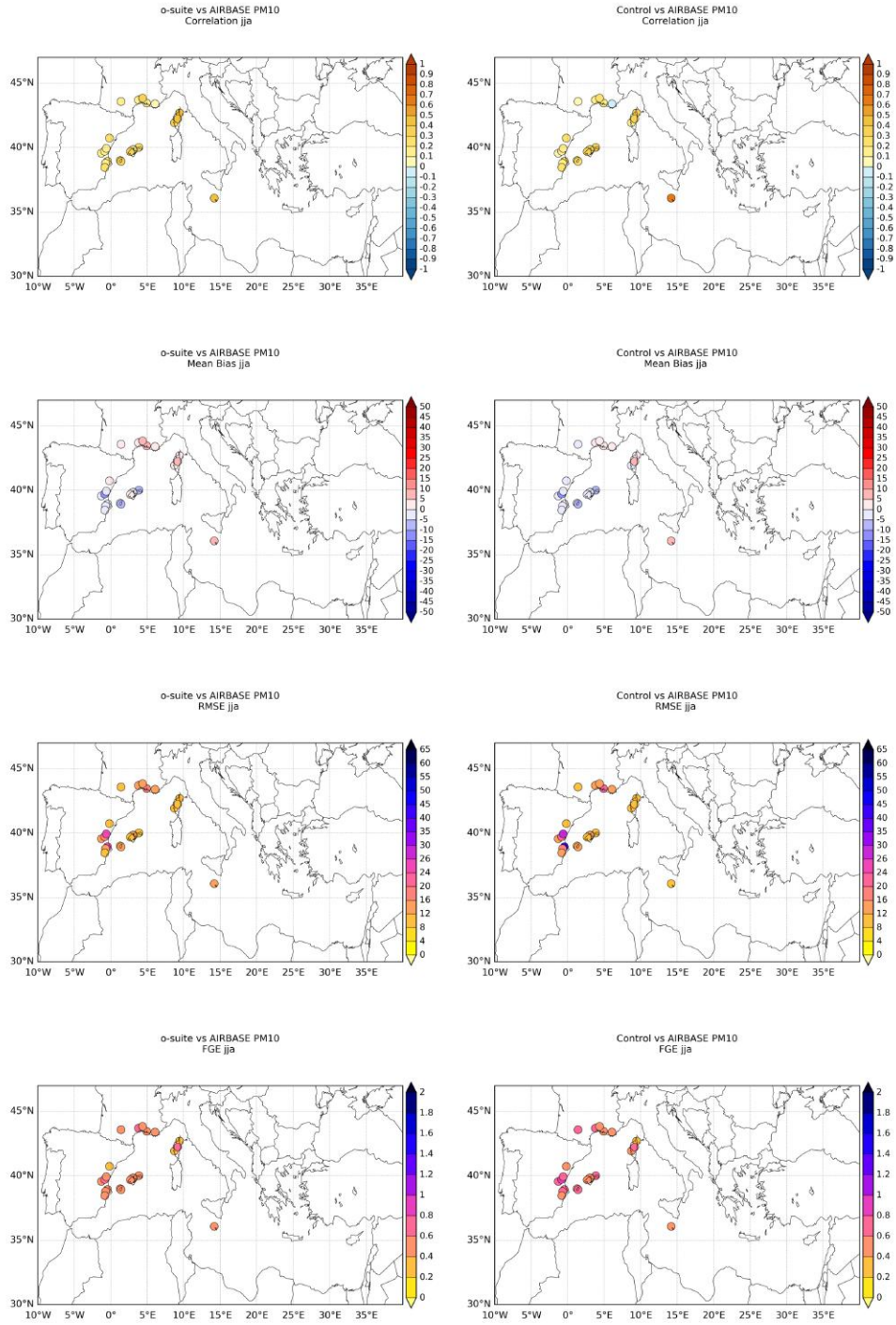

Figure 7.4.3: Skill scores (correlation coefficient, MB, RMSE and FGE) for 24-hour forecasts of CAMS o-suite and control for the study period. PM10 from EIONET are the reference. Only background suburban and rural available stations are displayed.

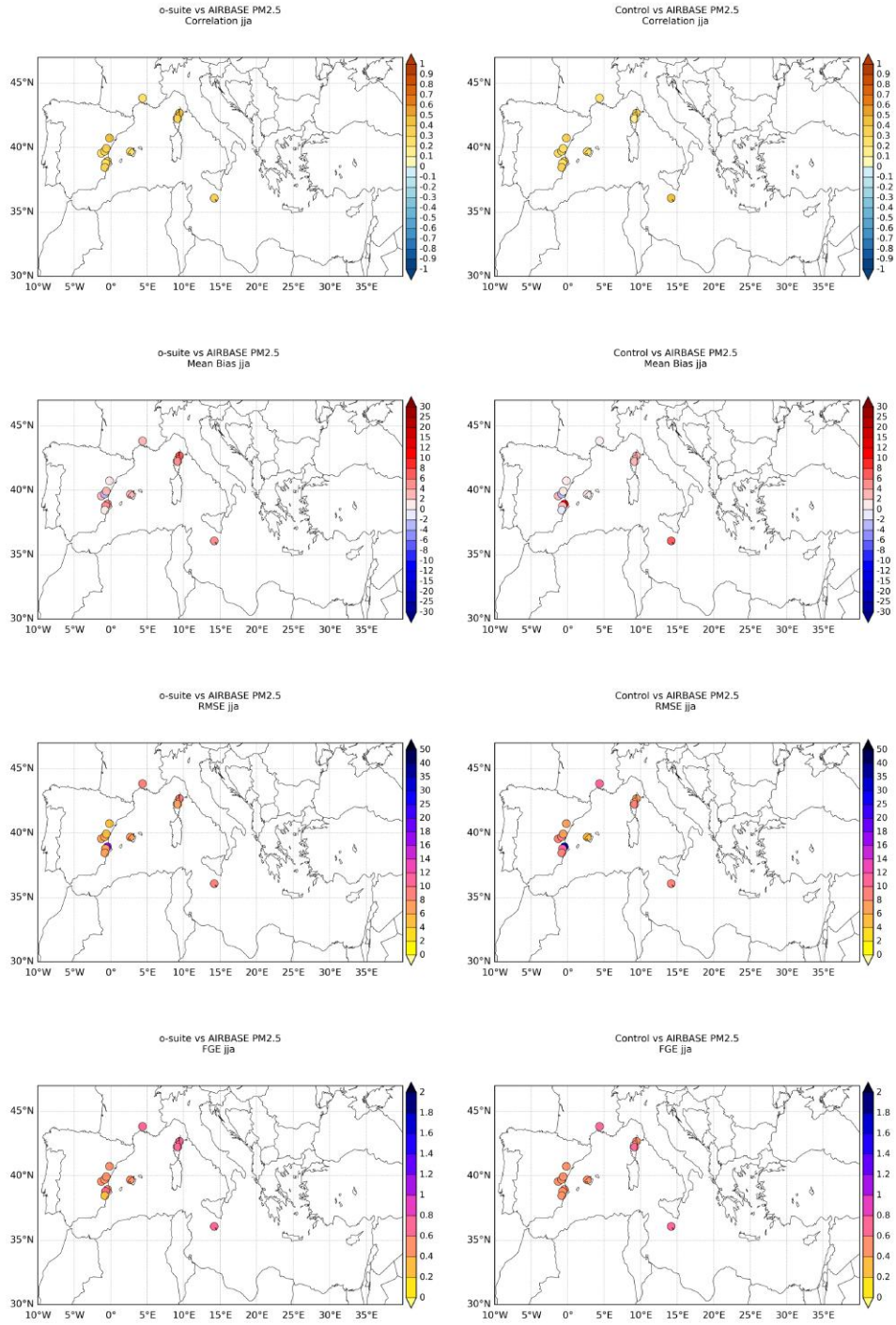

Figure 7.4.4: Skill scores (correlation coefficient, MB, RMSE and FGE) for 24-hour forecasts of CAMS o-suite and control for the study period. PM2.5 from EIONET are the reference. Only background suburban and rural available stations are displayed.

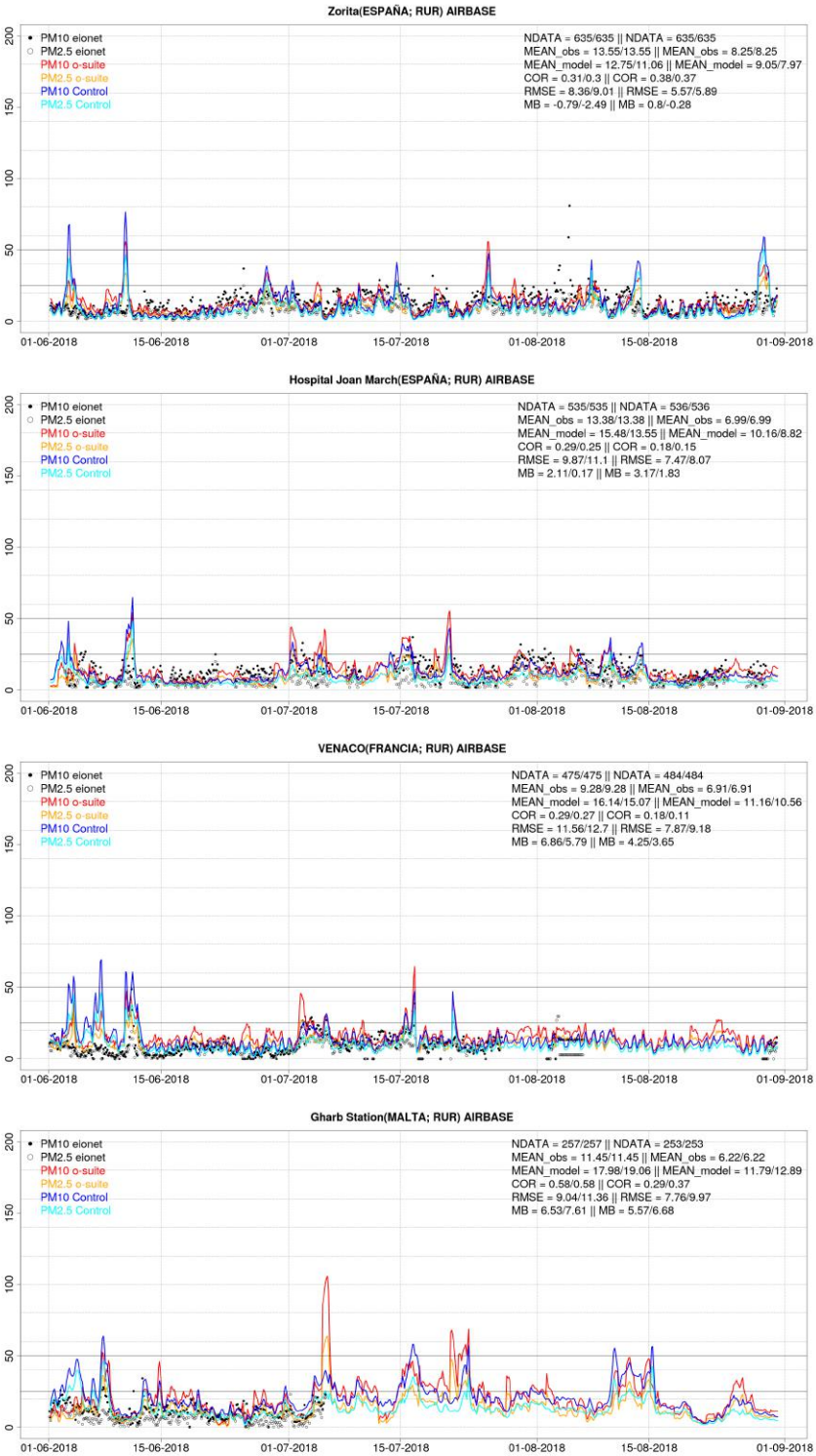

Figure 7.4.5: PM10 and PM2.5 Airbase observations (black and grey dots, respectively), PM10 and PM2.5 o-suite (red and orange lines, respectively) and PM10 and PM2.5 control (blue and cyan lines, respectively) for the study period over Zorita (Western Iberian Peninsula, Spain) as well as Hospital Joan March (Balearic Islands, Spain), Venaco (Corse, France) and Gharb (Malta). Skill scores per each individual site, model (o—suite/control) and PM10/PM2.5 are shown in the upper right corner (NDATA: available 3-hourly values used for the calculations, MEAN observations, MEAN_model, COR, RMSE, MB).

8. Stratosphere

8.1 Validation against ozone sondes

In this section, we present the results of the stratospheric ozone evaluation against ozone soundings from the NDACC, WOUDC, NILU and SHADOZ databases. The sondes have a precision of 3-5% (~10% in the troposphere for Brewer Mast) and an uncertainty of 5-10%. For further details see Cammas et al. (2009), Deshler et al. (2008) and Smit et al (2007). Model profiles of the o-suite are compared to balloon sondes measurement data of 44 stations for the period January 2013 to August 2018 (please note that towards the end of the validation period fewer soundings are available). As C-IFS-CB05 stratospheric composition products beyond O_3 in the o-suite is not useful we provide only a very limited evaluation of the control experiment. A description of the applied methodologies and a map with the sounding stations can be found in Eskes et al. (2016). The o-suite shows MNMBs within the range ±12%, for all regions and months (some exceptions with MNMBs of up to ±18% for single months in the high latitude regions). Figure 8.1.1. shows the results for the period August 2017 to August 2018.

Fig. 8.1.2 compares the averaged profiles in each region during March 2018. The vertical distribution of stratospheric ozone is quite well represented for all regions by the o-suite, with little overestimation in all latitude bands (MNMBs between 1 to 9% for MAM).

The control run shows a strong overestimation of stratospheric ozone in the upper stratosphere, and an underestimation between 40hPa (Arctic 100 hPa) and 300 hPa in the Arctic and the Northern Midlatitudes. In the Tropics, the underestimation is between 80 and 30 hPa. The Antarctic profile shows an underestimation between 300 and 30 hPa. Above, O_3 partial pressures are overestimated.

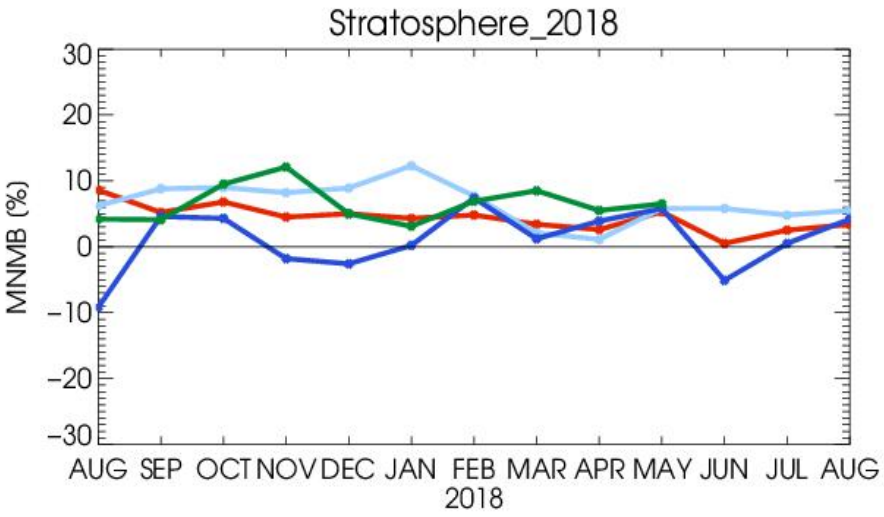

Figure 8.1.1: MNMBs (%) of ozone in the stratosphere from the o-suite against aggregated sonde data in the Arctic (light blue), Antarctic (dark blue) northern midlatitudes (red) and tropics (green).

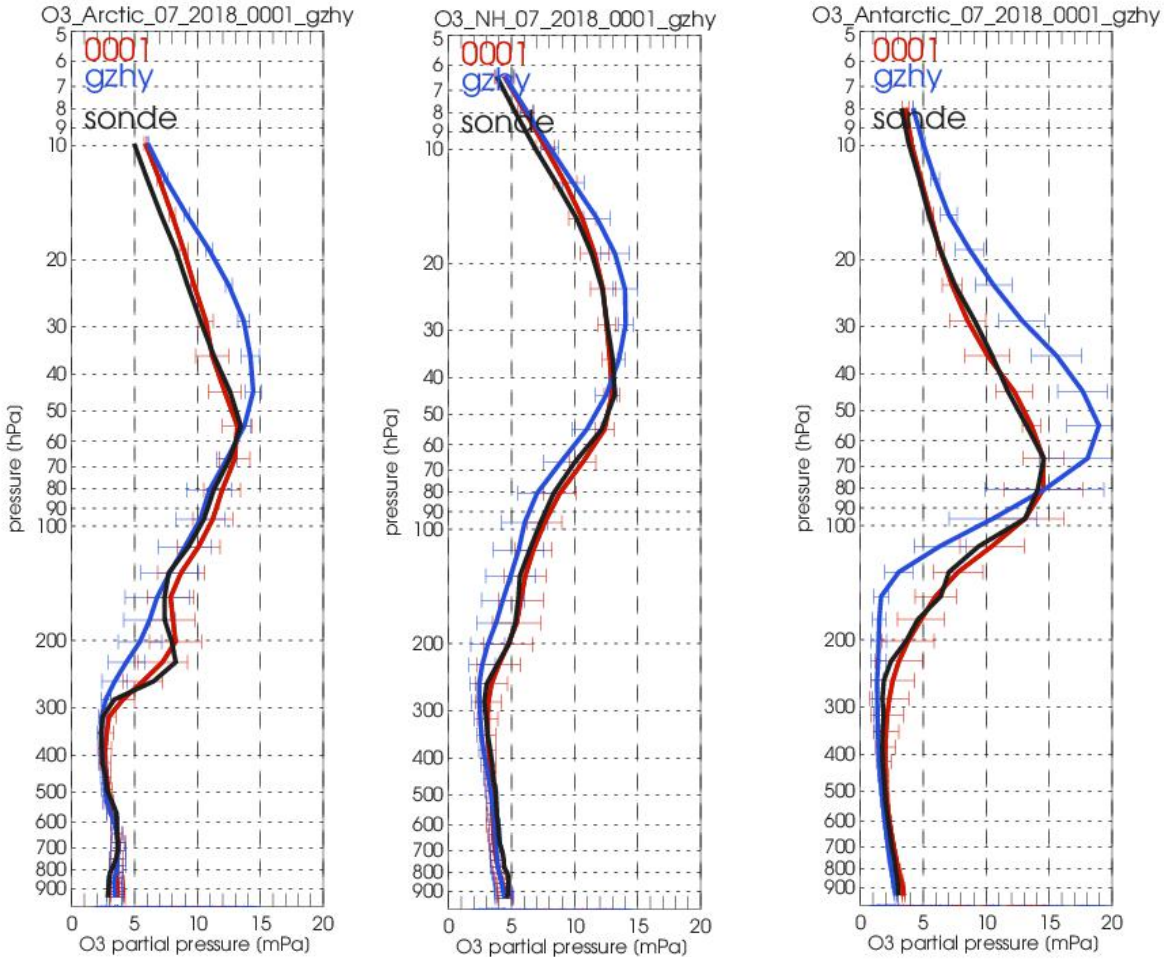

Figure 8.1.2: Comparison between mean O_3 profiles (units: mPa) of o-suite (red), and control (blue) in comparison with observed O_3 sonde profiles (black) for July 2018 for the various latitude bands: Arctic, NH-mid latitudes, Tropics and Antarctic.

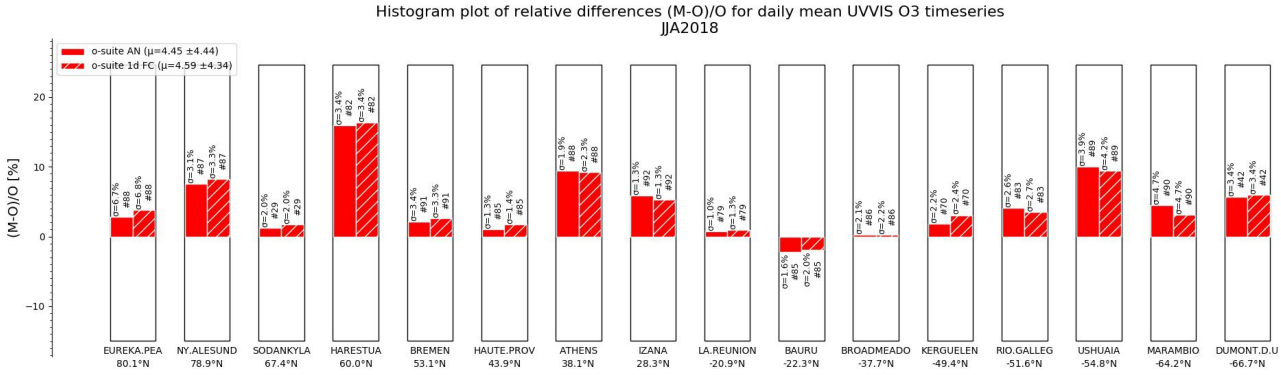

Figure 8.2.1 Relative biases during quarter JJA 2018 for 16 UVVIS stations measuring stratospheric ozone columns with ZENITH measurement geometry (stations sorted with decreasing latitude). The overall relative bias is positive for all latitudes and within the typical measurement uncertainty of 5% for most of the sites.

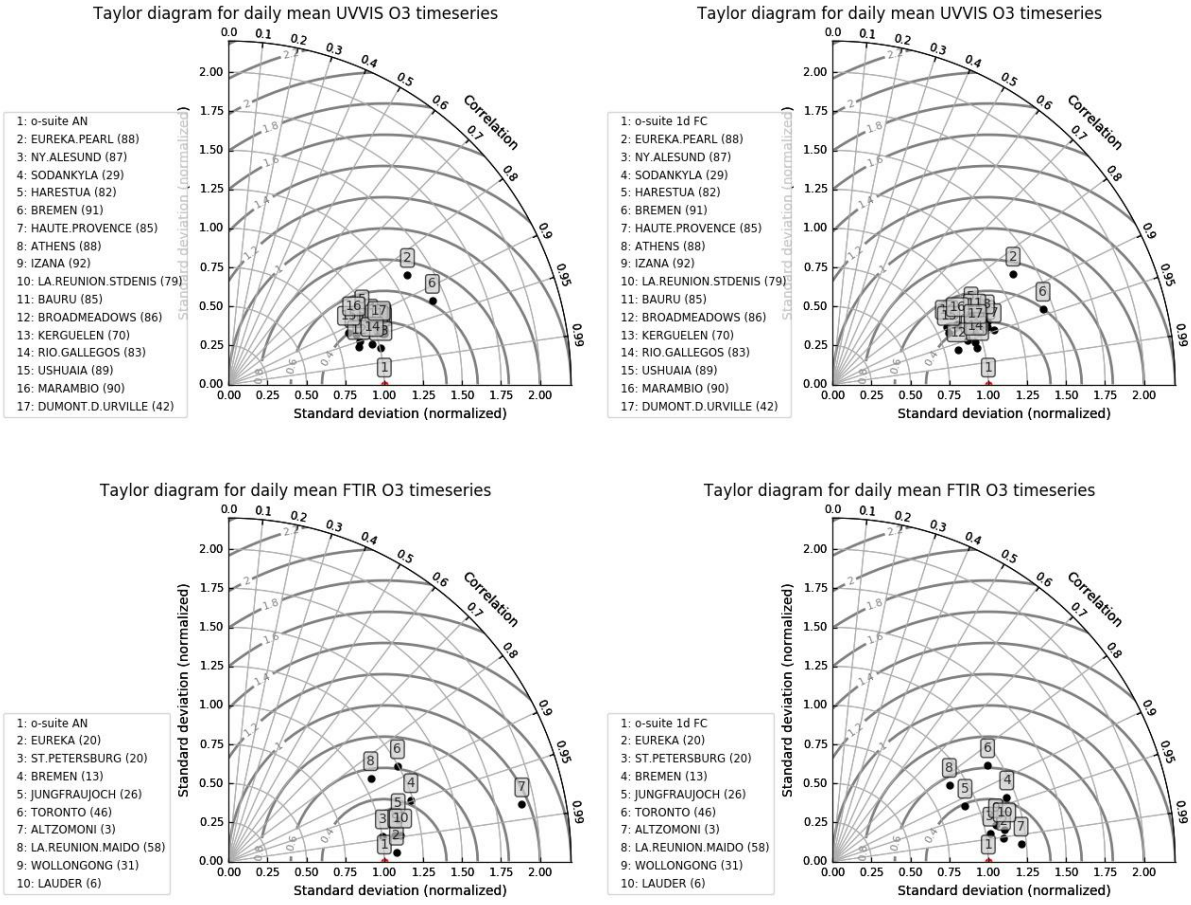

Figure 8.2.2 Taylor diagrams relating the standard deviations for the model and GB stratospheric column time series and their correlation for the time period JJA 2018. All time series are normalized such that the std of the model is 1. The performance for the osuiteAN is slightly better (averaged correlation is 0.96) compared to the 1d FC (averaged correlation is 0.93).

8.2 Validation against observations from the NDACC network (UVVIS, FTIR, MWR and LIDAR)

UVVIS and FTIR stratospheric columns

Since the start of the CAMS27 project, the number of UVVIS Zenith ozone measurements have increased on NDACC. Currently sixteen sites provided data in the recent quarter allowing for a representative picture on the latitude dependence of the model data.

The systematic uncertainty of the UVVIS measurements is typically 5%, hence the relative biases for most sites for both the AN and 1d FC of the o-suite are very close to each other and within the uncertainty ranges, see Figure 8.2.1. The averaged bias for the 16 UVVIS sites is 4.5% and the averaged correlation is 0.93.

Figure 8.2.3 depicts the FTIR stratospheric columns showing a discontinuity in the osuite 1d FC model for the tropical sites (Mauna Loa, Altzomoni and Reunion) in the June 2016 model update.

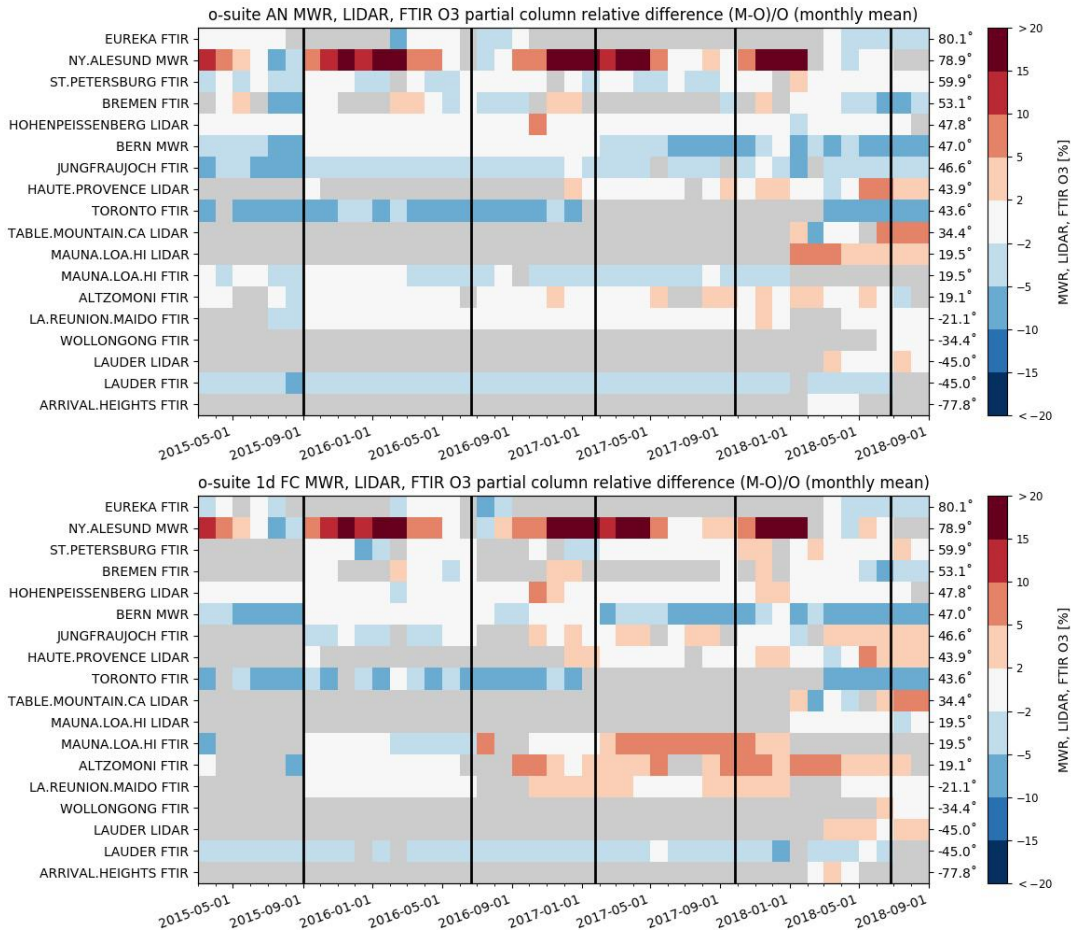

Figure 8.2.3 Time series of monthly mean relative differences for stratospheric columns (FTIR and LIDAR) and mesospheric (MWR) columns along with model cycle updates (black vertical lines) (o-suite AN top, o-suite 1d FC bottom). The stratospheric FTIR columns at St Peterburg, Jungfraujoch, Altzomoni and La Reunion show a slight positive trend in the relative differences, which is probably introduced by model updates.

The correlations between the sites and the model are presented in the Taylor diagrams in Figure 8.2.2. Again the o-suite AN and 1d FC perform very similarly in correlation coefficients. The FTIR Altzomoni (close to Mexico City) only has three co-located measurements days and no conclusions can be drawn from the apparent outlier in the analysis plot.

Profile comparison using LIDAR and MWR

In this section we present a comparison between the CAMS o-suite and control run models against MWR and LIDAR observations from the NDACC network. A detailed description of the instruments and applied methodologies for all NDACC instruments can be found at http://nors.aeronomie.be. MWR (microwave) at Ny Alesund (79°N, 12°E, Arctic station) and Bern (47°N, 7°E, northern midlatitude station). LIDAR at Observatoire Haute Provence (OHP), France (43°N, 5.7°E, altitude 650m) and Hohenpeissenberg, Germany (47°N, 11°E, altitude 1km)

From Figure 8.2.3 at Ny Alesund the o-suite overestimates the stratospheric ozone concentration with more than 10% during SON/DJF/MAM and the bias vanishes during summer JJA. Between the model upgrades from September 2015 and January 2017 the relative bias at Bern vanishes (i.e. is

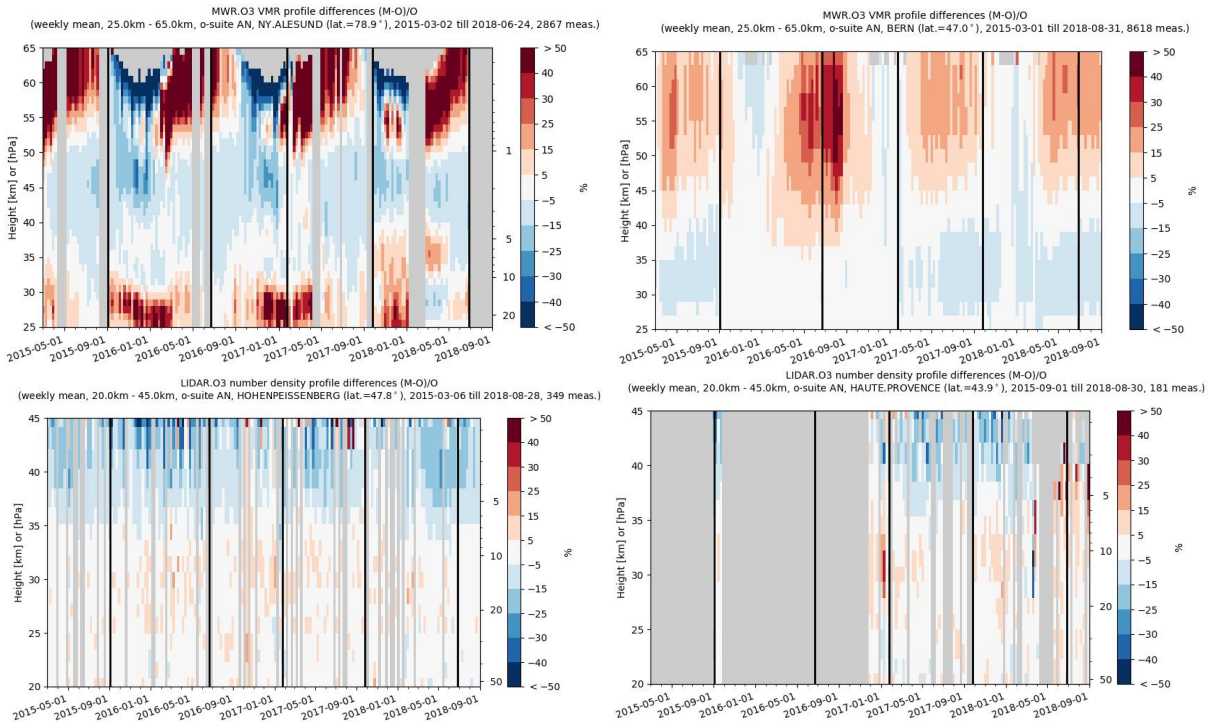

Figure 8.2.4: Comparison of the weekly mean profile bias between the O_3 mixing ratios of o-suite and the NDACC station at Ny Alesund, Bern, Hohenpeissenberg and OHP. For the LIDAR stations, the measurement uncertainty above 35km is comparable to the observed profile bias.

comparable to the measurement uncertainty). A discontinuity is observed for the mesospheric ozone column measured by the MWR at Bern in the Jan 2017 update which is due to an underestimation of the upper stratospheric ozone column (see Figure 8.2.4).

In MAM-JJA 2015-2018, both MWR stations observe a significant (i.e. comparable to the measurement uncertainty) overestimation of the upper stratospheric/mesospheric ozone content, and the converse is seen during autumn and winter SON-DJF, underestimating up to -30% (Ny Alesund), see also Figure 8.2.4.

At OHP and Hohenpeissenberg (LIDAR), the o-suite slightly overestimates the observed ozone (<10%) between 25km and 35km. The uncertainty on the LIDAR concentration increases with altitude and above 35km the observed differences are comparable to the measurement uncertainty (>10%, see http://nors.aeronomie.be/projectdir/PDF/NORS_D4.2_DUG.pdf)

8.3 Comparison with dedicated systems and with observations by limb-scanning satellites

This section compares the output of the o-suite for the last period with observations by limb-scanning satellite instruments, using the methodology described by Lefever et al. (2015). We also include the comparisons for the o-suite 4th day forecasts (96h to 120h) of stratospheric ozone. These forecasts are represented by dotted lines in the figures.

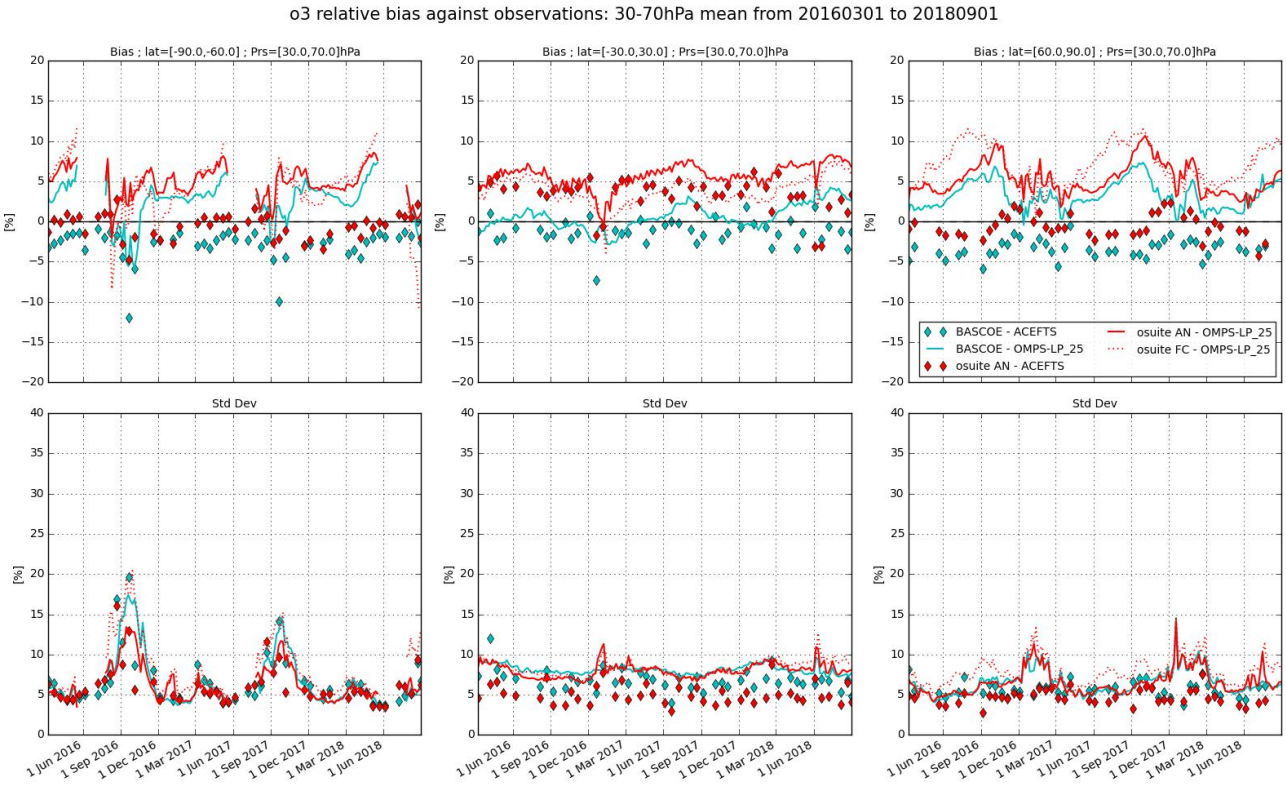

Figure 8.3.1: Time series comparing models to observations for the period 2016-03-01 to 2018-09-01 in the middle stratosphere (30-70hPa averages): o-suite analyses vs OMPS-LP (red, solid), o-suite forecasts 4th day vs OMPS-LP (red, dotted), o-suite analyses vs ACE-FTS (red markers), BASCOE vs OMPS-LP (cyan, solid) and BASCOE vs ACE-FTS(cyan markers). Top row, normalized mean bias (model-obs)/obs (%); bottom row, standard deviation of relative differences (%).

All datasets are averaged over all longitudes and over the three most interesting latitude bands for stratospheric ozone: Antarctic (90°S-60°S), Tropics (30°S-30°N) and Arctic (60°N-90°N). In order to provide global coverage, the two mid-latitude bands (60°S-90°S and 60°N-90°N) are also included in some comparisons with satellite observations.

In this section, we use on one hand the version 2.5 of OMPS-LP (i.e. the Limb Profiler) and the version 3.6 of ACE-FTS. For reference, we include also the BASCOE analyses which are very constrained by the AURA MLS offline profiles.

Figure 8.3.1 and Figure 8.3.2 present, in the upper row, the timeseries over the last 30 months of the bias of the o-suite against the two satellite measurements for respectively two regions of the lower stratosphere and UTLS (30-70hPa and 70-100hPa); the bottom row of the figures shows the standard deviation of the differences and can be used to evaluate the random error in the analyses.

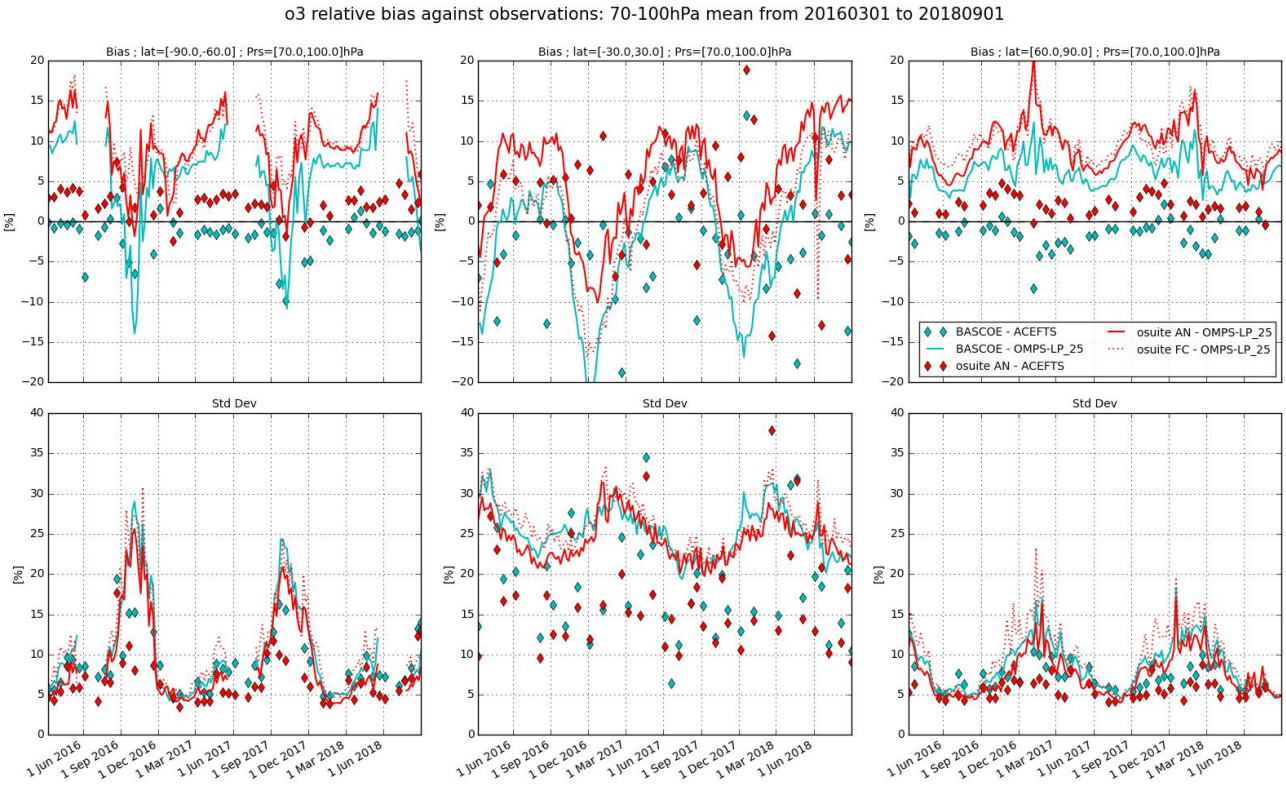

Figure 8.3.2: Time series comparing models to observations for the period 2016-03-01 to 2018-09-01 in the lower stratosphere (70-100hPa averages): o-suite analyses vs OMPS-LP (red, solid), o-suite forecasts 4th day vs OMPS-LP (red, dotted), o-suite analyses vs ACE-FTS (red markers), BASCOE vs OMPS-LP (cyan,solid) and BASCOE vs ACE-FTS(cyan markers). Top row, normalized mean bias (model-obs)/obs (%);bottom row, standard deviation of relative differences (%).

Compared to OMPS-LP in the 30hPa to 70hPa region, there is a systematic overestimation by the o-suite: up to 8% in the South polar region and in the tropics and up to 12% in the North polar region. Compared to OMPS-LP in the 70hPa to 100hPa region, the North polar bias increases up to 20% at various periods, while the variability of the bias is much stronger in the South polar region; the tropics exhibits a strong seasonal variation for the bias, with a high variability indicated by the standard deviation.

The agreement with ACE-FTS is much better: the bias is generally within ±5%, except in the tropics for 70hPa to 100hPa region, where the standard deviations indicate less reliable results.

The bias of BASCOE against the satellite observations for the considered regions is systematically lower, but follows a similar evolution as the o-suite.

Figure 8.3.3 and Figure 8.3.4 display vertical profiles of the relative biases between the o-suite or BASCOE and the satellite measurements. The difference is averaged over the most recent 3-month period considered in this validation report, i.e. June to August 2018.

The OMPS-LP profiles are much more irregular than the ACEFTS or MLS profiles, but the relative bias between o-suite and OMPS-LP is mostly within ±10% between 20km and 35km.

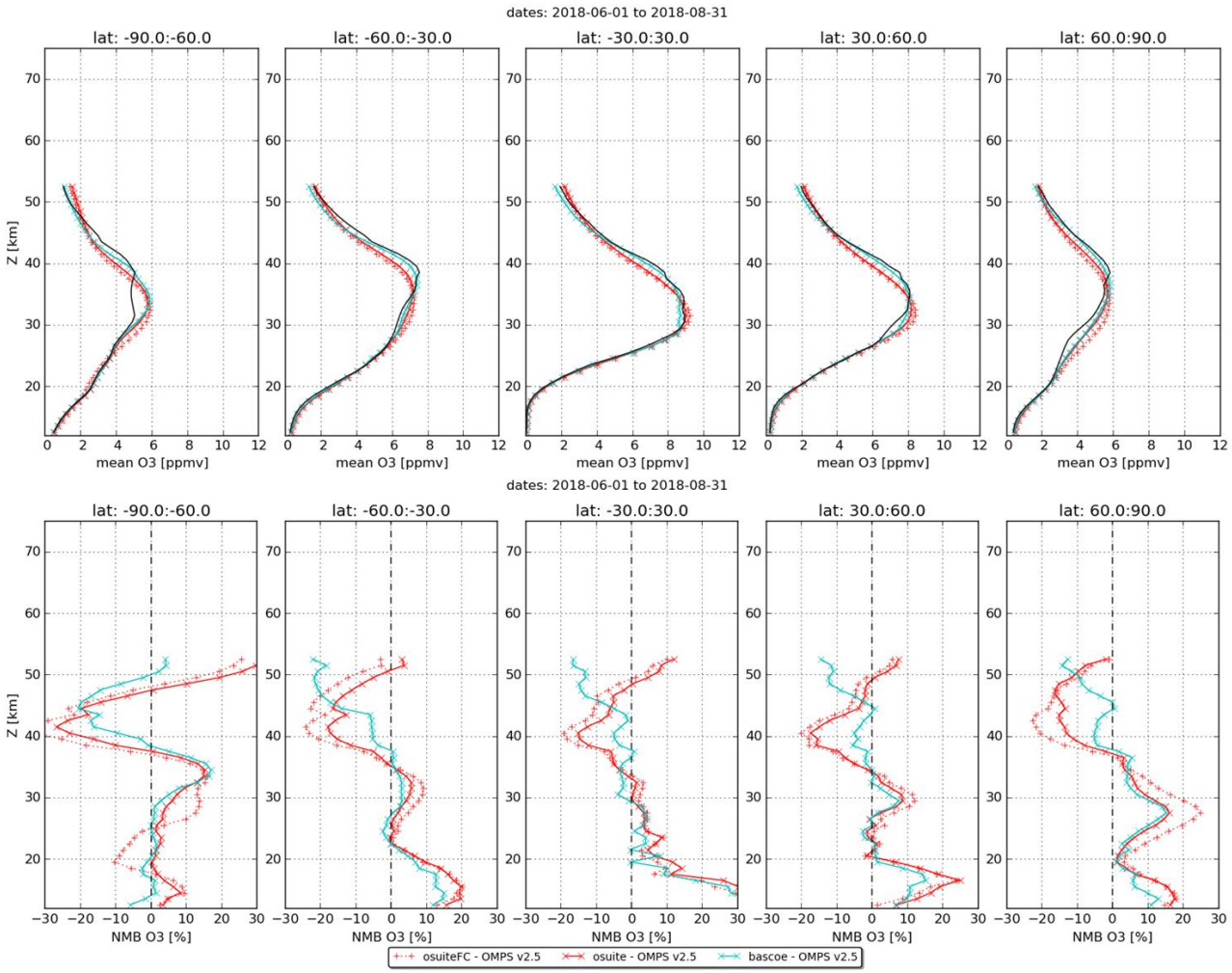

Figure 8.3.3: Mean value (top) and normalized mean bias (bottom) of the ozone profile between o-suite analyses (red, solid), o-suite forecasts 4th day (red, dotted) and BASCOE (cyan line) with OMPS-LP v2.5 observations for the period June to August 2018.

The negative bias above 40km is confirmed by the ACEFTS profiles, otherwise there is a good agreement in the middle and lower stratosphere.

It must be noted that the different instruments have a variety of spatial and temporal coverage: for a 3 month period and over the latitude bands considered, OMPS and Aura MLS (not shown) provide daily data with more than 40000 valid profiles, while ACE-FTS provides around 750 profiles in the polar region and 150 profiles in the tropics.

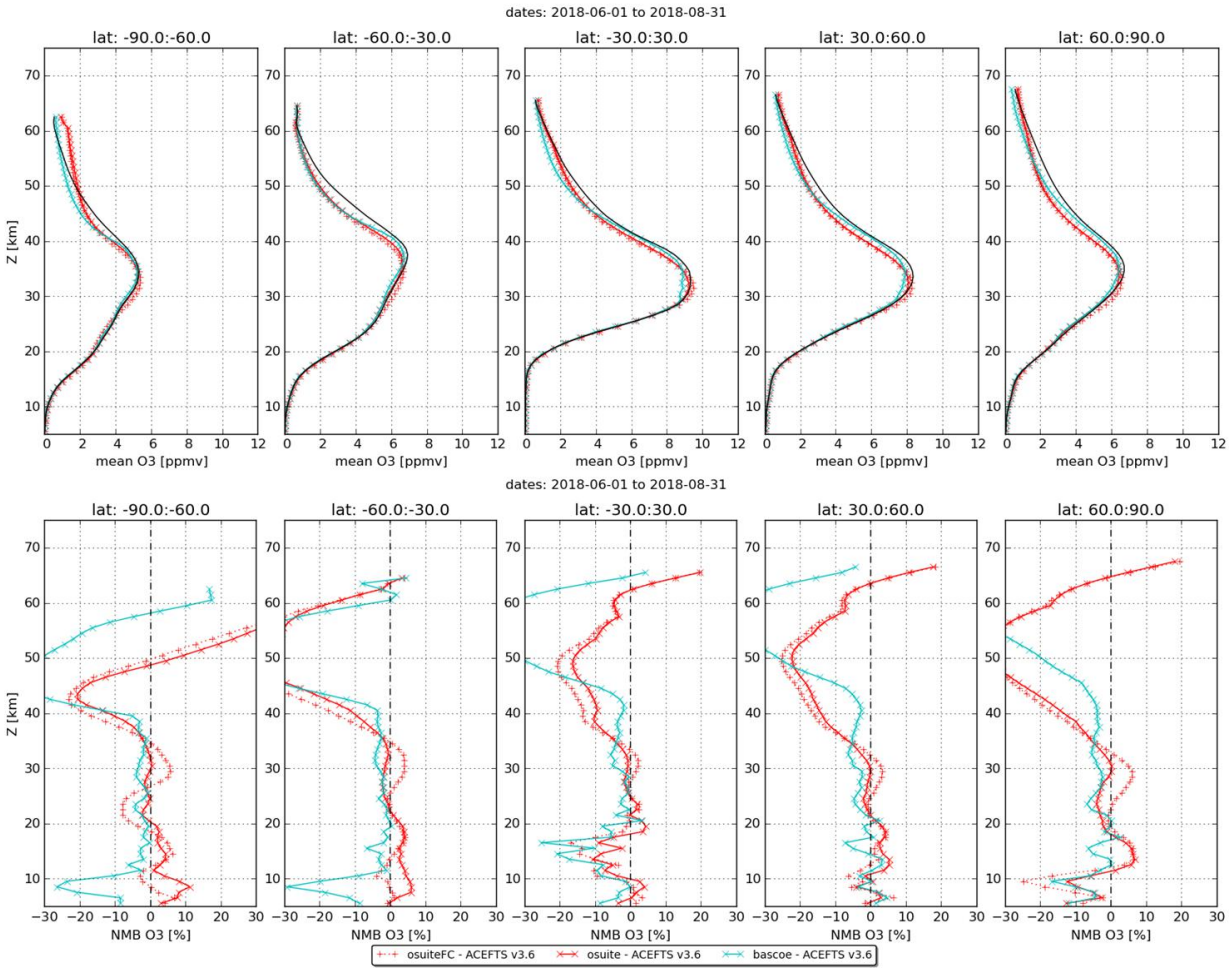

Figure 8.3.4: Mean value (top) and normalized mean bias (bottom) of the ozone profile between o-suite analyses (red, solid), o-suite forecasts 4th day (red, dotted) and BASCOE (cyan line) with ACE-FTS observations for the period June to August 2018.

8.4 Stratospheric NO_2

In this section, nitrogen dioxide from SCIAMACHY/Envisat satellite retrievals (IUP-UB v0.7) and GOME-2/MetOp-A satellite retrievals (IUP-UB v1.0) are used to validate modelled stratospheric NO_2 columns. Monthly mean stratospheric NO_2 columns from SCIAMACHY and GOME-2 have relatively small errors on the order of 20% in the tropics and in mid-latitudes in summer and even lower errors at mid-latitudes in winter. As the time resolution of the saved model files is rather coarse and NO_x photochemistry in the stratosphere has a large impact on the NO_2 columns at low sun, some uncertainty is introduced by the time interpolation at high latitudes in winter.

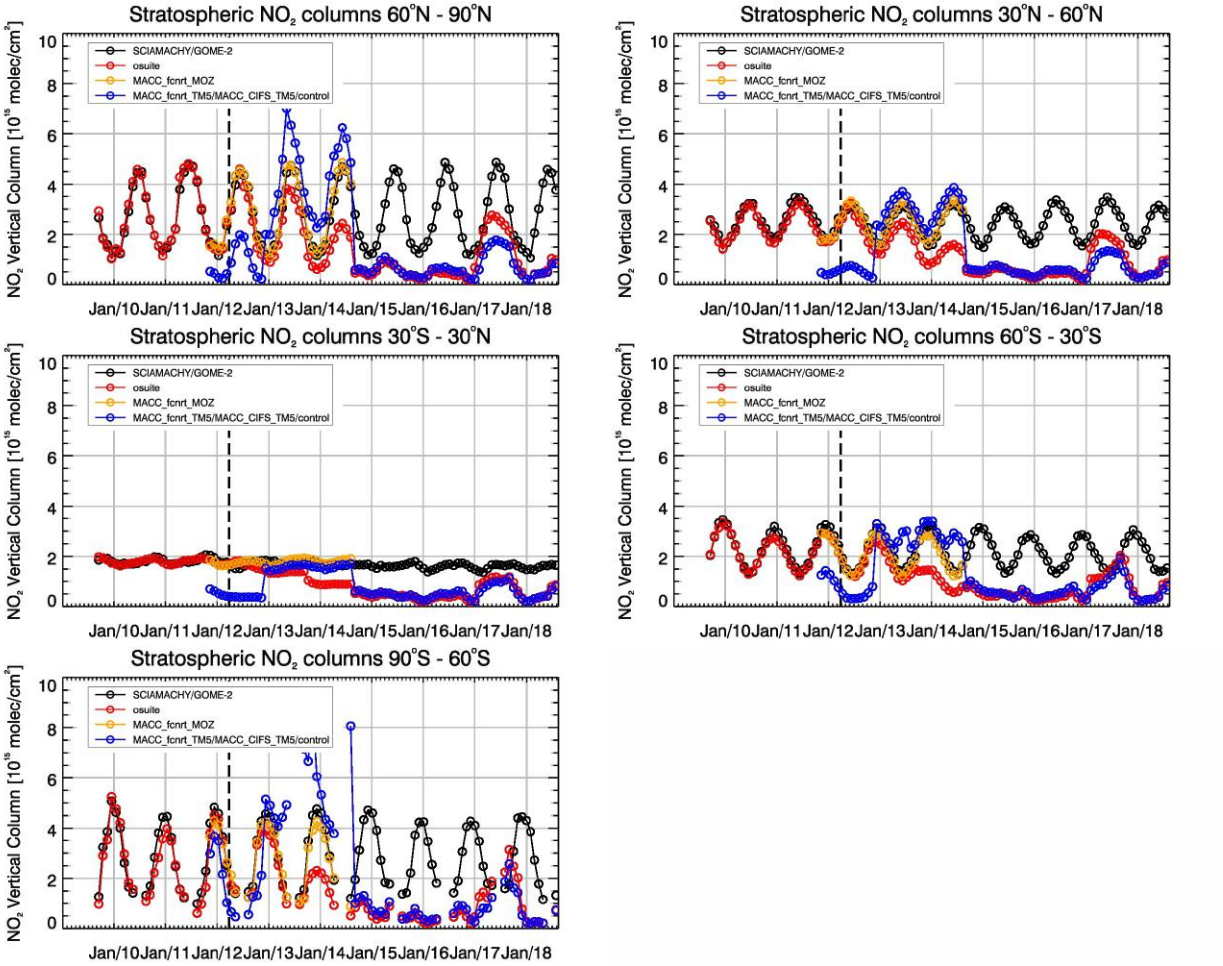

Figure 8.4.1: Time series of average stratospheric NO2 columns [1015 molec cm-2] from SCIAMACHY (up to March 2012) and GOME-2 (from April 2012) compared to model results for different latitude bands. See text for details. The blue line shows MACC_fcnrt_TM5 from November 2011 to November 2012, MACC_CIFS_TM5 results from December 2012 until August 2014 and control results from September 2014 onwards (the model run without data assimilation is termed control since Sep 2014). The vertical dashed black lines mark the change from SCIAMACHY to GOME-2 based comparisons in April 2012.

In this section, nitrogen dioxide from SCIAMACHY/Envisat satellite retrievals (IUP-UB v0.7) and GOME-2/MetOp-A satellite retrievals (IUP-UB v1.0) are used to validate modelled stratospheric NO_2 columns. Monthly mean stratospheric NO_2 columns from SCIAMACHY and GOME-2 have relatively small errors on the order of 20% in the tropics and in mid-latitudes in summer and even lower errors at mid-latitudes in winter. As the time resolution of the saved model files is rather coarse and NO_x photochemistry in the stratosphere has a large impact on the NO_2 columns at low sun, some uncertainty is introduced by the time interpolation at high latitudes in winter.

As shown in Figure 8.4.1, amplitude and seasonality of satellite stratospheric NO_2 columns are poorly modelled with CB05-based chemistry runs including the more recent versions of the o-suite. The significant differences between observations and CB05 chemistry runs, i.e. a strong underestimation of satellite retrievals by models, can be explained by the missing stratospheric chemistry for these model versions. The only constraint on stratospheric NO_x is implicitly made by fixing the HNO_3/O_3 ratio at the 10 hPa level. This assumption, in combination with the changing

model settings for stratospheric O_3 for control compared to MACC_CIFS_TM5, may explain some of the jumps we see in stratospheric NO_2. In any of these runs the stratospheric NO_2 is poorly constrained. It clearly indicates that stratospheric NO_2 in the latest versions of the o-suite is not a useful product and should be disregarded. However, model simulated values increased with an upgrade of the osuite in February 2017, so that simulations are closer to the satellite observations for 2017 only, especially for northern hemisphere latitude bands where seasonality seems to have been reproduced (in contrast to the Southern Hemisphere) by the o-suite apart from the pronounced underestimation. O-suite values are larger than the control in 2017 at all latitude bands. However, the better agreement found for 2017 does not continue for 2018 and values decreased again to the magnitude of 2015-2016 runs at all latitude bands.

Comparison of the o-suite from July 2012 until August 2014 with the other model runs and satellite observations shows that the previous version of the o-suite stratospheric NO_2 columns had a systematic low bias relative to those from MACC_fcnrt_MOZ and satellite observations for all latitude bands. For example, o-suite values are a factor of 2 smaller than satellite values between 60°S to 90°S for October 2013. Best performance was achieved with the MOZART chemistry experiments without data assimilation (MACC_fcnrt_MOZ, running until September 2014), especially northwards of 30°S. Details on the NO_2 evaluation can be found at: http://www.doas-bremen.de/macc/macc_veri_iup_home.html.

9. Validation results for greenhouse gases

This section describes the NRT validation of the pre-operational, high resolution forecast of CO_2 and CH_4 from 1st January 2017 to 1st September 2018 based on observations from 16 surface stations, mostly located in Western Europe; 13 TCCON stations measuring xCO_2 and xCH_4 total columns, and 13 NDACC stations measuring partial and total CH_4 columns. We compare the observations to the the high-resolution forecast experiment (*gqpe, Tco1279; 9x9 km*), coupled to the analysis experiment (*gqiq, Tco399, 25x25 km*). This forecast experiment is using the IFS model cycle CY43R1, and has been officially implemented on 1st Nov. 2017. In this report the *gqpe* experiment is used continuously since 1st January for the surface data, whereas column observations are compared to *ghqy* and *gqpe* experiments respectively from 1st March 2016 to 1st March 2018, and from this date onwards.

9.1 CH4 and CO2 validation against ICOS observations

Figures 9.1.1 and 9.1.2 show the CO_2 and CH_4 comparisons at four stations in South hemisphere (Amsterdam I.), North hemisphere (Mace Head, Trainou tall tower) and in the tropics (Lamto). There is no significant difference between the analysis experiment and the high resolution forecast regarding the trend and the seasonal scale variability, with the only exception of CO_2 at Lamto where the FC is closer to the observations from January to June 2018 (CO_2 concentrations in the analysis are 20 ppm or about 4% higher than the FC). At other stations only minor differences between the analysis and the high resolution FC can be observed at the synoptic scale, and those can be explained by the differences in the resolution. For example at the coastal site of MHD the analysis experiment displays more CO_2 spikes due to the local land based emissions.

The best agreement is obtained at the two north hemisphere sites for both CO_2 and CH_4. This is due particularly to the good representation of the wintertime pollution events observed regularly at MHD and TRN. The timing of those synoptic events are very well simulated even if their amplitudes are generally underestimated by 1 to 3% for CO_2. At the Trainou tall tower, located about 100km south of Paris, the synoptic variability agree within ±2% for CO_2, but the amplitude of the simulated CH_4 spikes is overestimated by up to 20%. The same patterns are observed at the Saclay tall tower (Figure 9.1.3), located 20km of Paris, indicating probably an overestimation of the CH_4 emissions in the Paris area.

The remote station of AMS, in South hemisphere, indicates a clear overestimation of the CO_2 trend (about +0.5%/year) and instead an underestimation of the CH_4 trend (about -0.7%/year). This is probably a common feature to all stations, which can only be detected at AMS thanks to the low seasonal and synoptic scale variabilities.

At the tropical station of Lamto, the model shows a very poor correlation coefficient for CO_2 (r^2=0.06) due to a poor representation of both synoptic events and seasonal cycle. The maximum values observed between October and March correspond to the period of fires in Western Africa. For CH_4 we observe a better correlation (r^2=0.5) but the model systematically underestimates the observed variabilities at synoptic and seasonal scales with a bias ranging from 0% to -6%.

The figure 9.1.3 presents the annual metrics for all surface stations based on comparisons of the daily means mole fractions, with a distinction between observed and simulated data obtained for daytime (12-16hr local time) and night time (00-04hr local time). There is a significant improvement of the performance of the model when looking exclusively at daytime time series, especially for CO_2. Some common features are emerging from the 16 sites.

First, for CO_2 we see a systematic improvement of the correlation coefficient, the RMSE and the bias with the sampling heights of the ICOS tall towers, especially during the night. During the day the correlation coefficients are greater than 0.75 for all sampling levels, a performance which is also reached during the night for sampling levels higher than 100m. We observe a convergence of the correlation coefficient, RMSE and biases (mostly negative during the night and positive during the day) with the elevation of the sampling lines. For sampling heights lower than 50m from the ground the mean CO_2 biases are +4.3 ppm and -2.6 ppm respectively during day and night, whereas above 100m they are down to +1.5 and -0.6 ppm. At tropical sites (CHC, GUY, LTO) the correlation coefficients are significantly poorer, ranging from 0.2 to 0.7.

For CH_4, there is much less difference of the model performance between day and night. The coefficient of correlations are generally higher than 0.75 with few exceptions, mostly at tropical sites. In North hemisphere the model has more difficulty to represent the variability observed at Saclay and Trainou tall towers. The model strongly overestimates the synoptic events associated to the emission from Paris area, located at 20 and 100 km respectively from the two stations. Apart from those two stations the mean biases in North hemisphere are 33, 7 and -6 ppb respectively for tall towers, coastal and mountain sites. At Amsterdam Island in South Hemisphere the mean bias is +1.2 ppb. All tropical sites appear as outliers compared to the North hemisphere stations, illustrating the difficulty of the model to represent those stations.

In figure 9.1.4 we have merged all European stations in one category (Northern hemisphere), whereas other sites are split in two categories, namely southern hemisphere and tropics. From this synthesis we can conclude that the seasonal cycle of the CO_2 is overestimated over Europe. Positive biases up to 4 ppm in winter/spring are followed by negative biases up to -5 ppm in late summer and autumn. For CH_4 in Europe the summertime values present a bias close to zero, whereas in winter and autumn the mean bias is around 20 ppb. South hemisphere and tropical station both display increasing trends (positive for CO_2, negative for CH_4).

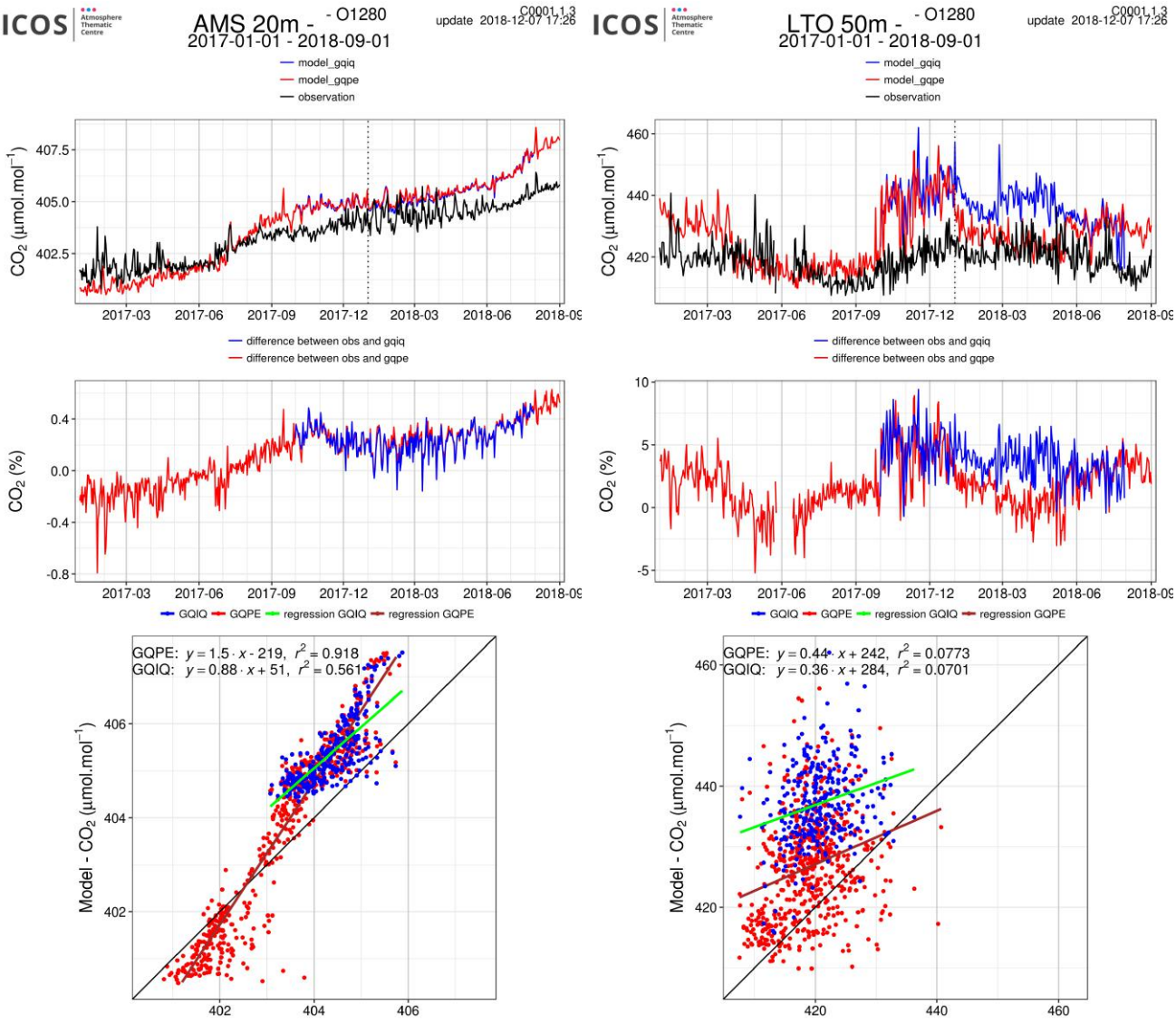
ICOS Atmosphere Thematic Centre
AMS 20m - O1280
2017-01-01 - 2018-09-01
update 2018-12-07 17:26
C0001.1.3
model_gqiq
model_gqpe
observation
CO2 (µmol.mol−1)
difference between obs and gqiq
difference between obs and gqpe
CO2 (%)
GQIQ GQPE regression GQIQ regression GQPE
GQPE: y = 1.5 · x - 219, r2 = 0.918
GQIQ: y = 0.88 · x + 51, r2 = 0.561
Model - CO2 (µmol.mol−1)
LTO 50m - O1280
GQPE: y = 0.44 · x + 242, r2 = 0.0773
GQIQ: y = 0.36 · x + 284, r2 = 0.0701

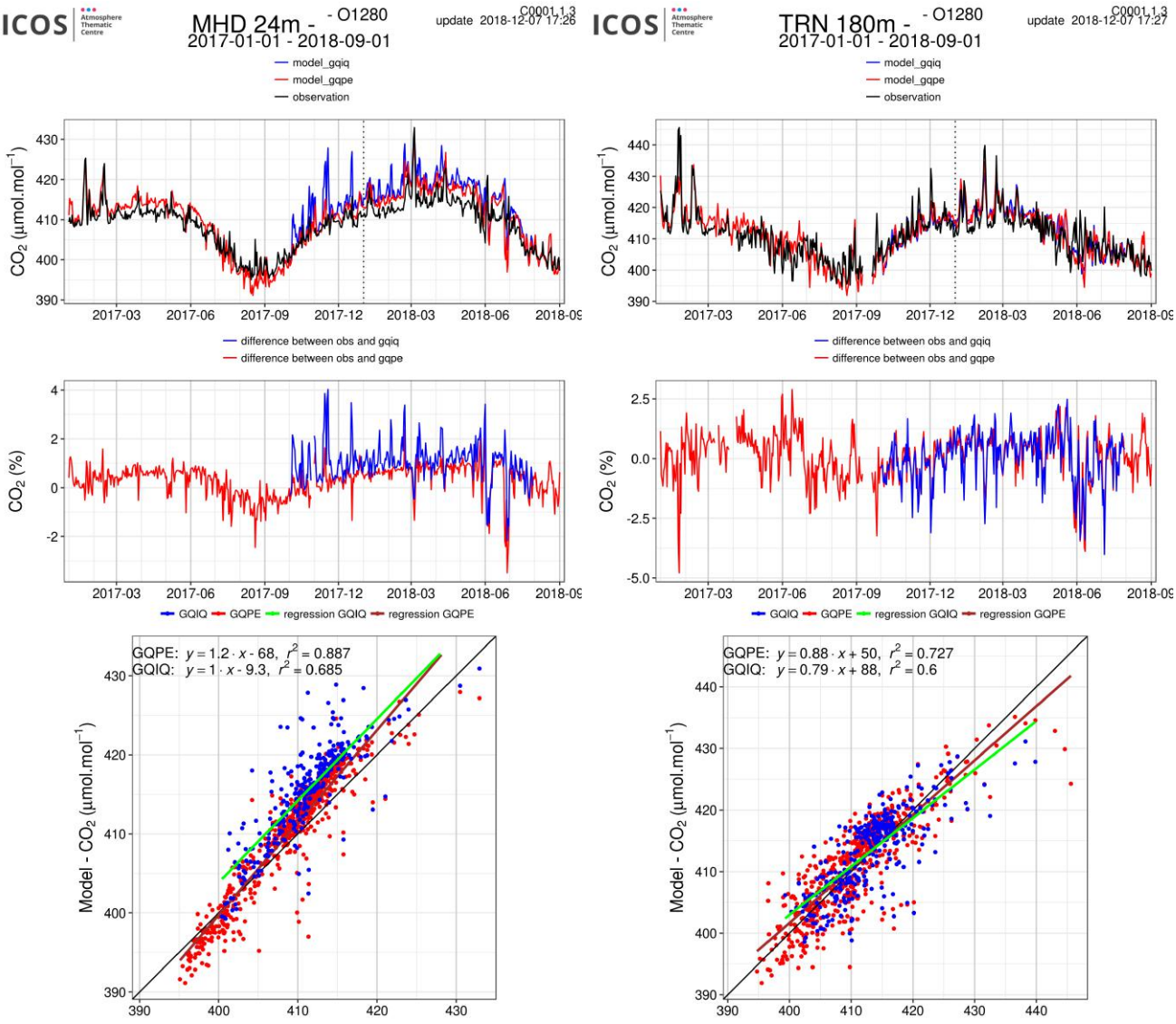

Figure 9.1.1: Above: Comparison of CO_2 daily means observed (black) with the analysis model (blue) and the high resolution forecast (red) at four stations (Amsterdam I. - AMS, Mace Head - MHD, Lamto - LTO and Trainou - TRN tall tower). Middle: differences of the observations minus the simulations. Below: Linear fit between observations and simulations.

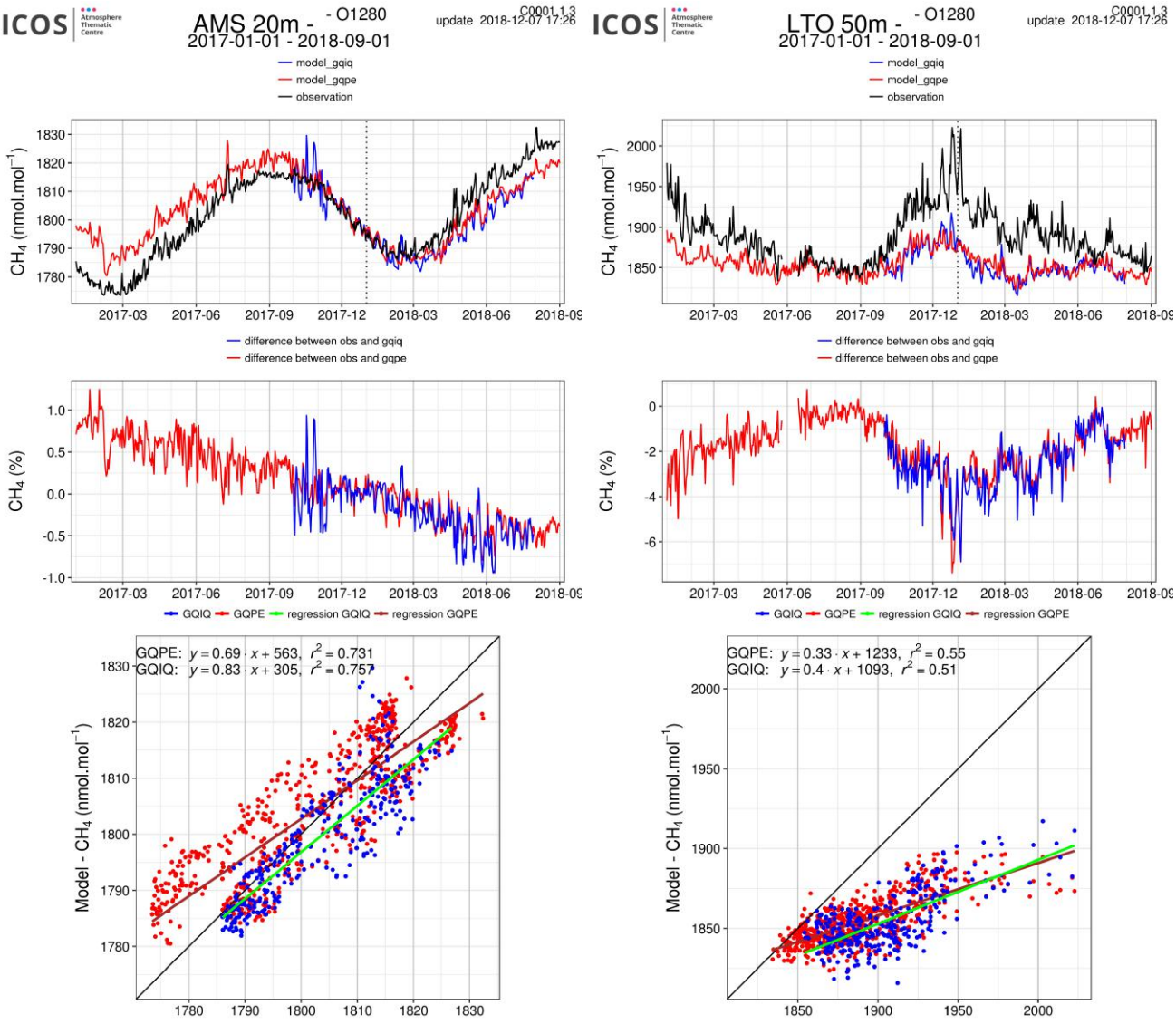
ICOS Atmosphere Thematic Centre
AMS 20m - O1280
2017-01-01 - 2018-09-01
update 2018-12-07 17:26
C0001.1.3
model_gqiq
model_gqpe
observation
CH4 (nmol.mol−1)
difference between obs and gqiq
difference between obs and gqpe
CH4 (%)
GQIQ GQPE regression GQIQ regression GQPE
GQPE: y = 0.69 · x + 563, r2 = 0.731
GQIQ: y = 0.83 · x + 305, r2 = 0.757
Model - CH4 (nmol.mol−1)
ICOS Atmosphere Thematic Centre
LTO 50m - O1280
2017-01-01 - 2018-09-01
update 2018-12-07 17:26
C0001.1.3
GQPE: y = 0.33 · x + 1233, r2 = 0.55
GQIQ: y = 0.4 · x + 1093, r2 = 0.51

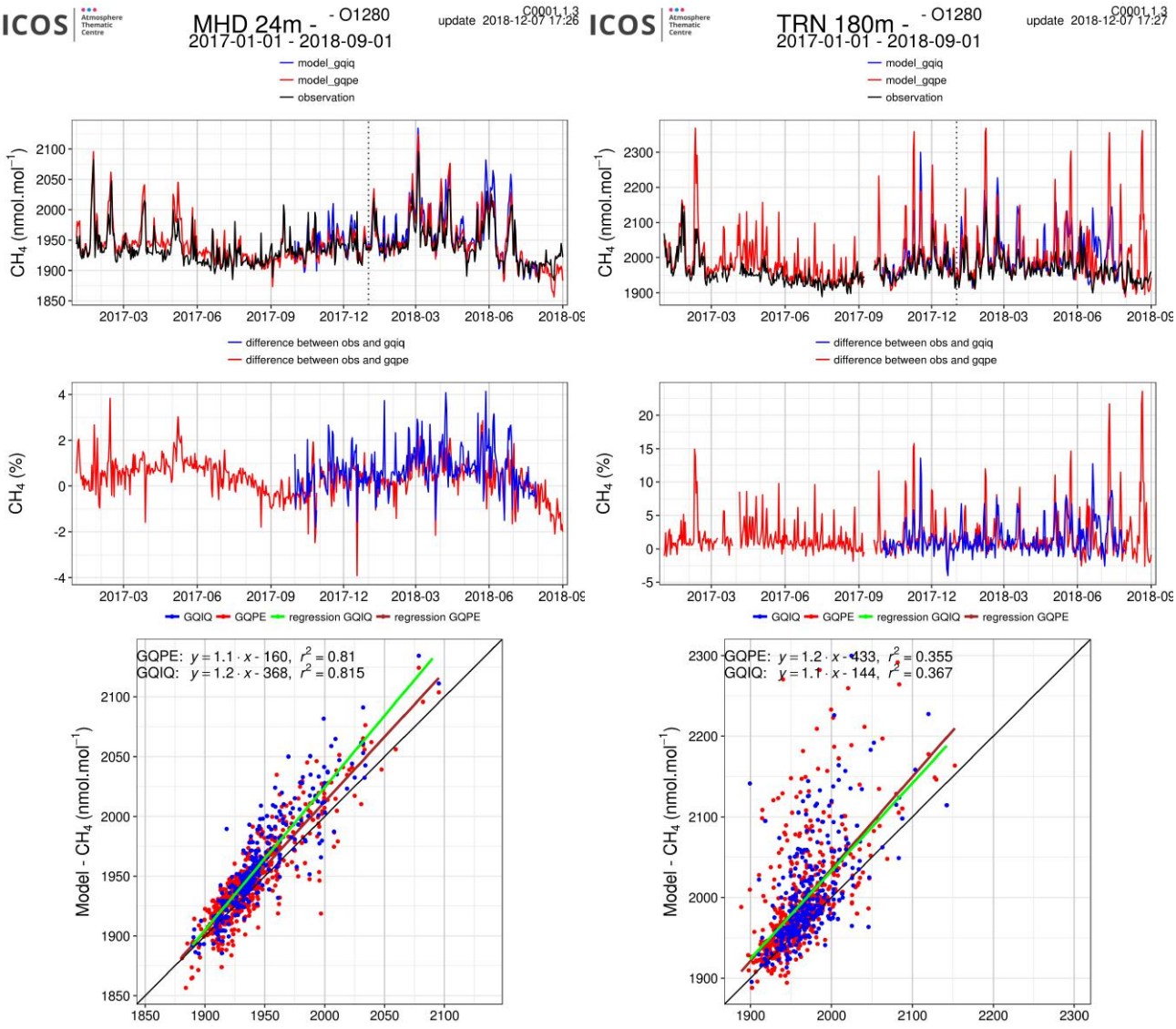

Figure 9.1.2: Same as figure 9.1.1 for CH_4

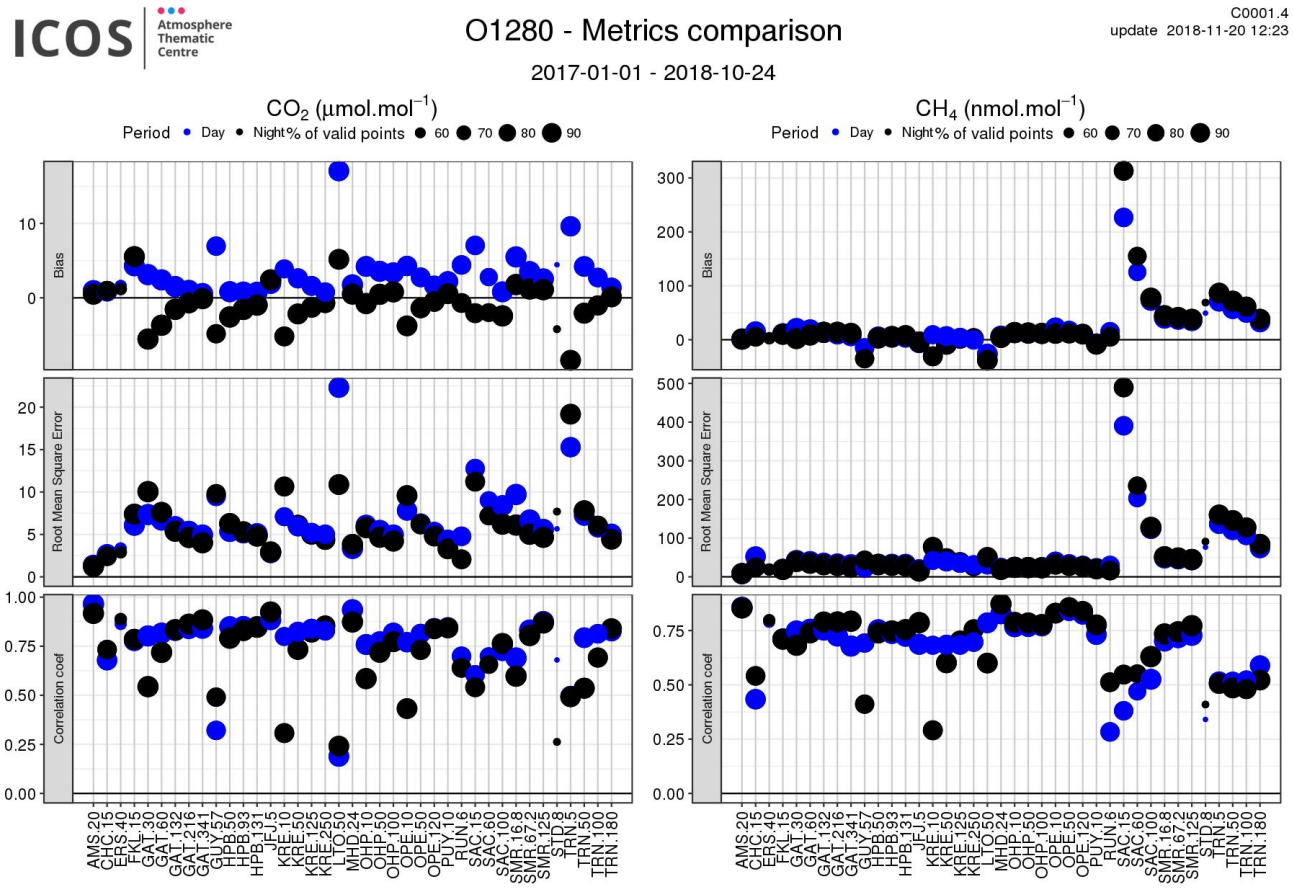

Figure 9.1.3: Annual metrics (bias, RMSE and coefficient correlation) calculated from the model-data comparison for daily means of CO_2 (left) and CH_4 (right) at the 20 sites (with multiple sampling heights at 8 tall towers). The size of each point relates to the percentage of available data. This figure uses the GQPE forecast experiment from 1st January 2017 to 25 March 2018. Daytime data (12-16 hr local time) are shown in blue, and nighttime data (00-04 hr local time) in black.

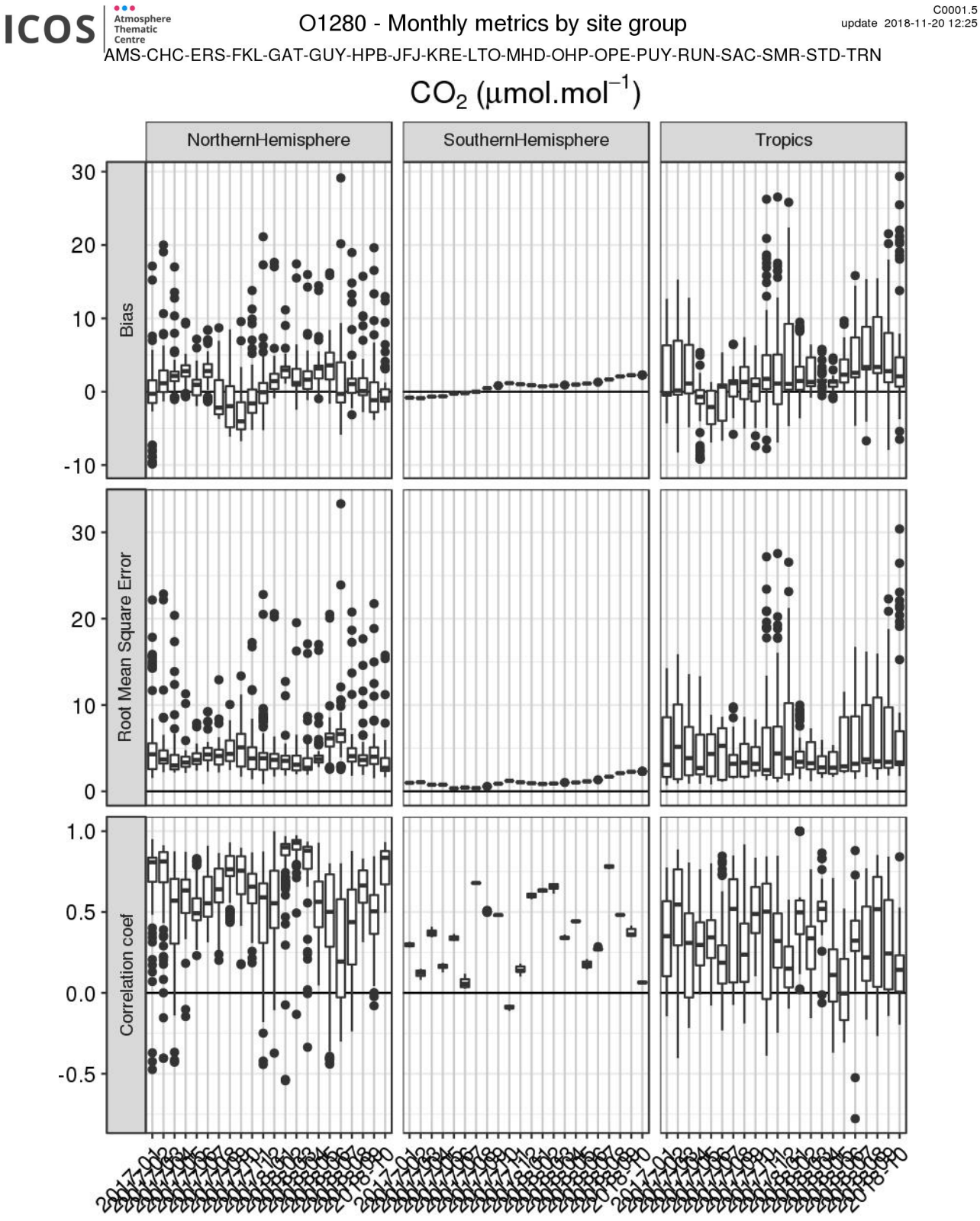
ICOS
Atmosphere Thematic Centre
O1280 - Monthly metrics by site group
C0001.5
update 2018-11-20 12:25
AMS-CHC-ERS-FKL-GAT-GUY-HPB-JFJ-KRE-LTO-MHD-OHP-OPE-PUY-RUN-SAC-SMR-STD-TRN
CO2 (µmol.mol−1)
NorthernHemisphere
SouthernHemisphere
Tropics
Bias
Root Mean Square Error
Correlation coef
30
20
10
0
-10
1.0
0.5
0.0
-0.5

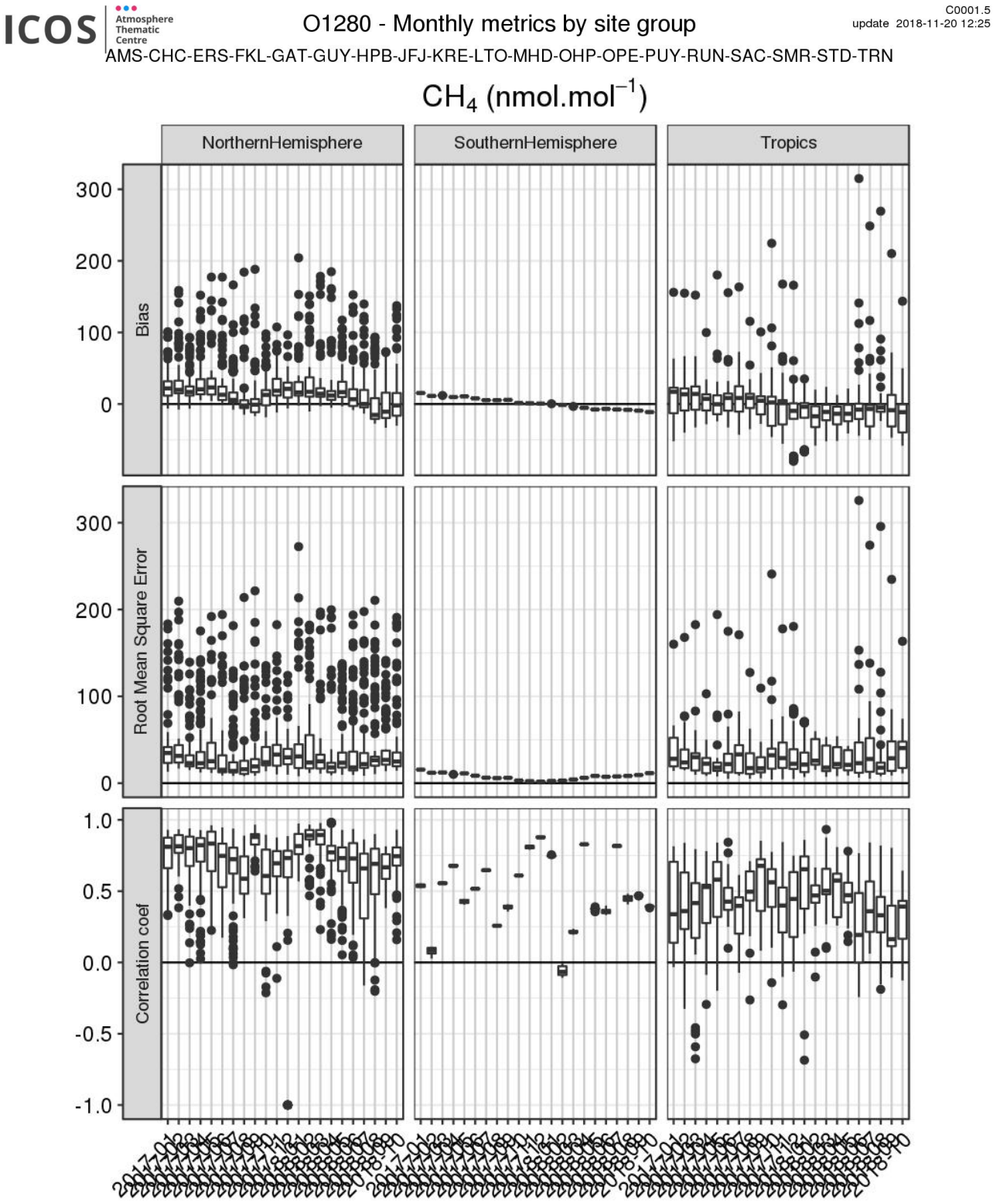

Figure 9.1.4: Annual metrics (bias, RMSE and coefficient correlation) calculated from the model-data comparison for daily means of CO_2 (left) and CH_4 (right) for three groups of stations: North hemisphere (Western Europe), Tropics and South hemisphere. This figure uses GQPE forecast experiment from 1st January 2017 to 1st November 2018.

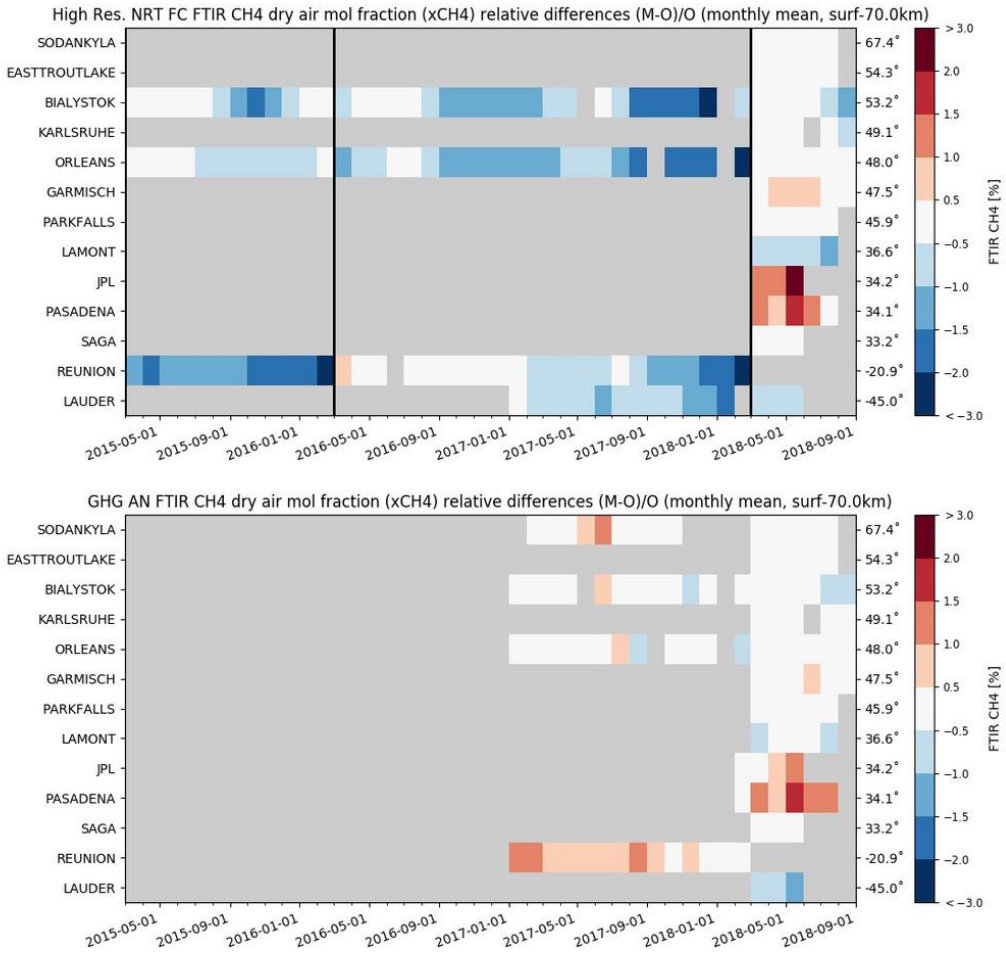

Figure 9.2.1: Monthly mean relative bias for column averaged CH_4 mole fractions for the period May 2015 – August 2018 for high resolution forecast (top) and for the analysis model (bottom).

9.2 CH_4 and CO_2 validation against TCCON observations

For the validation column averaged mole fractions of CO_2 and CH_4 (denoted as XCO2 and XCH4) from the Total Carbon Column Observing Network (TCCON) are used. Column averaged mole fractions provide different information than the in situ measurements and are therefore complementary to the in situ data. For example, if models suffer from problems in vertical transport, the combination of TCCON and surface in situ measurements will provide a means to detect this.

The validation routines used for TCCON data are the same as used for the NDACC network and are documented in Langerock et al. (2015). The routines have been adapted to use the TCCON data format. Only measurements within 2.5h around local noon have been used for the comparison. The reason is that at high solar zenith angles the comparison worsens due to the averaging kernels. This issue is being investigated.

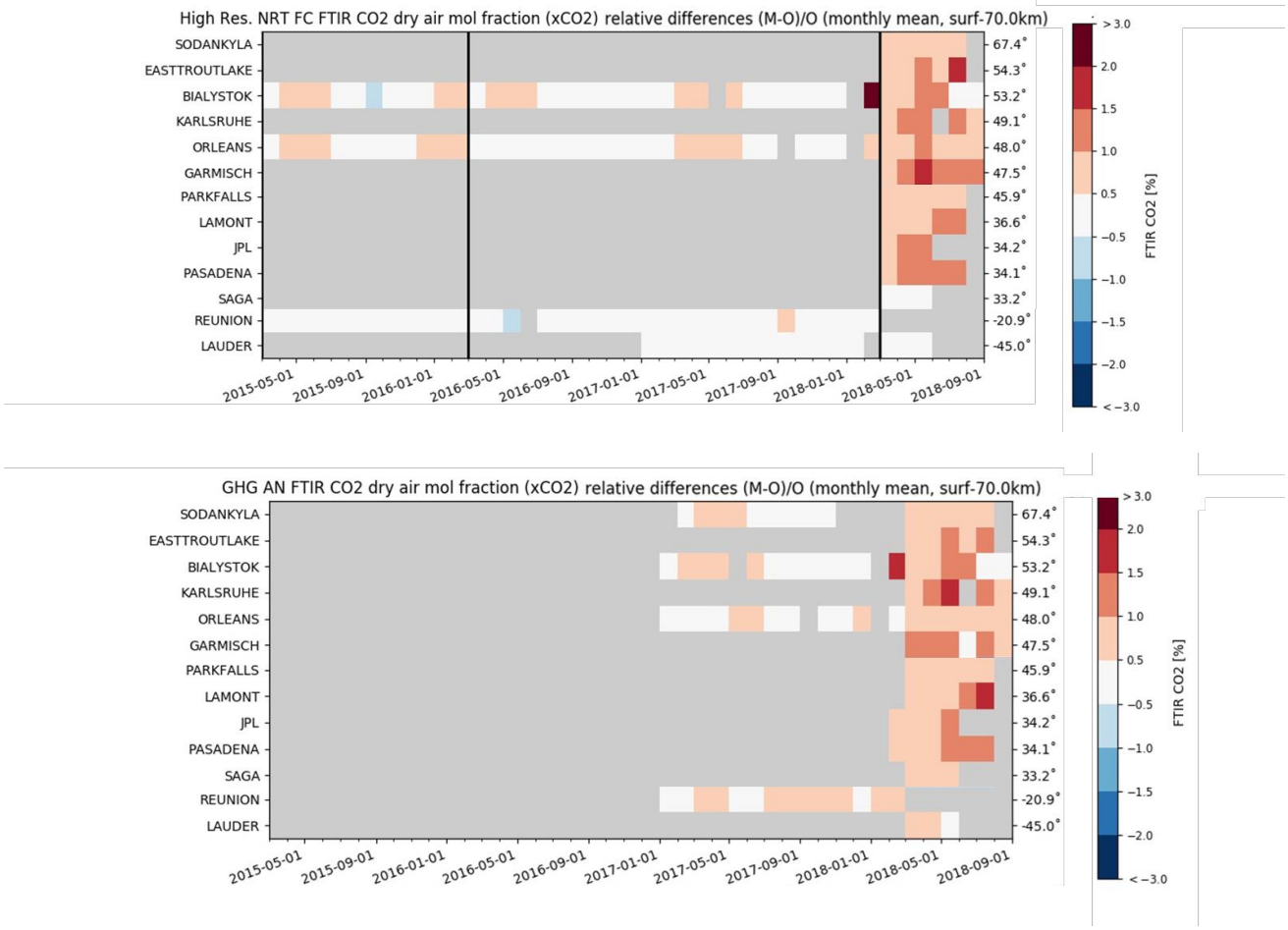

Figure 9.2.2: Monthly mean relative bias for column averaged CO_2 mole fractions for the period May 2015 – August 2018 for high resolution forecast (top) and for the analysis model (bottom).

For the model validation the official TCCON data is used and in addition rapid delivery data (RD-TCCON data), which is available at least one month after the measurement. TCCON sites that deliver RD-TCCON data currently include Trainou (France), Bialystok (Poland) and Reunion (France). TCCON requires that data providers make the data publically one year after the measurement.

The upper plot in Figure 9.3.1 shows the monthly mean relative bias for column averaged CH_4 mole fractions for the period May 2015 – August 2018. The stations on the vertical axis are ordered by latitude and the latitude is indicated on the vertical axis on the right side. The vertical black bars in the plot represent the timing of changes in the model. Prior May 2018 only the stations Bialystok, Orleans and Reunion have been used for the comparison, since only from these stations rapid data was available.

After the latest model change in May 2015 a very good agreement between measurements and high resolution model is seen in the northern hemisphere, except for the stations JPL and Pasadena. These two sites are strongly influenced by CH_4 emissions from urbanized Los Angeles basin. The model overestimates the CH_4 at these two stations. It has been reported that the individual contributions to the emission inventories are not well resolved for this area (Wunch et al., 2009, Wennberg et al., 2012). The comparison in Figure 9.3.1 suggest that the emissions of the CAMS

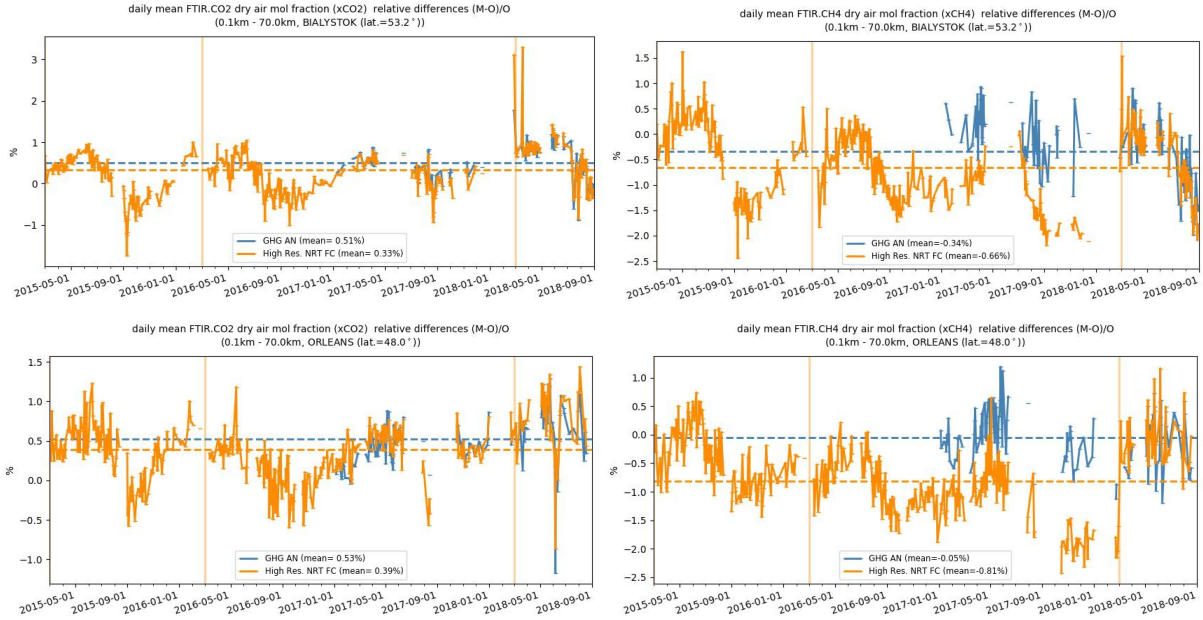

Figure 9.2.3: Daily mean of relative differences for CO_2 (left) and CH_4 (right) total columns (right) at Bialystok (top) and Orléans (bottom). The simulated columns are taken from three successive high resolution forecast experiments: gf39 (until 2016,3,1); ghqy (until 2018,3,1) and gqpe from 2018,3,1 onwards.

model are too high for the Los Angeles basin. At the southern hemispheric site Lauder the model underestimates the CH_4.

The analysis model shows qualitatively the same pattern than the high resolution model for the period after May 2018.

The upper plot in Figure 9.3.2 shows the monthly mean relative bias for column averaged CO_2 mole fractions for the period May 2015 – August 2018. The stations on the vertical axis are ordered by latitude and the latitude is indicated on the vertical axis on the right side. The vertical black bars in the plot represent the timing of changes in the model. Prior to May 2018 only the stations Bialystok, Orleans and Reunion have been used for the comparison, since only from these stations rapid data was available.

After the latest model change in May 2015 both, the high resolution and the analysis model, overestimate the CO_2 in the northern hemisphere up to 1.5%, which is significant in the case of CO_2. At the southern hemispheric site in Lauder the comparison is better. However, for a closer analysis a longer time period is needed for the northern as well as for the southern hemisphere. This will be done in the upcoming reports.

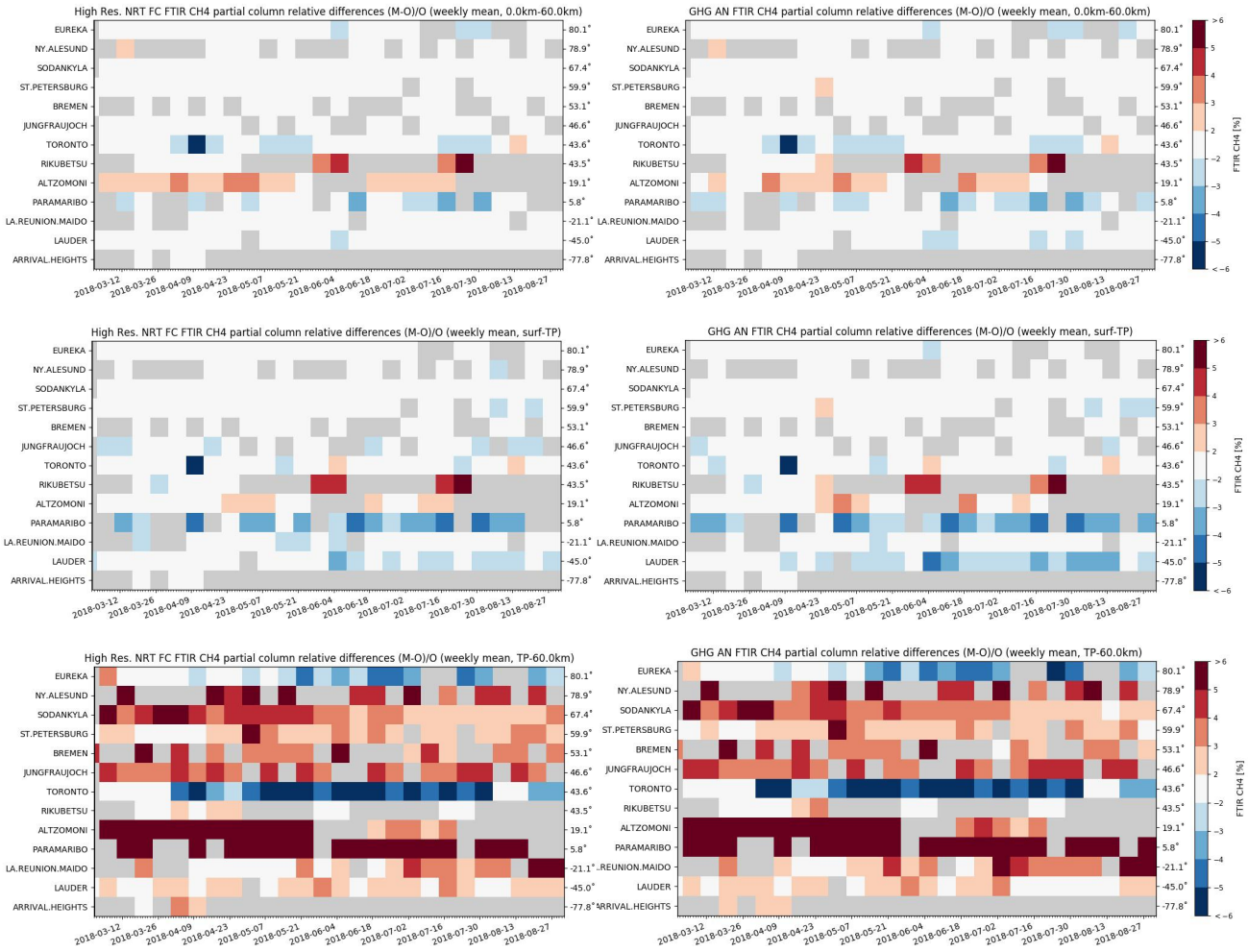

Figure 9.3.1: Weekly mean relative bias for total (top row), tropospheric (middle row) and stratospheric CH_4 columns (bottom row) for the period March 2018 – August 2018 for high resolution forecast (left) and the analysis (right). Stratospheric columns are plotted with a different color scale. The mid latitude stations at Rikubetsu and Altzomoni show a strong overestimation for both models of the CH_4 column. The overall uncertainty for the CH_4 total column measurements is approximately 4%.

9.3 Validation against FTIR observations from the NDACC network

In this section, we compare the CH_4 profiles of the CAMS GHG models with FTIR measurements at different FTIR stations within the NDACC network. These ground-based, remote-sensing instruments are sensitive to the CH_4 abundance in the troposphere and lower stratosphere, i.e. between the surface and up to 25 km altitude. Tropospheric and stratospheric CH_4 columns are calculated from the FTIR profile data and used to validate corresponding columns obtained from the model data. A description of the instruments and applied methodologies can be found at http://nors.aeronomie.be. The typical uncertainty on the FTIR tropospheric column is 3.5%, while the uncertainty on the stratospheric column is 7.5%, adding together to a 4% uncertainty on the total column. The systematic uncertainty is large for the NDACC methane product mostly due to higher spectroscopic uncertainties.

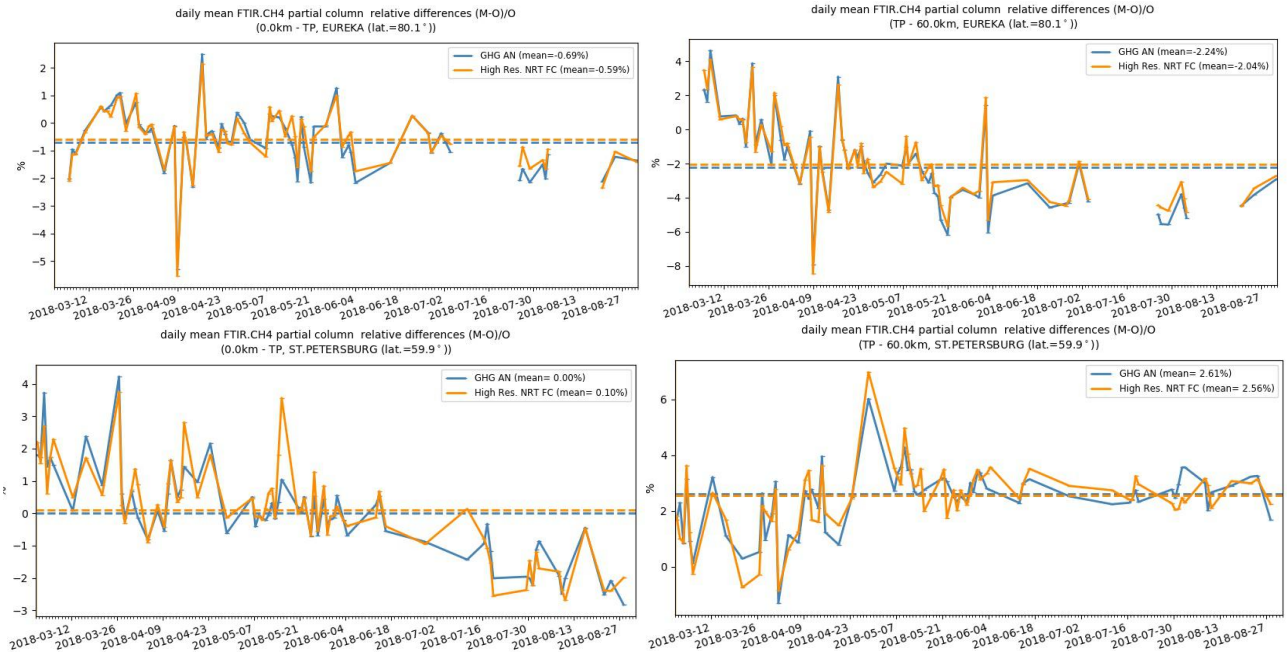

Figure 9.3.2: Daily mean of relative differences for tropospheric CH4 columns (left) and stratospheric CH4 columns (right) at Eureka (top) and St Petersburg (bottom). The performance change at Eureka changes from a positive bias in March-April for the stratospheric column to a negative bias in July-August, while at St Petersburg the tropospheric column performs worse during June-August.

Figure 9.3.1 shows that the tropospheric columns of CH_4 agree well and only small differences appear between the analysis and the high resolution model. The total column validation results correspond to the TCCON observations in Figure 9.2.1, where an overestimation is seen at the mid latitudes in the NH (Rikubetsu and Altzomoni) and an underestimation in Lauder (New Zeeland).

At some sites a clear trend is observed in either the tropospheric or stratospheric concentrations. Due to the limited time period, it is unclear if this is related to seasonal dependent model performance or a long term trend. In Figure 3.9.2 the tropospheric and stratospheric column time series are plotted at Eureka and St. Petersburg.

Figure 9.3.3 shows Taylor diagrams for the JJA time period and for a selected number of sites: stations with limited observations are left out and Toronto because its time series contains some outliers which impacts its correlation. Assimilation has a small effect on the correlation coefficients.

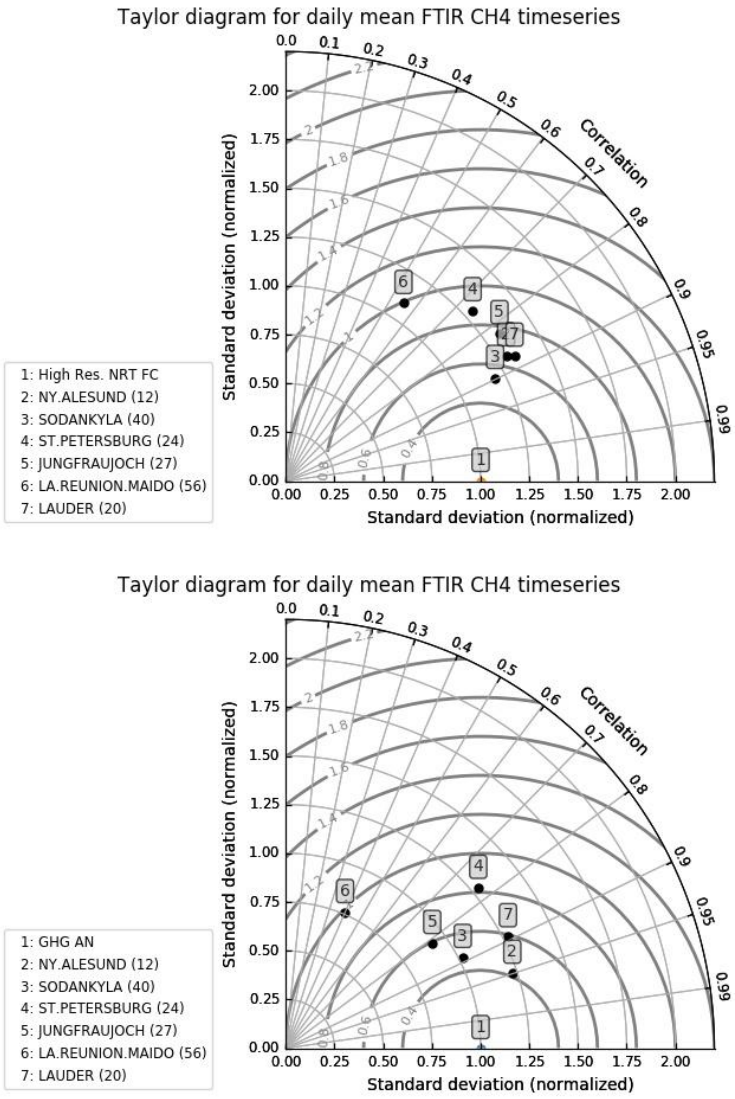

Figure 9.3.3: Taylor diagrams relating the standard deviations for the model /GB time series of total CH_4 column data and their correlation for the period JJA 2018 (the stations with a limited number of measurements are left out). All time series are normalized such that the std of the model is 1. The high resolution forecast (left) has lower performance on variability (> 1.25) compared to the analysis (right) with values <=1.25. The correlation for the analysis is larger for most sites.

10. Event studies

10.1 North Atlantic dust transport over the Iberian Peninsula during August 2018

In early-August 2018, MODIS satellite detected a North Atlantic dust plume with origin in Northern Algeria on 1st August. The dust plume moved to the East following an arc shape trajectory over the Atlantic, arriving in Southern Portugal on the 2nd of August, in North-western Spain on the early 3rd of August and Central Spain on the late 3rd of August. This North Atlantic dust trajectory was nicely tracked by the AERONET sunphotometers in the Iberian Peninsula (see Figure 10.1.2) and reached maximum AOD values of 1.2 over Portugal.

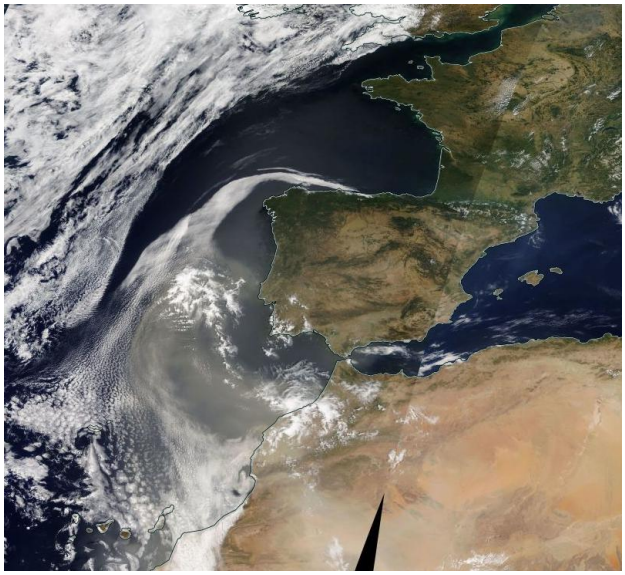

Figure 10.1.1: Daily composite of NASA MODIS/Terra on 2nd August 2018.

CAMS AOD o-suite did timely reproduce the spatial distribution of the dust plume over the Arabian Peninsula in comparison with AERONET in Evora (Portugal), Coruna (NW Spain) and Madrid (Central Spain), see Figure 10.1.2, despite the model tendency to underestimate the observed maximum values. At surface levels, the CAMS model predicts the spatial evolution of the dust transport over the Eastern Iberian Peninsula, with values up to 120 μg/m^3 on the 4th of August (see Figure 10.1.2 and 10.1.3).

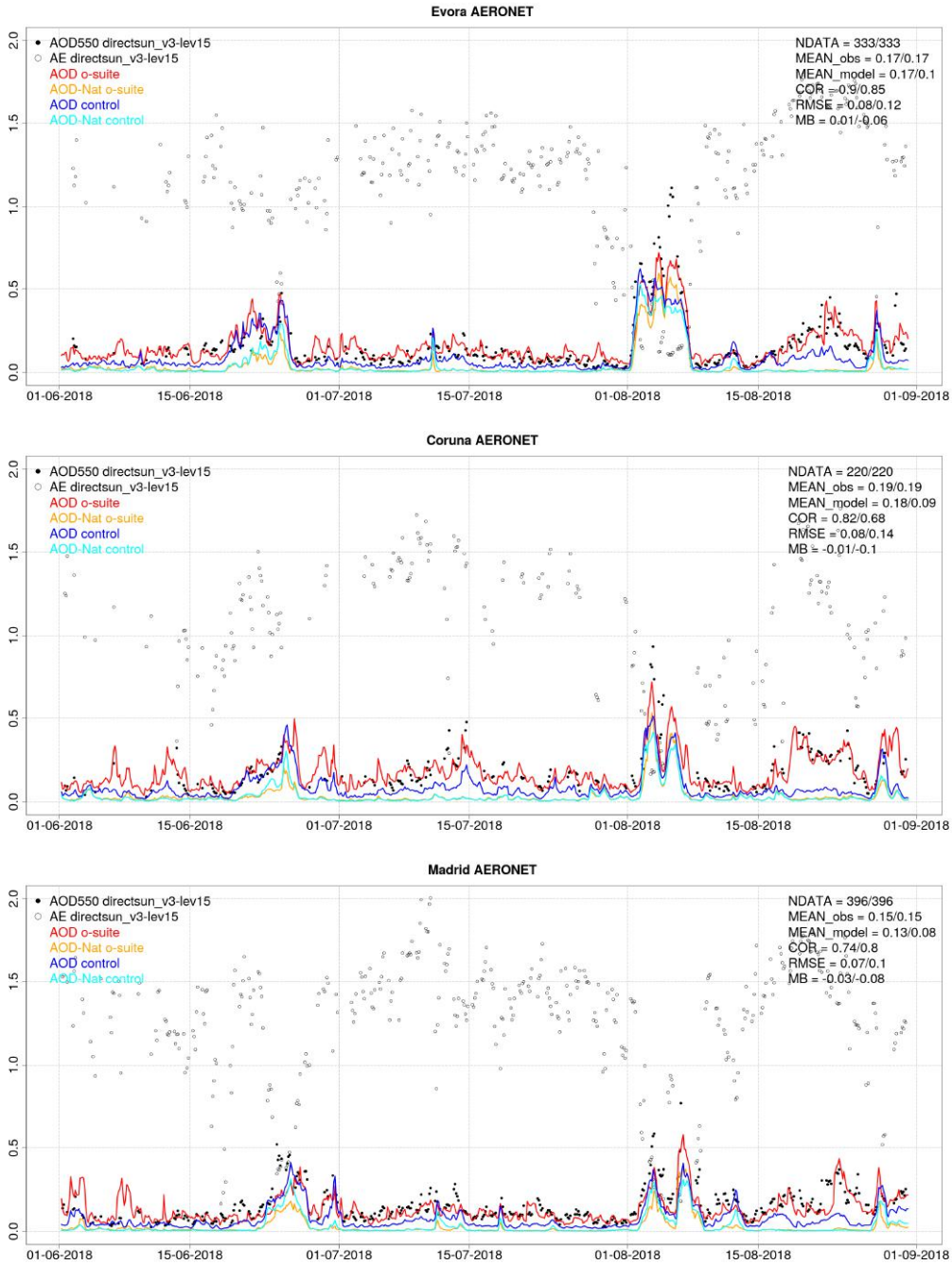

Figure 10.1.2: AOD from AERONET (black dot), AOD o-suite (red line), AOD control (blue line), AOD-Nat o-suite (orange line), AOD-Nat control (cyan line), for the study period over Evora (Portugal), Coruna (NW Spain) and Madrid (Central Spain). AOD-Nat corresponds to the natural aerosol optical depth that includes dust and sea-salt. Skill scores per each individual site and model (o—suite/control) are shown in the upper right corner (NDATA: available 3-hourly values used for the calculations, MEAN observations, MEAN_model, COR, RMSE, MB).

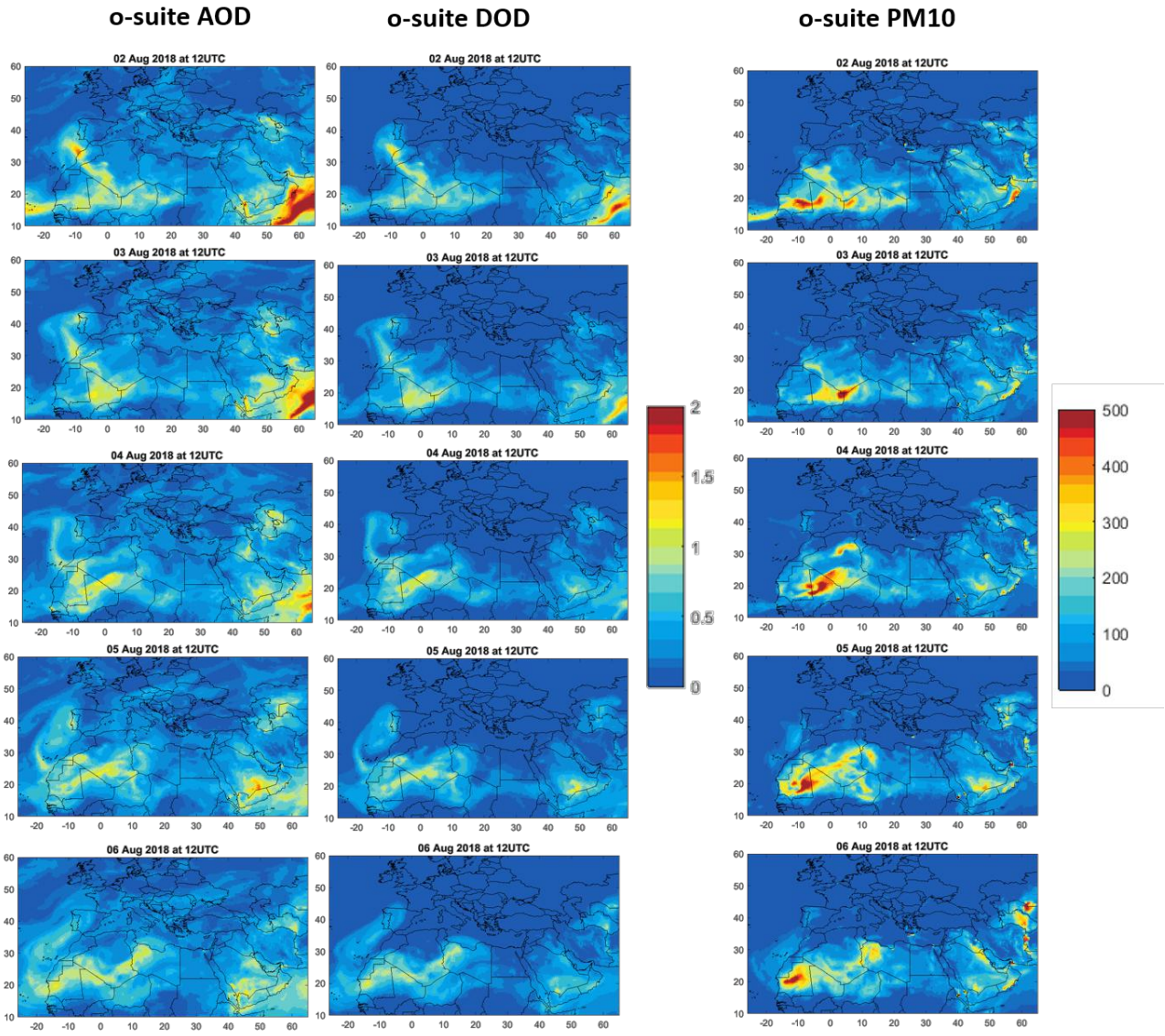

Figure 10.1.3. AOD and DOD at 12UTC from o-suite (left and central columns) and PM10 (in µg/m^3) at 12UTC from o-suite (right column) for 2-6 August 2018.

10.2. Fire events in Alaska in July 2018

Several fire events were detected during July 2018 in Alaska region. The first CO peak detected by MOPITT and IASI from July 7 to 9 was well captured by both model runs. A second fire event detected around July 22 was underestimated by both model runs by about 20%. Apart from the days with high CO values, the control run shows slightly better agreement with the satellite data compared to o-suite.

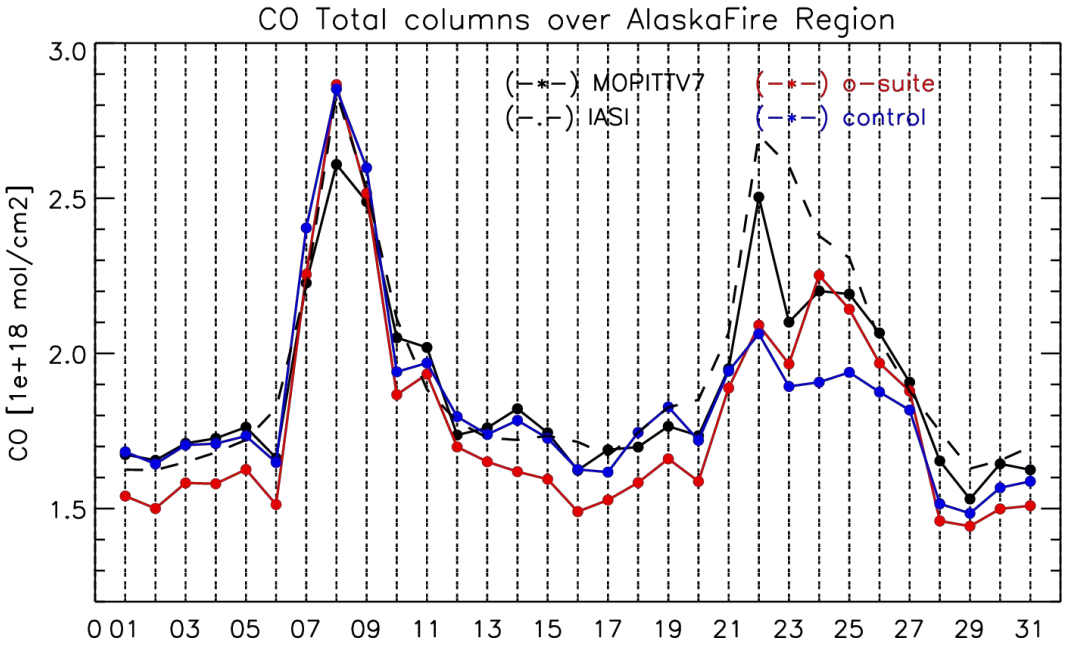

Fig. 10.2.1. Time series of CO total columns during July 2018 over Alaska regions from: MOPITT v7 (black), IASI (black), o-suite (red) and control (blue) runs.

11. References

Agusti-Panareda, A., Monitoring upgrades of analysis/forecast system, MACC-III Deliverable D44.04, June 2015.

Bergamaschi, P., Frankenberg, C., Meirink, J. F., Krol, M., Villani, M. G., Houweling, S., Dentener, F., Dlugokencky, E. J., Miller, J. B., Gatti, L. V., Engel, A., and Levin, I.: Inverse modeling of global and regional CH4 emissions using SCIAMACHY satellite retrievals, J. Geophys. Res., 114, D22301, doi:10.1029/2009JD012287, 2009.

Benedetti, A., J.-J. Morcrette, O. Boucher, A. Dethof, R. J. Engelen, M. Fisher, H. Flentjes, N. Huneeus, L. Jones, J. W. Kaiser, S. Kinne, A. Mangold, M. Razinger, A. J. Simmons, M. Suttie, and the GEMS-AER team: Aerosol analysis and forecast in the ECMWF Integrated Forecast System. Part II : Data assimilation, J. Geophys. Res., 114, D13205, doi:10.1029/2008JD011115, 2009.

Boussetta, S., Balsamo, G., Beljaars, A., Agusti-Panareda, A., Calvet, J.-C., Jacobs, C., van den Hurk, B., Viterbo, P., Lafont, S., Dutra, E., Jarlan, L., Balzarolo, M., Papale, D., and van der Werf, G.: Natural carbon dioxide exchanges in the ECMWF Integrated Forecasting System: implementation and offline validation, J. Geophys. Res.-Atmos., 118, 1–24, doi: 10.1002/jgrd.50488, 2013.

Braathen, WMO Arctic Ozone Bulletin No 1/2016, DOI:10.13140/RG.2.1.4929.6403, 2016.

Cammas, J.P., Brioude J., Chaboureau J.-P., Duron J., Mari C., Mascart P., Nédélec P., Smit H., Pätz H.-W., Volz-Thomas A., Stohl A., and Fromm M., Injection in the lower stratosphere of biomass fire emissions followed by long-range transport: a MOZAIC case study. Atmos. Chem. Phys., 9, 5829-5846, 2009

Cariolle, D. and Teyssèdre, H.: A revised linear ozone photochemistry parameterization for use in transport and general circulation models: multi-annual simulations, Atmos. Chem. Phys., 7, 2183-2196, doi:10.5194/acp-7-2183-2007, 2007.

Dee, D. P. and S. Uppala, Variational bias correction of satellite radiance data in the ERA-Interim reanalysis. Quart. J. Roy. Meteor. Soc.,135, 1830-1841, 2009.

Deeter, M. N., Emmons, L. K., Edwards, D. P., Gille, J. C., and Drummond, J. R.: Vertical resolution and information content of CO profiles retrieved by MOPITT, Geophys. Res. Lett., 31, L15112, doi:10.1029/2004GL020235, 2004.

Deeter, M. N., et al. (2010), The MOPITT version 4 CO product: Algorithm enhancements, validation, and long-term stability, J. Geophys. Res., 115, D07306, doi:10.1029/2009JD013005.

Dentener, F., et al., 2006: Emissions of primary aerosol and precursor gases in the years 2000 and 1750 prescribed data-sets for AeroCom, Atmos. Chem. Phys., 6, 4321 – 4344.

Deshler, T., J.L. Mercer, H.G.J. Smit, R. Stubi, G. Levrat, B.J. Johnson, S.J. Oltmans, R. Kivi, A.M. Thompson, J. Witte, J. Davies, F.J. Schmidlin, G. Brothers, T. Sasaki (2008) Atmospheric comparison of electrochemical cell ozonesondes from different maufacturers, and with different cathode solution strengths: The Balloon Experiment on Standards for Ozonsondes. J. Geophys. Res.113, D04307, doi:10.1029/2007JD008975

Douros, J., S. Basart, A. Benedictow, A.-M. Blechschmidt, S. Chabrillat, Y. Christophe, H. Clark, E. Cuevas, H.J. Eskes, H. Flentje, K. M. Hansen, J. Kapsomenakis, B. Langerock, K. Petersen, M. Ramonet, A. Richter, M. Schulz, A. Wagner, T. Warneke, C. Zerefos, Observations characterisation and validation methods document, Copernicus Atmosphere Monitoring Service (CAMS) report, CAMS84_2015SC2_D.84.8.1.1-2017_observations_v2.pdf, October 2017. Available from: http://atmosphere.copernicus.eu/user-support/validation/verification-global-services.

Dupuy, E., et al.: Validation of ozone measurements from the Atmospheric Chemistry Experiment (ACE), Atmos. Chem. Phys., 9, 287-343, doi:10.5194/acp-9-287-2009, 2009.

Elbern, H., Schwinger, J., Botchorishvili, R.: Chemical state estimation for the middle atmosphere by four-dimensional variational data assimilation: System configuration. Journal of Geophysical Research (Atmospheres) 115, 6302, 2010.

Emmons, L. K., D. P. Edwards, M. N. Deeter, J. C. Gille, T. Campos, P. Nédélec, P. Novelli, and G. Sachse, Measurements of Pollution In The Troposphere (MOPITT) validation through 2006 Atmos. Chem. Phys., 9, 1795-1803, 2009

Errera, Q., Daerden, F., Chabrillat, S., Lambert, J. C., Lahoz, W. A., Viscardy, S., Bonjean, S., and Fonteyn, D., 4D-Var Assimilation of MIPAS chemical observations: ozone and nitrogen dioxide analyses, Atmos. Chem. Phys., 8, 6169-6187, 2008.

Errera, Q. and Ménard, R.: Technical Note: Spectral representation of spatial correlations in variational assimilation with grid point models and application to the belgian assimilation system for chemical observations (BASCOE), Atmos. Chem. Phys. Discuss., 12, 16763-16809, doi:10.5194/acpd-12-16763-2012, 2012.

Eskes, H., Wagner, A., Schulz, M., Christophe, Y., Ramonet, M., Basart, S., Benedictow, A., Blechschmidt, A.-M., Chabrillat, S., Clark, H., Cuevas, E., Flentje, H., Hansen, K. M., Im, U., Kapsomenakis, J., Langerock, B., Petersen, K., Richter, A., Sudarchikova, N., Thouret, V., Warneke, T., and Zerefos, C.: Validation report of the CAMS near-real time global atmospheric composition service December 2016 - February 2017, CAMS84_2015SC2_D84.1.1.7_2017DJF_v1.1, June 2017. Available from: http://atmosphere.copernicus.eu/user-support/validation/verification-global-services

Eskes, H. J., T. Antonakaki, S. Basart, A. Benedictow, A.-M. Blechschmidt, S. Chabrillat, Y. Christophe, H. Clark, E. Cuevas, K. M. Hansen, U. Im, J. Kapsomenakis, B. Langerock, K. Petersen, A. Richter, M. Schulz, N. Sudarchikova, V. Thouret, A. Wagner, C. Zerefos, Upgrade verification note for the CAMS near-real time global atmospheric composition service, Copernicus Atmosphere Monitoring Service (CAMS) report, CAMS84_2015SC2_D84.3.1.3_201706_esuite_v1.pdf, July 2017.

Eskes, H. J., S. Basart, A. Benedictow, Y. Bennouna, A.-M. Blechschmidt, S. Chabrillat, Y. Christophe, H. Clark, E. Cuevas, K. M. Hansen, U. Im, J. Kapsomenakis, B. Langerock, K. Petersen, M. Schulz, A. Wagner, C. Zerefos, Upgrade verification note for the CAMS near-real time global atmospheric composition service, Copernicus Atmosphere Monitoring Service (CAMS) report, CAMS84_2015SC3_D84.3.1.5_201802_esuite_v1.pdf, February 2018; Eskes et al., Upgrade verification note for the CAMS near-real time global atmospheric composition service, Addendum July 2018, CAMS84_2015SC3_D84.3.1.5_201802_esuite_v1.pdf.

Flemming, J., Huijnen, V., Arteta, J., Bechtold, P., Beljaars, A., Blechschmidt, A.-M., Diamantakis, M., Engelen, R. J., Gaudel, A., Inness, A., Jones, L., Josse, B., Katragkou, E., Marecal, V., Peuch, V.-H., Richter, A., Schultz, M. G., Stein, O., and Tsikerdekis, A.: Tropospheric chemistry in the Integrated Forecasting System of ECMWF, Geosci. Model Dev., 8, 975-1003, doi:10.5194/gmd-8-975-2015, 2015.

Flemming, J., Benedetti, A., Inness, A., Engelen, R. J., Jones, L., Huijnen, V., Remy, S., Parrington, M., Suttie, M., Bozzo, A., Peuch, V.-H., Akritidis, D., and Katragkou, E.: The CAMS interim Reanalysis of Carbon Monoxide, Ozone and Aerosol for 2003–2015, Atmos. Chem. Phys., 17, 1945-1983, doi:10.5194/acp-17-1945-2017, 2017.

Franco, B., et al., Retrievals of formaldehyde from ground-based FTIR and MAX-DOAS observations at the Jungfraujoch station and comparisons with GEOS-Chem and IMAGES model simulations, Atmos. Meas. Tech., 8, 1733-1756, 2015

Gielen, C., Van Roozendael, M., Hendrick, F., Pinardi, G., Vlemmix, T., De Bock, V., De Backer, H., Fayt, C., Hermans, C., Gillotay, D., and Wang, P.: A simple and versatile cloud-screening method for MAX-DOAS retrievals, Atmos. Meas. Tech., 7, 3509-3527, doi:10.5194/amt-7-3509-2014, 2014.

Granier, C. et al.: Evolution of anthropogenic and biomass burning emissions of air pollutants at global and regional scales during the 1980–2010 period. Climatic Change (109), 2011

Holben, B. N., Eck, T. F., Slutsker, I., Tanré, D., Buis, J. P., Setzer, A., Vermote, E., Reagan, J. A., Kaufman, Y. J., Nakajima, T., Lavenu, F., Jankowiak, I., and Smirnov A.: AERONET – a federated instrument network and data archive for aerosol characterization, Remote Sens. Environ., 66, 1–16, 5529, 5533, 5537, 5544, 1998.

Hommel, R., Eichmann, K.-U., Aschmann, J., Bramstedt, K., Weber, M., von Savigny, C., Richter, A., Rozanov, A., Wittrock, F., Khosrawi, F., Bauer, R., and Burrows, J. P.: Chemical ozone loss and ozone mini-hole event during the Arctic winter 2010/2011 as observed by SCIAMACHY and GOME-2, Atmos. Chem. Phys., 14, 3247-3276, doi:10.5194/acp-14-3247-2014, 2014.

Huijnen, V., et al.: The global chemistry transport model TM5: description and evaluation of the tropospheric chemistry version 3.0, Geosci. Model Dev., 3, 445-473, doi:10.5194/gmd-3-445-2010, 2010.

Inness, A., Blechschmidt, A.-M., Bouarar, I., Chabrillat, S., Crepulja, M., Engelen, R. J., Eskes, H., Flemming, J., Gaudel, A., Hendrick, F., Huijnen, V., Jones, L., Kapsomenakis, J., Katragkou, E., Keppens, A., Langerock, B., de Mazière, M., Melas, D., Parrington, M., Peuch, V. H., Razinger, M., Richter, A., Schultz, M. G., Suttie, M., Thouret, V., Vrekoussis, M., Wagner, A., and Zerefos, C.: Data assimilation of satellite-retrieved ozone, carbon monoxide and nitrogen dioxide with ECMWF's Composition-IFS, Atmos. Chem. Phys., 15, 5275-5303, doi:10.5194/acp-15-5275-2015, 2015.

Janssens-Maenhout, G., Dentener, F., Aardenne, J. V., Monni, S., Pagliari, V., Orlandini, L., Klimont, Z., Kurokawa, J., Akimoto, H., Ohara, T., Wankmueller, R., Battye, B., Grano, D., Zuber, A., and Keating, T.: EDGAR-HTAP: a Harmonized Gridded Air Pollution Emission Dataset Based on National Inventories, JRC68434, EUR report No EUR 25 299–2012, ISBN 978-92-79- 23122-0, ISSN 1831-9424, European Commission Publications Office, Ispra (Italy), 2012.

Jaross, G., Bhartia, P.K., Chen, G., Kowitt, M., Haken, M., Chen, Z., Xu, Ph., Warner, J., Kelly, T. : OMPS Limb Profiler instrument performance assessment, J. Geophys. Res. Atmos 119, 2169-8996, 2014.

Kaiser, J. W., Heil, A., Andreae, M. O., Benedetti, A., Chubarova, N., Jones, L., Morcrette, J.-J., Razinger, M., Schultz, M. G., Suttie, M., and van der Werf, G. R.: Biomass burning emissions estimated with a global fire assimilation system based on observed fire radiative power, Biogeosciences, 9, 527-554, doi:10.5194/bg-9-527-2012, 2012.

Kramarova, N. A., Nash, E. R., Newman, P. A., Bhartia, P. K., McPeters, R. D., Rault, D. F., Seftor, C. J., Xu, P. Q., and Labow, G. J.: Measuring the Antarctic ozone hole with the new Ozone Mapping and Profiler Suite (OMPS), Atmos. Chem. Phys., 14, 2353-2361, doi:10.5194/acp-14-2353-2014, 2014.

Lahoz, W. A., Errera, Q., Viscardy, S., and Manney G. L., The 2009 stratospheric major warming described from synergistic use of BASCOE water vapour analyses and MLS observations, Atmos. Chem. Phys. 11, 4689-4703, 2011

Lambert, A, et al., Aura Microwave Limb Sounder Version 3.4 Level-2 near real-time data user guide, http://disc.sci.gsfc.nasa.gov/Aura/data-holdings/MLS/documents/NRT-user-guide-v34.pdf

Langerock, B., De Mazière, M., Hendrick, F., Vigouroux, C., Desmet, F., Dils, B., and Niemeijer, S.: Description of algorithms for co-locating and comparing gridded model data with remote-sensing observations, Geosci. Model Dev., 8, 911-921, doi:10.5194/gmd-8-911-2015, 2015.

Lefever, K., van der A, R., Baier, F., Christophe, Y., Errera, Q., Eskes, H., Flemming, J., Inness, A., Jones, L., Lambert, J.-C., Langerock, B., Schultz, M. G., Stein, O., Wagner, A., and Chabrillat, S.: Copernicus stratospheric ozone service, 2009–2012: validation, system intercomparison and roles of input data sets, Atmos. Chem. Phys., 15, 2269-2293, doi:10.5194/acp-15-2269-2015, 2015.

Liu, Z., et al., Exploring the missing source of glyoxal (CHOCHO) over China, Geophys. Res. Lett., 39, L10812, doi: 10.1029/2012GL051645, 2012

Massart, S., Flemming, J., Cariolle, D., Jones, L., High resolution CO tracer forecasts, MACC-III Deliverable D22.04, May 2015, available from http://www.gmes-atmosphere.eu/documents/macciii/deliverables/grg

Morcrette, J.-J., O. Boucher, L. Jones, D. Salmond, P. Bechtold, A. Beljaars, A. Benedetti, A. Bonet, J. W. Kaiser, M. Razinger, M. Schulz, S. Serrar, A. J. Simmons, M. Sofiev, M. Suttie, A. M. Tompkins, and A. Untch: Aerosol analysis and forecast in the ECMWF Integrated Forecast System. Part I: Forward modelling, J. Geophys. Res., 114, D06206, doi:10.1029/2008JD011235, 2009.

Richter, A., Burrows, J. P., Nüß, H., Granier, C, Niemeier, U.: Increase in tropospheric nitrogen dioxide over China observed from space, Nature, 437, 129-132, doi: 10.1038/nature04092, 2005

*Richter, A., Begoin, M., Hilboll, A., and Burrows, J. P.: An improved NO2 retrieval for the GOME-2 satellite instrument, Atmos. Meas. Tech. , **4**, 1147-1159, doi:10.5194/amt-4-1147-2011, 2011*

Sindelarova, K., Granier, C., Bouarar, I., Guenther, A., Tilmes, S., Stavrakou, T., Müller, J.-F., Kuhn, U., Stefani, P., and Knorr, W.: Global data set of biogenic VOC emissions calculated by the MEGAN model over the last 30 years, Atmos. Chem. Phys., 14, 9317-9341, doi:10.5194/acp-14-9317-2014, 2014.

Smit, H.G.J., W. Straeter, B.J. Johnson, S.J. Oltmans, J. Davies, D.W. Tarasick, B. Hoegger, R. Stubi, F.J. Schmidlin, T. Northam, A.M. Thompson, J.C. Witte, I. Boyd: Assessment of the performance of ECC-ozonesondes under quasi-flight conditions in the environmental simulation chamber: Insights from the Juelich Ozone Sonde Intercomparison Experiment (JOSIE), J. Geophys. Res. 112, D19306, doi:10.1029/2006JD007308, 2007.

Solomon, S., Haskins, J., Ivy, D. J. and Min, F.: Fundamental differences between Arctic and Antarctic ozone depletion, PNAS 2014 111 (17) 6220-6225, doi:10.1073/pnas.1319307111, 2014.

Stavrakou,T., First space-based derivation of the global atmospheric methanol fluxes, Atm. Chem. Phys., 11, 4873-4898, 2013.

Strahan, S.E., A.R. Douglass, and P.A. Newman, The contributions of chemistry and transport to low arctic ozone in March 2011 derived from Aura MLS observations, J. Geophys. Res. Atmos., 118, 1563–1576, doi:10.1002/jgrd.50181, 2013.

Taha, G.; Jaross, G. R.; Bhartia, P. K.: Validation of OMPS LP Ozone Profiles Version 2.0 with MLS, Ozone Sondes and Lidar Measurements, American Geophysical Union, Fall Meeting 2014, abstract #A33J-3322, 2014.

Taylor, K.E.: Summarizing multiple aspects of model performance in a single diagram. J.Geophys. Res., 106, 7183-7192, 2001.

van der A, R. J. , M. A. F. Allaart, and H. J. Eskes, Multi sensor reanalysis of total ozone, Atmos. Chem. Phys., 10, 11277–11294, doi:10.5194/acp-10-11277-2010, www.atmos- chem-phys.net/10/11277/2010/, 2010

van der A, R., M. Allaart, H. Eskes, K. Lefever, Validation report of the MACC 30-year multi-sensor reanalysis of ozone columns Period 1979-2008, MACC-II report, Jan 2013, MACCII_VAL_DEL_D_83.3_OzoneMSRv1_20130130.docx/pdf.

van der A, R. J., Allaart, M. A. F., and Eskes, H. J.: Extended and refined multi sensor reanalysis of total ozone for the period 1970–2012, Atmos. Meas. Tech., 8, 3021-3035, doi:10.5194/amt-8-3021-2015, 2015.

*Vrekoussis, M., Wittrock, F., Richter, A., and Burrows, J. P.: GOME-2 observations of oxygenated VOCs: what can we learn from the ratio glyoxal to formaldehyde on a global scale?, Atmos. Chem. Phys., **10**, 10145-10160, doi:10.5194/acp-10-10145-2010, 2010*

Wennberg, P. O., Mui, W., Wunch, D., Kort, E. A., Blake, D. R., Atlas, E. L., Santoni, G. W., Wofsy, S. C., Diskin, G. S., Jeong, S., and Fischer, M. L.: On the sources of methane to the Los Angeles atmosphere, Environ. Sci. Technol., 46, 9282–9289, https://doi.org/10.1021/es301138y, 2012

Wittrock, F., A. Richter, H. Oetjen, J. P. Burrows, M. Kanakidou, S. Myriokefalitakis, R. Volkamer, S. Beirle, U. Platt, and T. Wagner, Simultaneous global observations of glyoxal and formaldehyde from space, Geophys. Res. Lett., 33, L16804, doi:10.1029/2006GL026310, 2006

WMO (2010), Guidelines for the Measurement of Atmospheric Carbon Monoxide, GAW Report No. 192, World Meteorological Organization, Geneva, Switzerland, 2010.

WMO (2013), Guidelines for the Continuous Measurements of Ozone in the Troposphere, GAW Report No. 209, World Meteorological Organization, Geneva, Switzerland, 2013.

Wunch, D., Wennberg, P. O., Toon, G. C., Keppel-Aleks, G., and Yavin, Y. G.: Emissions of greenhouse gases from a North American megacity, Geophys. Res. Lett., 36, 1–5, https://doi.org/10.1029/2009GL039825, 2009.

Annex 1: Acknowledgements

Listed below are the authors contributing to the sections in this report. The authors contributing to the model description are also provided, as well as acknowledgements to the validation datasets.

Tropospheric reactive gases reactive gases

Annette Wagner, MPG (editor, O3 sondes, GAW data)
Yasmine Bennouna, Valerie Thouret, CNRS-LA (IAGOS)
Harald Flentje, DWD (O3 sondes, GAW data)
Anne Blechschmidt and Andreas Richter, IUB Bremen (GOME-2 NO2, HCHO)
John Kapsomenakis, Christos Zerefos, AA (ESRL)
Natalia Sudarchikova, satellite IR observations (MPG)
Kaj Hansen, Ulas Im, AU (Arctic theme)
Bavo Langerock, BIRA (NDACC)

Tropospheric aerosol

Michael Schulz, MetNo (editor, Aerocom, Aeronet)
Anna Benedictow, Jan Griesfeller, MetNo (Aerocom, Aeronet)
Sara Basart, MTeresa Pay, Oriol Jorba, BSC-CNS (Aeronet, MODIS, AirBase, SDS-WAS NAMEE RC)
Emilio Cuevas, AEMET (Aeronet, MODIS, AirBase, SDS-WAS NAMEE RC)
Harald Flentje, DWD (Backscatter profiles)

Stratospheric reactive gases

Yves Christophe, BIRA (editor, model-satellite intercomparisons)
Simon Chabrillat, BIRA (model intercomparisons)
Annette Wagner, MPI-M (O_3 sondes)
Bavo Langerock, BIRA (NDACC FTIR, MWR, UVVIS DOAS, LIDAR)
Anne Blechschmidt and Andreas Richter, IUB-UB Bremen (SCIAMACHY/GOME-2 NO_2)

Greenhouse gases

Michel Ramonet, IPSL (ICOS)
Olivier Jossoud and Leonard Rivier, LSCE (ICOS)
Thorsten Warneke, UBC (TCCON)
Bavo Langerock, BIRA (TCCON)

Reactive gases and aerosol modeling

Johannes Flemming (ECMWF), Antje Inness (ECMWF), Angela Benedetti (ECMWF), Sebastien Massart (ECMWF), Anna Agusti-Panareda (ECMWF), Johannes Kaiser (KCL/MPIC/ECMWF), Samuel Remy (LMD), Olivier Boucher (LMD), Vincent Huijnen (KNMI), Richard Engelen (ECMWF)

Acknowledgements for the validation datasets used

We wish to acknowledge the provision of NRT GAW observational data by: Institute of Atmospheric Sciences and Climate (ISAC) of the Italian National Research Council (CNR), South African Weather Service, National Centre for Atmospheric Science (NCAS, Cape Verde), National Air Pollution Monitoring Network (NABEL) (Federal Office for the Environment FOEN and Swiss Federal Laboratories for Materials Testing and Research EMPA), Atmospheric Environment Division Global Environment and Marine Department Japan Meteorological Agency, Chinese Academy of Meteorological Sciences (CAMS), Alfred Wegener Institut, Umweltbundesamt (Austria), National Meteorological Service (Argentina), Umweltbundesamt (UBA, Germany)

We are grateful to the numerous operators of the Aeronet network and to the central data processing facility at NASA Goddard Space Flight Center for providing the NRT sun photometer data, especially Ilya Slutker and Brent Holben for sending the data.

The authors thank to all researchers, data providers and collaborators of the World Meteorological Organization's Sand and Dust Storm Warning Advisory and Assessment System (WMO SDS-WAS) for Northern Africa, Middle East and Europe (NAMEE) Regional Node. Also special thank to Canary Government as well as AERONET, MODIS, U.K. Met Office MSG, MSG Eumetsat and EOSDIS World Viewer principal investigators and scientists for establishing and maintaining data used in the activities of the WMO SDS-WAS NAMEE Regional Center (http://sds-was.aemet.es/).

We wish to acknowledge the provision of ozone sonde data by the World Ozone and Ultraviolet Radiation Data Centre established at EC in Toronto (http://woudc.org), by the Data Host Facility of the Network for the Detection of Atmospheric Composition Change established at NOAA (http://ndacc.org), by the Norwegian Institute for Air Research and by the National Aeronautics and Space Administration (NASA).

We wish to thank the NDACC investigators for the provision of observations at Ny Alesund, Bern, Jungfraujoch, Izaña, Xianghe, Harestua, Reunion Maido, Uccle, Hohenpeissen, Mauna Loa, Lauder and Haute Provence.

The authors acknowledge the NOAA Earth System Research Laboratory (ESRL) Global Monitoring Division (GMD) for the provision of ground based ozone concentrations.

The MOPITT CO data were obtained from the NASA Langley Research Center ASDC. We acknowledge the LATMOS IASI group for providing IASI CO data.

SCIAMACHY lv1 radiances were provided to IUP-UB by ESA through DLR/DFD.

GOME-2 lv1 radiances were provided to IUP-UB by EUMETSAT.

The authors acknowledge Environment and Climate Change Canada for the provision of Alert ozone data and Sara Crepinsek – NOAA for the provision of Tiksi ozone data. Surface ozone data from the Zeppelin Mountain, Svalbard are from www.luftkvalitet.info. Surface ozone data from the Villum Research Station, Station Nord (VRS) were financially supported by "The Danish Environmental Protection Agency" with means from the MIKA/DANCEA funds for Environmental Support to the Arctic Region. The Villum Foundation is acknowledged for the large grant making it possible to build VRS in North Greenland.

We acknowledge the National Aeronautics and Space Administration (NASA), USA for providing the OMPS limb sounder data (http://npp.gsfc.nasa.gov/omps.html) and the Aura-MLS offline data (http://mls.jpl.nasa.gov/index-eos-mls.php).

We thank the Canadian Space Agency and ACE science team for providing level 2 data retrieved from ACE-FTS on the Canadian satellite SCISAT-1.

The TCCON site at Orleans is operated by the University of Bremen and the RAMCES team at LSCE (Gif-sur-Yvette, France). The TCCON site at Bialystok is operated by the University of Bremen. Funding for the two sites was provided by the EU-project ICOS-INWIRE and the University of Bremen. The TCCON site at Réunion is operated by BIRA-IASB, in cooperation with UReunion and is funded by BELSPO in the framework of the Belgian ICOS program.

We acknowledge the provision of CO_2/CH_4 data from SNO-RAMCES/ICOS network coordinated by LSCE/OVSQ (CEA-CNRS-UVSQ, Université Paris-Saclay), as well as Laboratorio de Física de la Atmósfera (UMSA, Bolivia), Environmental Chemical Processes Laboratory (ECPL/UoC, Greece), Station Géophysique de LAMTO, Ivory Coast), C-CAPS/NUIG/EPA (Ireland), BIRA-IASB (Belgium) and the following research institutes in France: LaMP/OPGC, P2OA/LA/OMP, OPE/ANDRA, OHP/PYTHEAS, OPAR/LACY/OSUR, UMR EcoFoG, IPEV, IRD.

The European Environment Information and Observation Network (Eionet) Air Quality portal provides details relevant for the reporting of air quality information from EU Member States and other EEA member and co-operating countries. This information is submitted according to Directives 2004/107/EC and 2008/50/EC of the European Parliament and of the Council.

Copernicus Atmosphere Monitoring Service

ECMWF - Shinfield Park, Reading RG2 9AX, UK

Contact: info@copernicus-atmosphere.eu